INSPECTION OF STEEL BRIDGE WELDS USING PHASED ARRAY ULTRASONIC TESTING

by

Curtis J. Schroeder

A Dissertation

Submitted to the Faculty of Purdue University

In Partial Fulfillment of the Requirements for the degree of

Doctor of Philosophy

Lyles School of Civil Engineering

West Lafayette, Indiana

December 2018

THE PURDUE UNIVERSITY GRADUATE SCHOOL
STATEMENT OF COMMITTEE APPROVAL

Dr. Robert J. Connor, Chair

Lyles School of Civil Engineering, Purdue University

Dr. Mark D. Bowman

Lyles School of Civil Engineering, Purdue University

Dr. Amit H. Varma

Lyles School of Civil Engineering, Purdue University

Dr. Glenn A. Washer

Department of Civil and Environmental Engineering, University of Missouri

Approved by:

Dr. Dulcy Abraham

Head of the Graduate Program

This work is dedicated to my wife, Shana, who supported and believed in me.

ACKNOWLEDGMENTS

I would like to thank my advisor, Dr. Robert J. Connor, for his immense support and guidance during both my Master of Science and Doctor of Philosophy research projects. I am very grateful for his leadership and mentorship. I would not have returned to Purdue to pursue my PhD without Rob's guidance and instruction.

I would also like to thank the other members of my graduate committee, Dr. Mark Bowman, Dr. Amit Varma, and Dr. Glenn Washer, for their expert review and contribution to my research.

I would like to give special thanks to Bridget Crowley for her diligent effort and contribution to the NCHRP research project. I would also like to thank my friends and colleagues at Bowen Laboratory for their support including Dr. Cem Korkmaz, Leslie Campbell, Thomas Bradt, Dr. Ryan Sherman, Dr. Jason Lloyd, Dr. Francisco Bonachera Martin, and Adam Cullison.

This research is part of NCHRP (National Collaborative Highway Research Program) Project 14-35, "Acceptance Criteria of Complete Joint Penetration Steel Bridge Welds Evaluated Using Enhanced Ultrasonic Methods". I would like to acknowledge the industry sponsors who loaned round robin test plates and ultrasonic equipment, including Federal Highway Administration, University of Missouri, Fickett Structural Solutions, Olympus, and Zetec, as well as High Steel Structures for performing digital radiography services. Finally, I would like to thank the anonymous industry professionals who generously donated their time by taking part in the round robin testing program.

TABLE OF CONTENTS

LIST OF TABLES

LIST OF FIGURES

ABSTRACT

Author: Schroeder, Curtis, J. PhD
Institution: Purdue University
Degree Received: December 2018
Title: Inspection of Steel Bridge Welds Using Phased Array Ultrasonic Testing
Major Professor: Dr. Robert J. Connor

The objective of this research is to develop recommendations on calibration standards, scanning procedures, and acceptance criteria for phased array ultrasonic testing (PAUT) of complete joint penetration butt welds within the AWS D1.5 Bridge Welding Code. These recommendations include the development of a rational acceptance criteria which is based in engineering analysis and fracture mechanics. It is expected that the updated scanning procedures and acceptance criteria will result in improved reliability for bridges and improved consistency in bridge fabrication quality.

While PAUT was included in the 2015 edition of AWS D1.5 in Annex K, the acceptance criteria for this procedure was developed as an adaptation of an existing conventional ultrasonic testing (UT) acceptance criteria in AWS D1.1. Therefore, the acceptance criteria in AWS D1.5:2015 is a workmanship-based criteria and is not based on engineering analysis of the criticality of weld flaws. The scanning procedures and application of PAUT inspections of bridge welds according to this procedure differ greatly from the scanning procedures outlined in AWS D1.5 for conventional UT inspections. Previous research has shown that differences in flaw rejection are possible for PAUT and conventional UT ultrasonic methods under the AWS D1.5:2015 approach.

In order to develop recommendations for improved calibration standards, scanning procedures, and acceptance criteria for PAUT within AWS D1.5, this research project utilized both analytical techniques and experimental testing. This research project included determination of target critical flaw sizes for routine detection and rejection through fitness-for-service evaluations. This was followed by a round robin ultrasonic testing program in order to collect data on the variability of inspection results of eleven weld samples with nineteen weld flaws using different ultrasonic inspection techniques. Next, calibration requirements were developed to account for differences

in ultrasonic attenuation and shear wave velocity between calibration blocks and test objects. Development of these requirements included experimental testing of base metals and weld metals, along with simulations of ultrasonic inspection using commercial software. Finally, minimum requirements for weld scanning procedures, reference standard reflectors, and corresponding amplitude limits for detection and rejection of target critical weld flaws were developed using ultrasonic inspection simulations and verified through experimental testing of weld samples with known weld flaws.

1. INTRODUCTION

1.1 Motivation

Reliable detection of internal weld flaws using any nondestructive testing (NDT) technique is essential to ensuring the desired performance of a structure. Presently, two NDT methods are used for evaluation of complete joint penetration (CJP) groove butt welds in steel bridges: radiographic testing (RT) and ultrasonic testing (UT). Using RT, discontinuities are distinguished from sound weld or base metal based on contrast variations that appear on a radiographic film. UT, on the other hand, utilizes reflections from high-frequency sound waves to inspect for internal discontinuities within the weld and base metal. While RT can reliably identify volumetric discontinuities, this method is typically not as effective for thin planar discontinuities such as cracks and lack of fusion. UT typically launches the sound waves at an angle into the material in such a way that planar discontinuities can be readily detected.

A set of *acceptance criteria* provides a measure or reference by which a standard of quality is applied to provide adequate structural performance. One definition of acceptance criteria is "a set of rules formulated in terms of the requirements to NDE recorded parameter values for judgement of whether flaws are acceptable or rejectable [1]." It would be ideal for acceptance criteria to reject and repair all imperfections which could be harmful to the structure while accepting all harmless imperfections, but this idea is unattainable in a rational weld acceptance criteria. If one takes into account the economic considerations of repairing a fatigue failure due to undersizing a flaw compared to the cost of repairing a benign imperfection, it may be found that the acceptance criteria needs to be set so that many harmless imperfections may need to be repaired in order to eliminate one harmful imperfection [2].

On a very broad level, all acceptance criteria can be placed into one of two categories: *workmanship* criteria or *fitness-for-service* (fracture mechanics based) criteria. *Workmanship* criteria are based on a general, arbitrary control on the level of quality [3] and is aimed at ensuring that an acceptable workmanship level is met [1]. Many welding codes employ a workmanship criteria such as the AWS D1.1 Structural Welding Code [4] and AWS D1.5 Bridge Welding Code

[5]. Generally speaking, although workmanship criteria have historically provided adequate performance, they are often based on experience and do not give an objective comparison to the actual size that would result in component failure. Further, the apparent "success" of workmanship criteria (i.e., the observation that bridges are not having critical failures so the criteria are working) may not necessarily be due to the criteria themselves, but due to a series of factors that are unknown or unaccounted for since the criteria were arbitrarily crafted.

Fitness-for-service (FFS) criteria, also known as Engineering Critical Assessment (ECA), are based on fracture mechanics which uses information on member loading and material properties to determine an acceptable initial discontinuity size for the intended service life. FFS will typically permit larger discontinuities than "workmanship" criteria, but require accurate and reliable measurements of flaw size and location [6]. Further, FFS requires accurate estimates of material properties and residual stresses, in addition to static and cyclic stresses over the service life of the structure.

Advances in ultrasonic methods, including the development of phased-array ultrasonic testing (PAUT), provide enhanced ability to detect and characterize weld flaws, perform automated data collection, and generate images of ultrasonic results. Although improvements have been made to the ultrasonic equipment, the current acceptance criteria for PAUT in the 2015 edition of American Welding Society (AWS) D1.5 Bridge Welding Code provided in Annex K are not based on the criticality of a weld discontinuity on bridge performance measures such as the resistance to fatigue and fracture. Rather this acceptance criteria is a workmanship criteria meant to provide an arbitrary control on the level of quality.

Previous research has found large variability in the inspection results using encoded, line scanned PAUT according to AWS D1.5:2015 Annex K compared with manual, raster scanned conventional UT or RT. These variations could result in acceptance of a weld discontinuity which would have been previously rejected. While amplitude-based acceptance criteria have been traditionally applied to ultrasonic results, it has been shown in previous research that amplitude is not a direct measurement of discontinuity size since many factors will affect the amplitude, including the shape of the discontinuity, ultrasonic incidence angle, tilt and skew of the discontinuity, etc. According to fracture mechanics, the critical dimensions of weld discontinuities are the discontinuity height and length, not the ultrasonic amplitude.

Therefore, the ability to use PAUT to measure the physical discontinuity height and length was investigated as part of this research project. As discussed in Chapter 4, it was found that the variability of discontinuity height sizing was too great to result in consistent determination of weld discontinuity rejection. Therefore, this research instead focused on improvements to the amplitude-based acceptance criteria to increase reliability of inspection results. Research under NCHRP 14-35 [7], [8] has also noted large variability in ultrasonic material attenuation and ultrasonic material velocity which would result in decreased inspection reliability if not properly accounted for during the calibration and scanning procedures. Since AWS D1.5:2015 does not account for these factors, modifications to the code to provide additional requirements on calibration requirements and scanning procedures are warranted.

Therefore, development of updated acceptance criteria for evaluation of CJP butt welds in steel bridges using PAUT is expected to result in improved reliability for bridges and improved consistency in bridge fabrication quality. Development of a PAUT acceptance criteria based on engineering analysis and flaw criticality requires determination of the following five items:

1. Target critical flaw size that needs to be routinely detected and rejected by the inspection procedure
2. Ultrasonic probe parameters that will enhance detectability of target critical flaws while limiting calibration issues due to variations in weld thickness and base and weld metal ultrasonic properties
3. Calibration requirements to account for differences between the calibration block and the test specimen
4. Scanning procedures and acceptance criteria amplitude limits corresponding to a reference standard reflector that will result in detection and rejection of target critical flaws
5. Accounting for variability in inspection results due to human factors and technology factors (i.e., equipment errors, variation in process or procedure, etc.)

Therefore, based on the current status of ultrasonic inspection procedures in AWS D1.5:2015, the motivation of this research project will be to aid in the development of rational acceptance criteria based in fracture mechanics for ultrasonic inspection using PAUT of steel bridge CJP butt welds by evaluating items one through four in the list above. Item five (i.e., inspection variability) will be evaluated during future research.

1.2 Current AWS D1.5 Requirements

AWS D1.5 conventional UT employs workmanship criteria based on the amplitude of the reflected sound along with the flaw length. Conventional UT technicians perform bridge weld testing under the AWS D1.5 code by utilizing a manual, raster scanning approach where the probe is rotated and translated on the testing surface to provide coverage of the entire weld volume and to maximize the signal response amplitude. Thresholds for flaw rejection using conventional UT in AWS D1.5 were developed through calibration to criteria used traditionally for RT that were not based on structural performance [3], [9]. RT and UT utilize very different approaches for discontinuity detection due to the actual physics associated with the technologies. For example, RT responds to changes in density which is recorded on a 2-D film while UT measures reflection of sound in both the amplitude and time domain. Therefore, it cannot be assumed, nor is it reasonable to assert that UT or PAUT can always detect the same discontinuities as RT.

For conventional UT inspections according to AWS D1.5, the Indication Rating is determined based on the indication amplitude compared to the reference standard reflector and the sound path distance. Decreasing values (i.e., more negative) of Indication Rating are more severe. The Indication Rating is derived by subtracting the reference gain and an attenuation factor from the equipment gain when the indication amplitude matches the reference amplitude. The attenuation factor is included to account for the ultrasonic attenuation due to the loss of amplitude as the sound travels through the steel. Discontinuities larger than the reference reflector, which is a 1.5 mm (0.06”) diameter side drilled hole (SDH), should reflect more sound than the reference reflector. Therefore, the equipment gain will be lower when the indication amplitude matches the reference level. A negative Indication Rating would result if the sound traveled the same distance in the inspection as the reference reflector and lower equipment gain is required to match the reference amplitude. Assuming that the sound path remains the same, a positive Indication Rating would result if the more equipment gain is required to match the reference amplitude.

Based on the loading (compression or tension), Indication Rating, plate thickness, and testing angle, the indication is classified by assumed severity:

- Class A (large flaws): Any indication in this category is rejected (regardless of length)
- Class B (medium flaws): Any indication with a length greater than ¾ inch is rejected.
- Class C (small flaws): Any indication in this category with a length greater than 2 inches or ¾ inch for an indication in the top or bottom quarter of a tension weld is rejected.
- Class D (minor flaws): Any indication in this category is accepted regardless of length or location in the weld.

For plate thicknesses up to 1.5 inches, the range for intermediate classifications (i.e., Class B and Class C) is 1 decibel (dB). Therefore, only 3 dB separates a Class A (automatically rejectable) indication from a Class D (automatically acceptable) indication. For plate thicknesses greater than 1.5 inches, the range for intermediate classifications is 2 dB, and 5 dB separates a Class A indication from a Class D indication.

AWS D1.5:2015 includes alternate acceptance criteria in Annex K to allow for the implementation of PAUT in lieu of conventional UT for testing of bridge welds. This testing procedure employs a line scanning approach where the probe remains perpendicular to the weld at a constant index position. The procedure uses a sectorial focal law which produces a sound wave over a range of incidence angles. This helps to insonify the weld volume. However, multiple scans at varying index points may be necessary for complete coverage. The acceptance criteria in Annex K were developed as an adaptation of an existing conventional UT acceptance criteria in AWS D1.1 (Annex Q). Therefore, Annex K is also a workmanship criteria and the amplitude of the reflected sound along with the flaw length form the basis of the acceptance criteria. Similarly, Annex K uses the same size reference standard reflector and the same indication classifications (Class A – D). As will be discussed further in Chapter 6, the acceptance criteria in AWS D1.1 Annex Q and subsequently AWS D1.5 Annex K do not match the acceptance criteria in AWS D1.1 or D1.5 Clause 6 for conventional UT. This is a very important observation. While the classifications and their respective maximum length requirements are very similar for Annex K and conventional UT, the range of intermediate classifications (i.e., Class B and Class C) are much larger. Class B has a 5 dB range, and Class C has a 6 dB range. Therefore, 11 dB separates a Class A (automatically rejectable) indication from a Class D (automatically acceptable) indication. For Annex K, the reference amplitude is consistently used as the distinction between a Class B or Class C indication, while the reference amplitude does not correlate to a distinct flaw classification in the conventional UT tables.

Instead of using an Indication Rating and an attenuation factor to evaluate the amplitude of the indication such as is performed in Clause 6 conventional UT inspections, PAUT utilizes a calibration method with reference reflectors placed at various depths (i.e., Time Corrected Gain (TCG)). With this correction, the amplitude measured in percentage of full screen height (%FSH) is compared directly with the reference amplitude. Therefore, indications with a greater amplitude in %FSH are more severe. This is unlike conventional UT where more negative Indication Ratings are more severe.

1.3 Comparison to Other UT Codes

A collection of reference standard provisions, both national and international, related to ultrasonic testing have been summarized below. Specifically, a comparison of each standard's policy on acceptance criteria, material attenuation, and probe frequency have been presented in Table 1.1, Table 1.2, and Table 1.3, respectively. The ultrasonic codes included in this summary are:

- Canadian Standards Association (CSA) W59 code, which is applicable to bridges [10]
- European Standard (EN) and International Organization for Standardization (ISO) codes which are applicable to bridges
- American Society of Mechanical Engineers (ASME) Boiler and Pressure Vessel Code (BPVC), which is applicable to the nuclear and petrochemical industry [11], [12]
- Japanese Industrial Standard (JIS) Z 3060 code, which is applicable to bridges [13]

1.3.1 Acceptance criteria

Codes which included an acceptance criteria based on measuring the flaw size of weld flaws require that the flaw sizing procedures be developed by the PAUT technician and verified for accuracy through performance qualification of the PAUT procedure on weld mockups representative of those being inspected before performing testing. None of the PAUT codes provide a prescriptive procedure for measuring the through-thickness height of weld flaws.

AWS D1.5:2015 Annex K uses maximum amplitude and length for the acceptance criteria for PAUT. It does not require any performance qualification testing be performed. It outlines the requirements of performing a mockup verification at the option of the PAUT technician or when required by the Engineer.

CSA W59 added a TCG approach in the 2018 edition for conventional UT or raster scanned manual PAUT which is intended to provide an equivalent level of quality as the current conventional UT acceptance tables but has one table for all angles. The CSA W59 acceptance criteria is compared graphically to the AWS D1.5 Annex K acceptance criteria in Chapter 6. As noted by the authors of the CSA acceptance criteria [14]–[16], the CSA acceptance criteria will generally be quite conservative compared with the current AWS method. The CSA code also provides requirements for use of encoded line scanned PAUT or other alternative ultrasonic systems in lieu of conventional UT if agreed to in writing by the Engineer and Contractor prior to inspection. In order to use encoded PAUT, it requires that a written procedure be developed and that performance qualification tests of the procedure be performed to verify that the minimum required sensitivity is provided. No prescriptive procedures are provided for flaw sizing or scanning of the welds.

ISO 19285:2017 [17] provides acceptance criteria for PAUT which may be applied to bridge welds. This code allows for either evaluating the welds using the flaw size (e.g. flaw height and length) or maximum amplitude and flaw length. This code requires performance qualification for all PAUT inspection procedures on a test block of the same material and similar thickness as the test object with reflectors of prescribed size and location. No prescriptive procedures are provided for flaw sizing and verification of flaw sizing procedures is required.

ASME BPVC Code Case 2235-13 [12] provides acceptance criteria for PAUT in lieu of RT for the nuclear and petrochemical industries. The code case allows for evaluation of final acceptance only be performed by flaw sizing, but amplitude may be used for detection. The code case requires performance qualification of all PAUT inspection procedures on a test block of the same material with multiple reflectors throughout the thickness of the part. Requirements are given for the size and location of the reflectors. No prescriptive procedures are provided for flaw sizing and verification of flaw sizing procedures is required.

JIS Z 3060-2015 does not provide an acceptance criteria specifically for PAUT. This code provides classification of discontinuities based on conventional UT results, but no acceptance criteria is included.

Table 1.1 Acceptance Criteria Summary Table

Specification	Acceptance Criteria based on Flaw Sizing using PAUT	Prescribes Flaw Sizing Procedure	Acceptance Criteria based on Max Amplitude & Length using PAUT	Requires Performance Qualification
AWS D1.5-15	X	n/a	✓	X
CSA W59-18	✓*	X	✓	✓(Flaw Sizing)
ISO 19285-17	✓	X	✓	✓
ASME BPVC CC 2235-13	✓	X	X	✓
JIS Z 3060-15	X	X	X	X

*CSA W59-18 does not provide any specific acceptance criteria for PAUT based on flaw sizing, but gives minimum requirements and allows for other acceptance criteria which have been deemed to be equivalent.

1.3.2 Calibration requirements

AWS D1.5:2015 Annex K is the only code which <u>does not</u> require PAUT technicians to account for differences in material attenuation between the calibration block and the test specimen. In fact, there is no discussion on the acoustic properties of the calibration block compared to the test object in the AWS code. For conventional UT, both the AWS D1.5 and CSA W59 account for attenuation in the test specimen by the application of an attenuation factor and use of an International Institute of Welding (IIW) "type" reference block to set the reference amplitude. However, the 2018 edition of CSA W59 provides a TCG approach in lieu of the fixed attenuation approach for conventional UT, while the TCG approach is required for manual raster scanned PAUT. While there is limited discussion in the CSA code on how to account for differences in material attenuation, it states that the calibration block shall be "acoustically equivalent" to the test object. For encoded line scanned PAUT inspections, the CSA code requires a calibration procedure be developed on a case-by-case basis as part of a written procedure.

The ISO and ASME codes specifically state that modifications to calibration are required if the material attenuation differs between the calibration block and the test object, including both base metal and weld metal. This is typically in the form of a transfer correction. ISO 17640 [18] requires a transfer correction be applied when a difference of 2 dB to 12 dB is observed at the longest inspection sound path. Any difference less than 2 dB is negligible and any difference greater than 12 dB is a cause for reevaluation of the calibration procedures. ASME BPVC [11] states, if *"the block material is not of the same product form or has not received the same heat treatment, it may be used provided it meets all other block requirements and a transfer correction for acoustical property differences is used"*. ASME does not provide requirements on the use of a transfer correction instead it is left to an inspector's discretion. JIS Z 3060 [13] provides five different calibration blocks to be used in different circumstances. Each reference block is required to be of a steel material with equivalent acoustic characteristics to the test object. JIS Z 3060 states that the difference in the ultrasonic velocity of the test object and the calibration block shall be within ±2% and that the transfer correction shall be within ±2 dB. Measurement of the acoustic properties require ultrasonic testing of the test object and calibration block including the use of normal incidence shear wave probes and/or pitch-catch methods.

Table 1.2 Material Attenuation Summary Table

Specification	Accounts for the material attenuation due to varying grade or microstructure	If so, how?	
		Conventional UT	**PAUT**
AWS D1.5-15	NO	n/a	n/a
CSA W59-18	NO (UT) / YES(PAUT)	n/a	Qualification testing through same medium.
ISO 17640-17	YES	Requires a calibration block. If the calibration block and test object are not acoustically the same, a transfer correction is to be applied.	
ASME BPVC-17	YES	Requires a calibration block of the same product form and material specification of the material being examined. If any acoustic differences remain between the calibration block and test object, a transfer correction is to be applied.	
JIS Z 3060-15	YES	Requires all calibration blocks to be of a steel material with equivalent acoustic characteristics to the test object.	

1.3.3 Probe selection

AWS D1.5 and CSA W59 restrict the probe frequency for conventional UT due to the fixed attenuation factor which is only valid for a specific probe size, shape, and frequency [15]. The 2018 edition of the CSA W59 code allows a wide range of probe frequencies for the TCG approach, but, as noted above, this requires that the calibration block be acoustically equivalent to the test object. The other codes also allow a wider range of probe frequencies but also require that a calibration be performed to take into account material attenuation. The ISO 17640 code [18] states that lower frequencies are recommended for conventional UT where acceptance is determined based on maximum amplitude and length rather than flaw characterization and sizing. While removed for the 2017 edition, the 2010 edition of ISO 17640 stated that initial testing use frequencies as low as possible, but within the specified range. JIS Z 3060 [13] stipulates the allowed probe frequency be determined based on the sound path distance with longer sound paths having lower frequencies. JIS Z 3060 allows 3.5 to 5 MHz probes be used on sound paths that are 100 mm (3.9") or less. For 2nd leg scans, this limit would be exceeded for a thickness of 1.4" at a 45° incidence angle and at a thickness of 0.7" at a 70° incidence angle. Anything over 250 mm (9.8") is only allowed to be inspected using 2 MHz.

Table 1.3 Probe Frequency Summary Table

Specification	Probe Shear Wave Frequency Range (MHz)		Notes
	Conventional UT	PAUT	
AWS D1.5-15	2-2.5	1-6	-
CSA W59-18	2-2.5 (Fixed Attenuation) 2.25-10 (TCG)	2.25-10 (TCG)	-
ISO 17640-17	2-5	No stipulation	Lower frequencies may be necessary for testing at long sound paths and/or high material attenuation
ASME BPVC-17	1-5	1-5	-
JIS Z 3060-15	2-5	2-5	Sound path length stipulations are put on using higher frequencies

1.4 Phased Array Ultrasonic Testing (PAUT)

Since phased array relies on the same basic physics as conventional UT to generate and receive ultrasound, many of the details of PAUT inspection do not change from conventional UT. However, unlike the single element transducer used in conventional UT, PAUT uses multiple element transducers and electronic time delays to generate and receive ultrasound. The electronic time delays use constructive and destructive interference which allow the ultrasonic beam to be steered, scanned, swept, and focused electronically. Figure 1.1 shows the electronic time delays for 16 active elements of a 64 element transducer (i.e., elements 1-16 active) in order to produce a 40° incidence angle (left) and 70° incidence angle (right).

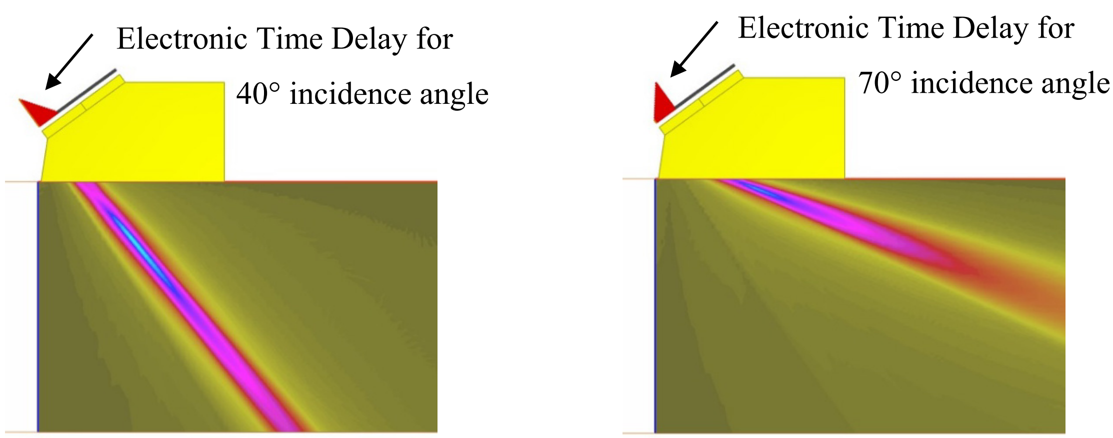

Figure 1.1 PAUT Time Delays for Sectorial Sweeping

The array in the transducer can be constructed from a linear array, a two-dimensional matrix array, or a circular array. Linear arrays are used for most applications since they are cheaper than more complex arrays and easier to program [19]. Phased array probes commonly have between 16 to 128 elements. Focal laws are calculated by the software which controls the time delays and firing sequence of the transducer. The frequency of PAUT is very similar to conventional UT, typically between 2-5 MHz for bridge weld testing.

Two types of scans are typically used for PAUT:

- Electronic scans (E-scans) are performed by multiplexing the same focal law along a linear array. This will produce a scan which is similar to manual scanned conventional UT.
- Sectorial scans (S-scans) are performed by altering the time delays as the elements are fired which creates a beam which sweeps through a range of incidence angles.

PAUT can utilize encoded scanners to capture a continuous stream of data from different transducer positions either automatically or semi-automatically. Semi-automatic scanning, using a wheel or string encoder attached to the transducer, is typically utilized for bridge welds due to the variation in geometry associated in bridge fabrication. PAUT using encoded scans have multiple views which can be displayed to the technician including:

- A-scan (x-y plot of amplitude vs time for a single beam; top left of Figure 1.2)
- B-scan (end view when volume corrected)
- C-scan (top view when volume corrected; bottom of Figure 1.2)
- D-scan (side view)
- E-scan (end view of all A-scans when multiplexing same focal law)
- S-scan (end view of all A-scans for a range of incidence angles, top right of Figure 1.2)

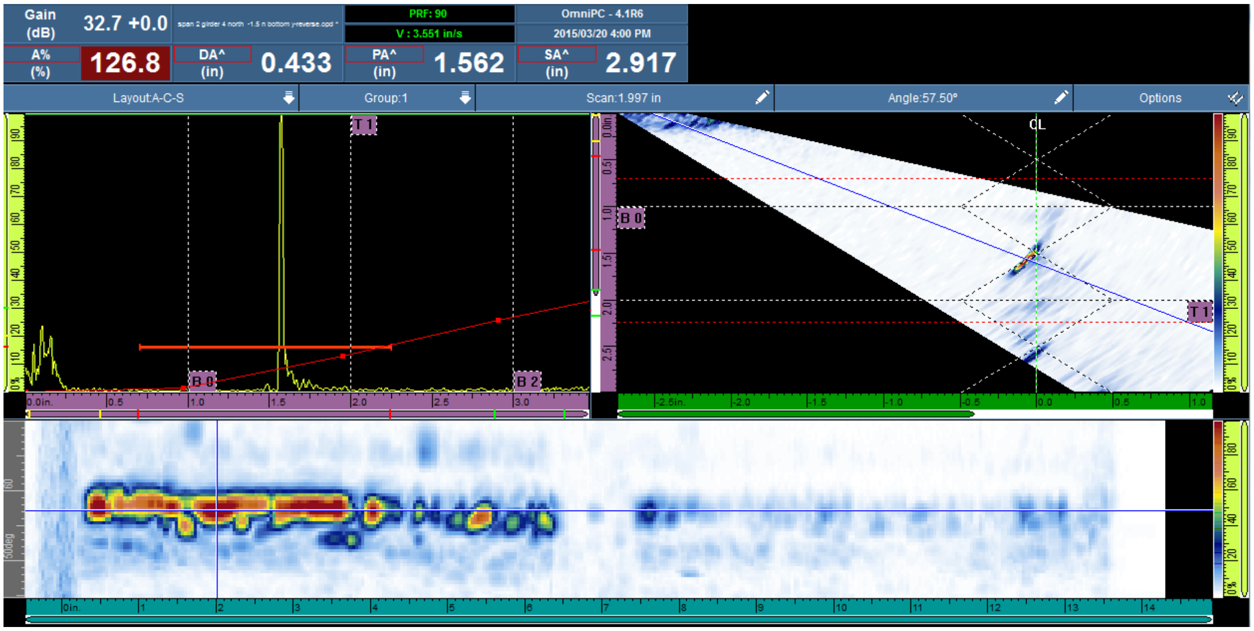

Figure 1.2 Sample PAUT Image (top left) A-scan, (bottom) C-scan, and (top right) S-scan

PAUT calibration involves correction of the wedge delay and sensitivity calibration. For conventional UT, sensitivity calibration involves measuring the reference amplitude of a standard 1.5 mm diameter (0.06”) SDH reflector on an IIW-type calibration block. In conventional UT, material attenuation at other sound paths is accounted for by implementing a correction through the attenuation factor equation. For PAUT, the reference amplitude is calculated across the full range of angles that will be used during the scanning. The standard SDH reflector on the IIW-type block is still used, but the beam is swept through all of the angles by moving the transducer along the IIW-type block surface. After calibration, the reference reflector will have the same amplitude at each angle (i.e., 70 degrees and 45 degrees). Time Corrected Gain (TCG) is used to account for material attenuation by sweeping the ultrasonic beam through SDH reflectors at varying depths. After performing TCG calibration, identical reflectors will have the same amplitude regardless of the depth or beam angle.

PAUT has many advantages over conventional UT. One advantage that cannot be disputed is the increased sound coverage provided by PAUT. Compared to conventional UT, PAUT can provide the UT technician with the ability to scan a material using multiple beam angles simultaneously. The UT technician also has additional views such as the S-scan and E-scan, which are two-dimensional representations of all of the A-scans plotted simultaneously. This can greatly aid the technician to distinguish false call signals due to geometric indications. It can also help in flaw characterization, through the use of tip diffraction signals or signals at the surface. Weld overlays showing the geometry of the weld preparation can also be drawn on the S-scan or E-scan views which can help UT technicians inspect locations where discontinuities are more likely, such as the fusion face or weld root. If PAUT is used as a direct replacement of conventional UT in manual raster scanning, these advantages are likely to improve flaw detection and rejection if the same amplitude-based acceptance criteria were implemented.

An advantage of encoded PAUT scanning is the ability to collect the raw scan data and save it for future reference or viewing. Conventional UT indications are typically reported as tabulated values of indication amplitude, length, and location. Operator error is introduced into the reporting process since these values often are manually transferred from physical measurements or instrument results. Conventional UT A-scan data is typically not saved for future reference.

Although PAUT can provide more coverage than conventional UT, full coverage of the weld does not ensure that all discontinuities within the covered region will be detected. When line scanning is performed with a single transducer, each point in the volume of the weld will only be primarily covered by sound with a single angle of incidence. (*It is recognized that due to beam spread, a given location will be "hit" by more than one angle of incidence but not with significant amplitude.*) If the flaw is not oriented in a manner to reflect adequate ultrasound back to the transducer based on the specific angle of incidence, the discontinuity may not be detected (or very little sound reflected) even though sound is covering that region. For this reason, it is often recommended to scan with angles that are normal to "expected" discontinuities such as fusion faces of welds.

When line scanning is performed, the probe is typically kept normal to the weld axis to inspect for discontinuities which are primarily orientated parallel to the weld axis. Conventional UT, on the other hand, is typically performed by raster scanning where the probe is moved with rotation, transverse, and longitudinal movements. This movement helps to maximize the amplitude response from discontinuities that are not oriented perfectly parallel to the weld axis. Prior PAUT research found that a skew angle of only 10° from the alignment of the discontinuity caused the signal amplitude to drop considerably and flaw detection become marginal [20]. A change in skew angle of 20° from perpendicular to the discontinuity resulted in total loss of discontinuity response. Therefore, lack of raster scanning when line scanning with PAUT is likely to result in decreased amplitude for some weld flaws.

2. PRIOR RESEARCH

A comprehensive review of the vast literature on conventional UT and PAUT was performed as part of the current research. There is very little documented use of enhanced ultrasonic methods within the bridge industry for the inspection of CJP welds. This is likely due to the fact that there was not an acceptance criteria utilizing enhanced ultrasonic methods in the AWS D1.5 Bridge Welding Code [5] until 2015 when Annex K was added.

The following chapter contains a brief description of the seven studies thought to be most significant to the current work. When necessary, references have been provided throughout this document to additional work reviewed. The first summary includes two studies from research in Japan that investigated the acoustic anisotropy of thermo-mechanical controlled processed (TMCP) steels along with summarizing requirements in the Japanese UT code for acoustic anisotropy. The second summary includes recent research under NCHRP 14-35 that collected information on the material attenuation and shear wave velocity of US bridge steels. The third summary includes the research that FHWA performed assessing the application of PAUT on bridge structures. Next, a study from Florida DOT is summarized that compared the rejection rate of AWS D1.5 Annex K to the current combined AWS conventional UT and RT acceptance criteria. This is followed by research that collected data on the scatter of reported amplitude and flaw length of conventional UT technicians during performance testing on plates with known weld flaws and later compared this scatter to testing which included PAUT. Finally, a study is included that investigated the use of PAUT to measure the flaw height and length of weld flaws and compared conventional UT, PAUT, and RT acceptance criteria. Each of these studies offered great value to the current research.

2.1 Various Studies in Japan on TMCP Acoustic Anisotropy (1987-2004)

Researchers in Japan first noted issues with detectability and location estimation of flaws due to acoustical anisotropy of TMCP steel plates in 1987 [21]. It was discovered that the shear wave velocity of some TMCP plates was higher in the rolled direction and lower in the transverse to rolled direction. The velocity difference due to scanning orientation (i.e., acoustic anisotropy) results in changes to the refraction angle of the sound beam due to Snell's Law. Changes in the refraction angle result in error in estimating the location of flaws. In accordance with Snell's Law, the change in the refraction angle is greater at higher incidence angles (i.e., greater for 70° than 45°). For instance, the research [21] found that the refraction angle that was supposed to be at 70° was actually at 79° in the test specimen while the 60° beam was actually refracted at 65°. A rearranged version of Snell's Law used to calculate the actual refraction angle is shown below:

$$\theta_{actual} = \sin^{-1}\left(\frac{v_{actual}}{v_{reference}} \times \sin\theta_{reference}\right)$$

Along with impacting the refraction angle, the researchers noted significant effect on the amplitude of the sound beam at high incidence angles which could negatively affect sensitivity to flaw detection. Due to variation in the material velocity between different TMCP plates, the drop in amplitude also had high variability, with some plates having a change in amplitude of -20 dB at 70° and others not experiencing any drop in amplitude. This research recommended limiting the refraction angle to 65° for plates exhibiting acoustic anisotropy.

Requirements are included in the Japanese UT code, JIS Z 3060 [13], which require measurements of the actual shear wave velocity of the test specimen in order to determine which refraction angle to use for inspection. There are also requirements that the actual refraction angle in the test specimen be measured and used for calculating the flaw location when the velocity is ~+2% or ~-0.5% compared with standard velocity. This code also includes requirements for amplitude correction for differences in material attenuation between the test specimen and calibration block. For the calibration block to be considered acoustically equivalent to the test object, the velocity must be within +/- 2% and attenuation within +/- 2 dB.

Additional research was performed by other researchers in 2004 [22] which also noted large scatter in the anisotropy of TMCP plates due to variations in processing. This research noted that velocity near to the surface of the plate may be increased even further than the velocity in the center of the plate due to the TMCP processing techniques. This research noted that measurements of the through-thickness velocity of the plate may underestimate the localized velocity at the surface. Since the refraction of the sound beam occurs as it first enters the plate and is related to the change in velocity from wedge to the surface of the plate, this increased velocity on the surface of the plate may result in a larger change in the actual refracted angle at the surface compared to what is anticipated from the through-thickness velocity measurement. This additional refraction will result in a greater drop in amplitude due to more of the sound beam reaching the second critical angle (i.e., refraction angle is parallel to the surface). The increased velocity at the surface was noted to be further exaggerated for thinner plates. It was noted in this research that measurements of the velocity in accordance with JIS Z 3060 will result in an average value through the plate thickness. Use of this value to calculate the actual refraction angle may underestimate the actual refraction at the surface which could result in the sound beam being closer to the critical angle than originally calculated.

2.2 Crowley (2018)

Testing was performed under NCHRP 14-35 [7], [8] to measure the typical material attenuation and shear wave velocity of bridge base metals along with the attenuation of narrow-gap electroslag welds (NGI-ESW). Ultrasonic testing using various conventional UT and PAUT probes was performed on five historical bridge base metal specimens including grades A373, A441, and A36 and seven modern base metal specimens including A709 Gr. 50, A709 HPS 70W quenched and tempered (QT), A709 HPS 70W TMCP, and A709 HPS 100W QT. This testing involved machined specimens with multiple 1/16” dia. SDH reflectors. It was found that the A36 specimen had the greatest attenuation while the A709 100W and 70W QT specimens had the least attenuation. The material attenuation was found to correlate with the grain size of the steel. Attenuation measurements with 5 MHz probes were found to have significantly more variability than with 2.25 MHz probes. This is due to the shorter wavelength which is more sensitive to grain size variation. The experimental data from this report was used in this research study to benchmark CIVA models for various grades of steel in order to develop recommendations for optimal probe parameters. The attenuation data from TMCP processed steel in the rolled and transverse to rolled direction was also used to compare to testing in an oblique orientation to the rolled direction.

The shear wave velocity of the specimens was also measured. Similar to the findings in the prior research from Japan, it was found that many of the TMCP specimens experienced increased velocity in the rolled direction and decreased velocity in the cross-rolled direction. This resulted in a change of the refraction angle and a significant decrease in the amplitude at high incidence angles. The experimental velocity and attenuation data from this report was used in this research project to develop recommendations for the scanning procedures such as limits to the incidence angles to be used during inspection of bridge welds.

Finally, attenuation testing was performed on narrow gap improved electroslag welds (NGI-ESW) weld specimens to evaluate the effect of scanning through the heat affected zone (HAZ) and weld metal. While the HAZ did not seem to have a major effect on the amplitude of the sound, it was found that scanning through NGI-ESW weld metal may result in a significant loss of amplitude and steering of the sound beam due to large grain size. Once again, the amplitude difference is greater for high frequencies such as 5 MHz compared with 2.25 MHz, but it is still present for 2.25 MHz probes. Similar testing was performed in this research project to evaluate the attenuation of ultrasound passing through the HAZ and weld metal of submerged arc welds (SAW).

2.3 FHWA (2014)

Two FHWA TechBriefs [23], [24] have been published on the application of PAUT to inspect CJP butt welds. The final report on this research has not been published as of the preparation of this report.

Phase 1 [23] of this research involved reviewing the current practices for PAUT testing, developing test specimens, calibration blocks, and testing procedures. Eight test specimens were fabricated using SAW and NGI-ESW processes with plate thicknesses varying from 1" to 3.3". Four of the specimens were thickness transition butt welds while the other four specimens had consistent thickness. Testing was performed using two phased-array probes with frequencies of 5 and 2.25 MHz. The calibration block included ten side-drilled holes (SDH) that were 0.05" in diameter.

Phase 2 [24] of this research performed conventional UT, PAUT, and RT testing of the test specimens. It was found that conventional UT was able to identify most of the flaws compared with RT, but some of the flaws were not detected using conventional UT. This was attributed to the fact that flaws located close to each other or at different depths can be difficult to discern using raster scanning, especially when scanning large specimens. Good correlation between PAUT scanning and the RT images was found for the location and the length of the flaws in four butt weld specimens. Significant errors were found for flaws representing a cluster of slag or porosity when inspected from different angles due to the interpretation of the analyst.

The physical height and length of the flaws was not included in the TechBrief reports, and the intended sizes of the flaws were not reported. The plots for estimated flaw lengths and heights from the PAUT measurements show that the flaws were approximately between 0.01” to 0.75” in height and 0.5” to 6” in length. The sizing variability comparing the different scans for the four butt weld specimens were ±0.3” for depth, ±0.3” for length, and ±0.1” for height. The welds were not destructively tested so the error compared to the actual flaw size was not reported.

2.4 Florida DOT (2014)

Florida DOT sponsored a PAUT research project [25] to compare the findings of PAUT, RT, and conventional UT testing of steel bridge butt welds in a fabricator’s shop. The results of this data compared the methods to determine whether PAUT may be a suitable substitute for RT. The PAUT procedures that were developed for testing in this project were in accordance with the draft AWS D1.5 Annex K (then Annex X) procedures. Testing was performed using a 2.25 MHz, 20 element PAUT transducer. The findings of this study were that the rejection rates were similar for PAUT according to the developed procedure as conventional UT and RT according to AWS D1.5.

A caveat to this finding is that these rejection rates were based on the entire data set for each method but not every specimen was tested using each method. Therefore, the number of critical flaws may have been different for each method. The rejection rate was also based on the number of tests performed, not on the number of samples. Typically, each plate was tested twice with PAUT and RT but only once with conventional UT. As a result, no real conclusions can be drawn from the rejection rate data since the rejection rates are not based on inspection of the same flaws by each method and the rejection rate was based on the number of tests and not the number of flaws.

A Type I error, defined as rejectable to RT and acceptable to PAUT and UT, was found on one plate. Thus, replacing RT with PAUT would have resulted in a rejectable plate under the old protocol being acceptable under the new protocol. A Type II error, defined as rejectable to RT and conventional UT and acceptable to PAUT, was also found in one plate. In this error, replacing RT with PAUT would have resulted in the same rejectable conclusion between the old and new protocol but only because of the rejectable conventional UT. This plate would have been acceptable if conventional UT was also replaced with PAUT. It was found that edge flaws were responsible for the Type I and Type II errors. Therefore, it was assumed by the authors that applying supplemental manual PAUT scanning on the edges of the plates would have resulted in a rejectable condition for these plates and matched the RT results. Supplemental manual PAUT scanning was included in the final version of AWS D1.5 Annex K as an option when edges and corners prevent access for encoded PAUT.

2.5 Washer, Connor, & Looten (2014)

This study primarily investigated the application of performance testing of conventional UT and magnetic particle (MT) technicians [26]. In this study, plates with known flaws were attached to a bridge and scanned by the technicians as a performance test before they were allowed to test the actual bridge welds. Seven conventional UT technicians were successful at completing the test. One technician was unsuccessful due to an excessive number of false calls and undersizing of the flaw length of a large flaw. Typically, the flaw length was oversized for the small flaws, but some flaw length measurements were undersized for the larger flaws. The reported amplitude also varied widely. The average range of dB values reported for the flaws was 12.5 dB. This is more than four times greater than the interval between an acceptable and rejectable indication, regardless of the flaw length, for a plate less than 1.5 inches thick.

Although not reported in the Transportation Research Record publication, the authors of this paper subsequently sent some of the plates for testing using combined PAUT and time-of-flight diffraction (TOFD) scanning to compare the results to the conventional UT results [27]. The combination of the PAUT and TOFD for the detection and characterization of the flaws was much more successful than using standard AWS approaches. Figure 2.1 shows the results from this blind study superimposed on the conventional UT performance test results. As shown in this figure, the combined TOFD/PAUT approach significantly reduced the error in the length measurements for the subsurface flaws studied.

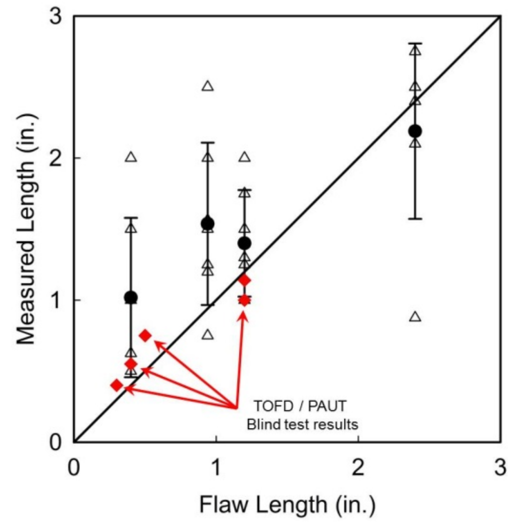

Figure 2.1 Comparison between flaw lengths as measured with PAUT and TOFD [26], [27]

2.6 Schroeder, Hardy, Fish, & Sauser (2017)

The U.S. Army Corps of Engineers (USACE) sponsored a PAUT research project [28] to investigate the ability to measure internal and surface discontinuities in butt welds by PAUT flaw sizing. The PAUT flaw size results were compared to the actual size of the discontinuities by destructive testing. A 5 MHz linear array PAUT transducer was used for this testing. Typically, good correlation was found for the length of the discontinuities when compared to RT results. Oversizing of discontinuities due to two indications being combined into one long indication was possible when 2nd leg data was included in the evaluation due to the beam spread. While the PAUT measurements of discontinuity height and length were very close for four of the seven butt weld samples, the other three butt weld samples had some issues with oversizing or undersizing of the weld flaws.

This research also compared the variability when the discontinuities were evaluated by various acceptance criteria for conventional UT, PAUT, and RT. Since all of the weld flaws were rejectable to combined conventional UT and RT, error from PAUT in accordance with Annex K rejecting an otherwise acceptable indication could not be evaluated. Two errors occurred where PAUT in accordance with Annex K accepted an indication which would have been rejectable to the combined AWS D1.5 conventional UT and RT requirements. One of these indications was a grouping of porosity which was rejectable to the applicable RT requirements but acceptable to the conventional UT requirements. The other indication was a small internal inclusion from a weld taken out of service which was rejectable to conventional UT, but was not inspected with RT.

The fracture mechanics based acceptance criteria of BS 7910:2005 [29] and ASME Code Case 2235:2013 [30] evaluations were applied to the PAUT flaw size measurements, and compared with the AWS conventional UT and RT acceptance criteria. Use of BS 7910 requires input parameters for the weld length, fracture toughness, tensile and yield strength, and stress in order to determine the critical flaw size. Using sample inputs for these parameters, three of the indications would have been acceptable per BS 7910 while they were rejectable per the current AWS D1.5 acceptance criteria. Evaluation per ASME Code Case 2235 was found to be more conservative than BS 7910 for the sample inputs, and only one of the flaws would have been acceptable.

3. CRITICAL FLAW SIZE

Analytical parametric studies have been performed in order to establish the critical flaw sizes that would be considered rejectable for typical bridge CJP welds. The results were utilized in identifying the critical flaw size that must be reliably detected and rejected to establish revised acceptance and rejection criteria. The critical flaw sizes were evaluated based on fracture mechanics using a BS 7910 [31] fitness-for-service (FFS) approach. Therefore, the internal flaws are assumed to be cracks. The parametric studies that were performed included various plate geometries, welds, residual stress fields, flaw types, flaw sizes, and locations.

3.1 Volumetric Flaws

Flaw severity is dependent on the flaw type (i.e., planar vs. volumetric). Therefore, volumetric (i.e., non-planar such as slag and porosity) flaws and planar flaws were considered separately. Fracture mechanics relies on an underlying assumption that a flaw is a crack, whether considering fatigue crack growth or fracture. This is a very conservative assumption for smooth, rounded volumetric flaws, but assuming that all volumetric flaws are void of any cracks or crack-like geometry is an unconservative assumption to make. During the literature review, it was apparent that all existing enhanced ultrasonic testing specifications do not distinguish between flaws that are volumetric as opposed to crack-like, other than including additional criteria for rejecting scattered volumetric flaws such as a limit on the number of point-like reflectors over a specific weld length.

The round robin testing performed during this research project and described in Chapter 4 requested inspectors to document whether a detected weld discontinuity is volumetric or planar. It was found that volumetric discontinuities and planar discontinuities could not be differentiated with reasonable accuracy. Not only were volumetric discontinuities often reported as being planar, but planar discontinuities were often reported as being volumetric. Obviously, the evaluation of truly planar discontinuities using an acceptance criteria developed for volumetric discontinuities will not capture the criticality of planar discontinuities and would be unconservative. Therefore, it was determined that PAUT acceptance criteria should not require flaw characterization as planar and volumetric flaws, but rather all indications should be evaluated against the same acceptance criteria.

In order to develop target critical flaw size for volumetric flaws, existing experimental test data on CJP welds with such flaws was explored. Harrison [32]–[34] investigated the fatigue resistance and strength of butt welds with embedded slag inclusions and porosity. That research found that the effect of slag inclusions and porosity below 10% volume on ductile strength was negligible due to the overstrength of the weld metal. The porosity limit was set to 10% since this was considered the limit that should be allowed without masking other indications during RT inspection. It was found that slag inclusions typically have limited through-thickness height, the critical dimension according to fracture mechanics, due to occurring between weld passes. During these studies, data from high-cycle fatigue tests performed by multiple researchers were collected by Harrison to develop an acceptance criteria based on S-N curves. This was used to set limits on the percentage of the volume of weld metal containing porosity and the maximum length of slag inclusions which were later incorporated into BS 7910. These limits assume that the flaw is verified to be volumetric and was developed to be used with RT. BS 7910 states "*The tolerable porosity sizes based on ultrasonic testing may be considerable less, particularly for thinner sections*". This is because BS 7910 recognizes that volumetric flaws can be easily undersized by ultrasonic testing. BS 7910 is silent on how specifically the allowable sizes should be reduced for ultrasonic testing; however, this would likely be determined through some kind of performance testing and POD evaluation.

The critical dimensions for slag inclusions in BS 7910:2013 are given in Table 3.1 when combining the height requirements for fracture (i.e., no length requirement for fracture) and the length limit for fatigue (i.e., no height requirement for fatigue) assuming infinite fatigue life. As shown in this table, the critical dimensions for slag inclusions in BS 7910 were already quite small before considering the effect of undersizing with ultrasonic testing.

Table 3.1 Combined BS 7910 Slag Fatigue and Fracture Requirements

Stress Range (ksi)	**Slag Height (2a) (0.5" thick weld)**	**Slag Height (2a) (> 1" thick weld)**	**Slag Length (2c)**
6.09	0.063"	0.118"	0.098"
5.37	0.063"	0.118"	0.157"
4.64	0.063"	0.118"	0.394"
4.06	0.063"	0.118"	1.378"
3.34	0.063"	0.118"	Infinite

AWS D1.5 RT acceptance criteria include limits on maximum indication length and spacing. While these limits are workmanship-based and not based on experimental results, they do help by highlighting the typical flaw size that has been traditionally accepted. A minimum slag height for RT sensitivity was also calculated by comparing the size and density of required wire-type image quality indicators (IQI) to determine the required slag height for the same change in density. This analysis assumed the density of slag to be 3.5 g/cm^3 based on literature [35], [36]. The maximum slag length and minimum slag height for each plate thickness are shown in Table 3.2. This confirmed that the BS 7910 maximum slag height would likely be detectable under RT inspection and that the BS 7910 maximum slag length requirements compare reasonably to the AWS D1.5 RT acceptance criteria for stress ranges of ~5 ksi.

Table 3.2 Slag RT Sensitivity and AWS D1.5 Length Requirements

Plate Thickness (in)	**Min. Slag Height (2a)**	**Max. Slag Length (2c)**
0.5"	0.028"	0.125"
1"	0.044"	0.313"
2"	0.057"	0.500"
3"-4"	0.089"	0.500"

The critical planar flaw sizes must also be considered when evaluating critical volumetric flaws since calculation of the stress intensity factors (K_I) show that any sharp or planar flaw extending from a slag inclusion or porosity will result in an equivalent planar flaw extending over the combined area of the volumetric and planar flaws. Thus, once a crack begins to extend from a volumetric flaw, it is equivalent to a crack which extends over the entire projected area.

An appropriate delta-K threshold (ΔK_{th}) to control fatigue crack growth of volumetric flaws was evaluated using fatigue test data. Using the combined fatigue and fracture limits on slag given by BS 7910 in Table 3.1, it was found that the ΔK_{th} varied from 1.5 to 2.0 ksi$\sqrt{\text{in}}$ depending on the stress range. In addition, NCHRP Report 335 [2] recommended using 2.5 ksi$\sqrt{\text{in}}$ for ΔK_{th} in the development of a modified RT acceptance criteria for bridge welds. NCHRP Report 335 included fatigue testing on weld samples with porosity and slag weld imperfections and reported that the calculated initial ΔK ranged from 2.25 to 3.7 ksi$\sqrt{\text{in}}$. As will be discussed in the following section, $2.5\ ksi\sqrt{in}$ was used for ΔK_{th} in this project for determination of the critical flaw size for planar flaws. Since this is also appropriate for volumetric flaws, planar and volumetric flaws have the same critical flaw size based on fatigue. Therefore, the target critical planar flaw sizes shown in the following sections were used to develop target critical volumetric flaw sizes for the CIVA parametric matrix shown in Chapter 6.

3.2 Critical Planar Flaw Sizes Based on Fatigue

Various planar flaws were modeled using FFS procedures to determine the maximum flaw size that will not grow in fatigue (i.e., infinite life). Failure was defined as the limiting flaw size at which crack growth is expected at a given stress range since the intention is to evaluate welds in a fabrication shop environment where the anticipated ADTT would not need to be taken into consideration for each individual weld. The inputs for the analysis accounted for variations in the plate thickness, flaw aspect ratio, flaw position, and magnitude of the applied live load stress range. Thickness transition weld geometries were also considered by accounting for stress concentrations through finite element analysis. It is noted that one could utilize a finite life approach and assume a number of cycles per day over the design life which could result in larger flaw tolerance. However, such an approach was not deemed to be implementable for several reasons. For example, the designer would need to provide detailed static and cyclic stress data for each weld. Then, the inspector would need to use this data to select the appropriate inspection criteria for the specific weld. Clearly, there is much room for error in this approach in addition to the fact it places considerable responsibility on the technician to interpret the data.

3.2.1 Cyclic stress range

To determine the stress range for evaluation, a reasonable approach is to use the stress range associated with infinite life; for example, using a stress range of 16 ksi for a Category B butt welded detail. However, the stress range associated with the CAFL of Category B (16 ksi) is very high in terms of actual in-service stress ranges for a fatigue resistant detail such as a CJP butt weld.

The FFS calculations indicated that a 16 ksi stress range results in a very small maximum permissible flaw size to ensure infinite life. It is noted that NCHRP 335 recommended using about half of the fatigue limit for the detail under consideration, for example 8 ksi to 9 ksi for Category B, as it better represents the upper bound in-situ effective stress range. NCHRP 335 even suggested using lower values if data exists for justification or if deemed acceptable by the engineer. Therefore, critical crack sizes were calculated for stress ranges from 4 ksi to 20 ksi in 4 ksi increments during the parametric study.

3.2.2 Delta-K threshold (ΔK_{th})

The delta-K threshold (ΔK_{th}) which correlates to initiation of fatigue crack growth was determined through review of previous research which had performed fatigue testing of welds in structural steels, including NCHRP Report 267 [37] and NCHRP Report 181 [38]. The appropriate value of ΔK_{th} depends on the R ratio which is the ratio of minimum applied stress to maximum applied stress. The typical R ratio at a butt weld is quite high due to the presence of residual and dead load stresses. According to Barsom and Novak [38], ΔK_{th} is equal to 2.05 ksi$\sqrt{\text{in}}$ for an R ratio of 0.8. According to Fisher [37], the constant amplitude crack growth threshold approaches 3 ksi$\sqrt{\text{in}}$ at high R ratios, but he found that ΔK_{th} approaches 2 ksi$\sqrt{\text{in}}$ for an R ratio of 0.8 for random variable block loading when only a small percentage of stress intensity factor range exceeds the constant amplitude crack growth threshold.

Therefore, based on the previous testing performed on ΔK_{th} for typical structural steels, $2.5\ ksi\sqrt{in}$ was used for ΔK_{th} in this project for both planar and volumetric flaws (i.e., planar and volumetric flaws have the same critical flaw size for fatigue). While the specific residual stresses were not considered in the fatigue evaluation, the effect of the residual stresses on the fatigue crack growth was accounted for in the determination of the ΔK_{th} through the R ratio. Since infinite life was utilized in the analysis, the effect of residual stresses on the da/DN curves did not affect the analysis. Therefore, the yield strength (i.e., grade) is not a variable in the test matrix.

3.2.3 Summary of parametric study

Using the inputs of the fatigue loading parametric study, the maximum crack height and length that would initiate crack growth for CJP butt welds was determined for various a/c ratios, crack position, plate thickness, stress range, and type of weld (i.e., equal thickness or thickness transition). The crack position and type of weld is shown in Figure 3.1 SignalFFS software [39] was used to perform this analysis by converting the fatigue crack growth problem to an equivalent fracture problem by setting the fracture toughness (K_c) equal to the ΔK_{th} value of 2.5 ksi$\sqrt{in}$ and the primary stress equal to the applied stress range. The specific joint types that were evaluated for fatigue are summarized in Table 3.3.

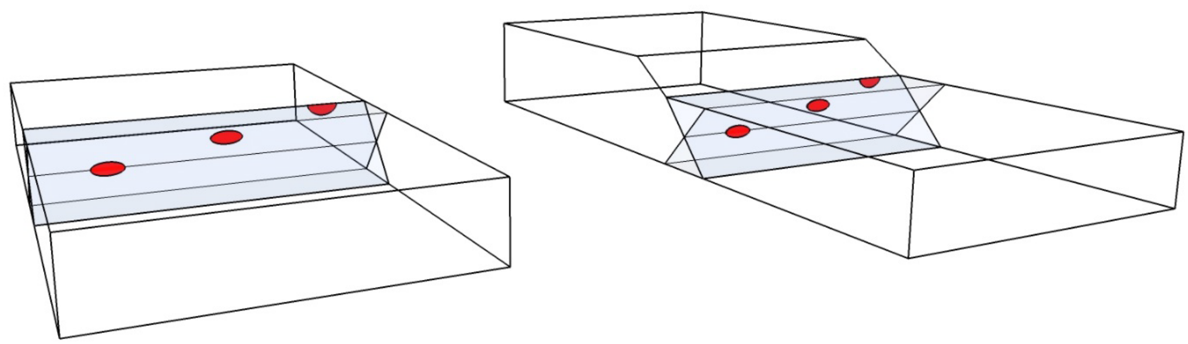

Figure 3.1 Typical Flaw Positions within Weld

Table 3.3 FFS Evaluation Matrix for CJP Butt Welds

Type of Crack/Position	**Type of Butt Weld**	**a/c ratio**	**Thickness**	**Applied Stress Range (Category B)**
Near Surface	Equal Thickness	0.01-1.5	0.5”, 1”, 2”, 3”, 4”	4 ksi, 8 ksi, 12 ksi, 16 ksi, 20 ksi
	Transition	0.01-1.5	0.5” to 1”, 1” to 1.5”, 1” to 2”, 2” to 3”, 2” to 4”, 3” to 4”	4 ksi, 8 ksi, 12 ksi, 16 ksi, 20 ksi
¼ depth	Equal Thickness	0.01-1.5	0.5”, 1”, 2”, 3”, 4”	4 ksi, 8 ksi, 12 ksi, 16 ksi, 20 ksi
	Transition	0.01-1.5	0.5” to 1”, 1” to 1.5”, 1” to 2”, 2” to 3”, 2” to 4”, 3” to 4”	4 ksi, 8 ksi, 12 ksi, 16 ksi, 20 ksi
Mid-depth	Equal Thickness	0.01-1.5	0.5”, 1”, 2”, 3”, 4”	4 ksi, 8 ksi, 12 ksi, 16 ksi, 20 ksi
	Transition	0.01-1.5	0.5” to 1”, 1” to 1.5”, 1” to 2”, 2” to 3”, 2” to 4”, 3” to 4”	4 ksi, 8 ksi, 12 ksi, 16 ksi, 20 ksi

The fatigue analysis and findings are presented in the following sections along with the fracture analysis findings for each geometry type including equal thickness butt welds and thickness transition butt welds.

3.3 Critical Planar Flaw Sizes Based on Fracture

Similar to the fatigue loading models, planar flaws have been modeled using FFS procedures to determine the maximum crack size that will not result in fracture. The Option 1 FFS procedure found in BS 7910:2013 was utilized to evaluate the effects of various flaw types on the performance of CJP welds. While finite element models were developed to evaluate the effects of plasticity for transition welds, the Option 1 failure assessment diagrams (FAD) curves were utilized to account for the inherent variability in the fracture mechanics inputs. A parametric study was performed to account for variations in the plate thickness, flaw aspect ratio, flaw position, magnitude of the combined dead and live stresses, residual stresses, and material properties (i.e., strength and fracture toughness).

3.3.1 Yield and tensile strength

Both yield and tensile strength must be included in the fracture analysis. Since steel products are generally delivered above the minimum specified yield strength, the analyses assumed that the expected yield strength is 10% greater than the minimum specified yield strength (i.e., $F_{yExpected}=1.1F_{yNominal}$). Similarly, the expected tensile strength was also assumed to be 10% greater than the minimum specified tensile strength. The expected yield and tensile strength of the as-placed weld were assumed to match the expected yield and tensile strength of the base material. Specific material grades considered in the parametric study are 36, 50, 70 and 100 ksi.

3.3.2 Fracture toughness

A fracture assessment requires toughness to be known or at least assumed. At present, the US bridge industry does not require any specific level of toughness or testing for as-placed production CJP welds or for the Heat Affected Zone (HAZ). In the absence of any specifications, one could conservatively use the lower bound estimate of K_{Ic} per the Master Curve of around 20 ksi$\sqrt{\text{in}}$. However, this will result in extremely conservative estimates of tolerable flaw sizes. Rather than assume a lower-bound toughness, the material toughness was included in the fracture analyses as a variable in the parametric study. Toughness was varied from a lower bound of 25 ksi$\sqrt{in}$ to 100 ksi$\sqrt{in}$ in 25 ksi$\sqrt{in}$ increments to establish the sensitivity and relationship between flaw size and toughness. It was assumed that the toughness used in the model corresponds to that of the as-placed weld and HAZ at the lowest anticipated service temperature.

Charpy v-notch (CVN) requirements are included in ASTM A709 [40] for base metal of production welds and AASHTO/AWS D1.5 [5] for weld metal of groove weld qualification test plates. These welds do not necessarily match the thickness or joint geometry of the production welds. While these requirements were used to estimate weld metal fracture toughness, previous research has found that production welds may have lower fracture toughness than the PQR test welds due to differences in the joint geometry so use of minimum Charpy requirements of PQR test welds may be unconservative in some cases [41].

The CVN values were converted into K_{Ic} values using the Charpy/fracture toughness correlation in BS 7910. This approach utilizes the master curve to calculate T_0 from T_{27J} or T_{40J}. Other factors in this equation are the probability that the material fracture toughness (K_{mat}) is less than estimated, the thickness of the material, and a factor (T_K) which describes the scatter in the Charpy versus fracture toughness correlation. The probability that K_{mat} is less than estimated was set to 50% since the Charpy value used in the correlation is only the minimum specified value and the scatter of the data is unknown. The thickness was taken as 4" unless the permissible thickness for a certain grade of steel was smaller. The recommended T_K term of +25 °C was used to account for the scatter in the Charpy correlation.

It was found that, except for non-fracture critical Grade HPS 100W, the base metal Charpy requirements resulted in lower K_{Ic} values than the weld metal requirements. In order to summarize the data, the minimum base or weld metal fracture toughness values in AASHTO Temperature Zone II at the maximum permissible thickness is shown in Table 3.4. Grades 36 through 50W have K_{Ic} of approximately 46 ksi$\sqrt{in}$ for fracture critical welds. Grade 70W has a K_{Ic} of approximately 60 ksi$\sqrt{in}$, and Grade 100W has K_{Ic} of approximately 75 ksi$\sqrt{in}$ for fracture critical welds. Therefore, use of 50 ksi$\sqrt{in}$ for Grade 36 through 50W and 75 ksi$\sqrt{in}$ for Grade 100W is probably reasonable. It should be noted that this is an approximate correlation and the fracture toughness in the HAZ is unknown.

Table 3.4 Typical Fracture Toughness Values for Bridge Welds

Steel	Minimum Base or Weld Metal in Zone II at Maximum Thickness (ksi$\sqrt{in}$)
Non-FC Gr. 36 - HPS 50W	NA
Non-FC Gr. HPS 70W	>56.5[1]
Non-FC Gr. HPS 100W	68.4
FC Gr. 36 - HPS 50W	45.8
FC Gr. HPS 70W	>60.4[1]
FC Gr. HPS 100W	>75.1[1]

[1]T_0 was slightly conservative since minimum Charpy energy was rounded down to either T_{27J} or T_{40J}

3.3.3 Primary stresses

The primary stresses (i.e., combined dead and live load stresses) were assumed to be 75% of the minimum specified yield strength of the base material. This correlates to the allowable stress level for the operating rating in the 2nd Edition Manual for Bridge Evaluation [42]. The HL-93 rating factor for the operating rating is 1.3 times greater than the inventory rating factor. A reasonable stress level for inventory loading is 0.55*F_y since this correlates to the historic allowable stress design limits. Multiplying 1.3*0.55 approximately results in the 0.75 factor. This is believed to be a reasonable level for maximum anticipated loads in a bridge member and that using 100% of the minimum specified yield strength would be overly conservative.

3.3.4 Residual stresses

The effects of residual stresses were included in analytical models for fracture by assuming a uniform tension stress. In reality, the actual residual stress profile highly depends on the type of weld and the welding procedure, etc. Further, the effects of repairs and starts/stops can drastically affect residual stress fields. For double bevel CJP welds, assumed residual stress profiles typically result in compressive residual stresses in the root of the weld. This compressive residual stress helps with resisting fracture for embedded discontinuities, but it results in different critical crack sizes depending on the location of the embedded discontinuity with respect to location within the weld. For new welds, the acceptance criteria would also need to be different depending on the weld type (e.g., single bevel, double bevel, electroslag) and the welding procedure (i.e., heat input). Further, different criteria would need to be developed for repair welds where the residual stress fields would also be considerably different. Therefore, a simplified approach for acceptance criteria for new welds was utilized due to the additional variables which would need to be included in the acceptance criteria (i.e., one would require knowledge of heat input, travel speed, top or bottom of the plate) in order to account for the different residual stress profiles and the location of the discontinuity in relation to the residual stress profile.

Use of a uniform residual stress profile equal to 100% of the expected yield strength is recommended by BS 7910 for an initial assumption. BS 7910 [31] includes additional non-uniform residual stress profiles in Annex Q, and API 579-1/ASME FFS-1 [43] released updated non-uniform residual stress profiles with the 2016 edition of the code. For both codes, the residual stress is equal to the assumed material yield strength at the surface of the weld. For embedded flaws, the maximum residual stress in the middle two-thirds of the thickness was evaluated. For BS 7910, this results in a residual stress of approximately 70% of the assumed material yield strength. For API 579-1/ASME FFS-1, the residual stress profile depends on the heat input of the weld divided by the weld thickness with lower heat inputs or thicker welds resulting in higher residual stresses. Previous research has found that typical bridge heat inputs are between 50 kJ/in to 90 kJ/in [41]. If the heat input was 50 kJ/in, the low heat input category would be invoked for welds greater than 1.5" thick. If the heat input was 90 kJ/in, the low heat input category would be invoked for welds 3" thick or greater. For the low input case, the maximum residual stress in the middle two-thirds of the thickness according to API 579-1/ASME FFS-1 would be 100% of the assumed material yield strength. The medium heat input case results in residual stresses of approximately 60% of the assumed material yield strength in the middle two-thirds of the thickness.

Two levels of residual stress were evaluated during the parametric study. The first level was residual stresses equal to the expected yield strength of the base metal ($1.1*F_{yNominal}$) as it seems that residual stresses of 100% of the expected material yield strength is an appropriate assumption for surface flaws. The second level was equal to two-thirds (66%) of the expected yield strength of the base metal as it seems that using 66% of the assumed material yield strength is appropriate for embedded flaws in most cases.

BS 7910 includes an additional equation which accounts for global relief of residual stresses due to primary loading of the structure. This equation was utilized in the evaluation which resulted in a reduction of the actual residual stresses at the surface from 100% of the expected yield strength to approximately 75% of the expected material yield strength for equal thickness butt welds and 60% of the expected yield strength for thickness transition butt welds.

3.3.5 Summary of parametric study

Using the inputs of the fracture parametric study, the maximum crack height and length that would resist fracture was determined for various a/c ratios, yield and tensile strength, fracture toughness, primary stress, and residual stress using SignalFFS software [39]. The specific joint types that were evaluated for fracture are same as those evaluated for fatigue shown in Table 3.3.

The fracture analysis and findings are presented in the following sections along with the fatigue analysis findings for each geometry type including equal thickness butt welds and thickness transition butt welds.

3.4 Critical Flaw Sizes for Equal Thickness CJP Butt Welds

For the analysis of CJP butt welds, the embedded and near surface flaws were assumed to be centered in a 12" wide plate. As expected, increasing the stress range resulted in a large decrease in the maximum flaw size which would not result in fatigue crack growth. Similarly, decreasing the fracture toughness of the material resulted in a large decrease in the maximum flaw size that can resist fracture. The maximum flaw size was very similar for embedded cracks at the ¼ point and the midpoint through the thickness of the plate expect for thin plates (i.e., 0.5" thick) at a 4 ksi stress range or for fracture toughness of 100 ksi$\sqrt{\text{in}}$. In these cases, a slight increase in maximum flaw size is seen for cracks at the midpoint compared with the ¼ point through the thickness of the plate. Due to the similarities of the ¼ point and midpoint embedded crack results, the results from the ¼ point were used for the critical crack size of embedded flaws. It was found that increasing the thickness of the plate, resulted in an increase in the critical flaw size for both surface and embedded flaws for both the fatigue and fracture analyses, but the sensitivity in critical flaw size to changes in plate thickness was much lower for limiting fatigue crack growth than limiting fracture. In other words, the critical flaw size was very similar for all thicknesses when accounting for fatigue crack growth.

The results from the fatigue and fracture parametric studies were combined in order to determine the target critical flaw size. Obviously, there was a wide spectrum of target critical flaw sizes depending on the inputs. Plots were created for both 100% and 66% residual stress assumptions for each plate thickness and for both surface and embedded cracks. Due to the wide variation in flaw size due to the underlying input parameter assumptions, the critical crack size data were grouped based on selected parameters that were reasonable for typical bridge welds. Based on the discussion of inputs noted above, the assumptions given in Table 3.5 were determined to be most reasonable for target critical flaw sizes of highway bridge welds.

Table 3.5 FFS Inputs for Target Critical Flaw Sizes

Residual Stresses (% of Expected Yield Strength)	100% for Surface Flaws, 66% for Embedded Flaws		
Yield Stress	Grade 36 - 50	Grade 70 - 100	Grade 36 - 100
Fracture Toughness	K_c=50 ksi$\sqrt{in}$	K_c=75 ksi$\sqrt{in}$	K_c=75 ksi$\sqrt{in}$
Fatigue Stress	≤ 4 ksi	≤ 4 ksi	≤ 8 ksi

After completing the review and grouping data, simplified tables for the combined fatigue and fracture analysis of equal thickness CJP butt welds were developed. The corresponding target critical flaw height and length for the cases in Table 3.5 are shown in the following tables: Table 3.6 for surface flaws in equal thickness welds, Table 3.7 for embedded flaws in equal thickness welds. The critical flaw height and length is shown at flaw aspect ratios (a/c) of 0.1, 0.5, 1.0, and 1.5 for surface flaws and 0.1, 0.5, and 1.0 for embedded flaws. The maximum a/c ratio for the embedded flaw in a 0.5” plate was 0.9 due to physical constraints.

Table 3.6 Target Surface Flaw in Equal Thickness Welds

Yield Stress	Grade 36 - 50	Grade 70 - 100	Grade 36 - 100
Fracture Toughness	Kc=50 ksi$\sqrt{\text{in}}$	Kc=75 ksi$\sqrt{\text{in}}$	Kc=75 ksi$\sqrt{\text{in}}$
Fatigue Stress	≤ 4 ksi	≤ 4 ksi	≤ 8 ksi
Plate Thickness	**Flaw Height (a) x Flaw Length (2c)**	**Flaw Height (a) x Flaw Length (2c)**	**Flaw Height (a) x Flaw Length (2c)**
0.5"	0.059" x 1.173” 0.091" x 0.363" 0.133” x 0.266” 0.149" x 0.199"	0.038" x 0.758” 0.058" x 0.231” 0.086” x 0.172” 0.095" x 0.127”	0.025" x 0.504” 0.038" x 0.153” 0.058” x 0.115” 0.063" x 0.084”
1"	0.062" x 1.234" 0.094" x 0.376" 0.141” x 0.282” 0.155" x 0.207"	0.038" x 0.768” 0.058" x 0.233” 0.088” x 0.176” 0.096" x 0.128”	0.025" x 0.508” 0.039" x 0.154” 0.058” x 0.116” 0.064" x 0.085”
2"-4"	0.063" x 1.252” 0.095" x 0.380” 0.143” x 0.287” 0.157" x 0.209”	0.039" x 0.771” 0.058" x 0.234” 0.088” x 0.176” 0.097" x 0.129”	0.025" x 0.509” 0.039" x 0.154” 0.058” x 0.117” 0.064" x 0.085”

Table 3.7 Target Embedded Flaw in Equal Thickness Welds

Yield Stress	Grade 36 - 50	Grade 70 - 100	Grade 36 - 100
Fracture Toughness	Kc=50 ksi$\sqrt{\text{in}}$	Kc=75 ksi$\sqrt{\text{in}}$	Kc=75 ksi$\sqrt{\text{in}}$
Fatigue Stress	≤ 4 ksi	≤ 4 ksi	≤ 8 ksi
Plate Thickness	**Flaw Height (2a) x Flaw Length (2c)**	**Flaw Height (2a) x Flaw Length (2c)**	**Flaw Height (2a) x Flaw Length (2c)**
0.5"	0.137" x 1.370” 0.183" x 0.366” 0.243” x 0.270”	0.098" x 0.978” 0.137" x 0.274” 0.200" x 0.200”	0.062" x 0.625” 0.089" x 0.177” 0.143" x 0.143”
1"	0.171" x 1.706” 0.243" x 0.485” 0.365” x 0.365”	0.107" x 1.072” 0.154" x 0.307” 0.251" x 0.251”	0.064" x 0.637” 0.091" x 0.181” 0.152" x 0.152”
2"-4"	0.184" x 1.842” 0.264" x 0.529” 0.437” x 0.437”	0.110" x 1.100” 0.157" x 0.313” 0.263" x 0.263”	0.064" x 0.639” 0.091" x 0.182” 0.153" x 0.153”

The results in Table 3.6 and Table 3.7 were compared to the closed fracture mechanics equations for a surface crack and embedded crack in an infinite plate. Using the equations provided by Anderson [44], the stress intensity factor for a circular surface crack in an infinite plate is $K_I=1.29\sigma\sqrt{a}$ and $K_I=1.13\sigma\sqrt{a}$ where “*a*” is the entire crack height for the surface crack and half the crack height for the embedded crack. These equations can be easily modified for fatigue crack growth by exchanging ΔK_{th} for K_I and the cyclic stress range (S_r) for stress (σ) resulting in $\Delta K_{th}=1.29S_r\sqrt{a}$ and $\Delta K_{th}=1.13S_r\sqrt{a}$ for surface and embedded cracks, respectively. Table 3.8 gives the results of the critical size of circular flaws in an infinite plate for fatigue loading only using inputs of 2.5 ksi$\sqrt{\text{in}}$ for ΔK_{th} and 4 ksi or 8 ksi for S_r. The 8 ksi stress range results given in Table 3.8 matched the target surface and embedded flaws for 4" thick plates given in Table 3.6 and Table 3.7. The 4 ksi stress range results given in Table 3.8 are larger than the target surface and embedded flaws for 4" thick plates given in Table 3.6 and Table 3.7 since these cases were controlled by fracture rather than fatigue crack growth.

Table 3.8 Circular Flaw in an Infinite Plate with Fatigue Loading Only

Flaw Type	**4 ksi Stress Range**	**8 ksi Stress Range**
Surface	0.234"x0.469"	0.058"x0.117"
Embedded	0.612"x0.612"	0.153"x0.153"

It quickly became apparent that the critical crack sizes were quite small in some cases. Therefore, to verify if the approach was yielding reasonable estimates, the simplified results were compared to the flaw size acceptance criteria in ISO 19285:2017 [17]. This PAUT inspection document includes acceptance criteria to be determined by either measuring the height and length of the flaw or measuring the length and the maximum amplitude. There are three levels of quality specified in this document, but Level 2 would typically be used for bridge welds. Table 3.9 includes the maximum flaw height and length for surface and embedded flaws over various plate thicknesses. For thin plates (i.e., 0.5"), the critical flaw height tends to be similar to those calculated during this project, but the critical flaw length tends to be a bit longer for the ISO acceptance criteria. As the plates become thicker, the ISO acceptance criteria allows larger flaws than were calculated during this project. Overall, the ISO acceptance criteria compares reasonably well with the critical flaw sizes computed in this project.

Table 3.9 ISO 19285:2017 Level 2 Acceptance Criteria

Plate Thickness	**Surface Flaws** **Flaw Height x Flaw Length**	**Embedded Flaws** **Flaw Height x Flaw Length**
0.5"	0.039" x ∞ 0.079" x 0.5"	0.039" x ∞ 0.079" x 0.5"
1"	0.039" x ∞ 0.079" x 1"	0.039" x ∞ 0.157" x 1"
2"-3"	0.079" x ∞ 0.118" x 1.969"	0.079" x ∞ 0.197" x 1.969"
4"	0.118" x ∞ 0.157" x 2.362"	0.118" x ∞ 0.236" x 2.362"

ASME Code Case 2235-13 [30] includes an acceptance criteria based on measurements of flaw height and length. The acceptance criteria vary by aspect ratio (a/c) and flaw height (a/t) for thicknesses 1" and greater. Therefore, at least three different aspect ratios were evaluated to compare the range of acceptable flaw sizes. It was found that the results developed in this study are typically conservative compared to the sizes in the ASME Code Case for the high strength steels or high stress ranges. For thin plates (i.e., 0.5"), the critical flaw height tends to typically be within 1/16" for approximately similar length flaws, but for thick plates (i.e., 3") the difference between the critical crack sizes developed in this project and the ASME limits increases and reaches values of approximately 5/8" in some cases. For the 4 ksi stress range cases, the critical crack sizes compare quite well, with the ASME Code Case allowing slightly smaller crack sizes for thin plates and slightly larger crack sizes for thick plates. For the 8 ksi stress range case, the critical crack size developed in this project is typically much smaller than the ASME limits. This is due to the limit placed on fatigue crack growth in this project while this was not a consideration during the development of the ASME Code Case 2235 limits [45].

3.5 Critical Flaw Sizes for Thickness Transition CJP Butt Welds

Butt welds with a transition in thickness have a stress concentration at the start of the transition. This stress concentration may decrease the fatigue and fracture resistance of cracks, especially if they are located near the surface of the plate. Typical girder flange welds utilize single-sided (offset) transitions since the web plate remains at a consistent height as shown in Figure 3.2. The butt weld is typically located in the region with the greatest stress concentration at the point where the thin plate begins the thickness transition. The general location of the butt weld and HAZ is visually apparent in Figure 3.2. In order to account for this effect, the magnitude of the stress concentration needs to be determined for various thickness transitions as shown in specimen matrix in Table 3.3.

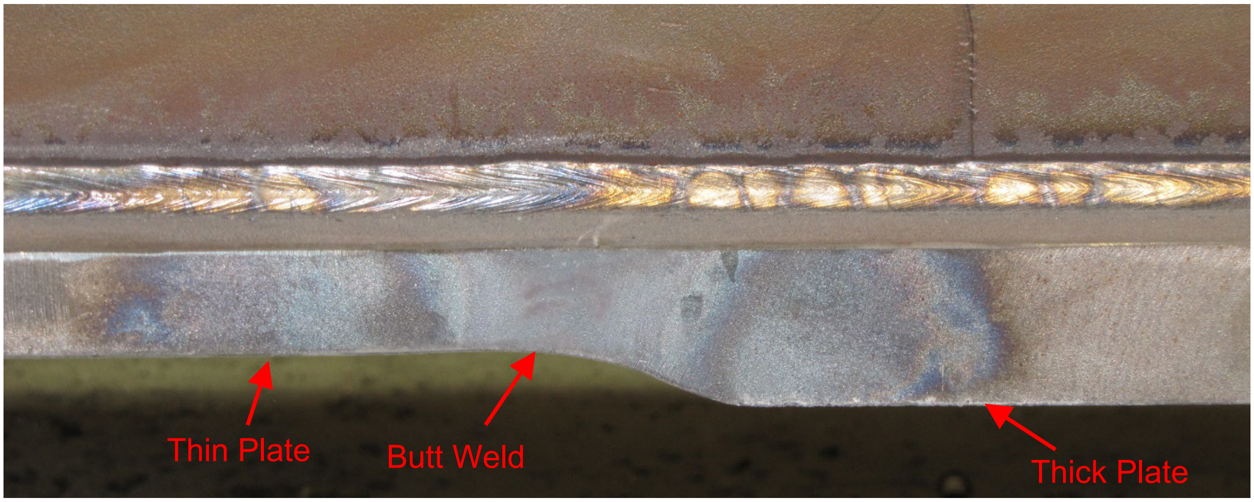

Figure 3.2 Typical Thickness Transition Butt Weld on Bridge Girder Flange Plate

Finite element analysis was used to calculate the magnitude of the stress concentration using the commercial solver ABAQUS. All of the thickness transitions used a 1 to 2.5 slope which is the maximum allowed by AASHTO for Category B butt welds. The thickness transitions with a minimum plate thickness of 0.5" were modeled as web plates while the thickness transitions with a minimum plate thickness equal to or greater than 1" were modeled as flange plates. For the flange plate models, the flanges were assumed to be 18" wide while the web was 0.5" thick by 36" deep. For the web plate models, various flange sizes were used to capture different levels of stiffness.

In order to capture the restraint provided by the web, the finite element analysis was performed using a 3D model. Typical transition butt weld geometries have a smooth radius as shown in Figure 3.2. Therefore, to better represent the actual conditions, a 2" radius was used at the change in slope. The model was loaded with a unit traction in the axial direction on the thin plate side while the thick plate side was restrained from movement in the axial direction.

Figure 3.3 displays the typical profile for stresses in the longitudinal direction of the girder. This figure shows a view cut through the flange at the point of maximum axial stress. As expected, there is a concentration of axial stresses at the radius of the transition to the thin plate. The lowest axial stresses occur where the thickness transition ends at the thick plate. The peak stress occurs within the radius, but the stresses in front of the radius within the thin plate are still increased in the region very close to the radius. Typically, the butt weld would be located in the thin plate near the thickness transition as shown in Figure 3.2. In this configuration, the far bevel face is located at the start of the transition radius. The upper portions of the weld near the top surface will therefore experience increased stresses compared to the rest of the thin plate.

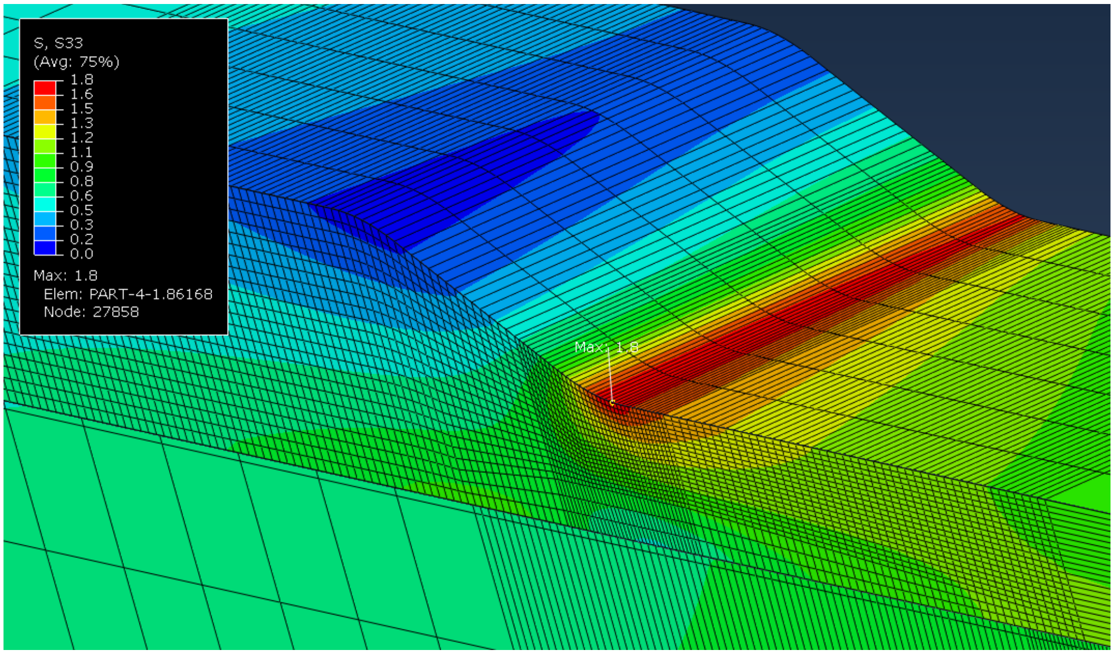

Figure 3.3 Stresses for 1” to 2” Transition Weld

The results from various thickness transitions were compared by plotting the stress at each integration point along a path extending from the point of maximum stress concentration vertically through the thickness of the flange. The location along the thickness of the flange was then normalized in order to compare the various transition geometries. As expected, the greatest stress concentration factor (SCF) occurred at the transitions with the greatest relative change in thickness such as 1” to 2” or 2” to 4”. It should be noted that the stress concentration occurred within the top half of the plate, and decreased quickly away from the plate surface.

In order to estimate the effect of the stress concentration on the fatigue resistance of transition welds, a polynomial trendline was fit to the results from the three transitions with the greatest SCF: 1” to 1.5”, 1” to 2”, and 2” to 4” transitions to obtain the following result, where t is the normalized depth in the plate with t=0 on the transition-side face and t=1 on the opposite face:

$$SCF_{Flange}(t) = 1.6587t^4 - 4.8158t^3 + 5.0949t^2 - 3.0826t + 1.7921$$

The SCF estimation was then multiplied by the various nominal stresses shown in Table 3.3 to obtain a through-thickness fatigue stress profile for each nominal stress level. The polynomial stress profiles were then entered into SignalFFS to obtain the maximum crack size which would not initiate fatigue crack growth for both embedded and surface cracks.

A separate web thickness transition model was developed for thickness transitions where the thin plate was less than 1" thick. Rather than the thickness transition occurring only on one side of the web, the web plate transition occurred on both sides of the web so that the web plate remained centered on the flange. The web plate thickness transition used in this analysis was 0.5" to 1" thickness since this was assumed as the largest anticipated thickness transition for a web plate. Unit axial traction was placed on the web and flange on the thin side of the weld.

It was found that the stress concentration factor of web thickness transitions had a dependency on the relative stiffness of the *flange plate*. Therefore, the flange size was varied as follows: no flange, 1"x6", 1.5"x9", and 4"x18". The location of the greatest SCF in the web thickness transition was located near the flange as shown in Figure 3.4. This figure shows axial stresses in the model with the lower limit on the color palette set to the nominal stress. When there is no flange, the web SCF is small since the average stress level is equal to the nominal stress. As the flange stiffness increases, the average stress level through the thickness of the web increases at the point of maximum SCF. Since the maximum SCF in web thickness transitions is dependent on the flange stiffness, the SCF was increased slightly compared to the highest FE results for the estimation to be used in the SignalFFS fatigue evaluations in order to be conservative for possible flange/web combinations. The following equation displays the resulting estimation of the SCF for web transitions, where t is the normalized depth in the plate with t=0 on the transition-side face and t=1 on the opposite face:

$$SCF_{Web}(t) = 0.8t^2 - 0.8t + 1.4$$

The equation for the SCF estimation was then multiplied by the nominal stress values given in the specimen matrix in Table 3.3 to obtain a through-thickness fatigue stress profile for each nominal stress level. The polynomial stress profiles were then entered into SignalFFS to obtain the maximum crack size which would not initiate fatigue crack growth for both embedded and surface cracks.

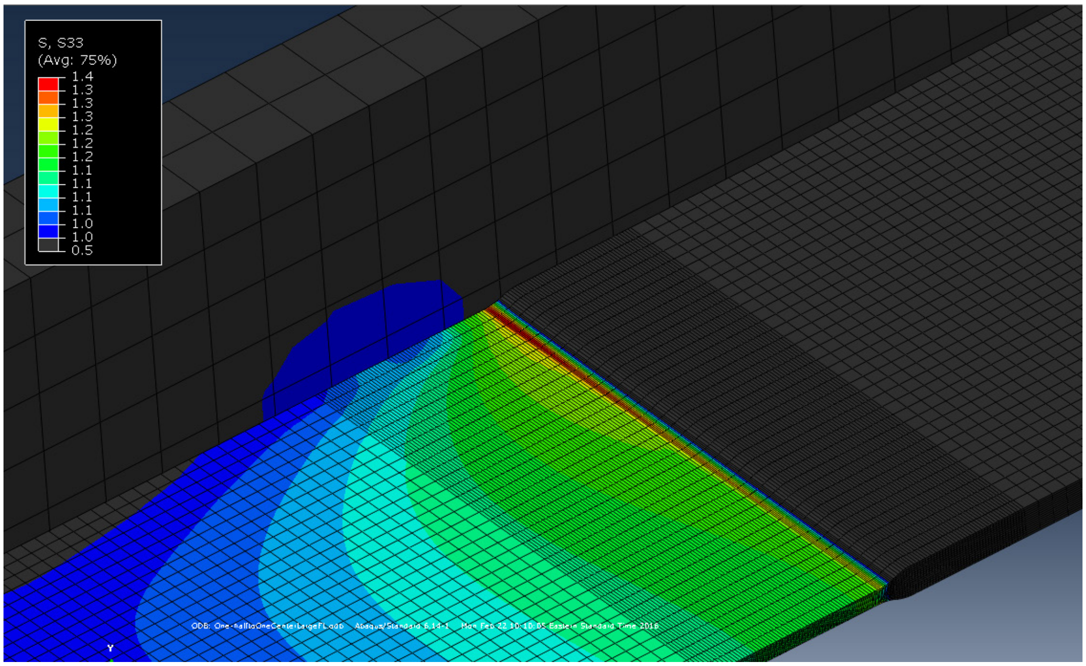

Figure 3.4 Web SCF for 4”x18” Flange

Similar finite element models were used for fracture resistance analysis as the fatigue resistance. Due to greater applied stresses in the fracture analysis, plasticity effects needed to be accounted for through the use of nonlinear FE analysis using stress-strain curves for ASTM A709 bridge steels. The plasticity effects flatten the SCF curves near the surface of the thickness transition due to localized yielding and increase the depth of the SCF below the surface. When all of the thickness transitions were plotted, it was discovered that the thickness transitions with the highest SCF were nearly linear for points between the maximum SCF and the midpoint of the plate. Since the critical flaws will be those on the top surface or ¼-point through the thickness, the model of the stresses in the FFS approach only needs to accurately represent the stress profile over the top half of the plate. Therefore, it was determined that a linear stress approximation could be used rather than a polynomial. The linear SCF estimation used for the fracture analysis of transitions were represented by using the following equations where S_m is the membrane (nominal) stress and S_b is the bending stress:

$$S_m = 0.75 * F_y$$

$$S_b = 0.6 * S_m$$

The values of S_m and S_b were then used in the SignalFFS software for the primary stresses along with the previously noted inputs for secondary stresses, thicknesses, fracture toughness, etc. to calculate the limiting crack size to resist fracture. Using this approach, the thickness transition CJP butt welds geometries in Table 3.3 were modeled as flat plates with a 12" width and a linearized primary stress profile for the primary stresses in the SignalFFS software to calculate the limiting crack size to resist fracture.

The results for the target surface and embedded weld flaws in thickness transition welds for the cases in Table 3.5 are given in Table 3.10 and Table 3.11, respectively. The critical flaw height and length is shown at flaw aspect ratios (a/c) of 0.1, 0.5, 1.0, and 1.5 for surface flaws and 0.1, 0.5, and 1.0 for embedded flaws. In these tables, the plate thickness correlates to the thickness of the thinner plate. The FFS results were determined based on the SCF listed above which were appropriate for the largest thickness transitions evaluated. Therefore, these results should be valid for typical thickness transitions, regardless of the thickness of the thicker plate.

Table 3.10 Target Surface Flaw in Thickness Transition Welds

Yield Stress	Grade 36 - 50	Grade 70 - 100	Grade 36 - 100
Fracture Toughness	Kc=50 ksi$\sqrt{\text{in}}$	Kc=75 ksi$\sqrt{\text{in}}$	Kc=75 ksi$\sqrt{\text{in}}$
Fatigue Stress	≤ 4 ksi	≤ 4 ksi	≤ 8 ksi
Plate Thickness	**Flaw Height (a) x Flaw Length (2c)**	**Flaw Height (a) x Flaw Length (2c)**	**Flaw Height (a) x Flaw Length (2c)**
0.5"	0.040" x 0.807" 0.063" x 0.254" 0.092" x 0.184" 0.102" x 0.136"	0.029" x 0.583" 0.045" x 0.180" 0.066" x 0.133" 0.073" x 0.097"	0.013" x 0.264" 0.020" x 0.081" 0.030" x 0.060" 0.033" x 0.044"
1"-2"	0.033" x 0.651" 0.050" x 0.201" 0.074" x 0.148" 0.081" x 0.107"	0.025" x 0.493" 0.038" x 0.150" 0.056" x 0.113" 0.062"x 0.082"	0.008" x 0.161" 0.012" x 0.049" 0.019" x 0.034" 0.020" x 0.027"
3"-4"	0.032" x 0.641" 0.049" x 0.196" 0.073" x 0.146" 0.080" x 0.106"	0.025" x 0.492" 0.037" x 0.149" 0.056" x 0.113" 0.061" x 0.082"	0.008" x 0.160" 0.012" x 0.049" 0.019" x 0.034" 0.020" x 0.027"

Table 3.11 Target Embedded Flaw in Thickness Transition Welds

Yield Stress	Grade 36 - 50	Grade 70 - 100	Grade 36 - 100
Fracture Toughness	Kc=50 ksi$\sqrt{\text{in}}$	Kc=75 ksi$\sqrt{\text{in}}$	Kc=75 ksi$\sqrt{\text{in}}$
Fatigue Stress	≤ 4 ksi	≤ 4 ksi	≤ 8 ksi
Plate Thickness	**Flaw Height (2a) x Flaw Length (2c)**	**Flaw Height (2a) x Flaw Length (2c)**	**Flaw Height (2a) x Flaw Length (2c)**
0.5"	0.101" x 1.013” 0.142" x 0.283” 0.205" x 0.205”	0.078" x 0.784” 0.110" x 0.221” 0.172" x 0.172”	0.040" x 0.395” 0.056” x 0.112” 0.094" x 0.094"
1"	0.110" x 1.096” 0.154" x 0.309” 0.245" x 0.245"	0.076" x 0.761” 0.107" x 0.214” 0.175" x 0.175"	0.036" x 0.361” 0.051” x 0.102” 0.084" x 0.084"
2"-4"	0.113" x 1.134” 0.160" x 0.320” 0.264" x 0.264"	0.077" x 0.772” 0.109" x 0.218” 0.181" x 0.181"	0.036" x 0.364” 0.051" x 0.103” 0.086" x 0.086"

Comparing the results for thickness transition CJP butt welds to the equal thickness CJP butt welds shown in Table 3.6 and Table 3.7, a larger reduction in critical crack sizes was seen for surface flaws in transition welds than for embedded flaws in transition welds. The reduction is also much greater for plates with a thickness 1” or greater since these plates were assumed to be flange plates with offset thickness transitions rather than web plates with centered thickness transitions for 0.5” plate thickness.

The thickness transition CJP weld results were compared to ISO 19285 and ASME Code Case 2235. Both of these documents do not have separate acceptance criteria for thickness transition welds so accounting for the SCF decreased the critical crack sizes calculated for thickness transition CJP welds in this project compared with those allowed in ISO 19285 and ASME Code Case 2235. In general, the target flaw sizes developed during this project are similar to those allowed in the other acceptance criteria for 0.5” and 1” plate thicknesses with a 4 ksi stress range. For the other cases, the target critical crack sizes developed during this project are smaller than those allowed for the other acceptance criteria, especially for an 8 ksi stress range. Along with not accounting for the stress concentration of thickness transition welds, the fatigue crack growth failure mechanism was not considered in the development of ASME Code Case 2235 [45]. It is not known whether either of these factors were considered during the development of ISO 19285 as no literature was found that documents the development of that acceptance criteria.

4. ROUND ROBIN EXPERIMENTAL TESTING

4.1 Introduction

A round robin testing program was performed in order to gain insight into the capabilities of the current technicians in the steel bridge industry and to identify best practices for improved flaw detection and flaw characterization. The round robin testing program was used to determine the minimum flaw size that could be reliably detected with enhanced ultrasonic methods and how the advanced methods compare with the historical conventional UT method. Scanning of a set of specimens containing weld flaws was performed by five PAUT technicians, two TOFD technicians, and five conventional UT technicians. Data was only received by four of the five PAUT technicians who participated. Conventional UT and PAUT technicians were qualified according to the requirements in AWS D1.5 as ASNT Level II for UT and PAUT, respectively. There was tremendous difficulty identifying TOFD technicians to participate in the round robin testing program due to lack of availability or lack of equipment. While eleven TOFD technicians were contacted and five of these technicians initially agreed to take part, only two technicians actually committed to testing of the plates. It is believed that this is directly related to the lack of TOFD technicians in the bridge and building fabrication industry.

PAUT technicians were requested to scan the plates in accordance to the requirements in Annex K and supplied copies of the scan plan details. Each technician provided details on the number of line scans, location of line scans (i.e., face and side of weld scanned and corresponding index offset), incidence angle range, angular sweep increment, calibration/TCG block details, equipment and transducer make, model, and settings, along with any other information included in AWS D1.5 Table K.2. Rather than providing the same scan plan to the technicians, having the technicians develop their own scan plan allowed for documentation of the variation in possible scan results for the same plate scanned within the requirements of Annex K. For instance, one technician scanned the thickness transition plates with six line scans, one technician used five line scans, one technician used four line scans, and one technician used only two line scans. If a single scan plan had been provided to the technicians, the scatter of results would be artificially limited since they would be provided with additional requirements beyond what is included in Annex K. Also, by providing a scan plan, the flaw rejection results would have been artificially influenced for PAUT by having the technicians either use an index offset which would maximize or minimize the amplitude response of the known flaws.

Table 4.1 provides the details of the flaws included in the round robin testing program. There was a total of 19 flaws implanted within the 11 plates which were circulated in the round robin. Some plates had multiple flaws while others did not have any flaws. In addition to the testing by the PAUT, TOFD, and UT technicians, the plates were tested with digital radiography and the full matrix capture (FMC) - total focusing method (TFM) PAUT to aid in determining the as-built flaw sizes. The digital RT and FMC/TFM results are also shown in the following sections. It was determined that digital RT gave the best estimate of the true flaw location and length for volumetric flaws while FMC/TFM gave the best estimate of the true flaw height. The digital RT images of each plate is shown in the Appendix. It should be noted that not all flaws could be distinguished on the digital RT scans, especially lack-of-fusion (LOF) flaws which do not produce a density change in the plan view. Testing was also performed using traditional film RT, but it was found that the contrast of the flaws was poor after digitizing the film. There were also many film artifacts and scratches. Therefore, the digital RT images were exclusively used for flaw location and length sizing.

The FMC/TFM testing was performed blind as to not skew the results by providing the intended flaw height. Two flaws were not detected by the FMC/TFM technician and therefore flaw heights were not reported for these flaws. The flaw sizes shown in Table 4.1 is therefore the size based on the flaw height from FMC/TFM and flaw length from digital RT where this information was available. If the flaw height or length was not available based on the FMC/TFM or digital RT results, the flaw sizes provided by FlawTech for planar flaws or the intended flaw sizes for implanted volumetric flaws was used.

A few of the implanted volumetric flaws also had unintended peripheral flaws which were noted on the digital RT scans. The peripheral flaws were included in the updated flaw location and length measurements. For these flaws, the accuracy in reported flaw location by the round robin technicians was considered both with and without the peripheral flaws in order to capture all possible hits since some technicians may have included the peripheral flaws while others may not.

The shear wave velocity of the round robin plates was measured and compared to a standard AISI 1018 calibration block to verify whether the plates would be considered acoustically equivalent to typical calibration standards. The shear wave velocity of all of the round robin plates were found to be within 0.5% of the AISI 1018 calibration block which had a shear wave velocity of 0.1275 in/μs. As will be explained further, this is within the ±1% tolerance which was determined to result in negligible error in the amplitude and incidence angle. The birefringence (i.e., ratio of shear wave velocity in the rolled and transverse to rolled direction) was 0.5% and lower. This is also within the 1% tolerance which was noted to result in acoustic anisotropic behavior and beam splitting.

The highlights of the results of the round robin testing program are summarized in the following sections, and a summary of the scatter in height and length measurements and reported amplitude are given in the Appendix.

Table 4.1 Round Robin Flaw Details

Flaw ID	Flaw Type	Height (in)	Length (in)
1	LOF	0.03	0.06
2	LOF	0.22	0.40
3	LOF	0.20	0.40
4	Toe Crack	0.02	0.04
5	Crack	0.43	0.80
6	Crack	0.40	0.74
7	Crack	0.17	0.40
8	LOF	0.45	1.00
9	LOF	0.20	0.60
10	LOF	0.43	0.80
11	LOF	0.23	1.00
12	Porosity	0.09	3.31
13	Slag	0.32	0.37
14	Slag	0.16	0.18
15	Slag	0.10	0.90
16	Porosity	0.13	3.27
17	Slag	0.24	0.49
18	Slag	0.06	0.03
19	Slag	0.17	3.61

4.2 Flaw Detection and Location

The accuracy in reported flaw location was very poor for many of the PAUT and conventional UT technicians. Therefore, a "hit" (simply defined as the technician noting that they detected an indication which matches a known flaw) was originally defined as any reported indication where any part of the reported indication was within 1 inch along the longitudinal weld axis of any part of a known flaw in the plate. In other words, the reported indication did not have to line up with a known flaw or even overlap with a known flaw, as long as the gap between the extents of the reported indication and known flaw was less than 1 inch. Clearly this is a very liberal criterion for counting a reported flaw as a hit, but all technicians, including PAUT, TOFD, and conventional UT, seemed to struggle with accurately locating flaws. For PAUT and TOFD technicians, this may be due to inaccuracy in encoder calibration or incorrectly using the encoder, while it may be due to physical measurement error for conventional UT technicians. No consideration was made for correctly measuring the through-thickness location since the flaw depth was not consistently reported (i.e., top of flaw or maximum amplitude).

It was determined not to be too stringent with developing a criterion for determining whether a reported flaw correlated to the intended flaw in order to have adequate data for flaw height and length sizing accuracy, along with variations in reported amplitude. API RP 2X *Recommended Practice for Ultrasonic and Magnetic Examination of Offshore Fabrication and Guidelines for Qualification for Technicians* [46] includes formulas for scoring the performance of ultrasonic technicians when performing a qualification examination. To be correctly located, this document recommends that the centerline of the reported indication be within the boundary of the actual indication or within ½ inch of the actual centerline of the indication (whichever is greater). This requirement is obviously stricter than the requirement developed during the initial review of the round robin data where flaws did not need to overlap at all as long as the gap between any portion of the reported flaw and actual flaw was less than or equal to 1 inch.

Therefore, the hit/miss data are reported using both criteria in the following tables with hits labeled as “1” and misses labeled as “0”. The criteria when the gap between the actual and reported flaw is less than 1 inch is shown in Table 4.3 while the API RP 2X flaw location criteria is shown in Table 4.4. Since these tables highlight accuracy of flaw detection, the data is only shown for the PAUT results where <u>all</u> relevant indications were asked to be reported regardless of the amplitude.

The average hit rate for all of the flaws, planar flaws (Flaws 1-11), and volumetric flaws (Flaws 12-19) is shown in Table 4.2. The overall hit rate for PAUT, conventional UT, and TOFD were quite similar when using the 1 inch gap criteria for flaw location. For planar flaws, PAUT had the highest hit rate and conventional UT had the lowest hit rate. For volumetric flaws, TOFD had the highest hit rate, and PAUT had the lowest hit rate. Under the more stringent criteria included in API RP 2X, the methods that utilize encoded line scanning had a larger drop in overall hit rate than the manual, raster scanned conventional UT method. For planar flaws, TOFD had the highest hit rate, and PAUT had the lowest hit rate. For volumetric flaws, conventional UT had the highest hit rate, and TOFD had the lowest hit rate.

Table 4.2 Average Hit/Miss Rate

Location Criteria	Method	Planar Flaws Only	Volumetric Flaws Only	All Flaws
1 Inch Gap	PAUT	0.97	0.68	0.86
	Conventional UT	0.91	0.83	0.87
	TOFD	0.95	0.94	0.95
API RP 2X	PAUT	0.65	0.64	0.64
	Conventional UT	0.75	0.83	0.78
	TOFD	0.91	0.63	0.79

The detection rate results for individual flaws were found to be highly variable. A small slag inclusion (Flaw 18: 0.06” high x 0.03” long) was not detected by any PAUT or conventional UT technician, but was detected by both TOFD technicians using the 1 inch gap criteria. It was noted in the inspection report for one of the TOFD technicians that this flaw had a low signal response. Another slag inclusion (Flaw 15: 0.10” high x 0.90” long) was detected by every PAUT and conventional UT inspection, but was missed by one of the TOFD technicians.

Table 4.3 Hit ("1")/Miss ("0") Comparison for 1 Inch Gap Criteria

Specimen Details		PAUT[1]					Conventional UT						TOFD		
Flaw ID	**Flaw Type**	**PAUT1**	**PAUT2**	**PAUT3**	**PAUT4**	**PAUT Avg**	**UT1**	**UT2**	**UT3**	**UT4**	**UT5**	**UT Avg**	**TOFD1**	**TOFD2**	**TOFD Avg**
1	LOF	1	1	1	1	1	1	1	1	1	1	1	1	1	1
2	LOF	1			1	1	1	1	1	1	1	1	1	1	1
3	LOF	1			1	1	1	1	1	1	1	1	1	1	1
4	Toe Crack	0	1	1	1	0.75	0	0	1	1	1	0.6	1	0	0.5
5	Crack	1			1	1	1	1	1	1	1	1	1	1	1
6	Crack	1			1	1	1	1	1	1	1	1	1	1	1
7	Crack	1			1	1	1	1	1	1	1	1	1	1	1
8	LOF	1	1	1	1	1	1	0	1	1	1	0.8	1	1	1
9	LOF	1	1	1	1	1	1	1	1	0	1	0.8	1	1	1
10	LOF	1	1	1	1	1	1	0	1	1	1	0.8	1	1	1
11	LOF	1	1	1	1	1	1	1	1	1	1	1	1	1	1
12	Porosity	0	0	1	1	0.5	0	1	1	1	1	0.8	1	1	1
13	Slag	0			1	0.5	1	1	1	1	1	1	1	1	1
14	Slag	1			1	1	1	1	1	1	1	1	1	1	1
15	Slag	1			1	1	1	1	1	1	1	1	0	1	0.5
16	Porosity	1			1	1	1	1	0	1	1	0.8	1	1	1
17	Slag	1			1	1	1	1	1	1	1	1	1	1	1
18	Slag	0	0	0	0	0	0	0	0	0	0	0	1	1	1
19	Slag	1	1	1	1	1	1	1	1	1	1	1	1	1	1
Total Hits		15	7	8	18	**48**	16	15	17	17	18	**83**	18	18	**36**
Hit Rate Avg.		0.79	0.78	0.89	0.95	**0.86**	0.84	0.79	0.89	0.89	0.95	**0.87**	0.95	0.95	**0.95**

[1]Cells blacked out were not tested by technician

Table 4.4 Hit ("1")/Miss ("0") Comparison for API RP 2X Criteria

Specimen Details		PAUT[1]					Conventional UT						TOFD		
Flaw ID	**Flaw Type**	**PAUT1**	**PAUT2**	**PAUT3**	**PAUT4**	**PAUT Avg**	**UT1**	**UT2**	**UT3**	**UT4**	**UT5**	**UT Avg**	**TOFD1**	**TOFD2**	**TOFD Avg**
1	LOF	1	0	1	1	0.75	0	1	0	1	1	0.6	0	1	0.5
2	LOF	1			1	1	1	1	1	1	1	1	1	1	1
3	LOF	1			1	1	1	1	1	1	1	1	1	1	1
4	Toe Crack	0	0	1	1	0.5	0	0	0	0	0	0	1	0	0.5
5	Crack	1			0	0.5	1	1	1	1	1	1	1	1	1
6	Crack	1			0	0.5	1	1	1	1	1	1	1	1	1
7	Crack	1			0	0.5	1	1	1	0	1	0.8	1	1	1
8	LOF	1	1	0	1	0.75	1	0	1	1	1	0.8	1	1	1
9	LOF	1	0	0	1	0.5	0	1	1	0	0	0.4	1	1	1
10	LOF	1	0	1	1	0.75	1	0	1	1	1	0.8	1	1	1
11	LOF	1	0	1	0	0.5	1	0	1	1	1	0.8	1	1	1
12	Porosity	0	0	1	1	0.5	0	1	1	1	1	0.8	0	1	0.5
13	Slag	0			1	0.5	1	1	1	1	1	1	0	1	0.5
14	Slag	1			0	0.5	1	1	1	1	1	1	0	1	0.5
15	Slag	1			1	1	1	1	1	1	1	1	0	1	0.5
16	Porosity	1			1	1	1	1	0	1	1	0.8	1	1	1
17	Slag	1			1	1	1	1	1	1	1	1	1	0	0.5
18	Slag	0	0	0	0	0	0	0	0	0	0	0	0	1	0.5
19	Slag	1	1	1	1	1	1	1	1	1	1	1	1	1	1
Total Hits		15	2	6	13	**36**	14	14	15	15	16	**74**	13	17	**30**
Hit Rate Avg.		0.79	0.22	0.67	0.68	**0.64**	0.74	0.74	0.79	0.79	0.84	**0.78**	0.68	0.89	**0.79**

[1]Cells blacked out were not tested by technician

4.3 Flaw Rejection and Flaw Type Characterization

Both flaw location criteria (i.e., the 1 inch gap criteria developed by the authors and the API RP 2X criteria) were evaluated to compare the rejection rate for PAUT Annex K and conventional UT. The criteria when the gap between the actual and reported flaw 1 inch or less is shown in Table 4.7 while the API RP 2X flaw location criteria is shown in Table 4.8 with rejection labeled as "1" and acceptance labeled as "0" in both tables. Flaw rejection from TOFD inspections cannot be compared to PAUT or conventional UT inspections since there is no acceptance criteria for this NDT technique in AWS D1.5. For the flaw to be considered rejected, it had to be located correctly as well as meeting any other criteria for rejection included in AWS D1.5. All flaws except Flaw 18, which is the very small slag inclusion, were considered rejectable by at least one conventional UT technician when using the liberal flaw detection criteria of the gap being 1 inch or less between the actual and reported flaw.

The average rejection rate for PAUT and conventional UT is shown in Table 4.5 for planar flaws, volumetric flaws, and all flaws. The rejection rates were lower for PAUT per Annex K than for conventional UT, especially when considering the API RP 2X location criteria. The rejection rate for PAUT and conventional UT are much closer for planar flaws when using the 1 inch gap criteria while PAUT has a much lower rejection rate than conventional UT for volumetric flaws. It was found that while PAUT has a lower rejection rate for the small planar flaws such as Flaw 1 and 4, all of the planar flaws 0.2" high by 0.4" long or larger were rejectable per Annex K for the 1 inch gap criteria while some of these flaws were not detected by conventional UT. Due to inaccuracy of locating these large planar flaws with PAUT, many of these large planar flaws would not have been rejected by PAUT according to the flaw location criteria in API RP 2X.

<u>It is important to recognize that the PAUT and conventional UT rejection rates are for the same set of samples and is providing a direct comparison of the two methods.</u> This is unlike some previous studies where the rejection rates of conventional UT and PAUT Annex K were computed using different sample sets which could skew the data. It should be noted that the rejection rates include Flaw 18 even though this flaw was not rejectable according to any conventional UT or

PAUT technicians. Therefore, this flaw has equally lowered the rejection rate for PAUT and conventional UT, but the rejection rates of critical flaws would be slightly increased.

Table 4.5 Average Rejection Rate

Location Criteria	Method	Planar Flaws Only	Volumetric Flaws Only	All Flaws
1 Inch Gap	PAUT	0.79	0.50	0.68
	PAUT w/o K10.2	0.76	0.45	0.64
	Conventional UT	0.87	0.83	0.85
API RP 2X	PAUT	0.53	0.50	0.52
	PAUT w/o K10.2	0.50	0.45	0.48
	Conventional UT	0.75	0.83	0.78

Two indications (Flaw 1 and Flaw 14) were rejected by PAUT technicians per Annex K due to being characterized as cracks rather than due to amplitude and length. The current AWS D1.5 Annex K10.2 states that "indications characterized as cracks shall be considered unacceptable regardless of length or amplitude." The rejection rate of PAUT Annex K without invoking Clause K10.2 (i.e., these flaws would instead be acceptable due to low amplitude) is included in Table 4.5 since PAUT flaw characterization is not always accurate and many PAUT technicians may not be comfortable with or capable of characterizing discontinuities as cracks. In fact, both of these indications were mischaracterized as cracks. Flaw 1 is a small lack of fusion indication which was acceptable per all other PAUT inspections but was rejectable to most conventional UT inspections. Flaw 14 is a slag indication and was acceptable per the other PAUT inspection but was rejectable to all conventional UT inspections.

While the rejection rate for PAUT and conventional UT was similar for many individual flaws, some individual flaws had much lower rejection rates for PAUT than for conventional UT. There were two reasons for these differences, the flaw classification (i.e., Class A - D) based on amplitude for PAUT was often lower than conventional UT and the reported location of the flaw was often more inaccurate for PAUT compared with conventional UT.

For instance, flaws with lower classifications according to PAUT compared to conventional UT include Flaw 1 and Flaws 12-15. This includes a small LOF flaw, a group of porosity, and three slag inclusions. In order to illustrate this difference, the average reported flaw classification for these five flaws are shown in Table 4.6. PAUT technicians had a much higher scatter in how these five flaws were classified. As shown in the table, the classification ranged from Class B, C, or D to as much as not reporting the flaw at all. However, these flaws were typically reported as Class A for conventional UT. It is thought that this difference is mainly due to the fact that PAUT scanning in accordance with Annex K is performed by line scanning where the reported amplitude is not maximized compared with the manual, raster scanned conventional UT approach. Another very important reason for these variations is due to differences in the amplitude limits between the flaw classifications for the PAUT code and the conventional UT code. In other words, the Class A-D limits for the PAUT code may not be equivalent to the Class A-D limits of the conventional UT code even if the amplitude was maximized for each method.

Table 4.6 Average Flaw Classification for Flaw 1 and Flaw 12-15

Method	No Reported Flaw	Class D	Class C	Class B	Class A
PAUT	21%	21%	29%	21%	7%
Conventional UT	4%	4%	4%	0%	88%

Another set of flaws, Flaw 5-7 and Flaw 11, show large decreases in the rejection rate for PAUT when applying the more stringent API RP 2X flaw location criteria. This can be seen when comparing the results for these individual flaws in Table 4.7 and Table 4.8 for PAUT and conventional UT. These flaws include three cracks and one LOF flaw. If one were to would group the results of these flaws, it was seen that the average rejection rate for PAUT decreased from 100% using the more liberal 1 inch gap criteria to 50% using the API RP 2X criteria while the conventional UT results only decreased from 100% to 90% using the same criteria, respectively. Therefore, poor flaw location of these planar flaws resulted in a large decrease in the rejection rate for PAUT compared with conventional UT.

Table 4.7 Rejection Rate (Reject "1"/Accept "0") for 1 Inch Gap Criteria

Specimen Details		**PAUT Annex K[1]**					**Conventional UT**					
Flaw ID	**Flaw Type**	**PAUT1**	**PAUT2**	**PAUT3**	**PAUT4**	**PAUT Avg**	**UT1**	**UT2**	**UT3**	**UT4**	**UT5**	**UT Avg**
1	LOF	0	0	0	1[2]	0.25	0	1	1	1	1	0.8
2	LOF	1			1	1	1	1	1	1	1	1
3	LOF	1			1	1	1	1	1	1	1	1
4	Toe Crack	0	0	0	0	0	0	0	1	0	1	0.4
5	Crack	1			1	1	1	1	1	1	1	1
6	Crack	1			1	1	1	1	1	1	1	1
7	Crack	1			1	1	1	1	1	1	1	1
8	LOF	1	1	1	1	1	1	0	1	1	1	0.8
9	LOF	1	1	1	1	1	1	1	1	0	1	0.8
10	LOF	1	1	1	1	1	1	0	1	1	1	0.8
11	LOF	1	1	1	1	1	1	1	1	1	1	1
12	Porosity	0	0	0	1	0.25	0	1	1	1	1	0.8
13	Slag	0			1	0.5	1	1	1	1	1	1
14	Slag	1[2]			0	0.5	1	1	1	1	1	1
15	Slag	0			0	0	1	1	1	1	1	1
16	Porosity	1			1	1	1	1	0	1	1	0.8
17	Slag	1			1	1	1	1	1	1	1	1
18	Slag	0	0	0	0	0	0	0	0	0	0	0
19	Slag	1	1	1	1	1	1	1	1	1	1	1
Total Rejected		13	5	5	15	**38**	15	15	17	16	18	**81**
Rejection Rate		0.68	0.56	0.56	0.79	**0.68**	0.79	0.79	0.89	0.84	0.95	**0.85**

[1]Cells blacked out were not tested by technician
[2]Rejected due to crack classification rather than amplitude and length

Table 4.8 Rejection Rate (Reject "1"/Accept "0") for API RP 2X Criteria

Specimen Details		**PAUT Annex K[1]**					**Conventional UT**					
Flaw ID	**Flaw Type**	**PAUT1**	**PAUT2**	**PAUT3**	**PAUT4**	**PAUT Avg**	**UT1**	**UT2**	**UT3**	**UT4**	**UT5**	**UT Avg**
1	LOF	0	0	0	1[2]	0.25	0	1	0	1	1	0.6
2	LOF	1			1	1	1	1	1	1	1	1
3	LOF	1			1	1	1	1	1	1	1	1
4	Toe Crack	0	0	0	0	0	0	0	0	0	0	0
5	Crack	1			0	0.5	1	1	1	1	1	1
6	Crack	1			0	0.5	1	1	1	1	1	1
7	Crack	1			0	0.5	1	1	1	0	1	0.8
8	LOF	1	1	0	1	0.75	1	0	1	1	1	0.8
9	LOF	1	0	0	1	0.5	0	1	1	0	0	0.4
10	LOF	1	0	1	1	0.75	1	0	1	1	1	0.8
11	LOF	1	0	1	0	0.5	1	0	1	1	1	0.8
12	Porosity	0	0	0	1	0.25	0	1	1	1	1	0.8
13	Slag	0			1	0.5	1	1	1	1	1	1
14	Slag	1[2]			0	0.5	1	1	1	1	1	1
15	Slag	0			0	0	1	1	1	1	1	1
16	Porosity	1			1	1	1	1	0	1	1	0.8
17	Slag	1			1	1	1	1	1	1	1	1
18	Slag	0	0	0	0	0	0	0	0	0	0	0
19	Slag	1	1	1	1	1	1	1	1	1	1	1
Total Rejected		13	2	3	11	**29**	14	14	15	15	16	**74**
Rejection Rate		0.68	0.22	0.33	0.58	**0.52**	0.74	0.74	0.79	0.79	0.84	**0.78**

[1]Cells blacked out were not tested by technician
[2]Rejected due to crack classification rather than amplitude and length

Table 4.9 shows the findings for all the PAUT flaw characterizations during the round robin testing program. Cracks were only correctly characterized 22% of the time, while many false calls were incorrectly characterized as cracks. It should also be noted that planar flaws such as cracks and lack of fusion were sometimes incorrectly characterized as volumetric discontinuities (11% and 4%, respectively). This is a major concern for developing separate acceptance criteria for planar and volumetric discontinuities. If a planar flaw is mischaracterized as volumetric, it would result in an unconservative evaluation.

Table 4.9 Flaw Characterization using PAUT

Actual Flaw Type	Reported Flaw Type			
	Crack	Planar (Non-Crack)	Volumetric	No Type Reported
Crack	22%	44%	11%	22%
LOF	21%	71%	4%	4%
Porosity	25%	25%	50%	0%
Slag	9%	64%	27%	0%
False Calls	71%	0%	29%	0%

Table 4.10 compares the flaw characterization results for PAUT and TOFD. It was found that the average TOFD technicians did not classify flaws as well as the average PAUT technician. While the classification of planar flaws was similar, TOFD more often incorrectly classified volumetric flaws as being planar.

Table 4.10 Comparison of Flaw Characterization of PAUT and TOFD

	Reported Flaw Type					
Actual Flaw Type	PAUT			TOFD		
	Planar	Volumetric	No Type Reported	Planar	Volumetric	No Type Reported
Planar	85%	6%	9%	86%	10%	4%
Volumetric	40%	60%	0%	86%	0%	14%
False Calls	71%	29%	0%	100%	0%	0%

4.4 False Calls

The reported indications that were not within +/- 1 inch of the total extents of the actual flaw were initially determined to be false calls. The digital RT results revealed that some of the plates included unintended weld flaws, especially near the edge. This was especially true for the FlawTech plates which seemed to have groups of sparse porosity intermittently within some of the plates as shown in the digital RT images in the Appendix. Therefore, indications which overlap with these unintended weld flaws should not be indicated as false calls. It was found that the number of false calls which the technicians classified as rejectable was relatively small after removal of these unintended weld flaws which were apparent on the digital RT results as shown in Table 4.11.

Table 4.11 Rejectable False Calls

Technician	# of Rejectable False Calls	Total Length of Rejectable False Calls
PAUT1	1	3.11”
PAUT2	0	0”
PAUT3	0	0”
PAUT4	3	2.76”
UT1	0	0”
UT2	1	0.45”
UT3	0	0”
UT4	0	0”
UT5	0	0”
TOFD1	2	0.95”
TOFD2	0	0”

4.5 API RP 2X Scoring Results

API RP 2X includes formulas for scoring the performance of ultrasonic technicians during a qualification examination. These formulas evaluate the detection of indications and include a penalty for false calls. This document also includes suggested minimum performance scores for qualification examinations. The performance scores are defined as follows:

$$P = \frac{L_c}{L_a} \times 100 \qquad \text{Formula 1}$$

$$R = \left(\frac{L_c}{L_1}\right)\left(1 - \frac{L_f}{L_1}\right) \times 100 \qquad \text{Formula 2}$$

Where:

P = percentage of actual reflectors correctly detected and sized

R = overall rating including penalty for false calls, 0 to 100

L_a = length of actual reflector contained in the test plate

L_c = credited length for indications that have been correctly sized and located. (Credit is given for the lesser of the reported length or actual length of the flaw.)

L_1 = accumulative length of all indications by the technician, right or wrong

L_f = accumulative length of indications above the stated disregard level where no reflector exists

To be correctly sized, this document recommends that the reported dimensions be within a factor of two of true dimensions (i.e., one-half to twice the actual dimension). To be correctly located, this document recommends that the centerline of the reported indication be within the boundary of the actual indication or within ½ inch of the actual centerline of the indication (whichever is greater).

API RP 2X suggests that minimum performance for ultrasonic technicians be a score of 70 or above for Formula 1 and a score of 50 or above for Formula 2. These criteria were applied to the round robin data to compare the performance of PAUT and conventional UT technicians. The small slag inclusion (Flaw 18) which was not detected by any PAUT or conventional UT technicians was not included in the analysis since it is not likely to be critical for any bridge structures.

The data was analyzed two ways: (1) only accounting for correctly measuring flaw length along with flaw location and (2) accounting for correctly measuring flaw length and flaw height along with the flaw location. Due to the presence of unintended peripheral indications outside of the extent of the intended indications, technicians were given credit if the reported location and dimensions were within the required tolerances for either the main grouping (intended) of the indication or the total flaw including the unintended peripheral indications. The length of the total flaw including unintended peripheral indications was used for the actual length (L_a). Table 4.12 displays the results considering detected discontinuities even if they were not deemed rejectable and disregarding height sizing errors for PAUT and TOFD technicians. No PAUT or TOFD technicians met the minimum requirements for *P* and *R* while two conventional UT technicians passed both requirements. The average score was much lower for the PAUT and TOFD technicians than the conventional UT technicians. Table 4.13 displays the results for PAUT and TOFD when length and height sizing were both required to be within one-half to twice the actual dimension along with being properly located. Due to the large inaccuracies with height sizing and the lack of reported flaw height for TOFD results, no PAUT or TOFD technicians were close to passing the minimum performance requirements.

Table 4.12 API RP 2X Results (not including Height Sizing Error)

	P	R
TOFD1	47	39
TOFD2	65	82
Avg. TOFD	56	61

	P	R
PAUT1	68	56
PAUT2	44	50
PAUT3	48	60
PAUT4	64	50
Avg. PAUT	56	54

	P	R
UT1	67	78
UT2	75	86
UT3	61	57
UT4	79	59
UT5	78	48
Avg. UT	72	66

Table 4.13 API RP 2X Results for PAUT and TOFD including Height Sizing

	P	R
TOFD1	17	14
TOFD2	29	37
Avg. TOFD	23	26

	P	R
PAUT1	29	24
PAUT2	10	11
PAUT3	20	25
PAUT4	33	26
Avg. PAUT	23	22

This simple performance test highlights that there is considerable room for improvement to the current PAUT procedures. This strongly highlights the need for performance testing of ultrasonic technicians in the bridge industry in order to test their abilities to detect (and reject) critical weld flaws.

4.6 Modifications to Future Scanning Procedures based on Round Robin Results

The initial round robin testing phase proved to be extremely useful and revealed much about the state-of-the-practice as related to UT and PAUT. However, based on the results of the round robin, moving forward with development of acceptance criteria based solely on the physical measurement of the flaw size was deemed not to be feasible at present with the accuracy and reliability provided with flaw size measurements using the current PAUT workforce. Acceptance criteria based on flaw height and length sizing was still provided as an alternative method if the PAUT technician develops a written procedure according to specified requirements and successfully completes a performance test on samples of similar material and with flaws similar to the critical flaw size. This would allow for other advanced methods such as FMC/TFM (Full Matrix Capture/Total Focusing Method) PAUT to be used to inspect bridge welds provided that they can detect and reject critical weld flaws if the shop, technician, engineer of record, etc. would request such methods.

It is also concluded that implementation of TOFD will be very difficult in the bridge industry. It seems that TOFD testing is very specialized and not readily available. It is clear that there are very few TOFD technicians that perform testing on structural welds and it appeared that there is not much interest in testing bridge welds with TOFD. Discussion with TOFD technicians noted that testing butt welds where there is a plate thickness transition will also be difficult with TOFD due to the special attention and jigs needed to scan these welds.

Therefore, in accordance with the research objectives, the focus of the research was to develop acceptance criteria based on maximum amplitude and flaw length for PAUT in the AWS D1.5. From the round robin results, it appeared that PAUT, when performed in accordance with Annex K, shows improved detection of planar flaws compared with conventional UT since data collected showed that PAUT did not miss large flaws when using the encoded line scans and the reported flaw location only had to be within 1 inch of the actual flaw to be counted as a hit. However, it seems that additional training or performance testing is required to improve the accuracy of encoded scans. The testing also confirmed that the lack of additional raster scanning, to maximize the amplitude associated with a given indication, reduces the *rejection* rate that results from using the current version of Annex K compared with using conventional UT. In other words, flaws that are rejected today using conventional UT would not be rejected using Annex K, though there is no fitness-for-service or engineering basis for allowing this to be the case.

Again, while ideally one would prefer to reject the flaw based on the size of the flaw and the type of flaw (planar vs volumetric), the round robin testing shows that neither of these can be reliably performed with the current workforce. To ensure that flaws that would be rejected today using conventional UT are not accepted with PAUT using line scanning alone, additional raster scanning of selected indications coupled with line scanning using an encoder is prudent. This will help ensure that the small flaws that were accepted when using line scanning alone in the round robin would be rejected in practice. PAUT has the advantage of producing ultrasound over a range of angles so additional raster scanning would not only maximize the amplitude at that angle, but it would do so over a wide range of angles. This should also help improve the rejection rate of volumetric flaws as well as small planar flaws. Further, use of an encoder would allow for a permanent record of the initial line scan.

In its most basic form, the proposed approach for inspection is to scan a weld using PAUT using an encoder along a specific index offset to be set during the development of the scan plan. If an indication is identified that meets a certain threshold, the technician would return to that location and raster scan using the PAUT probe in order to maximize the length and decibel reading. Then, the decision to accept or reject the indication would be based on an amplitude and length table. The round robin testing has shown conventional UT is already being used to reject very small planar flaws (0.03” x 0.06”). Thus, it does not seem that the proposed approach will result in *increased* rejection rates for small flaws (when using PAUT) which would have been acceptable under conventional UT thereby resulting in an unreasonable increase in weld repairs. However, as discussed above, while the line scanning approach is generally repeatable, the variability of the manual scanning approach after an indication is found using PAUT is problematic.

To better minimize the variability found during the round robin testing program, simulations were performed using CIVA-UT [47] to aid in the initial procedure development through modeling. The modeling incorporated weld flaws similar to the critical flaw sizes developed during the analytical program. These flaws serve as a “lower bound” flaw set from which improved acceptance criteria were developed to consistently <u>reject</u> these flaws. As long as flaws of this size or larger are consistently rejectable, the procedure can be deemed effective at removing critical flaws from service. Therefore, the acceptance criteria are grounded in fracture mechanics but will not use flaw height measurement for evaluation.

Two parametric modeling studies were performed using CIVA-UT. The first parametric study addressed the differences in reference amplitude possible due to differences in acoustic properties of various steel bridge base metal grades. This study involved (1) development of benchmarked CIVA material models based on experimental test results and (2) CIVA modeling of various probes and incidence angles to develop recommendations for AWS D1.5 in order to limit the amplitude differences between the calibration block and test object. The detailed results for the first parametric study are described in Chapter 5.

The second parametric study using CIVA evaluated the effects of variations in the amplitude response of weld flaws deemed critical per the FFS parametric study. This analysis provides a rational comparison of the amplitude from the target critical weld flaws to the acceptance criteria amplitude limits. These data were used to develop a rational fracture mechanics based PAUT inspection procedure and acceptance criteria which will detect and reject critical weld flaws. The parametric models varied the plate thickness along with the flaw type, size, position, tilt, and skew of target critical weld flaws in order to compare the maximum amplitude of the indication response with the reference amplitude and the associated acceptance criteria amplitude limits. The detailed results for the second parametric study are described in Chapter 6.

5. ACOUSTIC PROPERTY CALIBRATION REQUIREMENTS

5.1 Introduction

As previously discussed in Chapter 1, AWS D1.5 Annex K currently allows PAUT using probe frequencies from 1-6 MHz without any requirement accounting for the differences of the acoustic properties of the calibration block and test object. Experimental testing was performed under NCHRP 14-35 by Crowley [7] to measure the typical material attenuation and shear wave velocity of bridge base metals along with the attenuation of narrow-gap electroslag welds (NGI-ESW). These experimental test results highlighted that significant differences in ultrasonic amplitude are possible for the same reflector in different bridge base metals due to variations in acoustic properties (i.e., acoustic attenuation and shear wave velocity). These differences could result in significant variation in the reported amplitude and the reported location of weld flaws if not properly account for during calibration.

To aid in the develop calibration requirements to account for these variations, simulations using CIVA-UT [47] were performed to evaluate the differences in reference amplitude possible due to differences in acoustic properties of various steel bridge base metal grades. This study involved (1) development of benchmarked CIVA material models based on experimental test results by Crowley and (2) CIVA modeling of various probes and incidence angles to develop recommendations for AWS D1.5 in order to limit the amplitude differences between the calibration block and test object. The benchmarked material models include those representing the extreme cases of ultrasonic attenuation (i.e., Grade 36 and Grade 100W) noted during the experimental testing by Crowley along with other common grades of base metal and IIW-type calibration block materials. Additional simulations were also performed to evaluate the effect of variations in shear wave velocity found during the experimental testing of TMCP processed steels. These simulations were used to develop recommendations for AWS D1.5 to account for variations in shear wave velocity.

The experimental testing by Crowley included various grades of bridge base metals and four different NGI-ESW welds, but did not measure the attenuation of submerged arc welds (SAW).

Therefore, additional experimental testing was performed on four SAW welds to compare the attenuation of ultrasound passing through SAW weld metal and/or HAZ. These results were compared to the attenuation of ultrasound passing only through the base metal. This experimental testing was performed using similar machined specimens with SDH reflectors as the testing performed by Crowley, but supplemental testing was performed using pitch-catch ultrasound to compare with the pulse-echo results.

The experimental testing by Crowley included a machined specimen in both the rolled and transverse to rolled direction of one heat of TMCP plate. Significant differences were noted in these orthogonal directions. JIS Z 3060 [13] notes that the measurement of the shear wave velocity of the test object should account for the velocity in the same orientation with respect to the rolled direction that will be used for the inspection. If the velocity varies in the rolled and the transverse to rolled direction and testing will be performed in an oblique orientation compared to these directions, JIS Z 3060 requires that the calculation of the refraction angle (i.e., shear wave velocity) in the test object in the oblique scanning direction be computed using the pitch-catch technique. In order to evaluate the effect of inspection in an oblique direction of acoustic anisotropic material, additional experimental testing was performed on a machined specimen with an orientation of 45° to the rolled direction. This specimen was fabricated from the same heat of steel as the rolled and transverse to rolled direction specimens tested by Crowley. In addition, pitch-catch inspection was performed on this heat of steel in various scanning orientations to evaluate the effect of scanning TMCP processed steels in other orientations with respect to the rolled direction.

Finally, the variation of the shear wave velocity at different locations of the same heat of steel was evaluated by measuring the shear wave velocity in the rolled and transverse to rolled direction using a normal incidence shear wave probe. This testing was performed on a few different plates to measure the typical standard deviation in shear wave velocity for various processing methods. This testing included some grades of steel which were not evaluated by Crowley in order to document the shear wave velocity of additional grades of bridge steel.

5.2 Benchmarking CIVA Models

The parametric modeling using CIVA relies on benchmarking of attenuation models when simulating the acoustic characteristics and behavior of the various grades of bridge steels. The experimental data on ultrasonic testing of bridge base metals by Crowley [7] were used for benchmarking models in CIVA which replicate the physical material attenuation tests performed using the 5 MHz PAUT probe and the 2.25 MHz PAUT and conventional UT probes. The CIVA models were benchmarked against the physical results for three grades of bridge steel: (1) historical 1970's Grade 36 steel, (2) modern A709-50 steel, and (3) modern A709-HPS 100W steel. These steels represent the full range of material attenuation found during the physical testing from highest attenuation for Grade 36 to least attenuation for Grade 100W. This process not only helped with determining what material attenuation parameter to use in future CIVA models, but also helped to instill confidence in the accuracy of CIVA-UT to replicate physical testing. The process of determining what CIVA material attenuation parameter would minimize the error compared with the experimental results was repeated for each probe, specimen, and analysis type (2D or 3D).

Inputs for the CIVA models include exact probe and wedge specifications, specimen geometry, phased array settings, and probe location while varying the material attenuation parameter. During the analysis, the probe is scanned along the length of the specimen to sweep the ultrasonic beams through the side-drilled hole (SDH) reflectors, as shown in Figure 5.1.

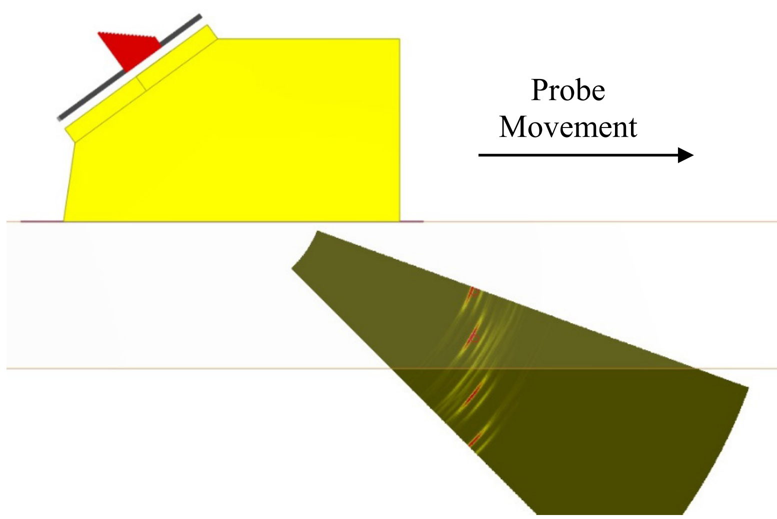

Figure 5.1 S-scan Output from CIVA Analysis Superimposed on Specimen

CIVA outputs amplitude data with 0 dB referenced as the highest amplitude signal in the entire analysis. In other words, there will always be a 0 dB signal in every scan analysis unless a post-processing calibration is applied to the data. Therefore, the drop in amplitude for a sound beam at a specific incidence angle as the sound path increases from various depth SDH reflectors was used to compare the CIVA analysis with the physical testing. This comparison is independent of any angle correction applied to the physical testing from the sensitivity calibration and can be easily obtained from the CIVA analysis.

The maximum amplitude for the 45°, 60°, and 70° beams were tabulated for each SDH and each probe to compare the drop in amplitude along the beam with the physical test results. The experimental data for 5 MHz PAUT probe and 2.25 conventional UT probes included skips off of the backwall of the specimens which increased the sound path to better capture the material attenuation. This experimental data was not available for 2.25 MHz PAUT probe.

CIVA allows for 2D or 3D modeling of the sound beam. In the 2D model, the probe and reflector are analyzed as only a strip along the centerline of the probe. In this model, the length of flaws perpendicular to this strip is not accounted for which could lead to overestimating the amplitude of small rectangular flaws compared with a long SDH. The 3D models are used when it is necessary to analyze the full surface of the probe and reflector. However, as expected these models take significantly more time to run than 2D models. Both 2D and 3D benchmarked models were performed for each probe and material combination.

The 2D CIVA results for the 5 MHz PAUT probe are compared with the experimental results for the Grade 50 specimen in Table 5.1. The material attenuation parameter was varied until the error in the results was minimized. As seen in Table 5.1, the CIVA results match well with all error in results within +/- 1 dB. The 3D CIVA results for the 5 MHz PAUT probe are compared with the experimental results for the Grade 50 in Table 5.2. Once again, the CIVA results match well with all error in results within +/- 1 dB.

Table 5.1 Comparison of 2D CIVA Results to Experimental Results for 5 MHz PAUT on Grade 50 Specimen

	45° Beam		60° Beam		70° Beam	
SDH Depth	**Exp. (dB)**	**CIVA (dB)**	**Exp. (dB)**	**CIVA (dB)**	**Exp. (dB)**	**CIVA (dB)**
0.6"	0	0	0	0	0	0
1.0"	2.3	2.3	4.3	4.3	5.5	5.7
1.0" Half Skip	5.6	5.8	8.6	8.8	NA[1]	NA
0.6" Half Skip	8.9	8.3	11.8	12.0	NA[1]	NA

[1]Could not collect data due to interference of other holes along the sound path

Table 5.2 Comparison of 3D CIVA Results to Experimental Results for 5 MHz PAUT on Grade 50 Specimen

	45° Beam		60° Beam		70° Beam	
SDH Depth	**Exp. (dB)**	**CIVA (dB)**	**Exp. (dB)**	**CIVA (dB)**	**Exp. (dB)**	**CIVA (dB)**
0.6"	0	0	0	0	0	0
1.0"	2.3	2.5	4.3	4.5	5.5	6.1
1.0" Half Skip	5.6	5.8	8.6	8.4	NA[1]	NA
0.6" Half Skip	8.9	8.3	11.8	12.1	NA[1]	NA

[1]Could not collect data due to interference of other holes along the sound path

The results for all of the 3D CIVA analyses for each probe are summarized in Figure 5.2. The CIVA material attenuation parameter at the center frequency of the probe (i.e., 2.25 MHz or 5 MHz) is plotted for each grade of steel and each probe. The 5 MHz PAUT probe shows a large difference in material attenuation amongst the various grades of steel with the attenuation parameter decreasing from 1.85 dB/in for the Grade 36 specimen to 0.9 dB/in for Grade 50 and 0.33 dB/in for the Grade 100W specimen. The 2.25 MHz probes had lower material attenuation than the 5 MHz probe. The material attenuation for the 2.25 MHz probes were very similar for the Grade 50 and Grade 100W specimens. The 2.25 MHz probes attenuation parameters were approximately 0.5 dB/in for the Grade 36 specimen and 0.14 dB/in for Grade 50 and Grade 100W specimens. It is apparent from this plot that use of a 2.25 MHz probe will greatly decrease the error resulting from using calibration blocks which do not have the same acoustic attenuation as the test object.

The results for all of the 2D CIVA analyses are summarized in Figure 5.3. The same trends from the 3D analyses were apparent during the 2D analysis, but the 2D results had higher material attenuation than the 3D results. This is likely due to the 3D CIVA analysis accounting for the beam spread in the width direction of the specimen which further decreases the amplitude as sound progresses along the sound path. While the trend for each probe is largely the same and just shifted to higher values of attenuation, the shift in attenuation for each probe was not the same. For instance, the 5 MHz PAUT probe shifted by approximately +0.30 dB/in, the 2.25 MHz PAUT probe shifted by approximately +0.50 dB/in, and the 2.25 MHz conventional UT probe shifted by approximately +0.20 dB/in.

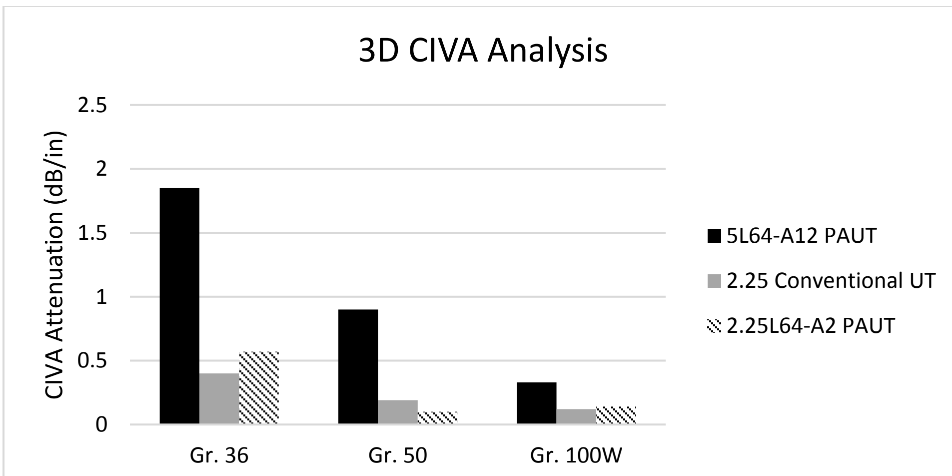

Figure 5.2 Summary of 3D CIVA Material Attenuation Models

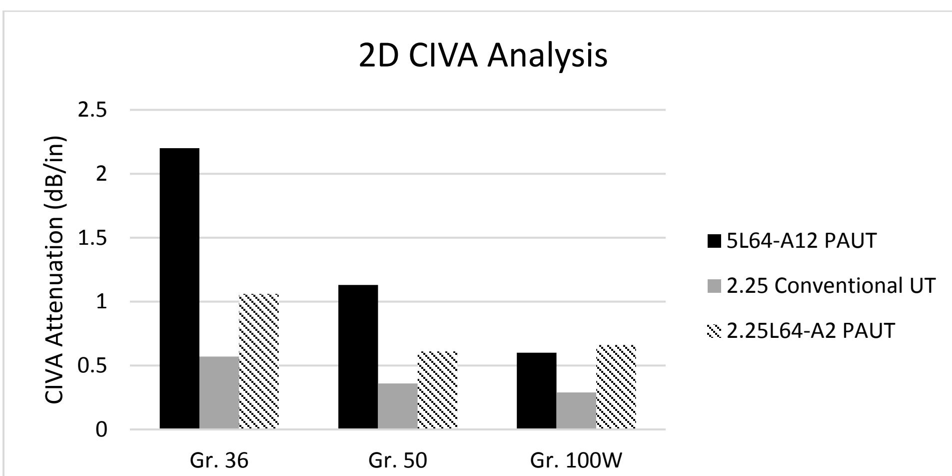

Figure 5.3 Summary of 2D CIVA Material Attenuation Models

The material attenuation of a typical AISI 1018 IIW-type block has also been evaluated experimentally. Due to the increased thickness of the calibration block and limited length of the block, skipping off of the backwall was not possible. Therefore, an additional 1.5 mm (0.06”) diameter SDH was drilled at 1” deep to provide additional experimental data along with flipping the block over to provide a data point at 3.4” depth from the 0.6” deep SDH. Due to the limited experimental data, an estimation of the material attenuation was assumed for the 1018 IIW-type calibration block by comparing the experimental data with the Grade 50 and 100W blocks results. This assumption was then verified through CIVA models and it was found that the drop in amplitude was within +/- 2 dB of the experimental results, which is a reasonable correlation.

Based on these results, material attenuation parameter models shown in Table 5.3 were developed for the parametric CIVA models for various grades of bridge base metals and a 1018 IIW-type calibration block. These parameters were used to model the effect of calibrating on one material and then scanning a material with very different attenuation. From this table, it seems that there is a negligible difference from the Grade 50 block to the Grade 100W block and 1018 IIW-type calibration block for the 2.25 MHz probes while there is a noticeable difference between these blocks for the 5 MHz probe. Therefore, use of a 2.25 MHz probe would greatly aid in diminishing the effects of varying amounts of material attenuation found in bridge steels.

Table 5.3 CIVA Material Attenuation Parameters

CIVA Attenuation Parameter at Probe Center Frequency (dB/in)								
Probe	Gr. 36		Gr. 50		Gr. 100W		1018 IIW-type	
	2D	3D	2D	3D	2D	3D	2D	3D
5 MHz	2.20	1.85	1.13	0.90	0.60	0.33	0.94	0.70
2.25 MHz	0.82	0.49	0.49	0.15	0.48	0.13	0.48	0.15

5.3 Probe Parameters and Material Attenuation CIVA Models

A parametric simulation program using CIVA-UT evaluated the effects of variations in the probe parameters such as frequency, number of active elements, and active aperture (element pitch and element elevation). These factors affect the focal point of the sound beam (i.e., near field distance) as well as the material attenuation. The near field distance is the location of the focal point of the sound beam as shown in Figure 5.4. The data shown in the figure are for a beam computation in

CIVA for a 2.25 MHz AWS conventional UT probe with a 70 degree wedge. It is preferred to keep the focal point of the probe close to the inspection zone to aid in flaw detection. A good rule of thumb is to keep try to keep most of the inspection zone over a range of one-half to three times the near field length.

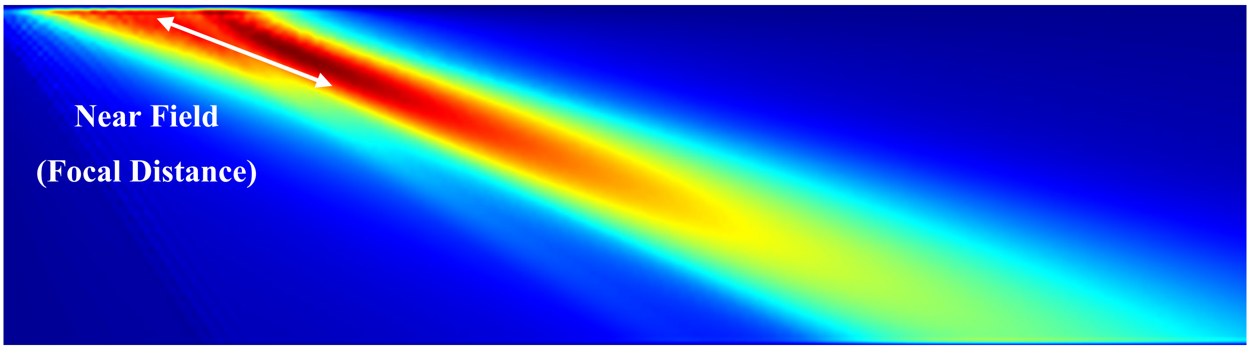

Figure 5.4 2.25 MHz AWS Conventional UT Probe 70° Sound Beam from CIVA

Based on the experimental attenuation testing and the benchmarked CIVA models, it is apparent that a 2.25 MHz probe would be more appropriate to limit the effects of attenuation than the 5 MHz probe which is typically used for PAUT inspection of bridge welds. Therefore, an evaluation was performed to determine whether a standard 2.25 MHz probe would potentially have the optimal parameters for typical butt weld inspections.

The near field length of 2.25 MHz PAUT probes was computed, and it was found that a 1 mm pitch and a 16 mm element elevation would generally be preferable for a 2.25 MHz probe with 16 active elements (i.e., active aperture of 16 mm (0.63") x 16 mm (0.63")) since the near field would be 1.8" of sound path after accounting for a typical wedge thickness. Use of only 16 active elements was chosen as most PAUT equipment in industry can only fire 16 elements at a single time (i.e., maximum single group). This aperture and frequency was also recommended by outside probe suppliers after they performed independent CIVA analysis. This aperture and frequency correlates perfectly with the size of the standard 2.25 MHz AWS conventional UT probe which has an aperture of 0.63"x0.63" or 0.63"x0.75". This does not seem like a coincidence, as it is much more likely that the standard AWS probe was selected to have a focal point near the typical inspection zone. Therefore, a 2.25 MHz probe with this active aperture when firing 16 elements was the starting point for the parametric study. While this aperture is preferable for 2.25 MHz probes used on a typical plate thickness for bridge welds (i.e., 0.75” to 2”), other probe apertures or frequencies may be preferable for welds on very thick or very thin plates. Typically, higher frequencies are necessary for inspection of very thin plates due to the increased resolution. Due to the short sound paths for inspection of thin plates, differences in material attenuation would also be minimal.

The matrix of probe parameters included in the CIVA parametric study is shown in Table 5.4. The focus of the parametric study was spent on the 2.25 MHz frequency. However, 5 MHz was also evaluated since this was the probe frequency used for all of the round robin testing. 2 MHz and 2.5 MHz frequencies were also included to evaluate the effect of the actual center frequency being slightly different than specified values. The actual center frequency for PAUT probes are typically required to be within +/- 10% of the specified frequency. Active probe aperture sizes were chosen based on near field calculations, standard probe availability, and recommended probe apertures given in JIS Z 3060 [13] for conventional UT.

Table 5.4 Probe Parameter Parametric Matrix

Frequency (MHz)	16 Element Aperture (mm)	32 Element Aperture (mm)
2.25	10x10, 16x16	24x24
2, 2.5	16x16	-
5	10x10	-

The 2, 2.25, and 2.5 MHz 16x16 mm aperture PAUT probes and the 5 MHz 10x10 mm PAUT probe were modeled in CIVA for the various base metal attenuation parameters given in Table 5.3 (i.e., Grade 36, 50, 100W, and 1018 for the IIW-type block) since this covered all of the probe frequencies of interest. The 2.25 MHz 10x10 mm and 24x24 mm aperture PAUT probes were modeled in CIVA for just the 1018 IIW-type block material in order to compare with the 2.25 MHz 16x16 mm aperture probe. This allowed for a comparison of the effect of modifications to the probe aperture.

The models involved placing 1.5 mm diameter (0.06”) SDHs at various depths as shown in Figure 5.5 and evaluating the difference in amplitude between the test object of a certain grade and the 1018 IIW-type calibration block for the same depth and incidence angle. This data was used to develop recommendations of probe parameters and calibration procedures to account for the error in amplitude due to differences in base metal attenuation. It should be noted that even with optimal probe parameters, the recommendations for AWS included a requirement that physical testing be performed to verify and account for the specific test specimen material attenuation before performing PAUT inspection.

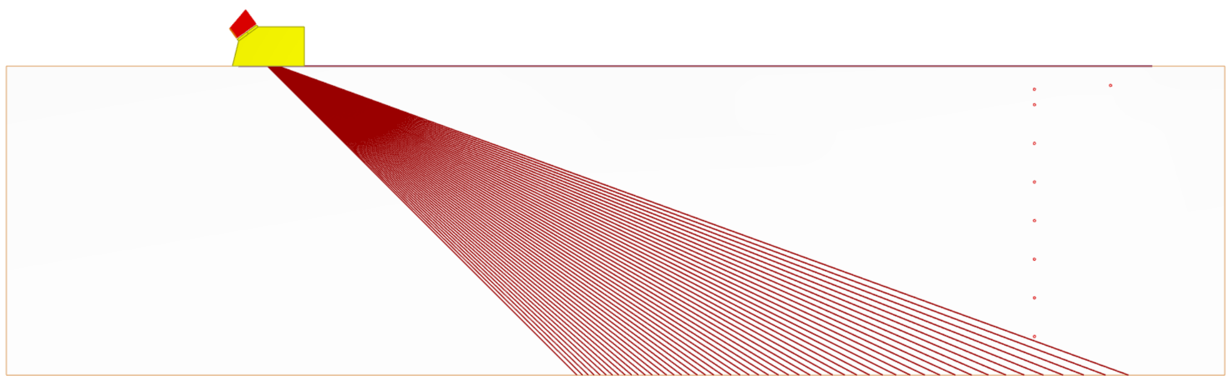

Figure 5.5 Probe Parametric SDH Model

The effect of variation in the shear wave ultrasonic velocity was also captured during this parametric simulation program. This factor affects the refraction angle of the sound beam and greatly diminishes the amplitude of sound beams at high refraction angles due to interference from the second critical angle (i.e., refraction of the shear wave along the surface). Therefore, both the probe parameters and the refraction angle affect the amplitude of the indication response, and recommendations are necessary to provide limits of probe parameters and scanning procedures in order to control inspection variability.

As noted in prior research [21], [22], variation of ultrasonic velocity has been noted with TMCP processed bridge steels. For instance, standard ultrasonic velocity for shear waves in steel is ~0.127 in/µs (~3230 m/s) while ultrasonic velocity for TMCP steels has been measured during the experimental testing of up to 0.133 in/µs (3374 m/s) in the rolled direction. While this variation may seem small, it is very significant at high incidence angles since the amplitude of the sound at these angles is greatly diminished. As noted in Chapter 1, previous research [22] has noted that the velocity on the surface of the plate may be higher than the velocity in the middle of the plate due to the TMCP processing. These researchers noted that a thin layer on the surface was found to have higher velocity than the measured velocity of the entire plate, which is an average velocity through the thickness.

To illustrate the effect that the velocity has on the amplitude of the sound beam, the beam profile of a standard 5 MHz PAUT probe with an incidence angle range of 45-70° was modeled in CIVA for three conditions: (1) test specimen velocity matching the standard velocity of 0.127 in/µs (3230 m/s) (Figure 5.6), (2) test specimen velocity of 0.133 in/µs (3374 m/s) constant throughout the thickness (Figure 5.7), and (3) a thin layer of 0.135 in/µs (3440 m/s) velocity on the surface while the rest of the thickness of the plate has a velocity of 0.133 in/µs (3374 m/s) (Figure 5.8). It is apparent that a significant amplitude drop occurs at high incidence angles for increases in shear wave velocity which must be accounted for when determining which incidence angles to use during the scanning procedures.

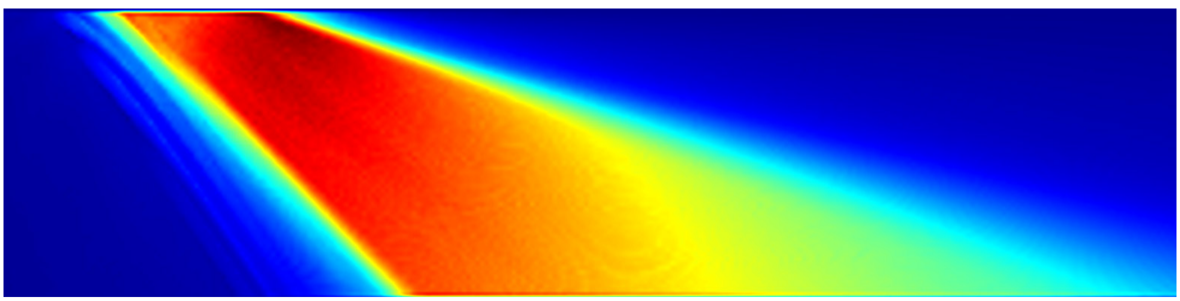

Figure 5.6 PAUT Sound Beam with Standard Velocity (0.127 in/µs)

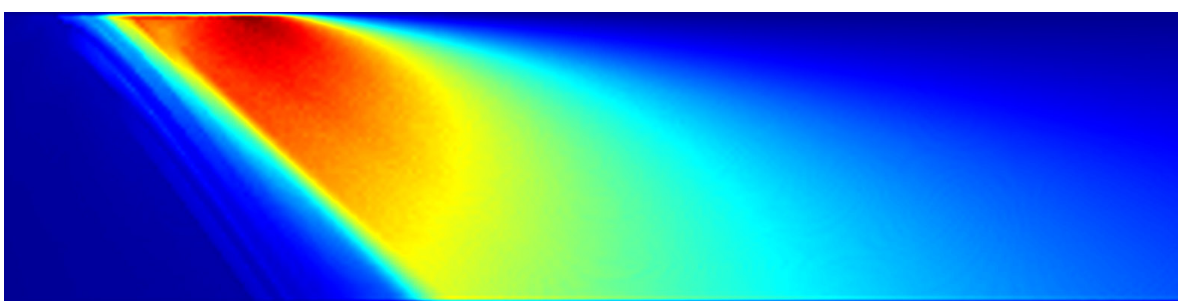

Figure 5.7 PAUT Sound Beam with TMCP Average Velocity (0.133 in/µs)

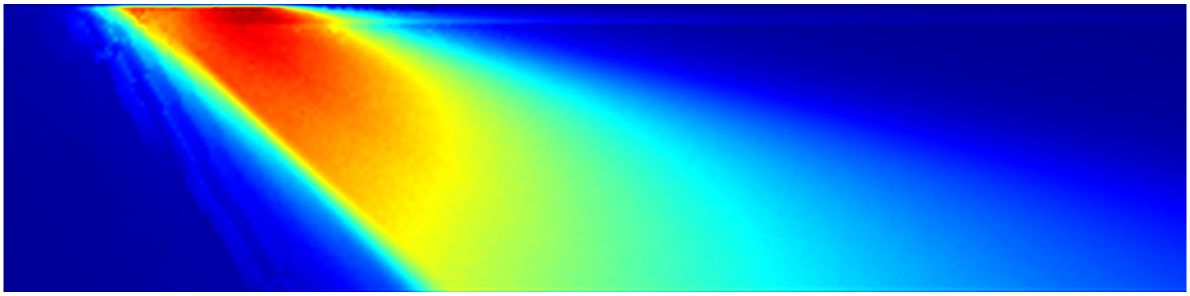

Figure 5.8 PAUT Sound Beam with 0.135 in/μs Layer on Top

It is very important to note that this phenomenon is present for both PAUT and conventional UT. Therefore, ultrasonic testing of TMCP plates (*where the velocity of a shear wave is significantly different than typically assumed as discussed above*) when using a 70° conventional UT probe could result in (1) a significant reduction in the amplitude which would diminish the likelihood of detecting and also rejecting a flaw and (2) error in locating flaws. Use of a 70° conventional UT probe is required for conventional UT in accordance with AWS D1.5 for testing of plates through 4" thickness, which would encompass basically all bridge butt welds. In fact, supplemental angles of 45° and 60° are not required by AWS D1.5 until the plate exceeds 3.5" thick unless the weld is not ground smooth, which is not common in modern bridges. The effect on conventional UT could result in a worse condition than testing with PAUT where other incidence angles are available. Therefore, it can be expected that conventional UT inspection of some current and historical welds in TMCP plate may have had decreased sensitivity to flaw detection and rejection. Plots for a 2.25 MHz AWS conventional UT probe with a 70° refraction angle is shown in Figure 5.9 - Figure 5.11. The effect of the change in shear wave velocity is obvious.

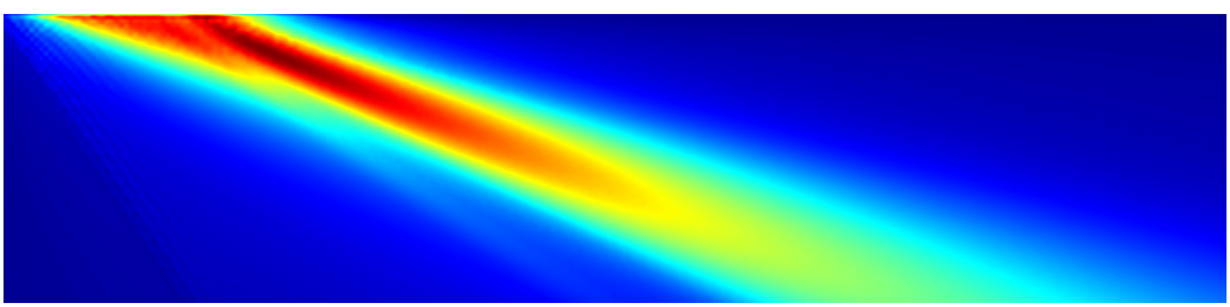

Figure 5.9 Conventional UT Sound Beam with Standard Velocity (0.127 in/μs)

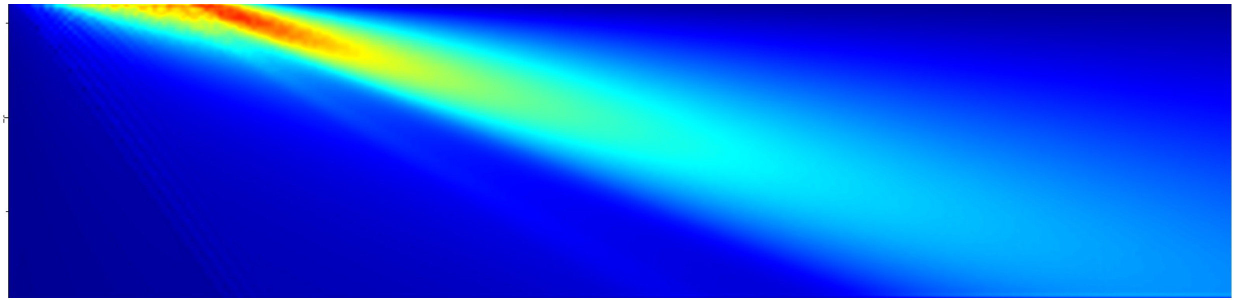

Figure 5.10 Conventional UT Sound Beam with TMCP Average Velocity (0.133 in/µs)

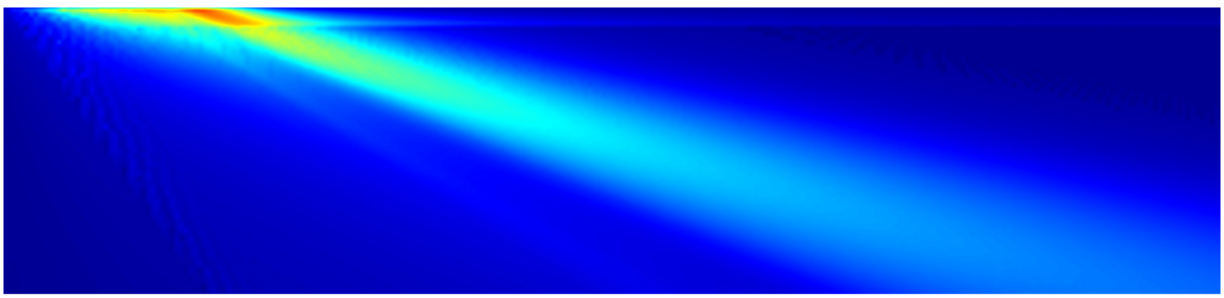

Figure 5.11 Conventional UT Sound Beam with 0.135 in/µs Layer on Top

The Japanese UT code, JIS Z 3060 [13], includes many references to the issue of mismatched ultrasonic velocity between the calibration block and the test object. For an ultrasonic velocity of 0.133 in/µs (3374 m/s) in the test object, JIS Z 3060 would only allow an incidence angle of up to 66° for up to 3" thickness and up to 61° over 3" thickness, where the incidence angle (i.e., wedge geometry) is based on the standard calibration block velocity.

The ultrasonic shear wave velocity measurements from the TMCP plates were modeled in CIVA to quantify the drop in amplitude across the standard incidence angle range of 45-70° and along various sound path distances by evaluating the amplitude of standard SDH reflectors. This data was used to develop simplified recommendations for PAUT scanning procedures to account for the error in amplitude due to velocity differences of TMCP steels. Based on the experimental velocity measurements by Crowley, the material velocity used in the following plots was 0.133 in/µs (3374 m/s). While the 0.133 in/µs (3374 m/s) shear wave velocity represents the worst case TMCP plate from the three samples which were tested experimentally by Crowley, it may not represent the worst-case TMCP plate that a mill may produce. The experimental attenuation measurements by Crowley for the 45° incidence angle in the TMCP plate were not largely affected by the change in shear wave velocity and had similar amplitude as the Grade 50 measurements. Therefore, Grade 50 material attenuation parameters were used to model TMCP base metals in CIVA.

Figure 5.12 displays the difference in amplitude due to different material attenuation or material velocity of the test object and calibration block for a SDH at the same depth and incidence angle scanned with a 2.25 MHz 16x16 mm aperture PAUT probe. In this plot, the amplitude from the SDHs in the 1018 IIW-type calibration block is used as reference, with the difference in amplitude for SDHs in other materials plotted along the Y-axis and the depth of the SDH from the surface along the X-axis. If the plates were acoustically equivalent the plot would be equal to 0 dB at all depths. For the 2.25 MHz probe, the Grade 100W and Grade 50 plates are nearly acoustically equivalent to the 1018 IIW-type calibration block model. The amplitude from the SDHs in the Grade 36 specimen were lower than the amplitude in the 1018 calibration block resulting in a negative change in amplitude (i.e., loss of amplitude for the reflector in the test object). This is expected due to the increased attenuation of the Grade 36 CIVA material attenuation model at 2.25 MHz compared with the 1018 IIW-type calibration block specimen.

This plot was used to determine the maximum sound path without incurring a significant amplitude difference from the calibration block. For instance, many codes require the amplitude of the calibration block and test object to be within +/-2 dB at the longest sound path used for the inspection before a correction is necessary (i.e., transfer correction). The Grade 36 block crosses this limit at 2” depth for 60° and 70° incidence angles or at 3” depth for a 45° incidence angle. Therefore, correction for the material attenuation will still be necessary for 2.25 MHz probes when testing objects with high material attenuation.

As expected, the TMCP model is very sensitive to the incidence angle. At a 45° incidence angle, the amplitude difference only exceeds 2 dB at 7” depth. At a 60° incidence angle, the amplitude difference exceeds 2 dB at 1” depth, but then it starts to level off so that it is within 4 dB at 7” depth. At a 70° incidence angle, the amplitude difference is -6.6 dB at a 0.5” depth and increases up to -10 dB at a 7” depth, indicating that this angle is almost entirely ineffective at scanning. This demonstrates that the amplitude of SDHs in TMCP plates may even be affected beyond a reasonable level (i.e., greater than 2 dB loss of amplitude) at a 60° incidence angle. While not shown on the plot, the 2.25 MHz conventional UT 70° incidence angle was also computed for the TMCP model and the amplitude difference was -7.6 dB at a 0.5" depth and increased to -11.4 dB at a 3" depth before leveling off. Therefore, the drop in amplitude due to the shear wave velocity difference of the TMCP plate was even worse for 2.25 MHz conventional UT than 2.25 MHz PAUT.

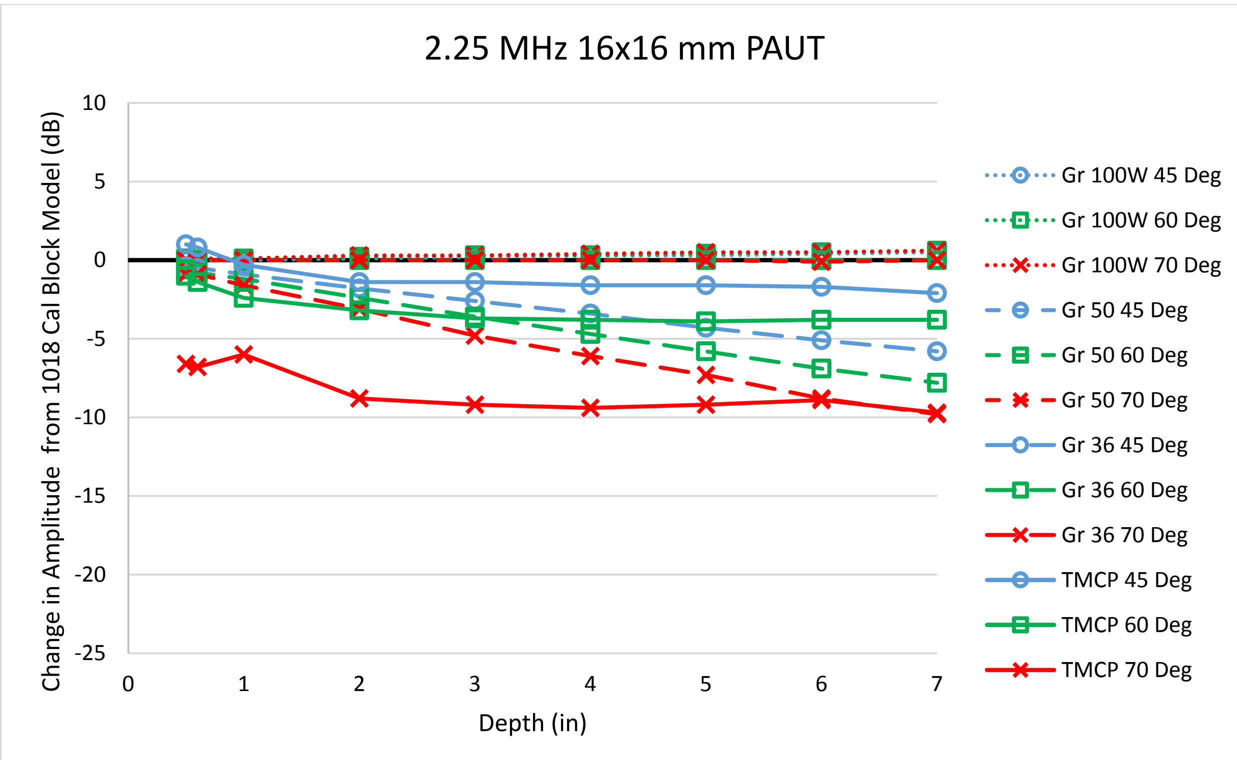

Figure 5.12 Amplitude Difference from 1018 Steel for 2.25 MHz 16x16 mm PAUT

Figure 5.13 and Figure 5.14 show the results using a 2 MHz and 2.5 MHz 16x16 mm aperture PAUT probe, respectively. These plots demonstrate the amplitude difference if the actual center frequency of a 2.25 MHz 16x16 mm PAUT probe was slightly different than the specified value. It was found that the Grade 100W and Grade 50 models were still acoustically equivalent through the 7" depth, but a slight increase in the amplitude difference for the Grade 36 and TMCP model was found for the 2.5 MHz probe. This drops the distance where the amplitude differs by more than 2 dB from the 1018 IIW-type calibration block to 1" depth for 70° incidence angle and 2" depth for 45° incidence angle for the Grade 36 specimen. The distance where the amplitude differs by more than 2 dB was the same in the TMCP specimen for the 2 MHz and 2.5 MHz probes as the 2.25 MHz probe since the velocity issue is not frequency dependent.

Figure 5.15 shows the results using a 5 MHz 10x10 aperture PAUT probe. A significant increase in the amplitude difference was found with the 5 MHz probe when compared with the 2.25 MHz probe. The Grade 100W model provided significantly higher amplitude from the SDH compared with the 1018 IIW-type calibration block model while the Grade 50, 36, and TMCP models all provide lower amplitude from the SDH than in the 1018 IIW-type calibration block model. The depth at which the amplitude differed by more than 2 dB is given in Table 5.5. While the Grade 50 model would still be considered acoustically equivalent to the 1018 IIW-type calibration block, the Grade 100W would only be within 2 dB up to ~2” depth while the Grade 36 and TMCP specimens would differ by more than 2 dB even at 0.5-0.6” depth. Therefore, the attenuation difference between various grades of bridge steels will result in significant calibration error for the 5 MHz probe other than for very thin plates.

Table 5.5 Depth where the Amplitude Difference exceeds 2 dB for 5 MHz Probe

Material Model	**45° Incidence Angle**	**60° Incidence Angle**	**70° Incidence Angle**
Grade 100W	3”	2”	2”
Grade 50	NA	NA	NA
Grade 36	1”	0.6”	0.5”
TMCP	2”	0.6”	0.5”

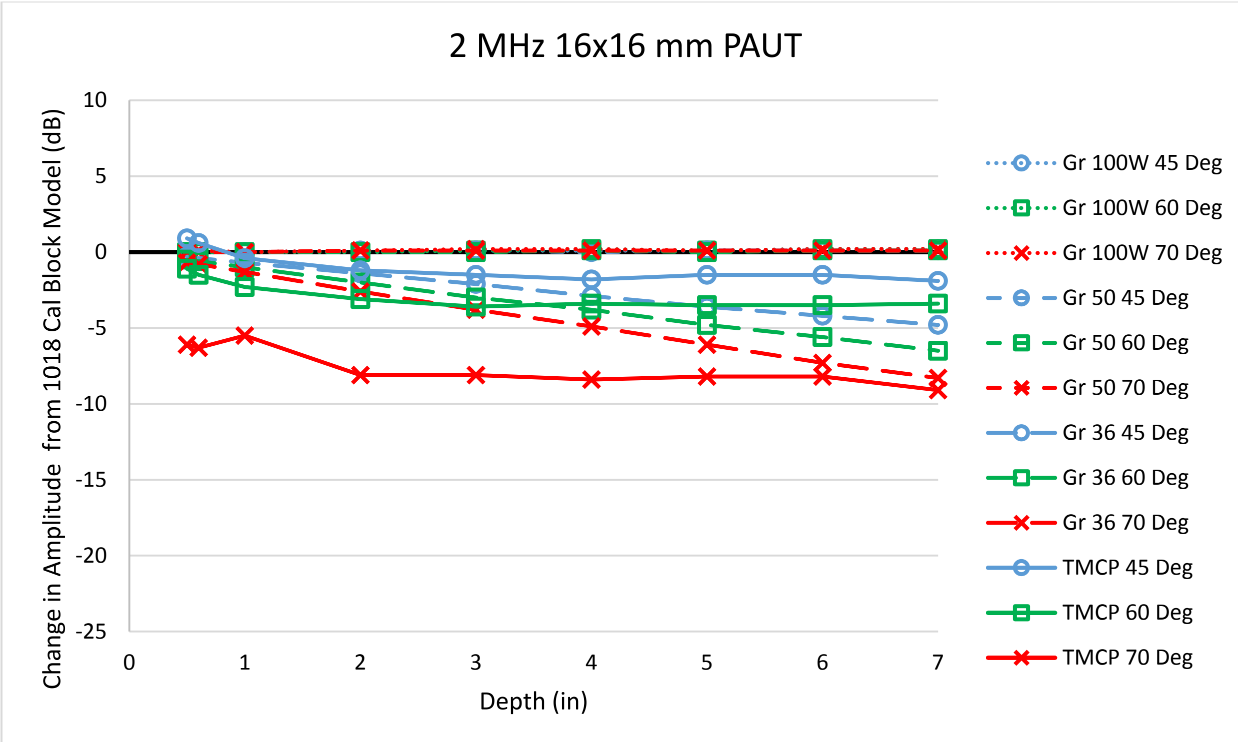

Figure 5.13 Amplitude Difference from 1018 Steel for 2 MHz 16x16 mm PAUT

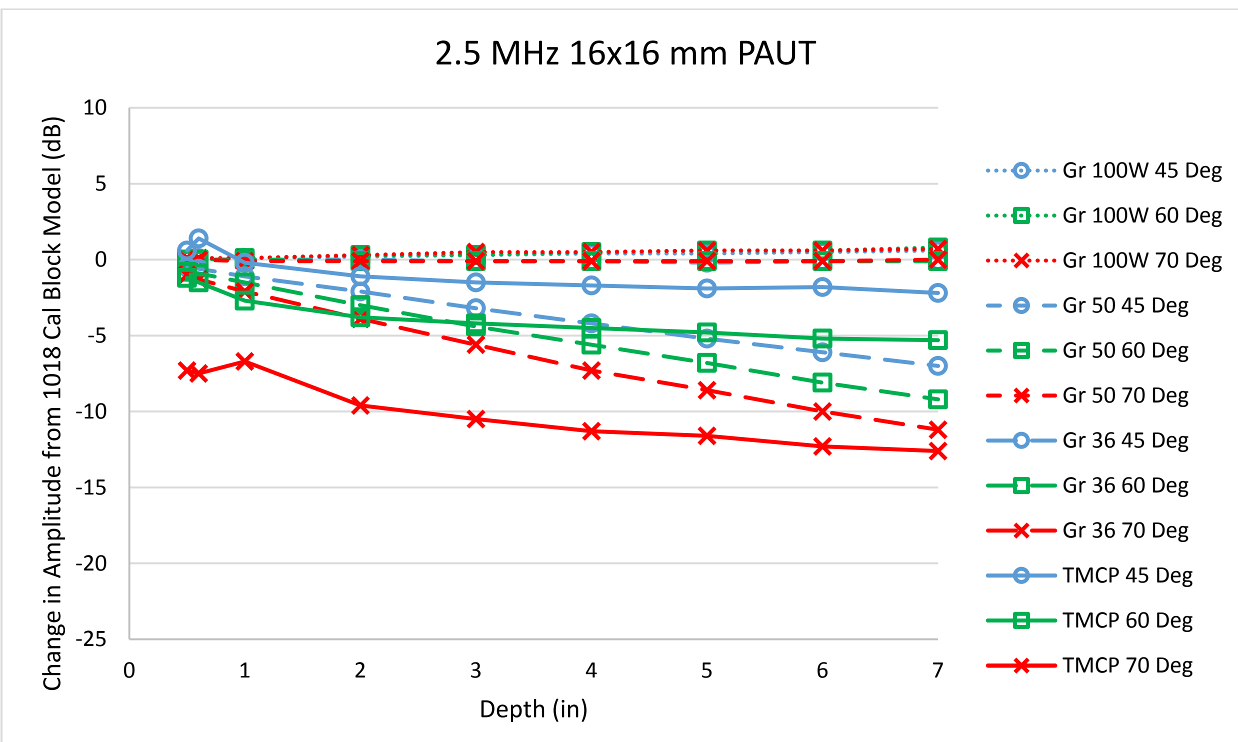

Figure 5.14 Amplitude Difference from 1018 Steel for 2.5 MHz 16x16 mm PAUT

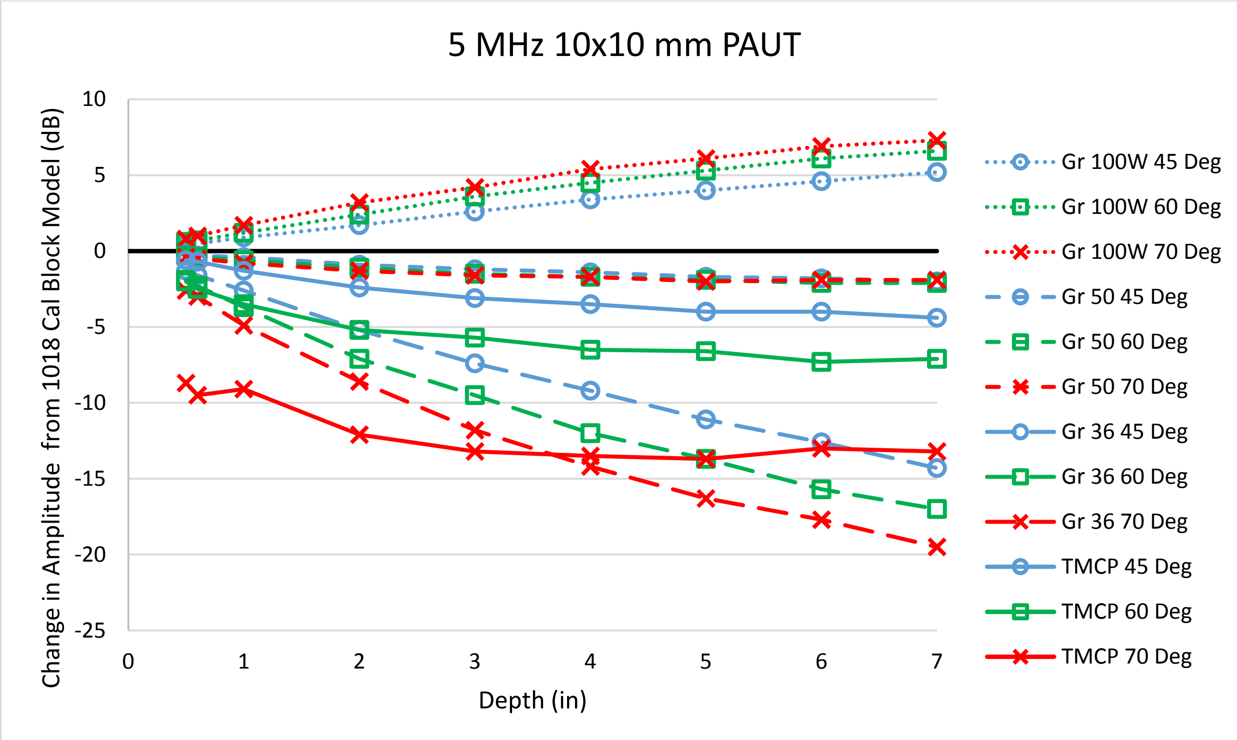

Figure 5.15 Amplitude Difference from 1018 Steel for 5 MHz 10x10 mm PAUT

Additional CIVA analysis was performed in order to identify the limiting velocity difference compared to the standard steel velocity of 0.127 in/µs (3230 m/s) which would result in an amplitude difference of 2 dB or less over a sound path covering 7” depth for the 60° and 70° incidence angles. A velocity increase of 2.5% compared to the standard velocity resulted in an amplitude difference of 2 dB or less across the 40°-60° incidence angles. Therefore, assuming a shear wave velocity of 0.127-0.128 in/µs for the calibration block which is typical for most steels, the 40°-60° incidence angles should be appropriate for plates with velocity of 0.130-0.131 in/µs. Two of the three TMCP samples from the experimental testing by Crowley had a shear wave velocity of 0.130 in/µs or less, and the amplitude difference for these two samples compared to the Grade 50 sample were 2 dB or less at the 60° incidence angle. This correlates well with the CIVA results regarding a recommended limit of 2.5% velocity difference for inspection up to a 60° incidence angle. While limiting the incidence angle range to 40°-60° for inspection of TMCP processed steels will result in much less amplitude error than using 40°-70° and may limit the amplitude error to 2 dB or less for many TMCP processed steels, there may be certain heats of TMCP processed steels where the amplitude loss may exceed 2 dB at the 60° incidence angle.

A velocity increase of 1.0% compared to the calibration block resulted in an amplitude difference of 2 dB or less across the 40°-70° incidence angles. Assuming a shear wave velocity of 0.127-0.128 in/µs, the 40°-70° incidence angles should be appropriate for plates with velocity of 0.128-0.129 in/µs. One of the three TMCP samples from the experimental testing by Crowley had a shear wave velocity of 0.1293 in/µs, and the amplitude difference for this sample compared to the Grade 50 sample (measured shear wave velocity of 0.1274 in/µs) was 2-4 dB at the 70° incidence angle. The velocity of this TMCP sample was 1.5% greater than the Grade 50 sample so a slight increase in sound loss exceeding 2 dB is expected at the 70° incidence angle. While a 1.0% limit on the velocity difference between the calibration block and the test object seems reasonable to limit the amplitude difference to 2 dB or less over the 40°-70° incidence angle range, the actual amplitude difference may exceed 2 dB in some cases. Especially when also including any differences in material attenuation.

The effect of aperture and frequency on the focal point (i.e., near field distance) was captured by measuring the amplitude of the SDH at various depths using the 1018 IIW-type calibration block model. This differs from the figures presented above since the previous figures evaluated the difference of amplitude from SDHs using the 1018 IIW-type calibration block compared with SDHs using the other material models. Rather, the following figures were used to evaluate the beam profile to determine the optimal probe aperture for testing typical bridge welds. For the following figures, the amplitude of the SDHs were normalized so that the maximum amplitude over the entire depth range and angular range (i.e., 45°, 60°, and 70°) was set to 0 dB for each aperture. 2.25 MHz apertures of 10x10 mm, 16x16 mm, and 24x24 mm and a 5 MHz aperture of 10x10 mm were evaluated. The plots for each incidence angle are shown in Figure 5.16 - Figure 5.18.

The focal point for the 2.25 MHz 10x10 mm and 5 MHz 10x10 mm probes is approximately 0.25" depth for 45° and 60° while it is less than 0.25" depth for 70°. While this would be good for very thin plates, the amplitude decreases quickly for thick plates. Rather, the 2.25 MHz 16x16 mm probe had a focal depth of approximately 1" at 45°, 0.35" at 60°, and 0.25" at 70°. As seen in the plots, the amplitude for the 16x16 mm probe does not decrease as quickly as the 10x10 mm probes due to less beam spread at longer depths. Finally, the 2.25 MHz 24x24 mm probe had a focal depth of approximately 2” at 45°, 0.75” at 60°, and 0.35” at 70°. While this probe had the highest amplitude at long depths, it is not appropriate for thin plates due to the large near field effect.

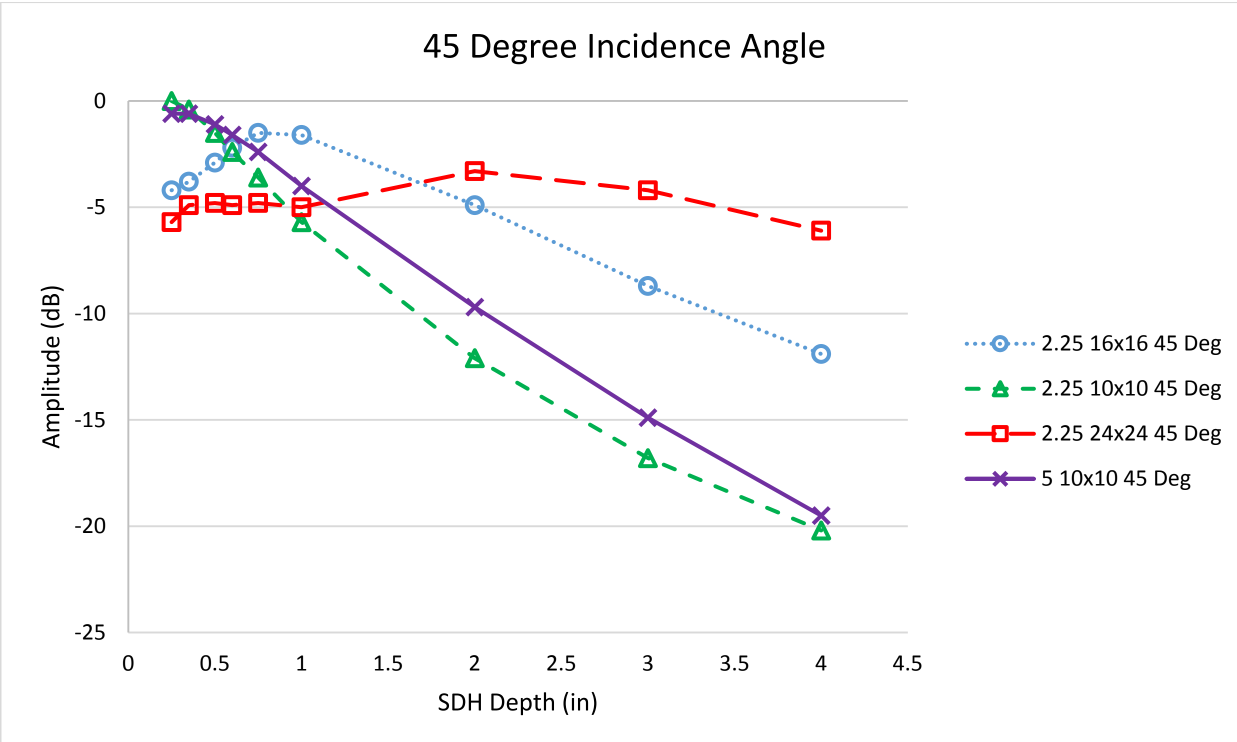

Figure 5.16 Variation in 45 Degree Amplitude due to Aperture/Frequency

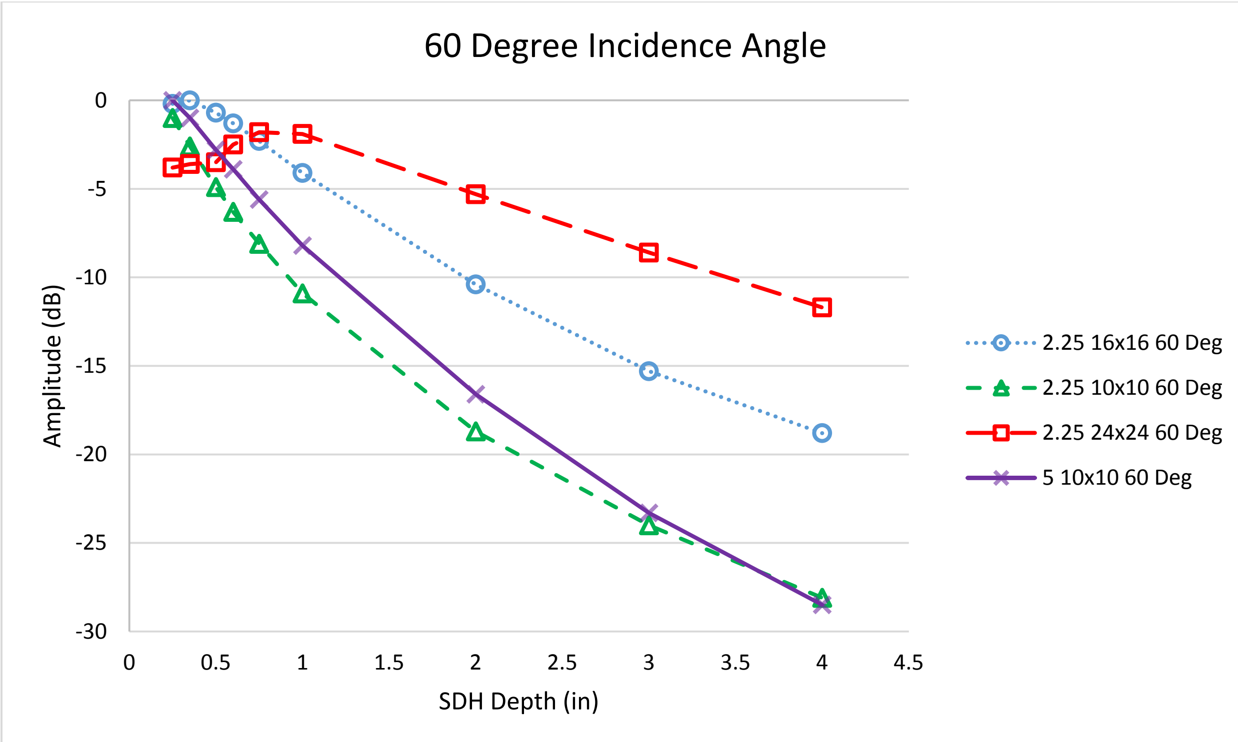

Figure 5.17 Variation in 60 Degree Amplitude due to Aperture/Frequency

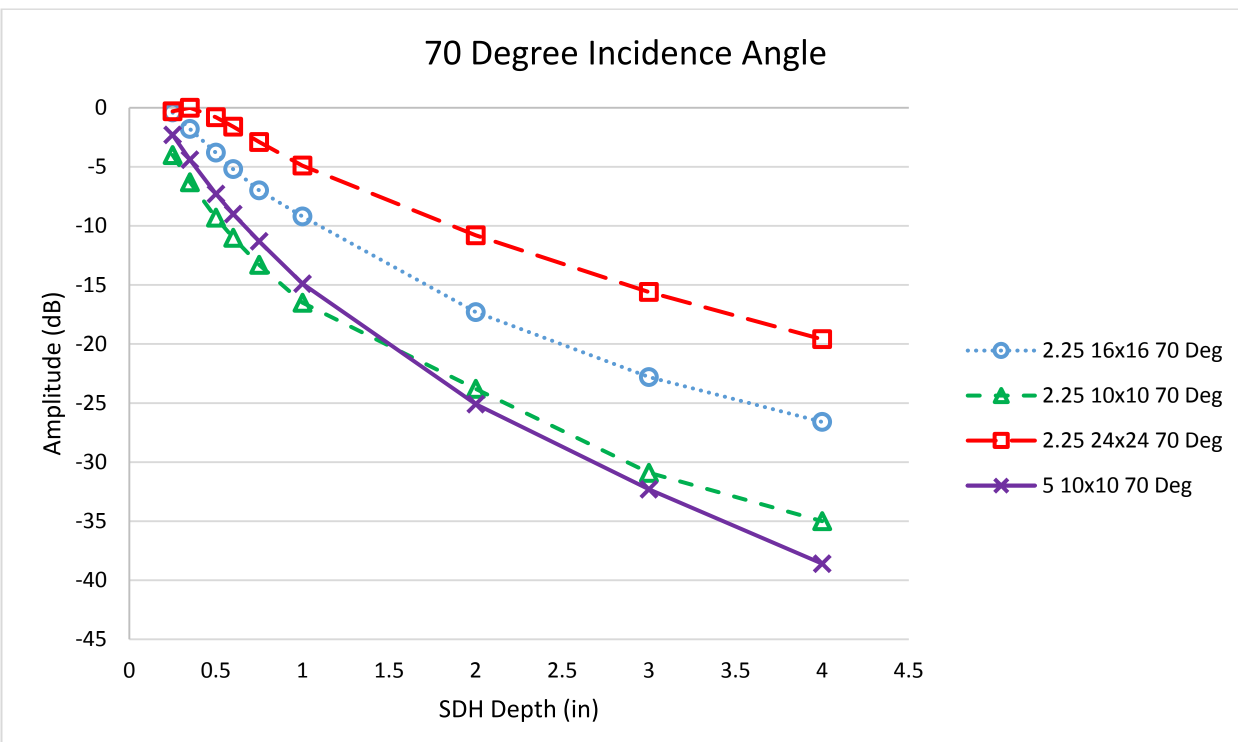

Figure 5.18 Variation in 70 Degree Amplitude due to Aperture/Frequency

The effect of probe frequency and aperture on the beam shape and near field can also be shown using the “cross-sectional” CIVA output plots for each probe at a specific incidence angle. Figure 5.19 shows the CIVA results for a 45° incidence angle for SDHs varying from 0.25” depth to 3” depth for each aperture/frequency combination. While the 10x10 mm apertures have very good resolution of the shallow SDHs, the amplitude drops off quickly for the deeper SDHs due to increased beam spread. The 16x16 mm aperture had fairly good resolution throughout the thickness range. On the other hand, the 24x24 mm aperture had two peak indications for each shallow SDH due to near field effects since the beam has not consistently formed yet.

Based on these results, it seems that that the 16x16 mm aperture is likely optimal for 2.25 MHz probes over the typical bridge CJP thickness range. The 2.25 MHz and 5 MHz 10x10 mm apertures may offer a slight improvement for the inspection of welds less than 0.5” thick, but the amplitude and resolution drop off quickly at longer sound paths, especially at 70° incidence angles. Also, one must keep in mind that, if not properly accounted for, the attenuation of 5 MHz probes can be an issue for thicknesses greater than 0.5”. Therefore, while it seems that 2.25 MHz and 5 MHz small aperture probes (~10x10 mm) may be appropriate for thin welds, the optimal probe to limit the effect of variation in acoustic properties is a 2.25 MHz probe with approximately 16x16 mm aperture. If proper calibration is performed to account for the attenuation, 5 MHz probes may be appropriate for thicker plates as well.

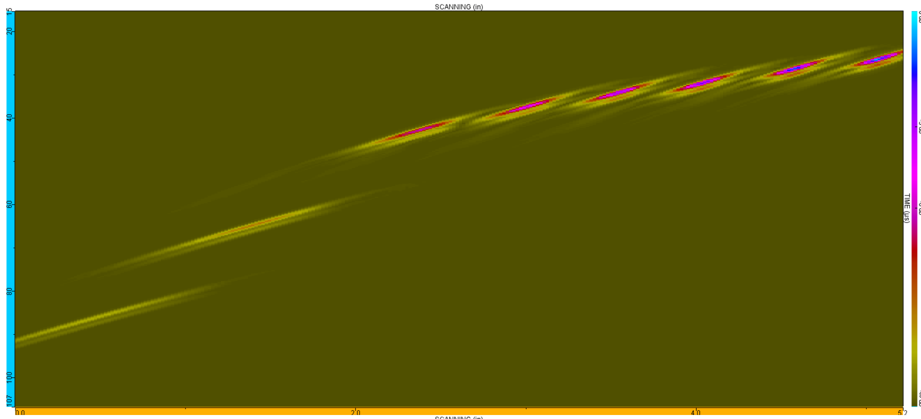

2.25 MHz
10x10 mm

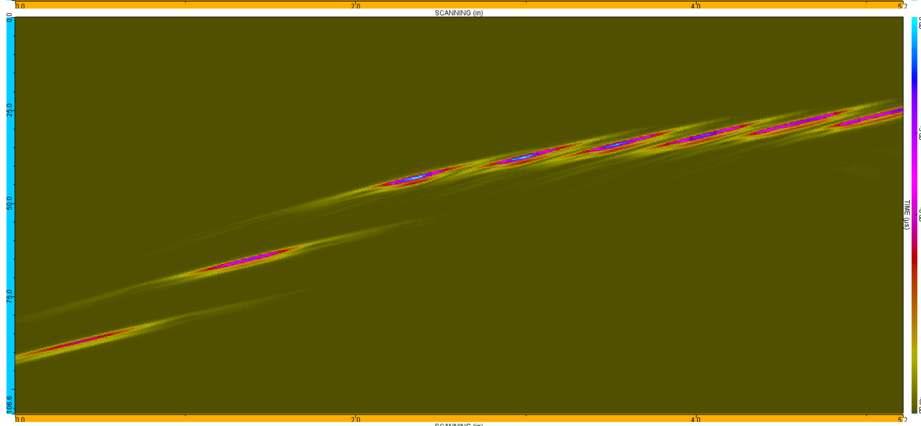

2.25 MHz
16x16 mm

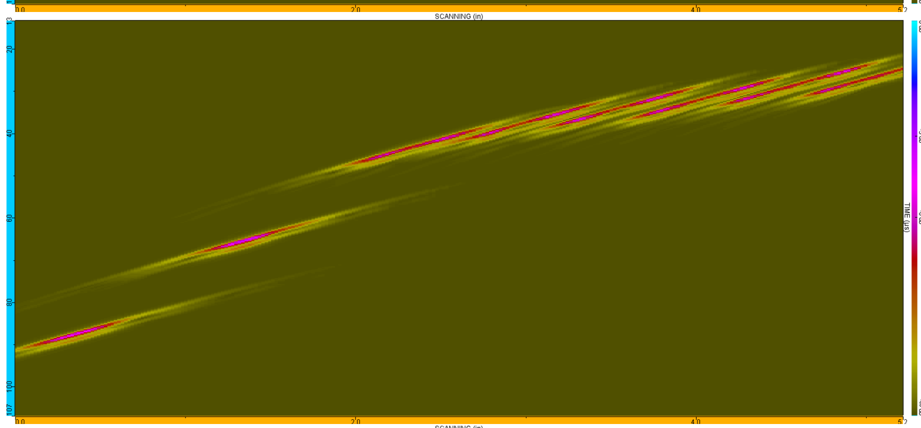

2.25 MHz
24x24 mm

5 MHz
10x10 mm

Figure 5.19 CIVA Results for 45 Degree Beam for 0.25”-3.0” Depth SDH

5.4 SAW Attenuation Testing

5.4.1 Introduction

Experimental testing was performed on four plates with typical bridge CJP SAW butt welds to collect material attenuation results and compare to the material attenuation of the base metal. All four welds were welded by major bridge fabricators and were requested to be fabricated using typical bridge welding practices. Unfortunately, welding procedure specifications (WPSs) were not available for these welds when requested from the fabricators. The details of the SAW welds is given in Table 5.6. All of the welds were two inches thick and included many individual passes to completely fill the weld. It should be noted that SAW welds of other thicknesses or weld parameters may have different attenuation characteristics.

Table 5.6 SAW Attenuation Specimen Details

ID	Weld Bevel	Fabricator	Plate Thickness	Fabrication Year
SAW1	Single-V	A	2”	2018
SAW2	Single-V	B	2”	2018
SAW3	Double-V	B	2”	2018
SAW4	Double-V	A	2”	2018

Two inch wide portions of the welds were cut out from the overall plate including the weld region and were polished and etched in order to determine appropriate placement of 1/16” diameter SDHs to be located in the base metal, HAZ, and weld metal. All SDHs were placed 1” below the top surface of the plate as shown in Figure 5.20. The plates were then machined in order to provide a smooth scanning surface on the top and bottom surface of the plate and a consistent width of 1.89” similar to the specimens used in the experimental testing by Crowley.

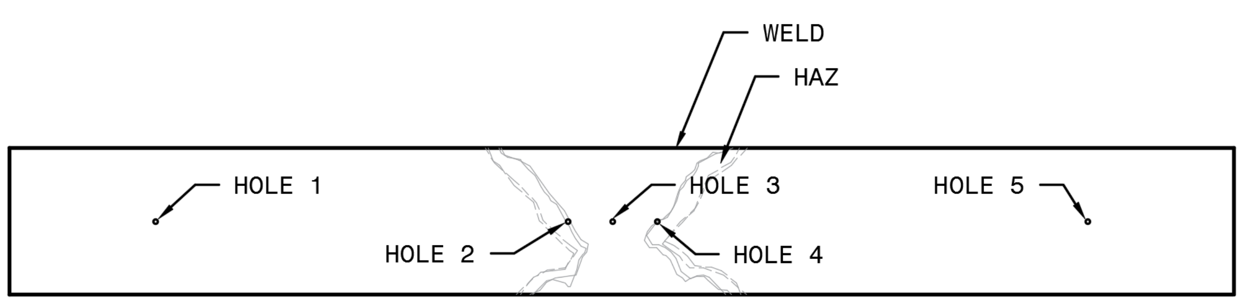

Figure 5.20 Overall SAW Specimen Configuration

Table 5.7 displays the test matrix for the SAW specimens. Initial testing of SAW1 was performed with 2.25 MHz and 5 MHz Zetec PAUT instrument and transducers. Final testing of all SAW specimens was performed using 2.25 MHz conventional UT and 5 MHz PAUT using an Olympus instrument. Each SDH was tested with three different incidence angles, 45°, 60°, and 70°. The SDHs in the weld metal and the HAZ were scanned from both sides (i.e., left and right as shown in Figure 5.20) while the SDHs in the base metal were scanned from only one side due to limited access. The same reference specimen was used for this testing as the experimental testing by Crowley which was the A709 Grade 50 base metal specimen with a SDH at 1" below the surface. The change in instrument gain to bring the indication amplitude to the reference amplitude was documented for each sound path.

The remaining portion of SAW2, SAW3, and SAW4 which were not machined were also tested using the pitch-catch technique using 2.25 MHz conventional UT transducers and the Olympus instrument. All pitch-catch testing used single V path (i.e., one backwall skip) to compare the instrument gain for ultrasound passing only through the base metal to ultrasound passing through the weld in each direction. SAW2 and SAW3 were inspected with pitch-catch using 45° incidence angle while SAW4 was inspected using 45° and 60° incidence angles since this plate was larger.

Table 5.7 SAW UT Test Matrix

Test Sequence-Number	Evaluated Specimens	Reference	Flaw Detector and Probe+Wedge Combination
1-1	1.0" deep holes of SAW1	Block 50 (Side A)	Zetec Topaz with Zetec AXL - 2.25MHz + AXL - 55SW
1-2	1.0" deep holes of SAW1	Block 50 (Side A)	Zetec Topaz with Zetec AM - 5MHz + AM - 55SW
2-1	1.0" deep holes of SAW1, SAW2, SAW3, and SAW4	Block 50 (Side A)	Olympus Omniscan MX2 with Panametrics-NDT C430 2.25 MHz/0.625"x0.625" + GE SF-AWS wedge (45°, 60°, and 70°)
2-2	1.0" deep holes of SAW1, SAW2, SAW3, and SAW4	Block 50 (Side A)	Olympus Omniscan MX2 with Olympus 5L64-A12 + SA12-N55S
3-1	Base Metal and Weld Metal of SAW2, SAW3, and SAW4	NA	Olympus Omniscan MX2 with Pitch-Catch (Tx: Panametrics-NDT C430 2.25 MHz/0.625"x0.625" + GE SF-AWS wedge) (Rx: Panametrics-NDT C430 2.25 MHz/0.625"x0.625" + Panametrics-NDT ABWS-8 wedge)

Test Sequence 1-1, 2-1, and 2-2 were performed similar to the experimental tests performed on the base metal and NGI-ESWs by Crowley with the probe placed in a jig and a ten pound weight centered over the wedge exit point and use of oil couplant. Test Sequence 1-2 was performed by free-hand scanning since the wedge was too small to mount in the jig and tended to tip rather than remain coupled. Test Sequence 3-1 (i.e., pitch-catch) was performed using two methods: (1) a jig was used to mount both probes at a constant probe center spacing and a ten pound weight was centered on the jig and (2) free-hand scanning was performed to allow for variation in the probe center spacing. Test Sequence 3-1 was performed with gel couplant since testing was performed on the remaining non-machined portion of the weld which had a slightly uneven surface. Therefore, oil couplant did not have high enough viscosity.

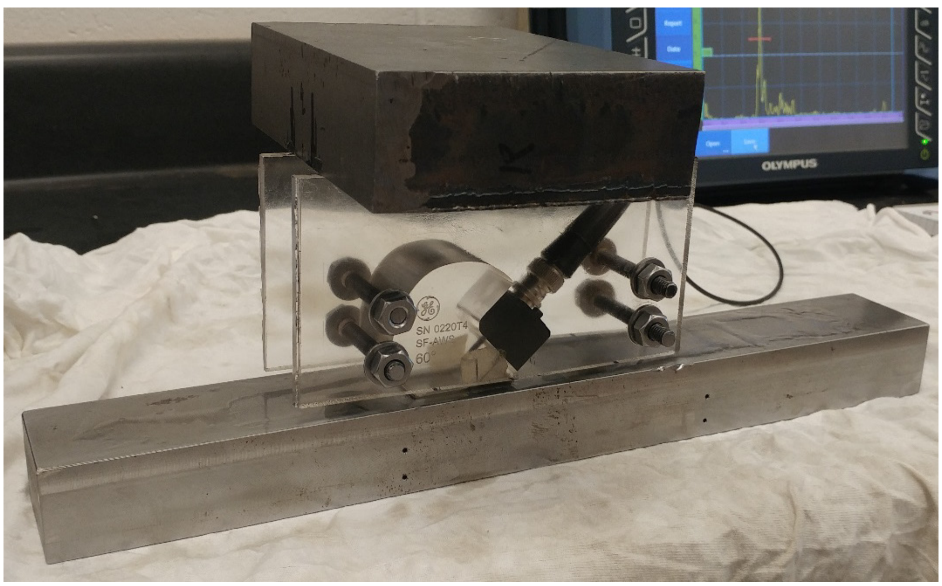

Figure 5.21 Jig used for Test Sequence 1-1, 2-1, and 2-2

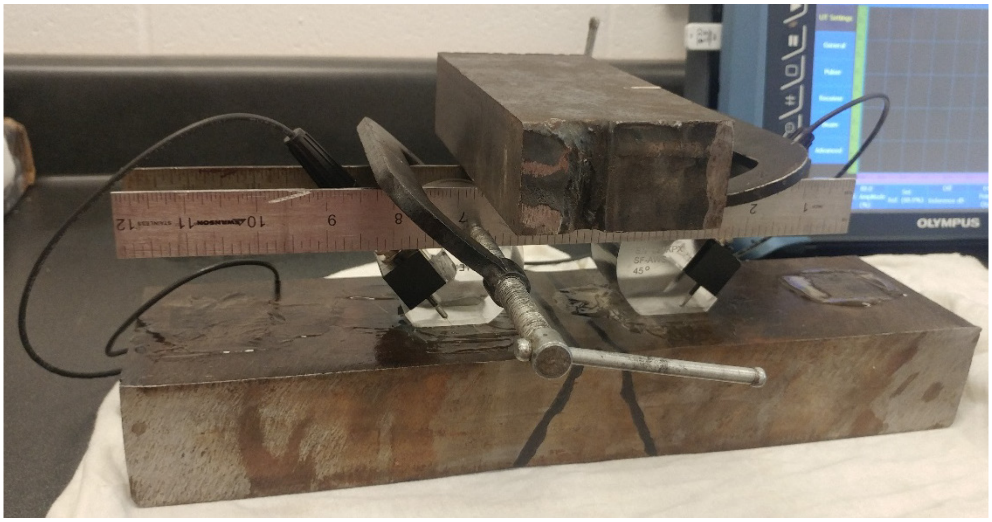

Figure 5.22 Jig used for Test Sequence 3-1

5.4.2 Specimen SAW1

Specimen SAW1 is shown in Figure 5.23 after etching the weld and HAZ region of the machined specimen. The red, green, and blue lines correspond to the sound paths for the 45°, 60°, and 70° incidence angles, respectively. The results for Test Sequence 1-1 through 2-2 are presented with the change in amplitude from the corresponding SDH in the reference specimen divided by the sound path distance (i.e., ΔdB/in) along the Y-axis. This is similar to the attenuation data reported by Crowley for the base metal and NGI-ESW specimens.

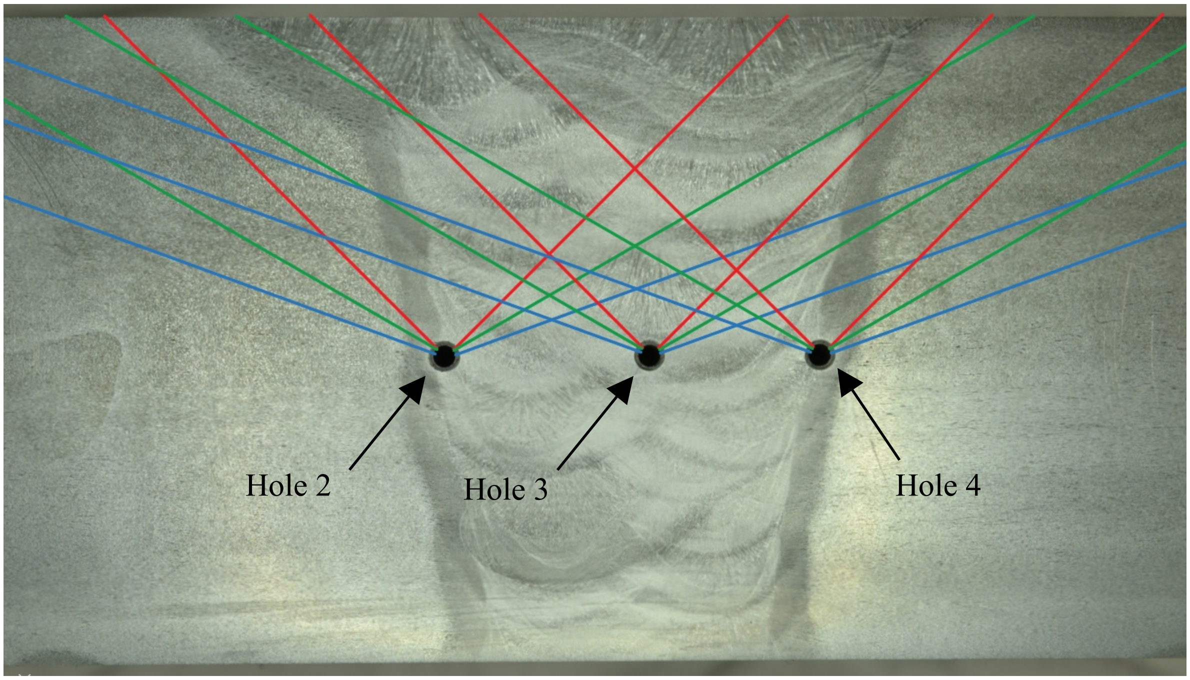

Figure 5.23 SAW1 Weld and HAZ with Sound Paths

The results of Test Sequence 1-1 is shown in Figure 5.24 with the average of the results from testing given as the black circle and the error bars giving the scatter of results for the 45°, 60°, and 70° incidence angles. The results for Hole 2 and Hole 4 are separated into two groups whether the sound originated in the base metal and only propagated into the HAZ (noted as BM) or whether the sound propagated through the weld metal and possibly far side HAZ (noted as WM). The results of Test Sequence 1-2 is shown in Figure 5.25. Unlike the NGI-ESW welds tested by Crowley which had very high attenuation compared to the base metal (i.e., ~+4-6 ΔdB/in), the SAW welds typically had less average attenuation when sound passed through the HAZ and weld metal compared with base metal only. This was seen for both the 2.25 MHz and 5 MHz results. Although the average attenuation decreased when passing through the weld metal, the scatter tended to increase. From Figure 5.23, it is apparent that the portion of the total sound path which passes through the weld metal varies widely for each incidence angle. Therefore, variations in the weld metal result are expected. The orientation of the sound path with relation to the weld metal grain structure also varies widely and, therefore, the amplitude can vary greatly depending on probe position.

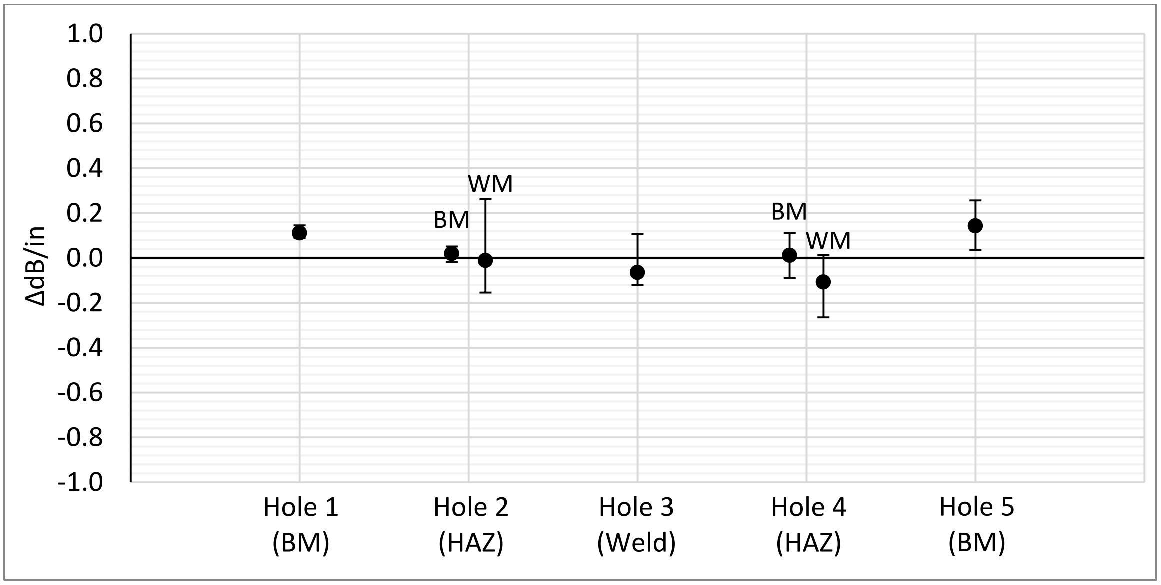

Figure 5.24 SAW1 Combined Results for Test Sequence 1-1

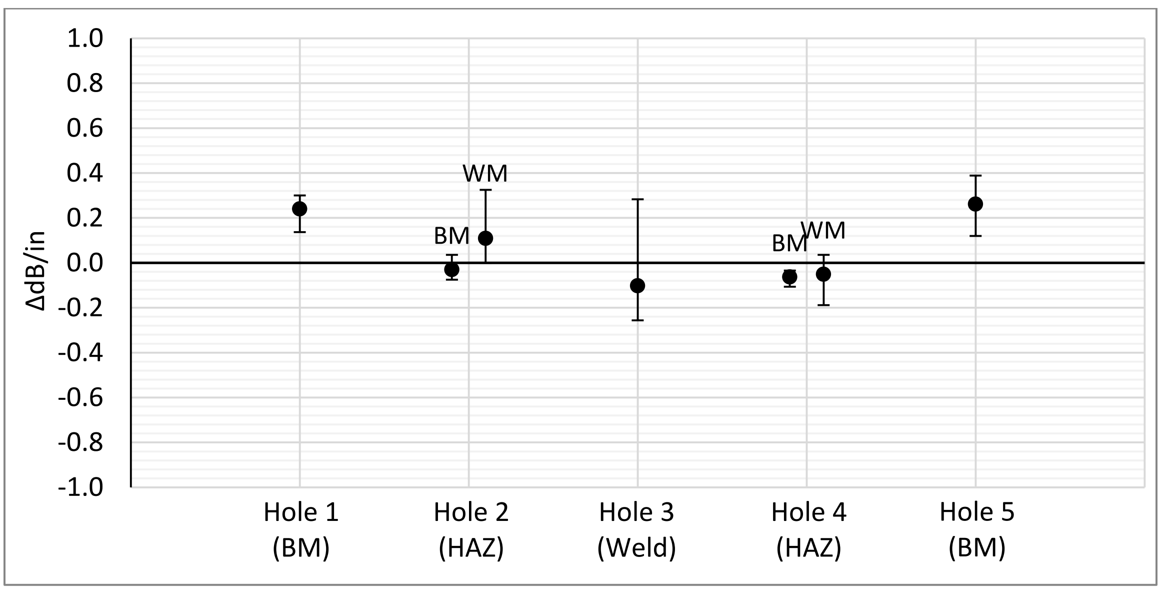

Figure 5.25 SAW1 Combined Results for Test Sequence 1-2

The results of Test Sequence 2-1 are shown in Figure 5.26 for the combination of the individual scans while Figure 5.27 shows the individual results for each incidence angle. The "L" and "R" labels in the individual results correspond to the direction that the sound was propagating with respect to the drawing shown in Figure 5.20 and the weld image shown in Figure 5.23. Therefore, for Hole 2, the data labeled "L" correspond to the "BM" data while those labeled "R" correspond to the "WM" data and vice versa for Hole 4. The results of Test Sequence 2-1 were very similar to the results of Test Sequence 1-1 since both used 2.25 MHz probes. This reinforces the findings from Crowley that the variation in attenuation is mainly affected by the frequency of the probe and that conventional UT and PAUT will give similar results.

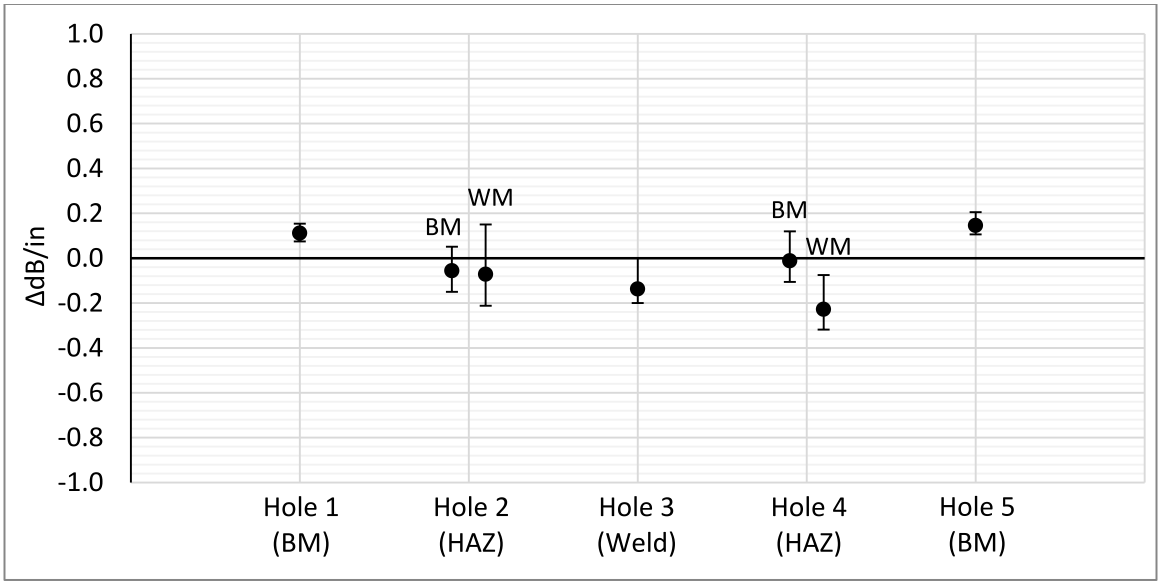

Figure 5.26 SAW1 Combined Results for Test Sequence 2-1

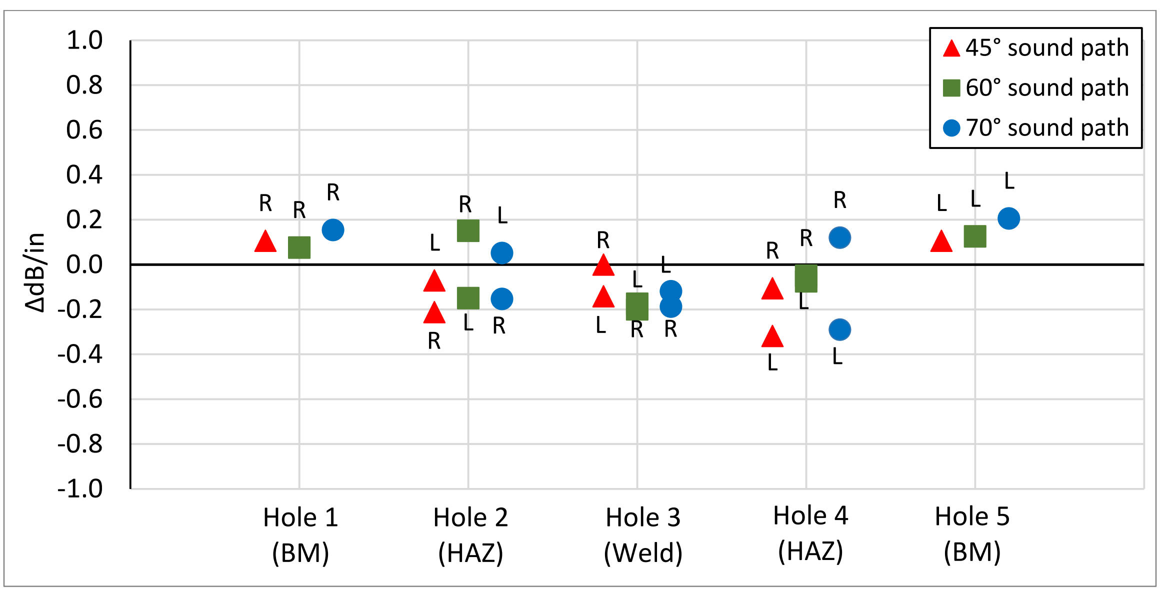

Figure 5.27 SAW1 Individual Results for Test Sequence 2-1

The results of Test Sequence 2-2 are shown in Figure 5.28 for the combination of the individual scans while Figure 5.29 shows the individual results for each incidence angle. Similar to Test Sequence 2-1, the 5 MHz probe used in Test Sequence 2-2 had much more scatter when the sound path propagated through the weld metal compared to the 2.25 MHz probe. In general, the attenuation for sound propagating through the HAZ and weld metal tends to be lower, but this is not always the case. For instance, the 45° sound path from the left side of Hole 3 had the most attenuation. Once again, it should be noted that the difference in attenuation is approximately an order of magnitude less than was measured through the NGI-ESW welds tested by Crowley.

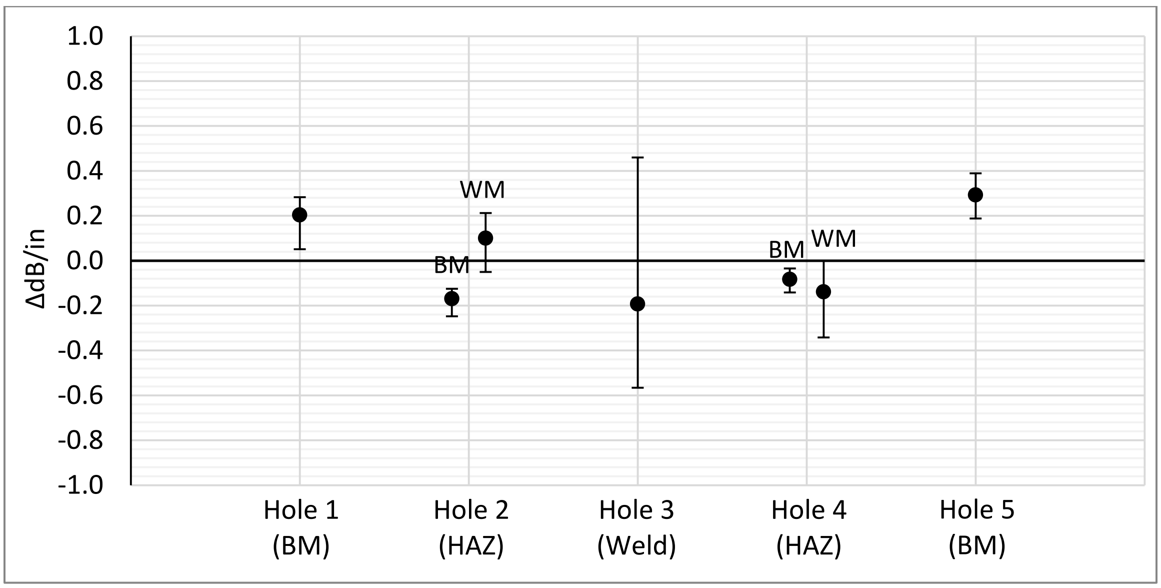

Figure 5.28 SAW1 Combined Results for Test Sequence 2-2

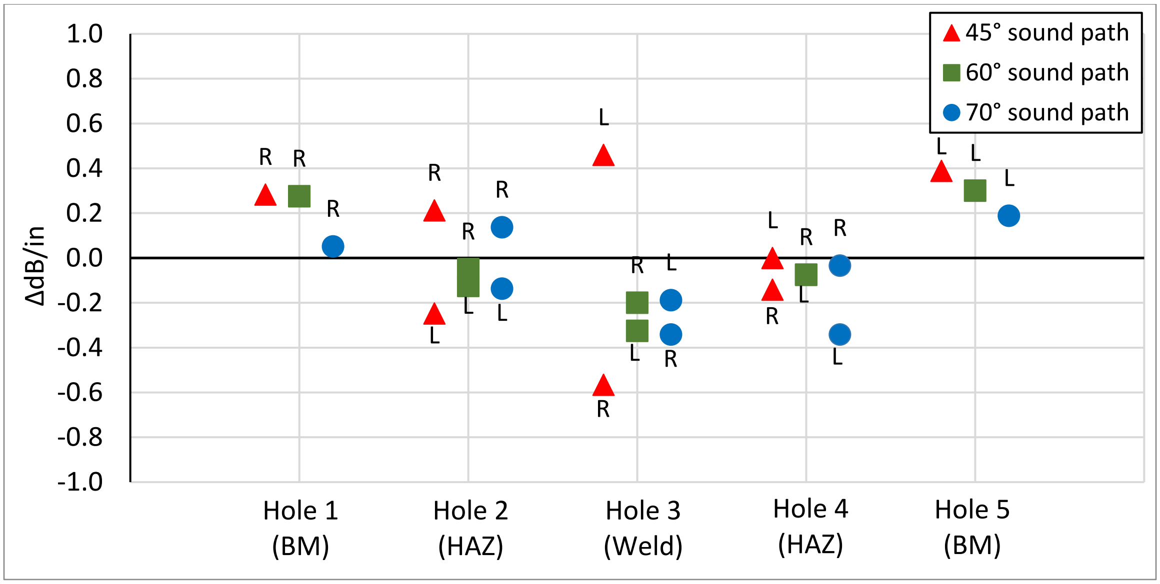

Figure 5.29 SAW1 Individual Results for Test Sequence 2-2

Another way to illustrate the variation in amplitude of ultrasound passing through the weld is to view the S-scan output of PAUT. Since the 1" hole in the Grade 50 specimen was used to set the reference amplitude correction, all of the SDHs should have similar amplitude in the S-scan view, regardless of the incidence angle. Figure 5.30 shows the S-scan view for Test Sequence 2-2 of the SDHs in the HAZ and weld metal for SAW1. Clearly, the amplitude of the middle SDH has the highest amplitude which is the SDH in the weld metal compared with the SDHs in the HAZ on either side of the weld.

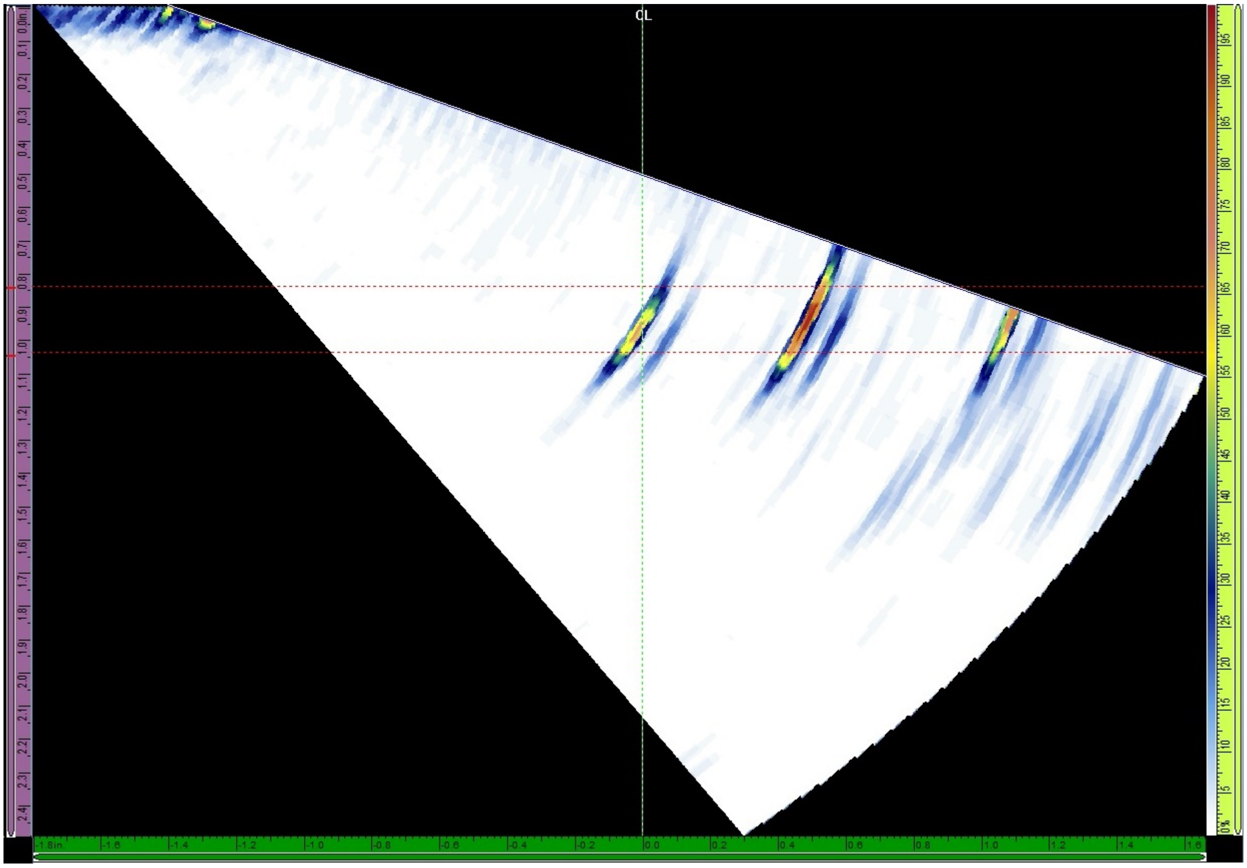

Figure 5.30 PAUT S-scan of SAW1 Weld

5.4.3 Specimen SAW2

Specimen SAW2 is shown in Figure 5.31 after etching the weld and HAZ region of the machined specimen. The results of Test Sequence 2-1 are shown in Figure 5.32 for the combination of the individual scans while Figure 5.33 shows the individual results for each incidence angle. Similar to Specimen SAW1, Specimen SAW2 had decreased average attenuation when sound propagated through the weld metal or HAZ compared to purely propagating through the base metal. It seems that the weld metal is responsible for the decrease more than the HAZ since Hole 2 “WM”, Hole 4 “WM”, and Hole 3 all had the lowest average attenuation.

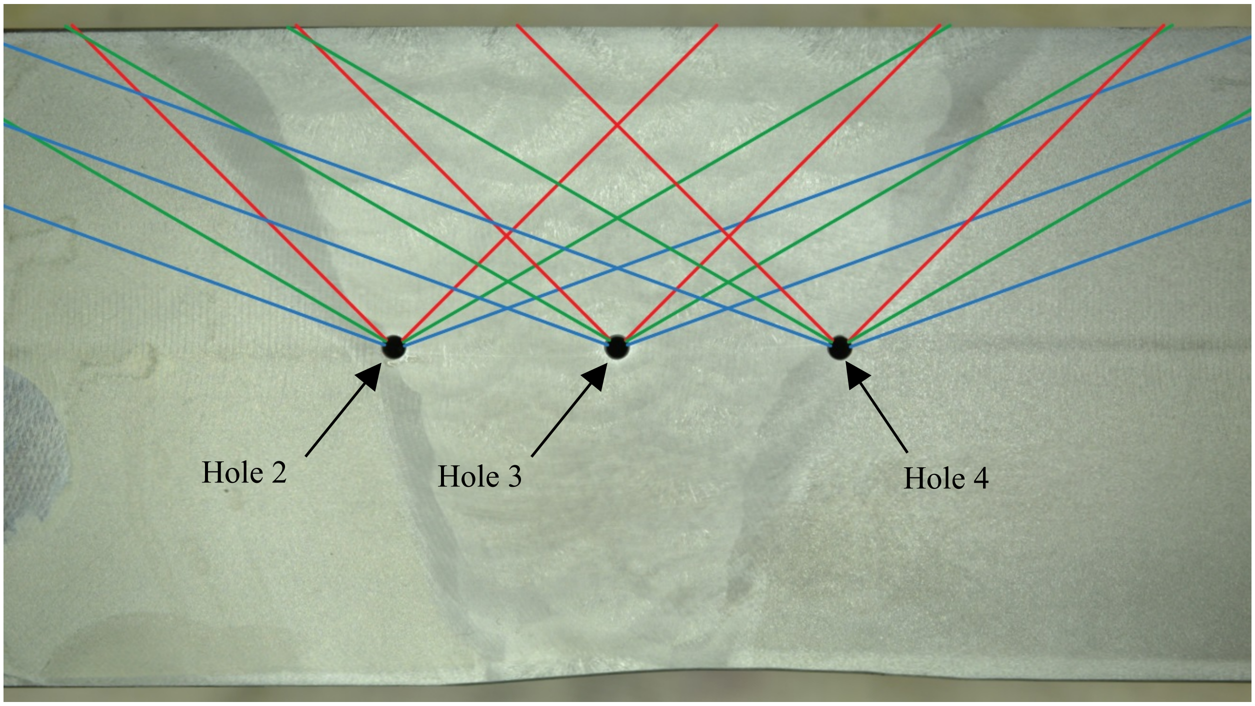

Figure 5.31 SAW2 Weld and HAZ with Sound Paths

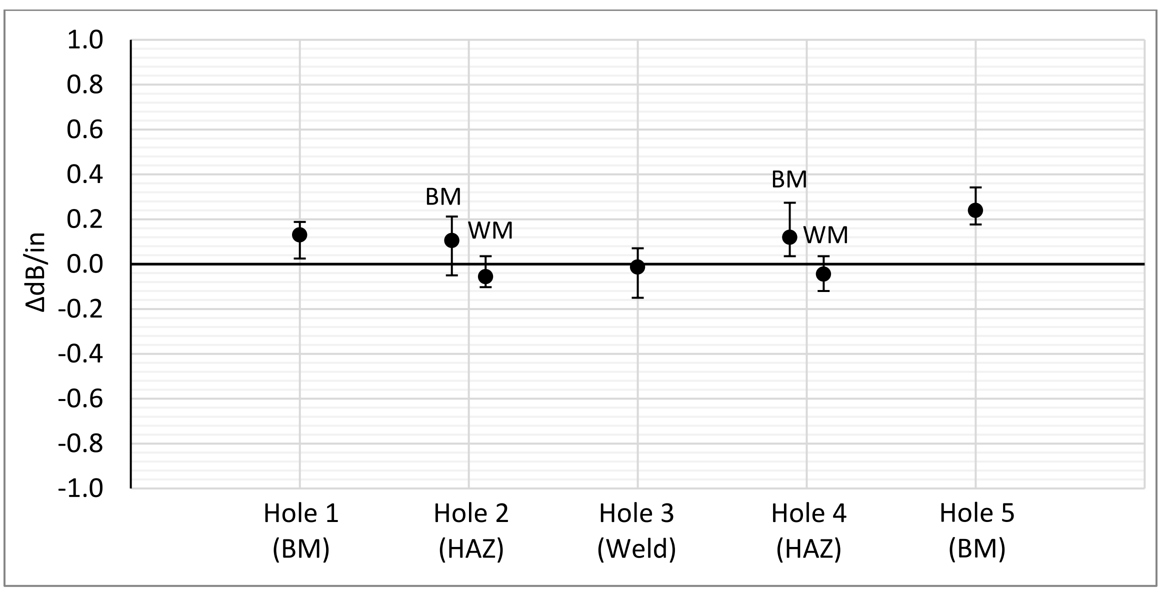

Figure 5.32 SAW2 Combined Results for Test Sequence 2-1

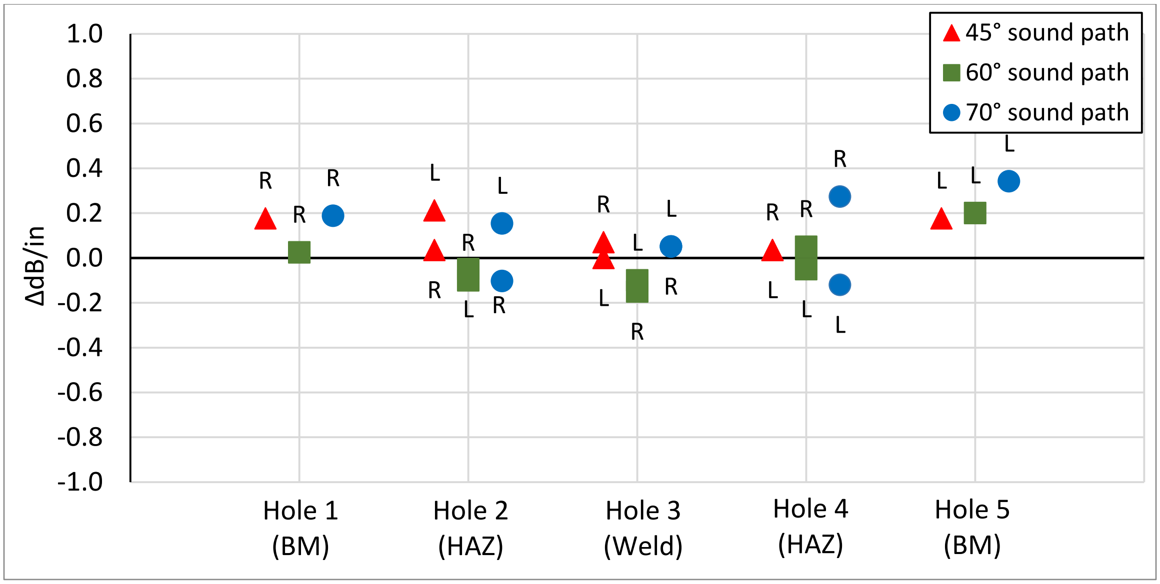

Figure 5.33 SAW2 Individual Results for Test Sequence 2-1

The results of Test Sequence 2-2 are shown in Figure 5.34 for the combination of the individual scans while Figure 5.35 shows the individual results for each incidence angle. The results are similar to SAW1 where use of the 5 MHz probe resulted in larger scatter between individual sound paths while the sound passing through the weld metal or HAZ tended to have decreased average attenuation.

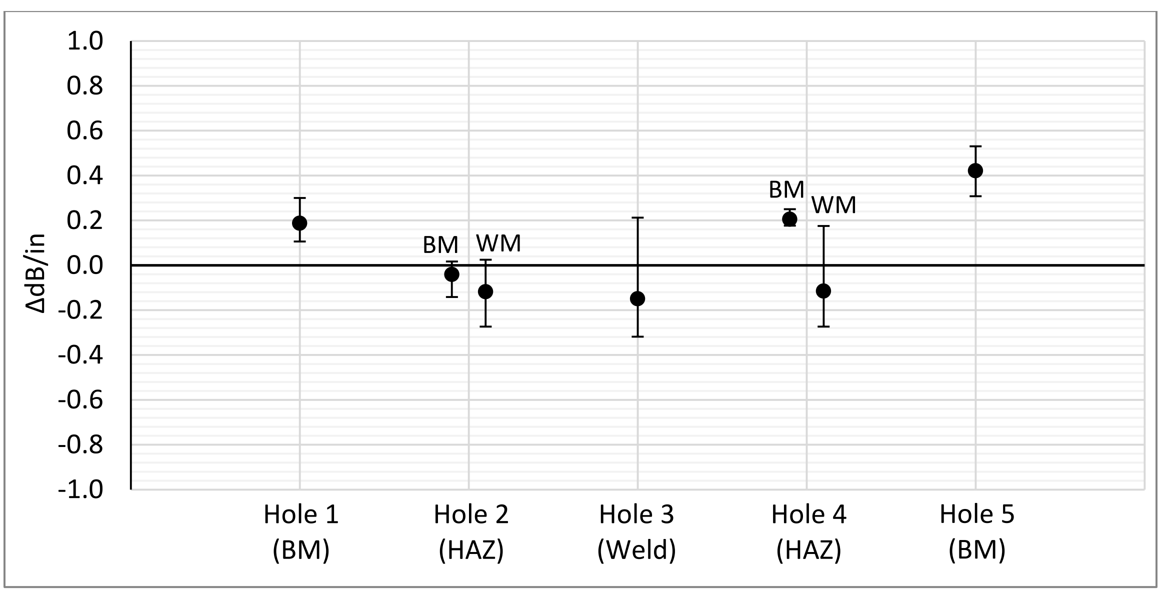

Figure 5.34 SAW2 Combined Results for Test Sequence 2-2

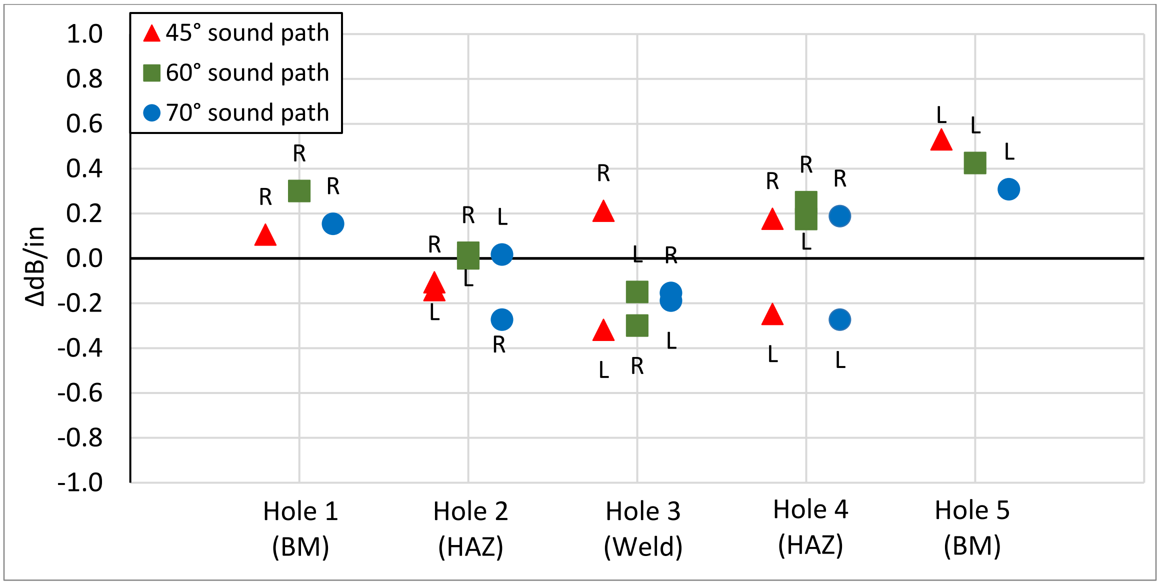

Figure 5.35 SAW2 Individual Results for Test Sequence 2-2

The results for pitch-catch testing in Test Sequence 3-1 are shown in Figure 5.36 for both the testing with the jig and free-hand. The probe center spacing between the index points was set to 4" for the scanning with the jig since this would result in peak signal for a 2" thick plate at 45° incidence angle. The instrument gain which resulted from adjusting the peak signal to 80% screen height is documented along with the direction of the corresponding sound path. The sound was propagated through the weld in both directions to compare any differences. When using the jig, additional gain was added for sound paths propagating through the weld. This is in disagreement with the pulse-echo results shown above. It is believed that this discrepancy is due to the lack of machining on the remaining weld used for pitch-catch testing since the backwall is not perfectly flat due to grinding of the weld. The pitch-catch results for the free-hand testing showed the sound path passing through the weld from the Hole 1 side to the Hole 5 side to have the lowest attenuation. It is likely that the backwall reflected sound at a slightly different incidence angle so the free-hand inspection resulted in higher amplitude (i.e., lower instrument gain) than using the jig with the assumed peak probe center spacing.

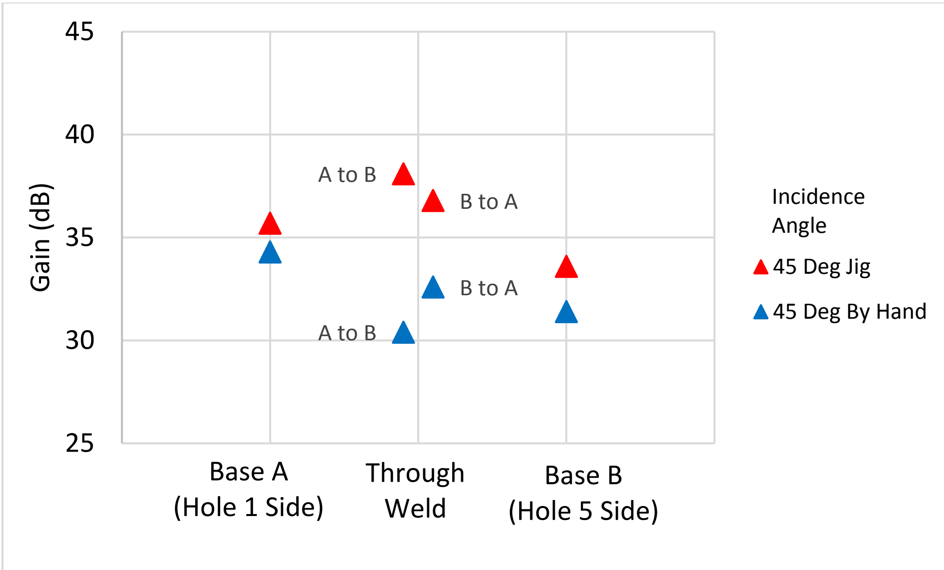

Figure 5.36 SAW2 Results for Test Sequence 3-1

5.4.4 Specimen SAW3

Specimen SAW3 is shown in Figure 5.37 after etching the weld and HAZ region of the machined specimen. The results of Test Sequence 2-1 are shown in Figure 5.38 for the combination of the individual scans while Figure 5.39 shows the individual results for each incidence angle. Specimen SAW3 also had decreased average attenuation when sound propagated through the weld metal or HAZ compared to purely propagating through the base metal.

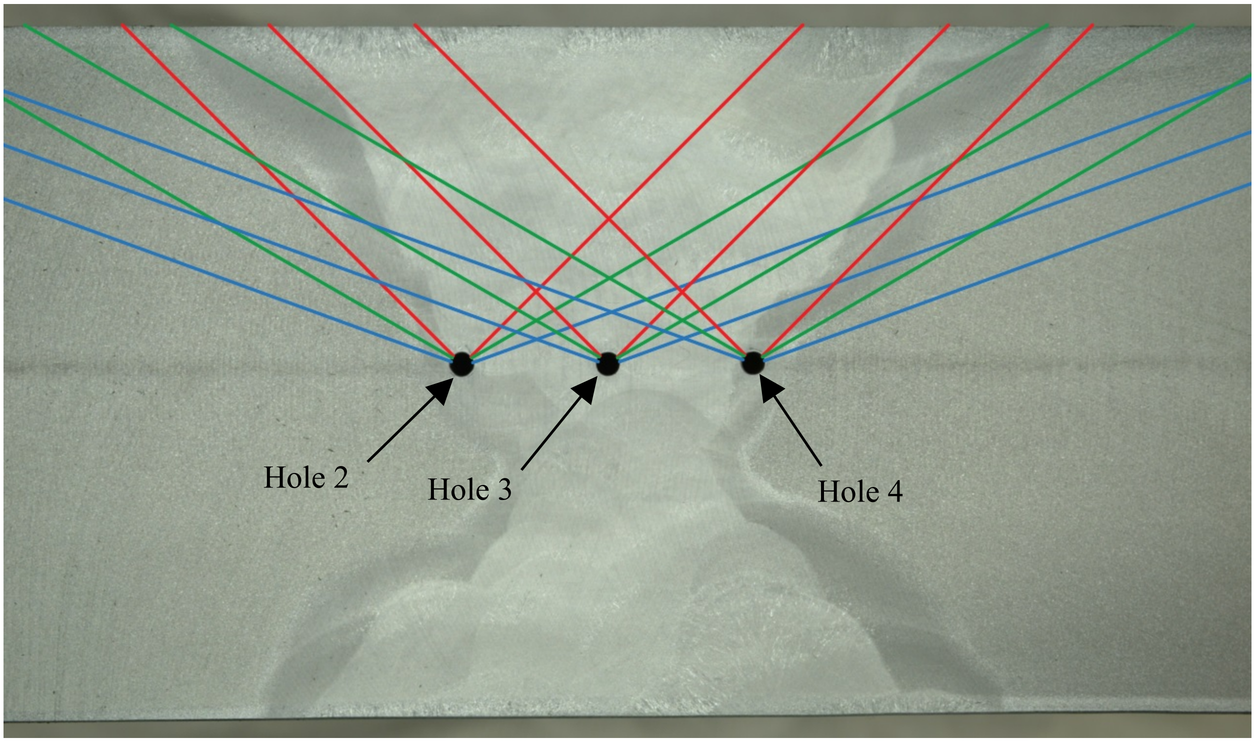

Figure 5.37 SAW3 Weld and HAZ with Sound Paths

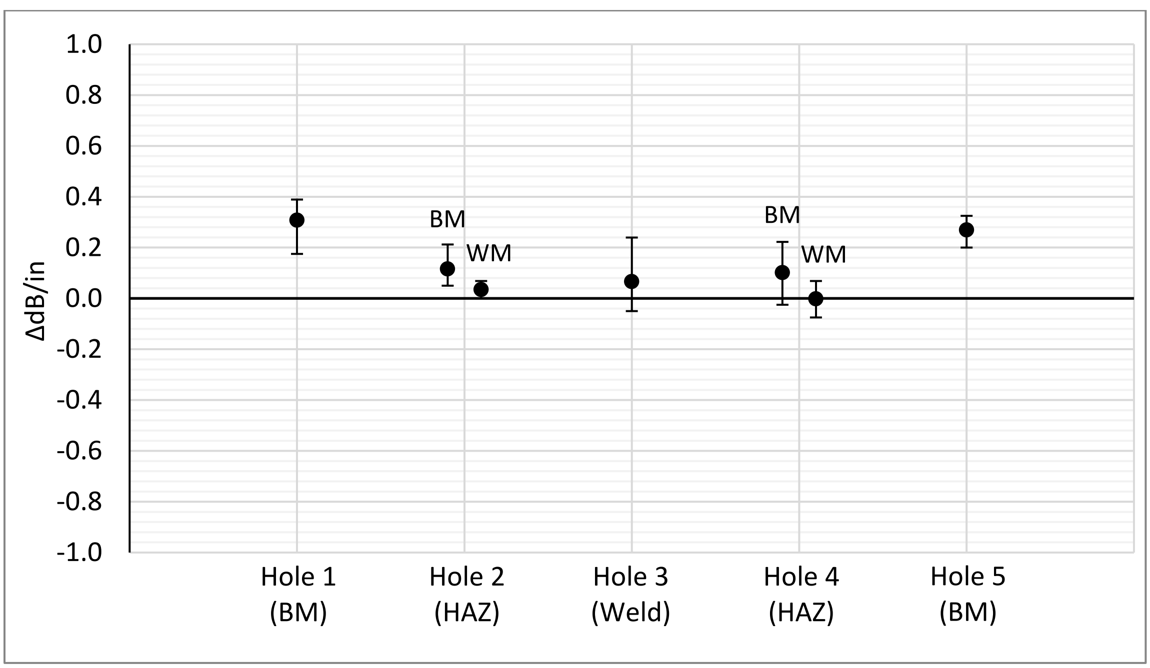

Figure 5.38 SAW3 Combined Results for Test Sequence 2-1

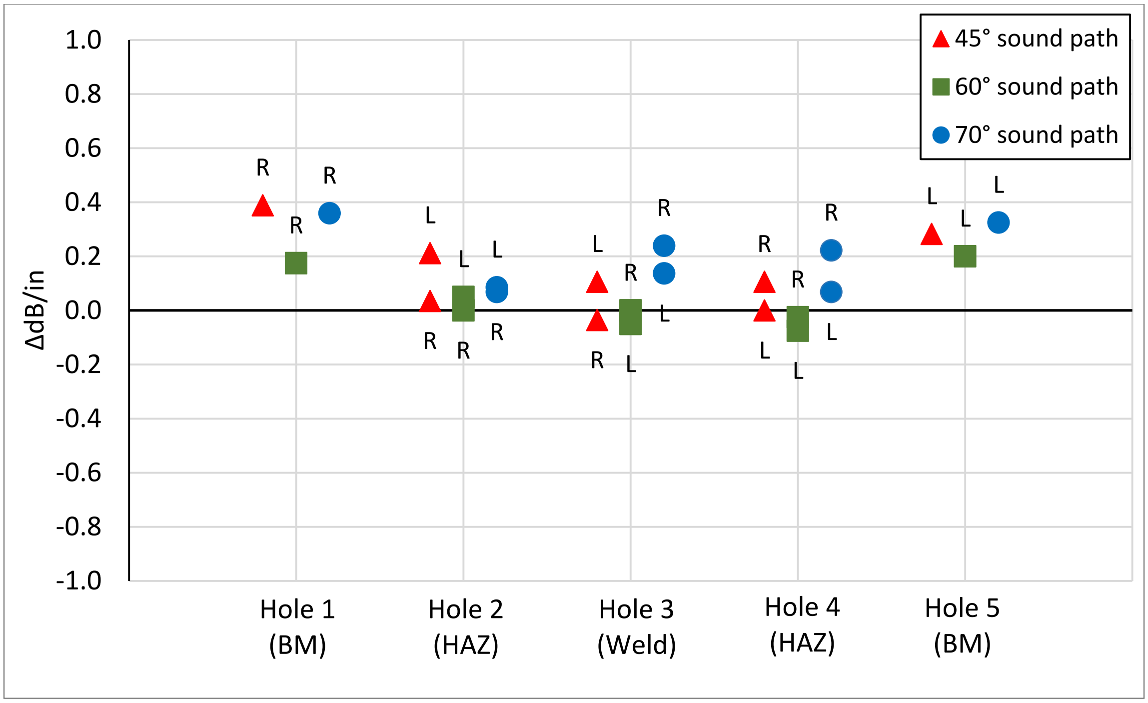

Figure 5.39 SAW3 Individual Results for Test Sequence 2-1

The results of Test Sequence 2-2 are shown in Figure 5.40 for the combination of the individual scans while Figure 5.41 shows the individual results for each incidence angle. Once again, the use of a 5 MHz probe resulted in larger scatter between individual sound paths while the sound passing through the weld metal or HAZ tended to have decreased average attenuation compared to the base metal. The sound paths passing through weld metal were typically lower than those only passing through the HAZ from the base metal side.

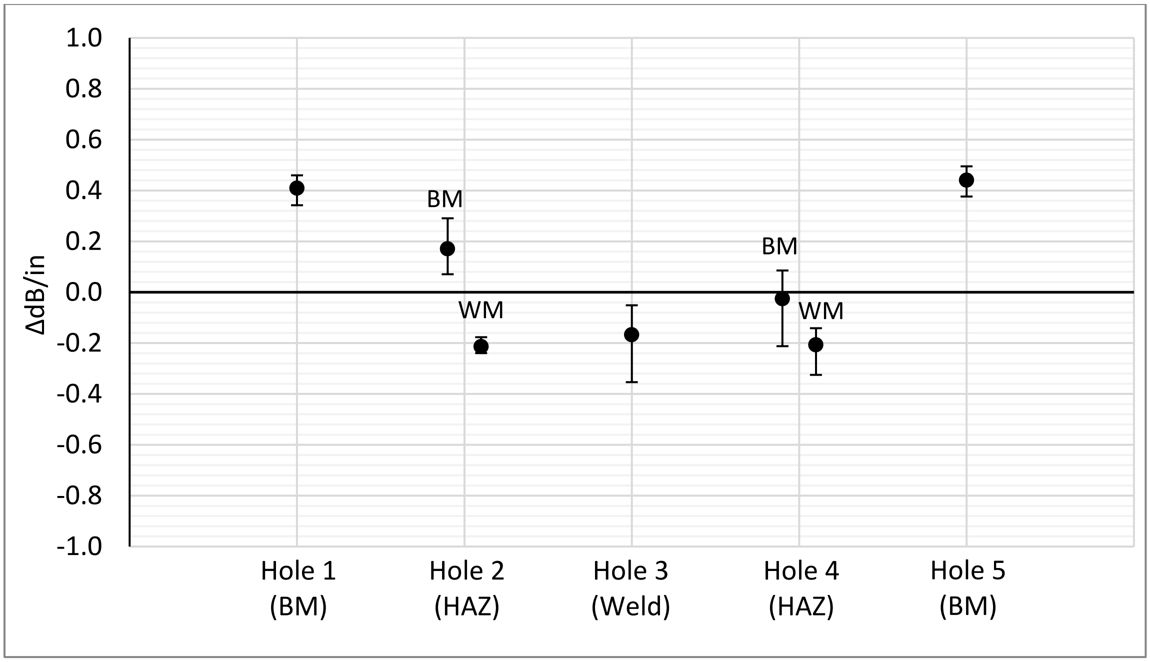

Figure 5.40 SAW3 Combined Results for Test Sequence 2-2

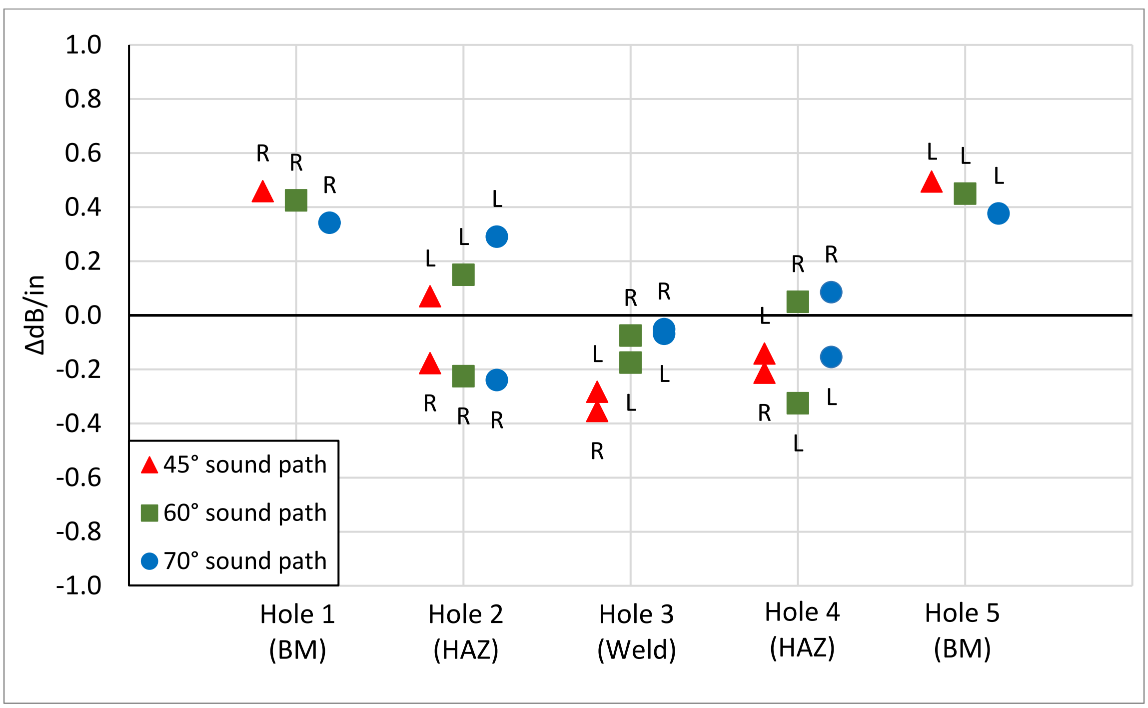

Figure 5.41 SAW3 Individual Results for Test Sequence 2-2

The results for pitch-catch testing in Test Sequence 3-1 are shown in Figure 5.36 for both the testing with the jig and free-hand. The probe center spacing at the index points was again set to 4" for the scanning with the jig since this would result in peak signal for a 2" thick plate at 45° incidence angle. When using the jig, additional gain was added for one of the sound paths propagating through the weld while gain was removed for the other sound path propagating through the weld. It is believed that this discrepancy is due to the lack of machining on the remaining weld used for pitch-catch testing since the backwall is not perfectly flat due to grinding of the weld. The pitch-catch results for the free-hand testing showed that both sound paths passing through the weld have the lowest attenuation.

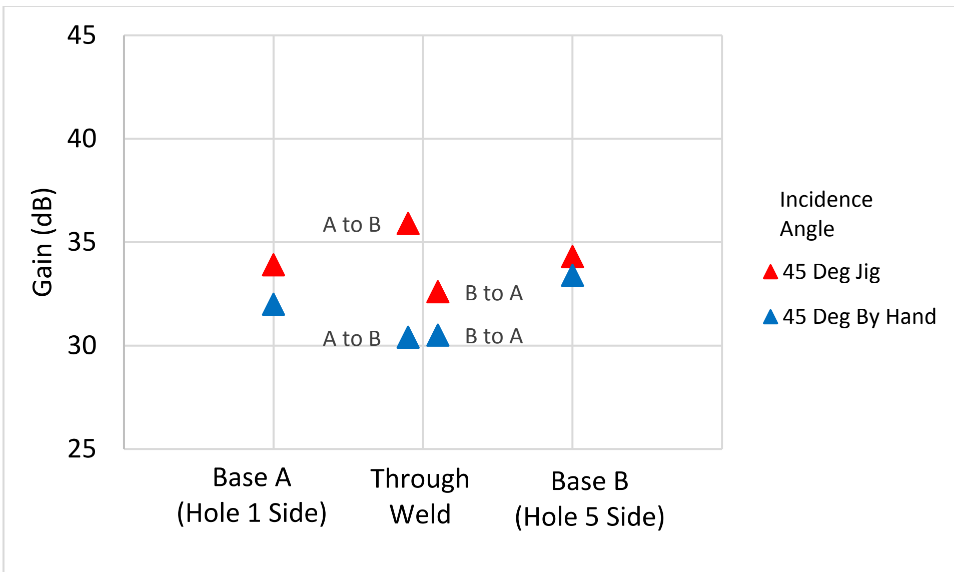

Figure 5.42 SAW3 Results for Test Sequence 3-1

5.4.5 Specimen SAW4

Specimen SAW4 is shown in Figure 5.43 after etching the weld and HAZ region of the machined specimen. The results of Test Sequence 2-1 are shown in Figure 5.44 for the combination of the individual scans while Figure 5.45 shows the individual results for each incidence angle. Unlike the other SAW specimens, Specimen SAW4 had increased attenuation in some cases when sound propagated through the weld metal or HAZ compared to purely propagating through the base metal. This seemed to be limited to only the 45° incidence angle while the 60° and 70° incidence angles had decreased attenuation. The exact reason for this is unknown but may be due to the orientation of the weld grain structure compared to the sound path orientation.

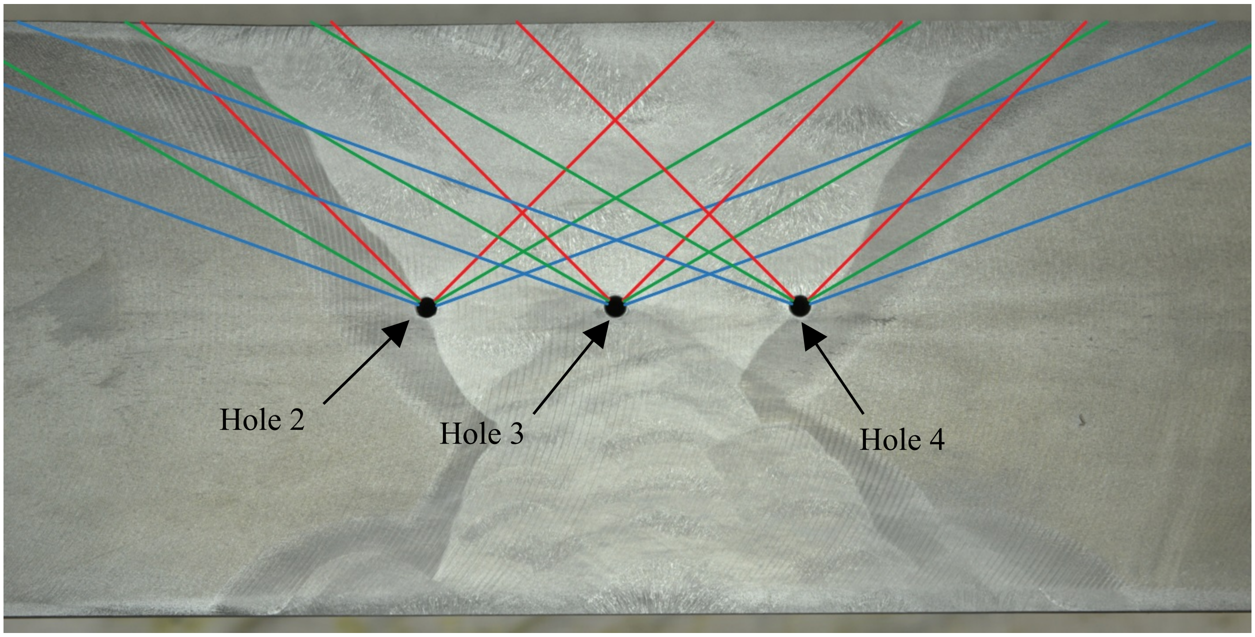

Figure 5.43 SAW4 Weld and HAZ with Sound Paths

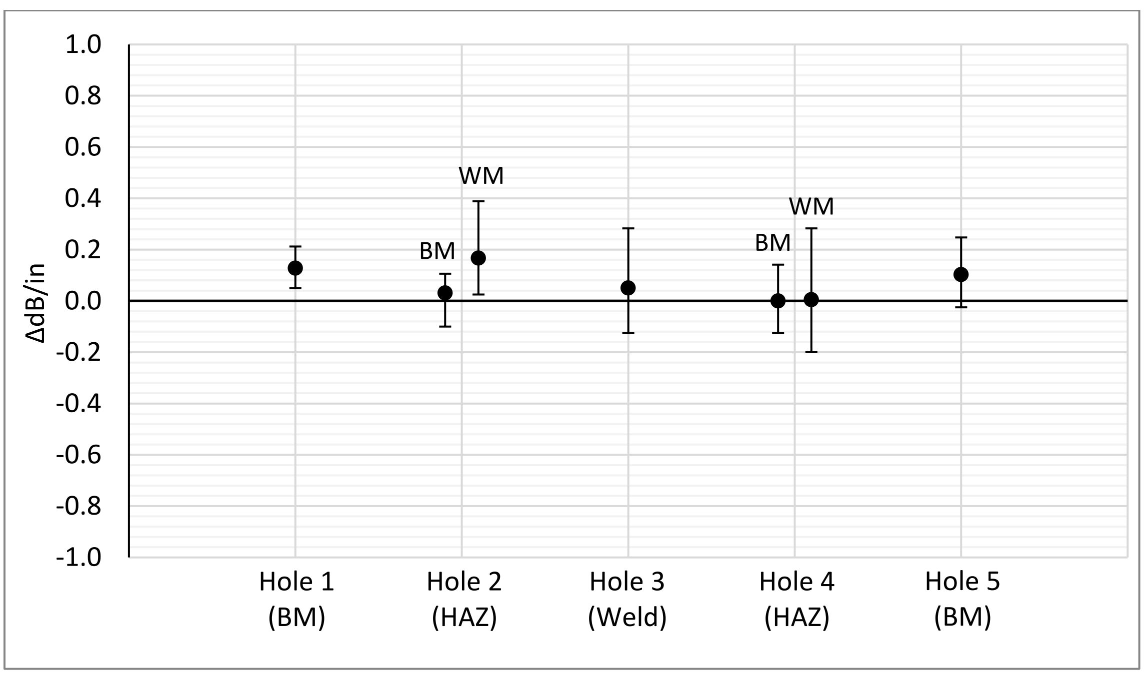

Figure 5.44 SAW4 Combined Results for Test Sequence 2-1

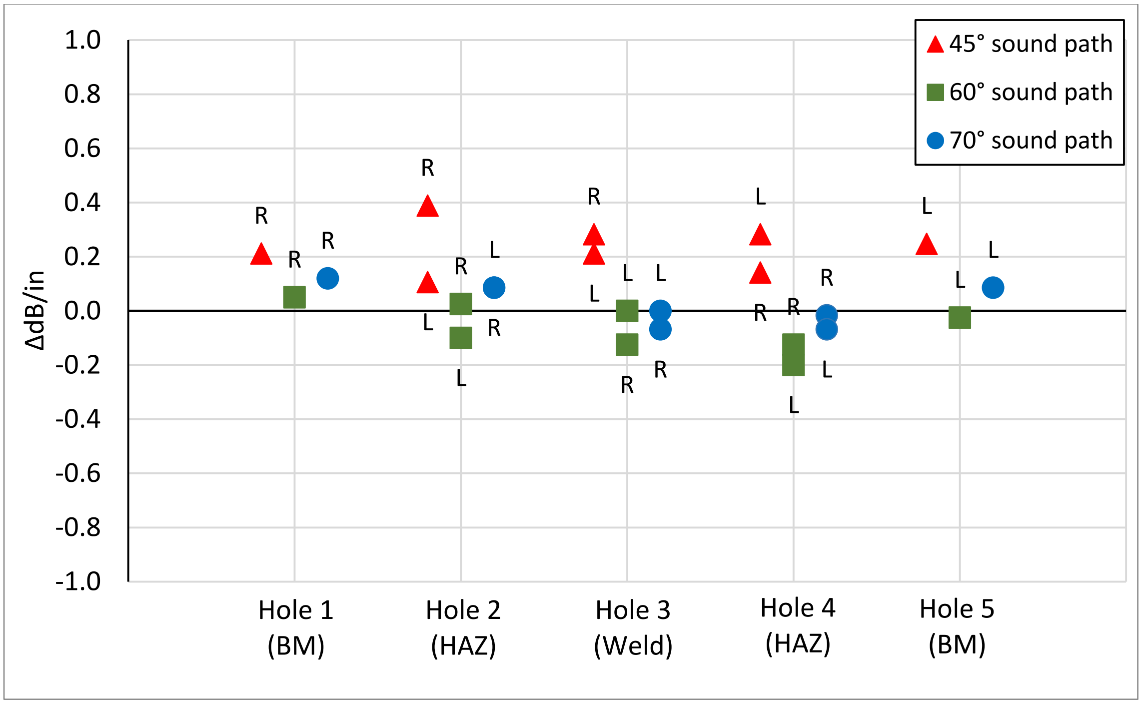

Figure 5.45 SAW4 Individual Results for Test Sequence 2-1

The results of Test Sequence 2-2 are shown in Figure 5.46 for the combination of the individual scans while Figure 5.47 shows the individual results for each incidence angle. Once again, the use of a 5 MHz probe resulted in larger scatter between individual sound paths. The 45° incidence angles which passed through the weld metal were particularly attenuating, similar to the testing with the 2.25 MHz probe shown above. The 60° incidence angle also had a large amount of scatter with some sound paths passing through the weld having higher attenuation and others (i.e., Hole 4 WM) being less attenuating than the base metal. The 70° incidence angle was slightly more attenuating through the weld than the base metal. While the weld metal and HAZ was more attenuating than the base metal for some of the sound paths used in the 5 MHz testing of SAW4, the total amplitude difference was only a bit more than 2 dB. Therefore, the effect of the SAW weld on attenuation is much less than the differences noted between different base metal grades for the 5 MHz probe and is not likely to be significant. Once again, it should be noted that this testing was limited to two inch thick SAW welds and that SAW welds of other thicknesses or welding parameters may have different attenuation characteristics.

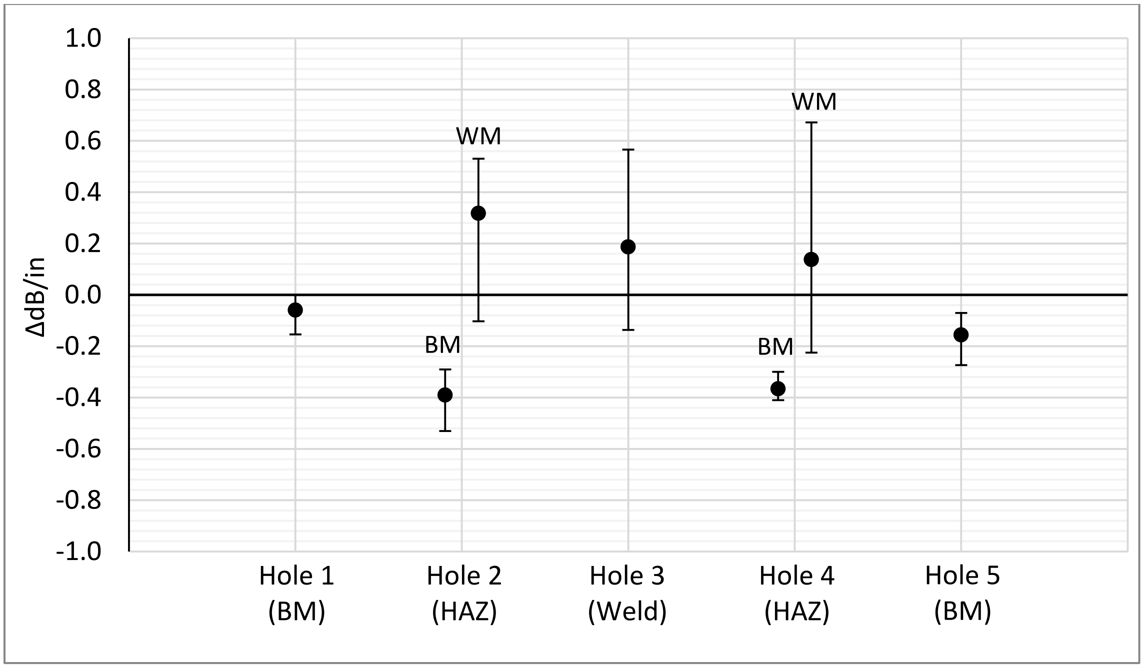

Figure 5.46 SAW4 Combined Results for Test Sequence 2-2

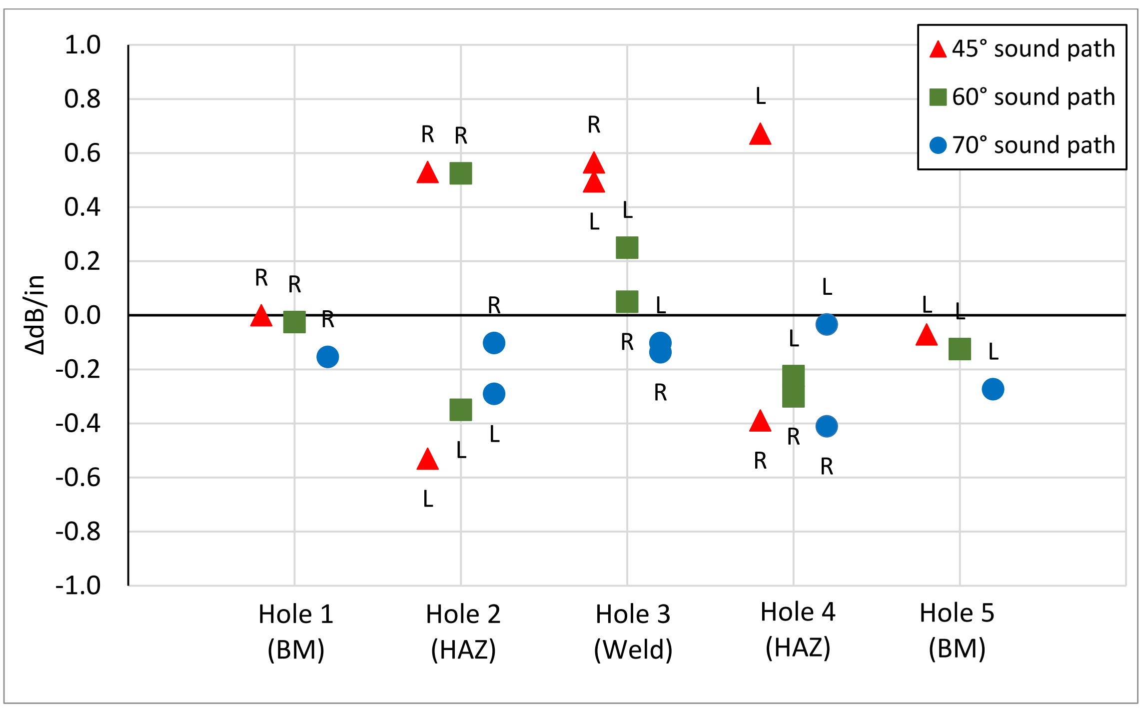

Figure 5.47 SAW4 Individual Results for Test Sequence 2-2

The results for pitch-catch testing in Test Sequence 3-1 are shown in Figure 5.48 for both the testing with the jig and free-hand. The probe center spacing at the index points was set to 4" for the scanning with the jig at the 45° incidence angle and 6.93" for scanning with the jig at the 60° incidence angle since this would result in peak signal for a 2" thick plate. The pitch-catch results for both the jig and the free-hand testing showed that the sound paths passing through the weld tended to have the lowest attenuation for both incidence angles evaluated.

Since the pulse-echo testing was performed with 2.25 MHz conventional UT probes and wedges, it is important that comparison is made to the 2.25 MHz pulse-echo results from Test Sequence 2-1, rather than the 5 MHz results from Test Sequence 2-2. The 60° incidence angle seem to correspond reasonably well with the pulse-echo results, but the 45° incidence angle for the pitch-catch testing were less attenuating through the weld than found during the pulse-echo results. This difference may be due to differences in the sound path used for testing and the location along the weld axis where testing occurred.

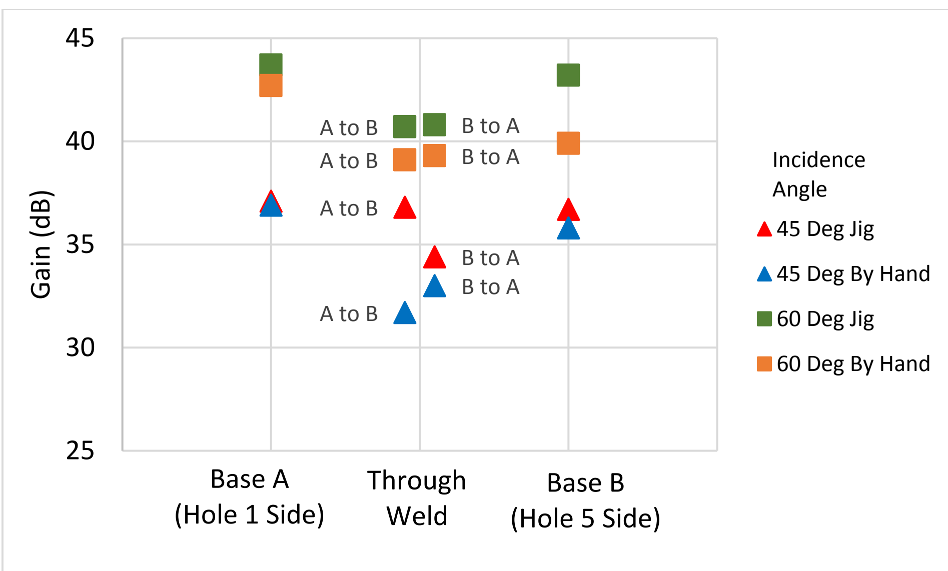

Figure 5.48 SAW4 Results for Test Sequence 3-1

5.5 Additional TMCP Testing

Since the TMCP steels have very different velocity in the rolled direction (RD) and the transverse to the rolled direction ($\perp_{RD}$), they are considered acoustic anisotropic materials. The amount of anisotropy is defined by the birefringence which is the ratio of the velocity in the rolled direction to the transverse to rolled direction as shown below.

$$Birefringence\ (\%) = \left(\frac{Velocity\ in\ RD}{Velocity\ in\ \perp_{RD}} - 1\right) \times 100$$

Experimental testing by Crowley was performed in the rolled and transverse to rolled directions, but no experimental data was collected using oblique orientations to the rolled direction. When scanning is performed oblique to the rolled direction (i.e., not parallel or perpendicular), the beam splits into two waves traveling at different velocities as shown in Figure 5.49 for the normal incidence shear wave probe. Since the beam is split, the amplitude is decreased and it is possible for two indications to appear on the screen as shown in Figure 5.50.

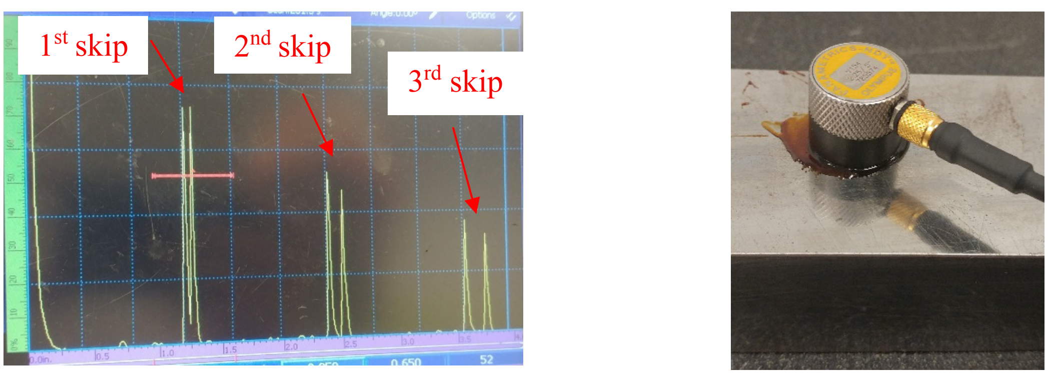

Figure 5.49 Normal Incidence Shear Wave Probe at 45° Angle

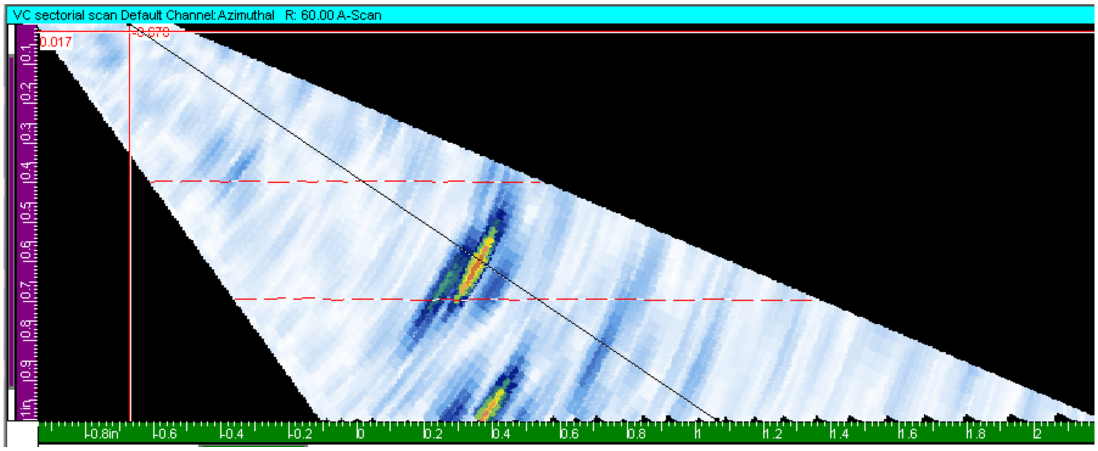

Figure 5.50 0.6” Deep SDH in 45° Orientation to RD TMCP Plate

Experimental testing was performed on a machined specimen cut at a 45° orientation to the rolled direction from Specimen TMCP2 plate (corresponding to Crowley’s designation) with 1/16” diameter SDHs at 0.6” and 1.0” depth. The machined specimen dimensions are similar to the other TMCP specimens tested by Crowley. Therefore, the results can be compared to the results of testing performed by Crowley for the TMCP2 0° and 90° orientations (i.e., rolled and transverse to rolled). TMCP2 had the largest birefringence ratio (i.e., difference in rolled and transverse to rolled velocity) during the experimental measurements by Crowley. The shear wave velocity was measured using a normal incidence shear wave probe to be 0.1333 in/µs in the rolled direction and 0.1267 in/µs in the transverse to rolled direction. The standard velocity of steel is typically assumed to be 0.127-0.128 in/µs. As shown in Table 5.8, experimental testing was performed using the same probes and wedges as the SAW experimental testing.

Table 5.8 TMCP Test Matrix

Test Sequence-Number	Evaluated Specimens	Reference	Flaw Detector and Probe+Wedge Combination
1-1	0.6” & 1.0" deep holes of TMCP2 45° Specimen	Block 50 (Side A)	Zetec Topaz with Zetec AXL - 2.25MHz + AXL - 55SW
1-2	0.6” & 1.0" deep holes of TMCP2 45° Specimen	Block 50 (Side A)	Zetec Topaz with Zetec AM - 5MHz + AM - 55SW
2-1	0.6” & 1.0" deep holes of TMCP2 45° Specimen	Block 50 (Side A)	Olympus Omniscan MX2 with Panametrics-NDT C430 2.25 MHz/0.625"x0.625" + GE SF-AWS wedge (45°, 60°, and 70°)
2-2	0.6” & 1.0" deep holes of TMCP2 45° Specimen	Block 50 (Side A)	Olympus Omniscan MX2 with Olympus 5L64-A12 + SA12-N55S
3-1	0°, 5°, 10°, 20°, 45°, 70°, 80°, 85°, and 90° Orientation of TMCP2 Plate	NA	Olympus Omniscan MX2 with Pitch-Catch (Tx: Panametrics-NDT C430 2.25 MHz/0.625"x0.625" + GE SF-AWS wedge) (Rx: Panametrics-NDT C430 2.25 MHz/0.625"x0.625" + Panametrics-NDT ABWS-8 wedge)

The amplitude difference for the 45°, 60°, and 70° incidence angles on the 45° orientation to rolled direction TMCP block compared to the Grade 50 block is shown in Figure 5.51 for Test Sequence 1-1 and Figure 5.52 for Test Sequence 1-2. The results are given in the change in amplitude (ΔdB) rather than the change in amplitude per sound path length (ΔdB/in) since the loss of amplitude is due to beam splitting rather than attenuation. The results are obviously not driven by attenuation since the loss of amplitude is very similar for the 0.6” and 1.0” deep holes. Rather than corresponding to the sound path distance, the total change in amplitude corresponds to the incidence angle with higher angles having more loss of amplitude. Based on Snell’s Law, higher incidence angles are more sensitive to changes in velocity (i.e., small changes in velocity result in large change in incidence angle). The loss of amplitude at the 70° incidence angle was approximately 6 dB which corresponds to the beam splitting into half. The loss of amplitude at the 60° incidence angle was approximately 4 dB, while the loss was approximately 2 dB at the 45° incidence angle.

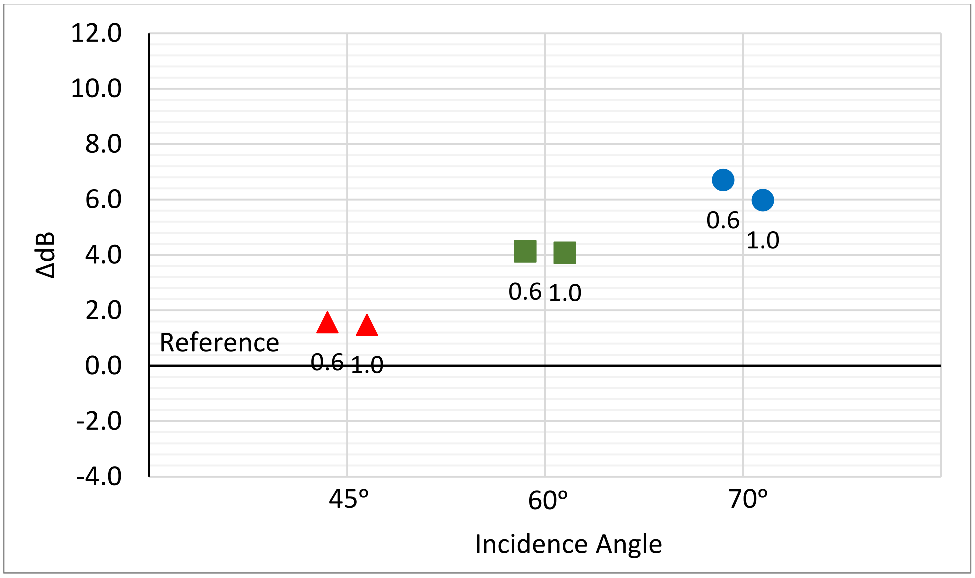

Figure 5.51 TMCP Plate 45° Orientation Results from Test Sequence 1-1

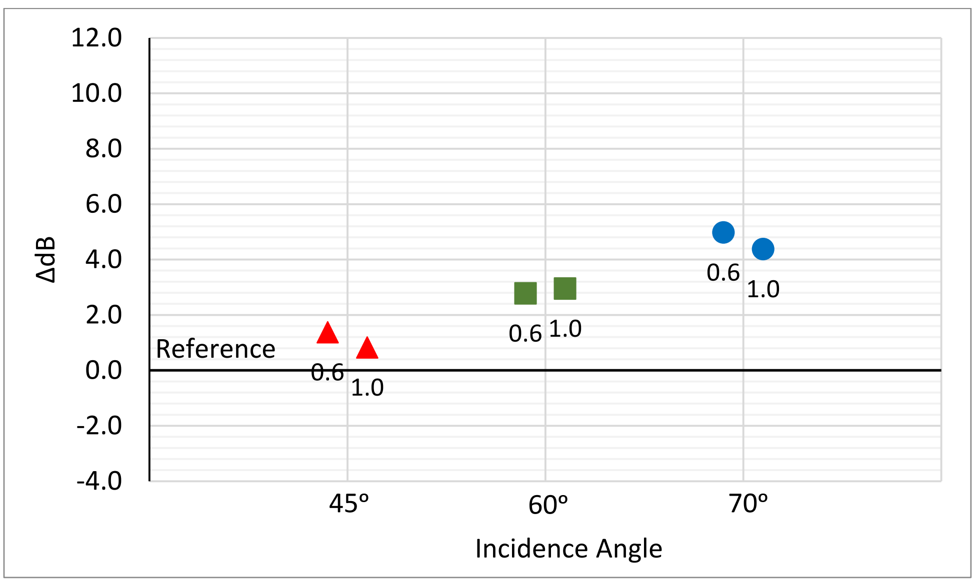

Figure 5.52 TMCP Plate 45° Orientation Results from Test Sequence 1-2

The results of Test Sequence 2-1 and 2-2 was compared to experimental testing by Crowley using the same heat of steel but in the rolled (0°) and transverse to rolled (90°) orientations since all testing was performed with the same probe frequency, probe and wedge dimensions, and active aperture. The results of the 2.25 MHz conventional UT testing under Test Sequence 2-1 for the 45° orientation are compared to the rolled direction (0°) and transverse to rolled direction results

(90°) in Figure 5.53. The results for the 5 MHz PAUT testing under Test Sequence 2-2 for the 45° orientation are compared to the rolled direction (0°) and transverse to rolled direction results (90°) in Figure 5.54.

The results for Test Sequence 2-1 and 2-2 for the 45° orientation were very similar to the results for Test Sequence 1-1 and 1-2, respectively. Therefore, slightly lower loss of amplitude for the 5 MHz probes compared with the 2.25 MHz probes was found for multiple probes. This slight difference in amplitude could be due to attenuation if the HPS 70W TMCP plate is slightly less attenuating than the Grade 50 reference specimen as this would result in less loss of amplitude at higher frequencies.

The 45° orientation with respect to the rolled direction seems to result in similar or slightly greater loss of amplitude at low incidence angles (i.e., 45° and 60°) compared to the rolled direction. At high incidence angles (i.e., 70°), the loss of amplitude in the 45° orientation was less than in the rolled direction. The loss of amplitude in the rolled direction is due to incorrect wedge dimensions for conventional UT or incorrect focal law generation for PAUT due to differences in velocity compared to the assumed value. This results in additional beam refraction, sound loss, and incorrect flaw location. This issue could be resolved for PAUT through measurement of the actual velocity in the scanning direction, correction of the generated focal laws, and use of calibration standards with similar acoustic properties as the test object. On the other hand, the loss of amplitude in the 45° orientation is caused by the beam splitting due to the anisotropic acoustic parameters in the rolled and transverse to rolled direction. Therefore, this issue cannot be readily resolved for conventional UT or PAUT other than accounting the amplitude loss during the calibration process.

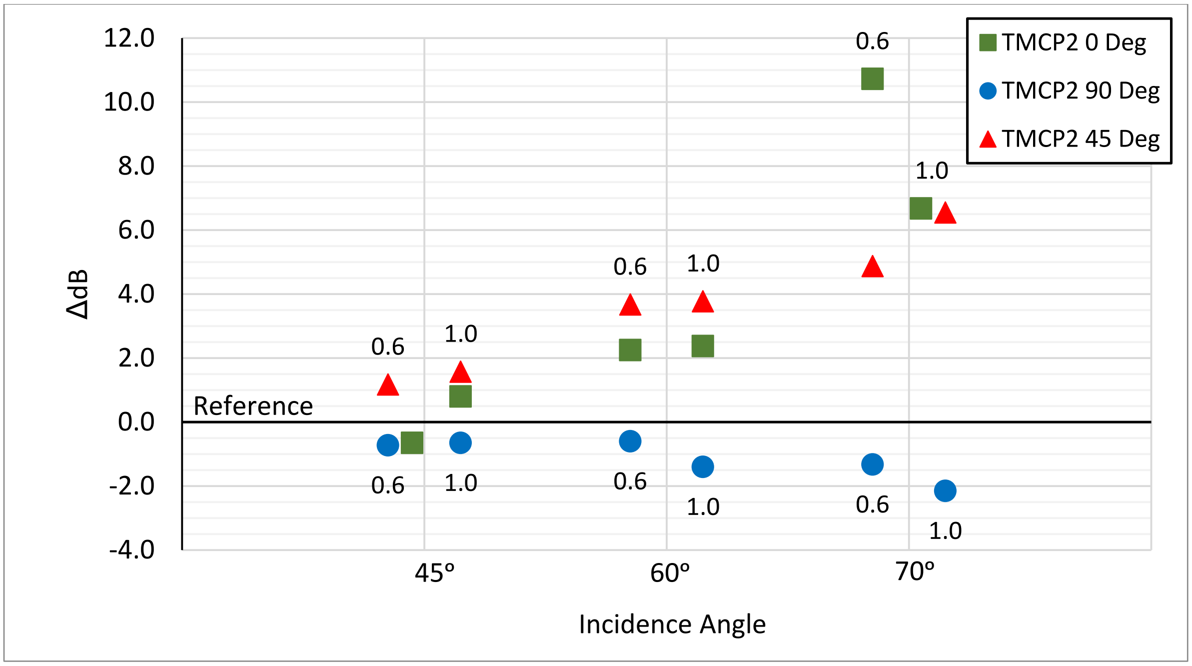

Figure 5.53 TMCP2 Results for Test Sequence 2-1

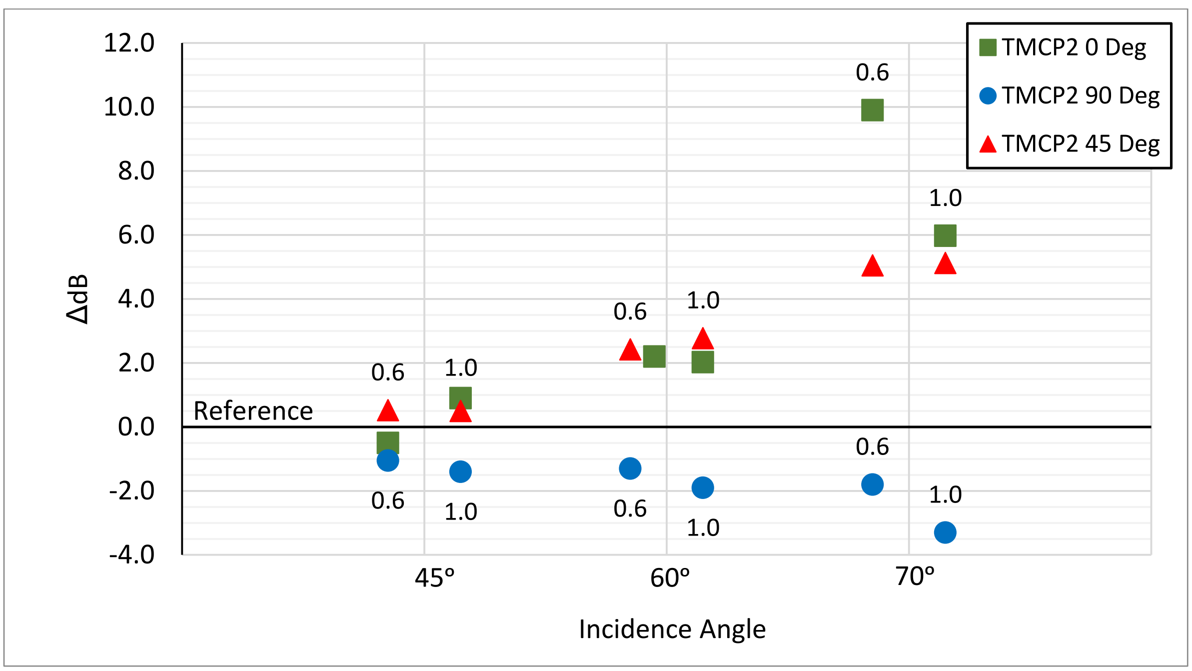

Figure 5.54 TMCP2 Results for Test Sequence 2-2

Pitch-catch testing was performed on the remaining TMCP2 plate in accordance with the details provided for Test Sequence 3-1. Data was collected at the following orientations with respect to the rolled direction: 0°, 5°, 10°, 20°, 45°, 70°, 80°, 85°, and 90°. For each orientation, the instrument gain at 80% screen height was documented for 45°, 60°, and 70° incidence angles with a jig using a specific probe center spacing shown in Figure 5.55 (left) and by free-hand scanning by varying the probe center spacing shown in Figure 5.55 (right). Probe center spacing (i.e., distance between index points of probes) for the testing with the jig were chosen in order to provide peak amplitude for a 1.25” thick plate for each incidence angle. The probe center spacing were as follows for the 45°, 60°, and 70° incidence angles, respectively: 2.5”, 4.33”, and 6.87”. Radial marks were placed on the plate for each orientation in order to ensure proper placement of the probe and repeatability between tests.

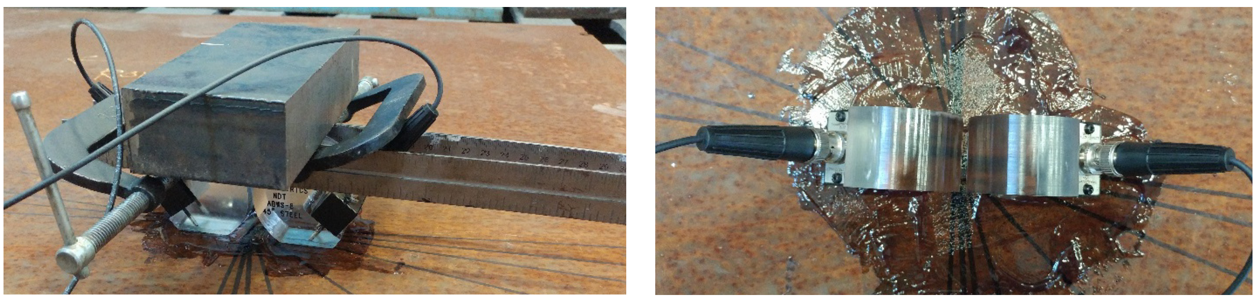

Figure 5.55 Pitch-catch Testing of TMCP2 Plate

The results for Test Sequence 3-1 is shown in Figure 5.56. It is apparent that a large loss of amplitude occurs for the 60° and 70° incidence angle when the probe was aligned or nearly aligned with the rolled direction (0°) compared to the transverse to rolled direction (90°). Along the transverse to rolled direction, the 70° incidence angle results required approximately 10 dB more gain than the 45° incidence angle. This difference is due to additional attenuation of the beam due to the longer sound path for the high incidence angle. There was a 24 dB difference in gain for the free-hand results along the rolled direction. This is an increase of 14 dB amplitude loss comparing the 70° incidence angle to the 45° incidence angle for the 0° orientation compared to the 90° orientation. Comparing the 60° incidence angle to the 45° incidence angle, an additional 4 dB loss of amplitude occurred for the free-hand testing in the rolled direction (0°) compared to the transverse to rolled direction (90°). These results are supported by the previously shown pulse-echo results.

It is also apparent that the use of the jig resulted in underestimating the amplitude by a significant amount for the 60° and 70° incidence angle when the probe was aligned or nearly aligned with the rolled direction (0°). For instance, there is approximately a 2 dB difference in instrument gain for jig and free-hand scanning of the 60° and 70° incidence angle in the transverse to rolled direction (90°) while approximately a 6 dB difference in the rolled direction (0°). This was expected since the change in the incidence angle is more affected at higher angles, and the velocity in the rolled direction differs more from the assumed standard velocity than the velocity in the transverse to rolled direction.

Finally, the largest loss of amplitude occurred at different orientations with respect to the rolled direction depending on the incidence angle. For instance, the 45° incidence angle required the greatest instrument gain in the 85° and 45° orientation. It was expected that the largest loss of amplitude would occur along the 45° orientation due to beam splitting. The loss along the 85° orientation is surprising, but was repeatable at other locations within the plate. The 60° incidence angle required the greatest instrument gain along the 10° and 5° orientation. This is likely due to the beam splitting effect compounded with the loss due to the additional beam refraction along the rolled direction. Therefore, the worst case orientation is not necessarily along the transverse to rolled direction. Likewise, the 70° incidence angle required the greatest instrument gain along the 5° and 0° orientation.

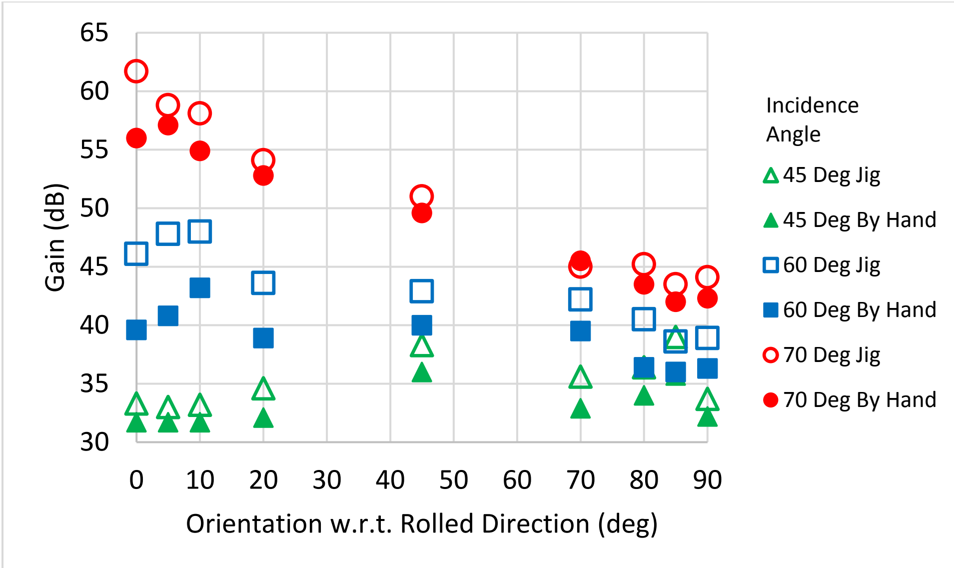

Figure 5.56 TMCP2 Instrument Gain Results for Test Sequence 3-1

Another way to plot the effect of the velocity on the incidence angle is through the depth recorded from the instrument and the corresponding probe center spacing when the amplitude was peaked. Figure 5.57 shows the depth recorded from the instrument. As expected, all of the data collected with the jig gave similar depth which were approximately 1.25” since this was the thickness of the plate and the probe center spacing was chosen to maximize the signal at this depth. The 45° incidence angle free-hand scanning also gave similar results with depths of approximately 1.25” due to the minimal effect on the incidence angle. The 60° incidence angle free-hand scanning gave a larger depth for orientations of 45° or less, with some reported depths as great as 1.54”. The 70° incidence angle free-hand scanning typically gave a larger depth for orientations of 45° or less, with some reported depths as great as 1.88”. The 70° incidence angle free-hand scanning gave a smaller depth for orientations of 80° or greater. The probe center spacing for the 70° incidence angle free-hand scanning is given in Figure 5.58. The probe center spacing varied from as small as 6.125” when in the transverse to the rolled direction up to 11” when along the rolled direction.

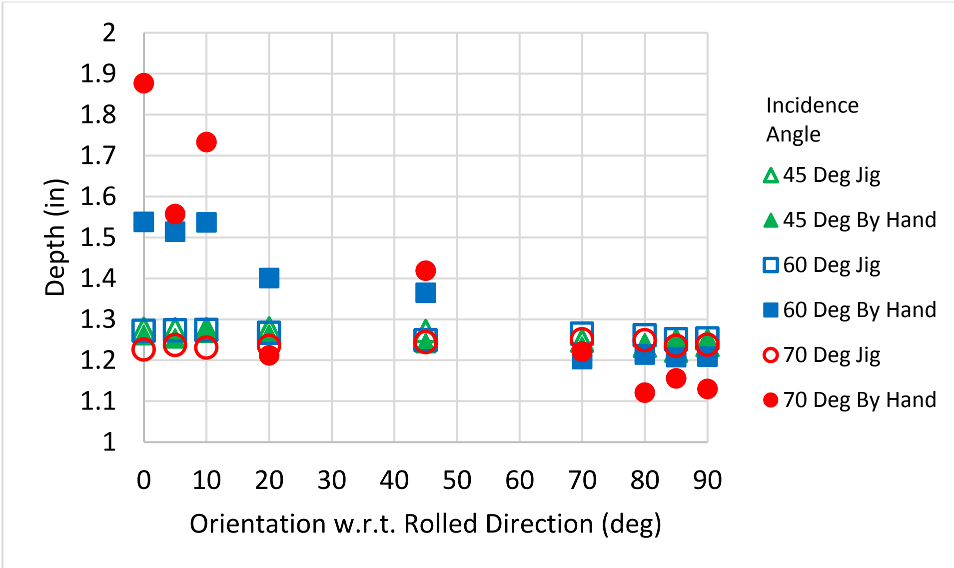

Figure 5.57 TMCP2 Depth Results for Test Sequence 3-1

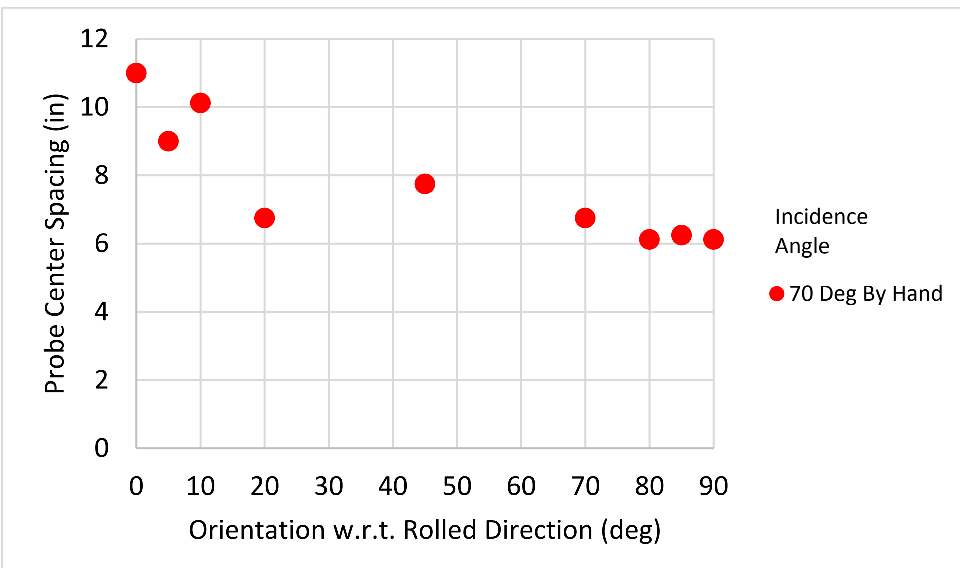

Figure 5.58 Probe Center Spacing for 70° Free-hand Scanning

5.6 Shear Wave Velocity Variation

The variation in the shear wave velocity within a heat of steel was measured for three different plates using a normal incidence shear wave probe. One plate was the TMCP2 plate used for the additional experimental testing with the location of the measurements shown in Figure 5.59 and the results shown in Table 5.9. The second plate was a newly acquired A709 HPS 70W TMCP plate with the location of the measurements shown in Figure 5.60 and the results shown in Table 5.10. The third plate was another newly acquired A709 HPS 50W plate with the location of the measurements shown in Figure 5.61 and the results shown in Table 5.11.

For all three plates, the variation in the shear wave velocity was very minimal across the plate. The maximum standard deviation in shear wave velocity for both the rolled direction and transverse to rolled direction was 0.0002 in/μs. The maximum standard deviation in birefringence ratio was 0.25%. Therefore, while there is a large difference in shear wave velocity between the rolled and transverse to the rolled direction for the TMCP processed plates, the velocity seems to be quite consistent in each direction across the plates.

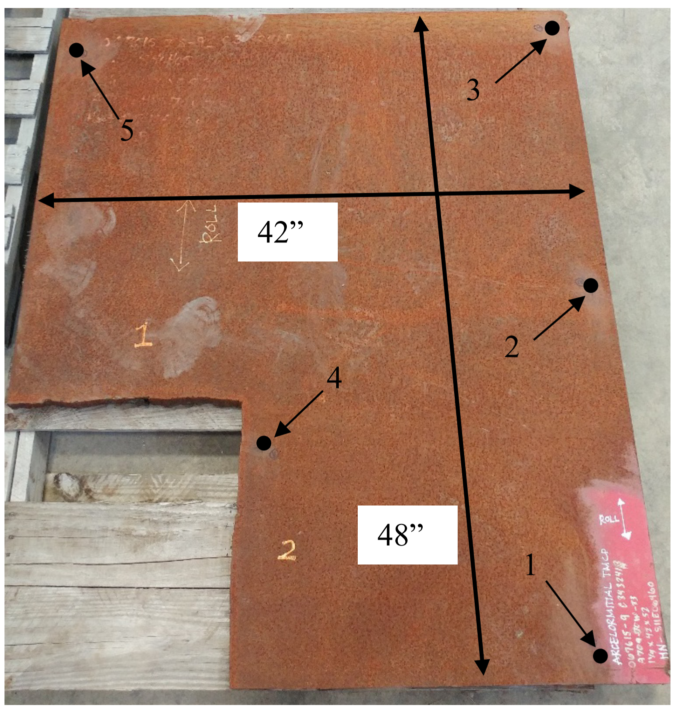

Figure 5.59 TMCP2 Shear Wave Velocity Variation Measurements

Table 5.9 TMCP2 Shear Wave Velocity Variation

Measurement Location	Velocity in Rolled Direction (in/μs)	Velocity in Transverse to Rolled Direction (in/μs)	Birefringence Ratio
1	0.1332	0.1266	5.21%
2	0.1334	0.1267	5.29%
3	0.1334	0.1268	5.21%
4	0.1331	0.1266	5.13%
5	0.1335	0.1267	5.37%
Average	0.1333	0.1267	5.24%
Std. Dev.	0.0002	0.0001	0.09%

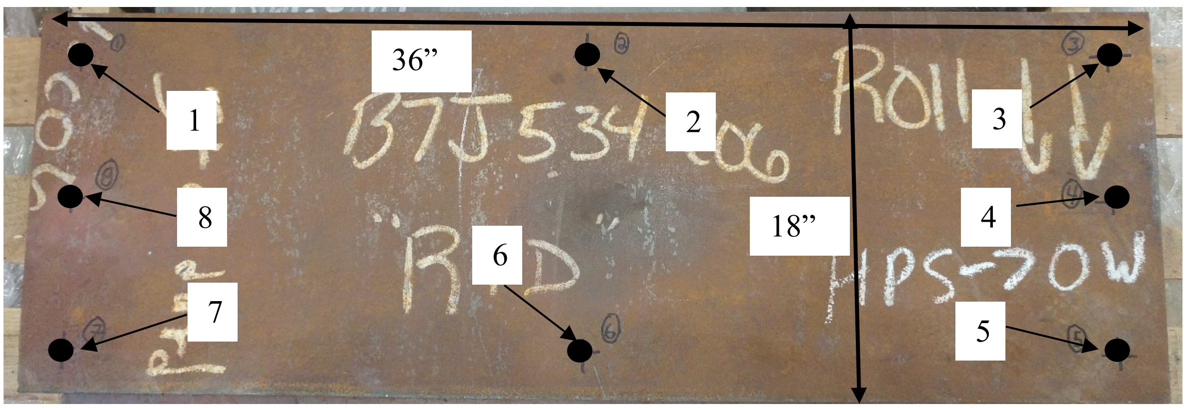

Figure 5.60 Additional A709 HPS 70W Shear Wave Velocity Variation Measurements

Table 5.10 Additional A709 HPS 70W Shear Wave Velocity Variation

Measurement Location	Velocity in Rolled Direction (in/μs)	Velocity in Transverse to Rolled Direction (in/μs)	Birefringence Ratio
1	0.1293	0.1265	2.21%
2	0.1295	0.1260	2.78%
3	0.1295	0.1261	2.70%
4	0.1294	0.1260	2.70%
5	0.1296	0.1263	2.61%
6	0.1295	0.1260	2.78%
7	0.1293	0.1265	2.21%
8	0.1292	0.1263	2.30%
Average	0.1294	0.1262	2.54%
Std. Dev.	0.0001	0.0002	0.25%

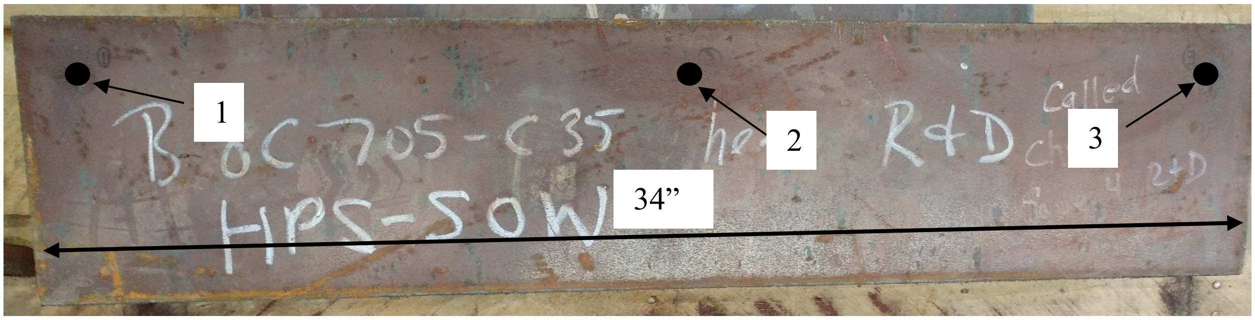

Figure 5.61 A709 HPS 50W Shear Wave Velocity Variation Measurements

Table 5.11 A709 HPS 50W Shear Wave Velocity Variation

Measurement Location	Velocity in Rolled Direction (in/µs)	Velocity in Transverse to Rolled Direction (in/µs)	Birefringence Ratio
1	0.1286	0.1270	1.26%
2	0.1287	0.1272	1.18%
3	0.1287	0.1269	1.42%
Average	0.1287	0.1270	1.29%
Std. Dev.	0.0001	0.0002	0.12%

The A709 HPS 50W steel plate shown above had significant difference in shear wave velocity between the rolled and transverse to rolled direction with average birefringence ratio of 1.29%. This grade of steel was not included in the test matrix by Crowley; thus, it was unknown whether other grades of steel beyond TMCP processed A709 HPS 70W possessed high birefringence ratios. Therefore, beam splitting during scanning in the oblique orientation may be possible for HPS 50W steels as well as HPS 70W TMCP steels. Also, the incidence angle range may need to be limited if the test object exceeds a 1% velocity difference compared to the calibration block in the scanning orientation.

The velocity of two additional grades of steel were also measured in one location for each plate to evaluate the birefringence ratio. This testing included another A709 50 plate in addition to the one tested by Crowley and an A709 50W plate (i.e., non-HPS) which was a grade of steel not included in the test matrix by Crowley. As shown in Table 5.12, neither of these plates experienced significant differences in shear wave velocity in the rolled and transverse to rolled direction with a maximum birefringence ratio of 0.36%.

Table 5.12 Shear Wave Velocity of Additional Grades of Steel

Plate	Velocity in Rolled Direction (in/µs)	Velocity in Transverse to Rolled Direction (in/µs)	Birefringence Ratio
A709-50	0.1281	0.1280	0.05%
A709-50W	0.1279	0.1275	0.36%

5.7 Recommendations for AWS

5.7.1 Attenuation

Differences in acoustic attenuation for common grades of base metals was noted during the experimental testing by Crowley. The differences in attenuation were significantly greater for 5 MHz probes than 2.25 MHz probes which results in large amplitude variations depending on the differences between the calibration block and the test object. CIVA models representing various grades of bridge base metals were developed and benchmarked to the experimental test results. The CIVA models were used to evaluate the amplitude differences that would result from testing different grades of base metals after performing calibration on a typical calibration block with AISI 1018 steel base metal.

Based on this analysis, proposed modifications to AWS D1.5 Annex K were developed in order to improve the calibration requirements to account for the differences in acoustic attenuation. These modifications include guidance that a 2.25 MHz probe should be used for plate thicknesses exceeding 0.5” unless the attenuation of the calibration block and test object is similar or the differences are accounted for through the use of a transfer correction. A transfer correction accounts for the differences in attenuation and coupling losses due to surface roughness between the calibration block and the test object. Transfer correction is referred to in many UT references [11], [13], [18], [46], [48] specifically as a method to account for acoustic differences between the calibration block and the test object. Two methods may be used to perform a transfer correction:

1. Fabricate a block with the same reference reflector including type, size, and depth as the calibration block and note the differences in the signal response between the calibration block and the test object. The sound path for this measurement should correspond to the longest sound path used for the inspection.

2. Perform pitch-catch measurement on the calibration block and the test object over two sound paths to develop the relationship between attenuation and sound path which can be used to correct the amplitude from the calibration block.

Since the first option involves fabrication of a new calibration block, the second option is often much more suitable for checking whether any amplitude correction is necessary between an existing calibration block and the test object. In this method, two probes are used with one acting as a transmitter and the other as a receiver. The sound is skipped off of the backwall of the calibration block and test object in a single V and double V-path (i.e., one skip and two skips off of the backwall), as shown in Figure 5.62, and the amplitude is measured at each location with the same transducer settings. These amplitude measurements are then plotted against the sound path and lines are drawn through the measurements corresponding to the calibration block and the test object, as shown in Figure 5.63.

The difference in amplitude at the maximum inspection sound path can be directly obtained from these lines. If the calibration block line is above the test object line, then the calibration block has less attenuation than the test object and additional gain must be added to the inspection of the test object. If the calibration block line is below the test object line then the calibration block has more attenuation than the test object. While gain may be removed from the inspection of the test object to correct for the difference in this case, this could result in removal of too much gain at shorter sound paths.

The thickness of the calibration block and the test object do not need to match, but the amplitude measurements must be made in the far field in order to ensure that the change in amplitude is due to attenuation. API RP 2X requires that the single V-path measurement sound path exceed 4 inches. If the single V-path measurement is within this sound path, it is recommended that additional skip distances be used to obtain longer sound paths.

For typical surface finishes, it is not believed that the loss of amplitude should be significant from scattering off of the surface when performing successive backwall skips. Previous research [49] used CIVA modeling to investigate the difference in amplitude for a SDH when scanned using successive backwall skips (up to four legs) compared with directly scanning a SDH at the same incidence angle and sound path in first leg only. This research found that the maximum amplitude loss for the third and fourth leg scans were 1.9 dB. Therefore, while the sound loss should be minimal for typical surface finishes, the loss of amplitude due to surface roughness from successive backwall skips should be considered when the surface roughness of the test object is poor.

While the inspection will be performed with PAUT probes, use of conventional UT probes with similar frequency and aperture which will be used for the PAUT inspection will be adequate to account for the attenuation. It is recommended that the conventional UT wedge be chosen to produce the largest incidence angle used in the PAUT inspection since this will increase the sound path and is more sensitive to amplitude differences due to velocity variations. During experimental testing, 2.25 MHz and 5 MHz conventional UT and PAUT probes were used for attenuation testing and the results of PAUT and conventional UT were very similar for the same incidence angle, frequency, and aperture.

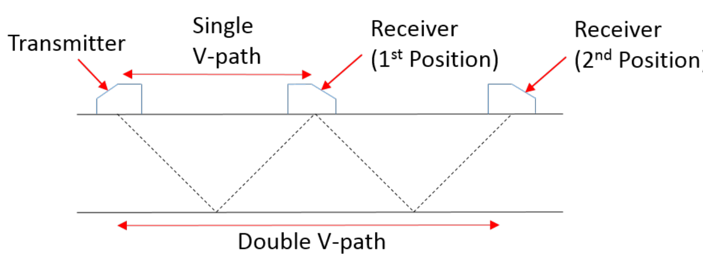

Figure 5.62 Transfer Correction Probe Locations

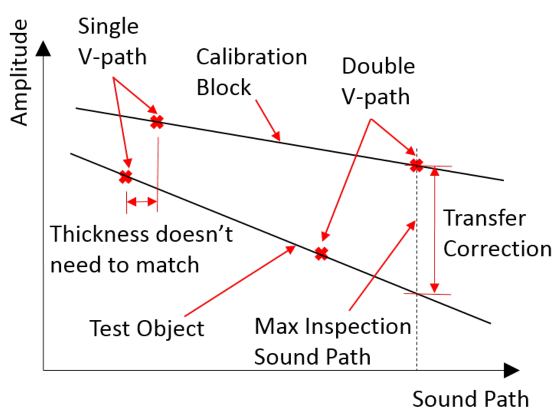

Figure 5.63 Transfer Correction Amplitude

According to ISO 17640 [18], no correction is required if the greatest difference in amplitude between the calibration block and the test object at the longest sound path is 2 dB or less. This code requires correction for amplitude differences greater than 2 dB but smaller than or equal to 12 dB. If the amplitude difference exceeds 12 dB, this code requires that the reason for this difference shall be considered or the scanning surface reconditioned.

In order to make the transfer correction when TCG is used, either (1) the entire TCG curve is corrected by modifying the reference gain which would offset the entire TCG curve up/down by the same amount or (2) separate corrections could be performed manually to each TCG point for each focal law. The first method is very simple, but may result in overcorrection at short sound paths. For instance, shifting the entire amplitude by the transfer correction at the longest sound path in Figure 5.63 would result in the test object amplitude being overestimated at shorter sound paths. This would obviously be conservative, but the opposite is true if the transfer correction resulted in removal amplitude (i.e., too much amplitude would be removed at short sound paths resulting in lower sensitivity than reference). Therefore, it is recommended that Annex K not allow for removal of amplitude unless consideration is given for the amplitude difference at shorter sound paths to avoid unconservative corrections.

The second method of TCG correction for attenuation differences described above involves manual adjustment to each TCG point for each focal law. While this would result in accurate correction over all sound paths, it would be a very time consuming process which will require input of at least 93 corrections considering 31 focal laws for a 40°-70° incidence angle range with 1° increment and a 3-point TCG. Therefore, unless automated in some way, this method is more sensitive to human error and unlikely to be practical for shop application.

It is recommended that AWS Annex K be modified to require verification of the differences in acoustic properties between the test object and calibration block. If the amplitude difference exceeds 2 dB at the longest sound path and the calibration block is less attenuating than the test object, a correction for this difference is required. Guidance for four methods of correction has been produced for the AWS Annex K commentary. The first correction method includes using a lower frequency probe such as 2.25 MHz. The second correction method involves using a calibration block that better matches the test object and results in less than a 2 dB amplitude difference at the longest sound path. The third correction method involves reconditioning the scanning surface of the test object in order to better match the calibration block. The fourth and final correction method involves adding gain equal to the difference between the calibration block and the test object at the longest sound path. It is noted that this may be overly conservative at shorter sound paths and it is not recommended to be performed for differences greater than 12 dB.

It is very likely that the base material on each side of a butt splice will be from different mills, grades, or heats. When this is the case, a separate transfer correction will be required to be performed on each plate at the weld to correct for differences in acoustic properties. Therefore, it is possible that the equipment settings may differ for inspection of the same weld depending on which side of the weld is being inspected.

The experimental testing of SAW welds showed that the attenuation through the HAZ and weld metal is typically lower than the attenuation of sound passing through only base metal of equivalent sound path. In the instances where the attenuation through the weld metal was greater than the base metal, the maximum absolute difference in amplitude between the base metal and the weld metal sound paths was only 2.4 dB. This location occurred on SAW4 with the 5 MHz PAUT probe. As stated above regarding base metal attenuation, differences of 2 dB or less are not considered significant according to most UT codes. Therefore, although the weld metal and HAZ of SAW welds were found to increase the scatter of reported amplitude of SDH reflectors, it is not believed that an additional correction is necessary in Annex K to account for these amplitude differences.

Unlike SAW welds, it is recommended that additional requirements be provided to account for the significant loss of amplitude reported by Crowley when sound propagates through coarse grained NGI-ESW welds. These requirements include verifying the amplitude and location of a 1.5 mm (0.06”) dia. SDH in a full-scale mockup of the weld. (*Note, full-scale means simply full thickness. The specimen need only be a few inches wide.*) The reflector would be required to be placed in a location which will maximize the sound path traveling through the weld metal. This recommendation will allow for an amplitude correction to be determined on a case by case basis in order to account for the high attenuation found when the sound beam passed through the weld metal of some NGI-ESW welds. Recommendations are also provided in the section which covers scanning coverage of welds that NGI-ESW welds shall be inspected from the outside of each fusion face. This recommendation will ensure that detection of fusion flaws will not depend on sound passing through the entire weld volume.

5.7.2 Shear wave velocity

5.7.2.1 Rolled direction or transverse to rolled direction

Differences in measured shear wave velocity for common grades of base metals was noted during the experimental testing by Crowley. For TMCP processed steels tested, the velocity increased in the rolled direction and decreased in the transverse to rolled direction. Therefore, these materials are considered acoustically anisotropic. Since the incidence angle is related to the ratio of the wedge velocity to the steel velocity by Snell's Law, differences in the incidence angle result in errors in properly locating flaws as well as affecting the amplitude reflected from the indications (i.e., a reduction in amplitude).

Previous experimental testing found that the amplitude was significantly decreased at high incidence angles (i.e., 60° or greater) when scanning was performed in a direction of increased velocity. CIVA models were developed which represented one of the TMCP processed steel samples from the experimental testing with a shear wave velocity of 0.133 in/μs (i.e., 4.5% increase compared to the calibration block). The CIVA models showed that the difference in amplitude of the TMCP steel to the 1018 calibration block would be ~2 dB at a 7" depth with 45° incidence angle, ~2 dB at a 1" depth and ~4 dB at a 7" depth with 60° incidence angle, and exceeded 2 dB for all sound paths with the 70° incidence angle. Therefore, while limiting the incidence angle range to 40°-60° will lessen the impact from the changes in the shear wave velocity, it will not limit the amplitude differences to 2 dB or less over all possible sound paths.

Additional CIVA analysis was performed in order to identify the limiting velocity difference compared to the standard steel velocity of 0.127 in/μs (3230 m/s) which would result in an amplitude difference of 2 dB or less over a sound path covering 7" depth for the 60° and 70° incidence angles. A velocity increase of 2.5% compared to the standard velocity resulted in an amplitude difference of 2 dB or less across the 40°-60° incidence angles while a velocity increase of 1.0% compared to the calibration block resulted in an amplitude difference of 2 dB or less across the 40°-70° incidence angles. This correlated well with the experimental test results from Crowley on three TMCP specimens. Therefore, assuming a shear wave velocity of 0.127-0.128 in/μs for the calibration block which is typical for most steels, the 40°-60° incidence angles should be appropriate for plates with velocity of 0.130-0.131 in/μs, and the 40°-70° incidence angles should be appropriate for plates with velocity of 0.128-0.129 in/μs.

It is recommended that the acoustic properties of the test object and calibration block be verified to be within certain tolerances. It is recommended that the shear wave velocity in the direction of sound propagation in the test object and the calibration block be required to be within ±2.5% of each other. When the difference exceeds this amount, it is recommended that a new calibration block which has velocity within 2.5% of the test object be fabricated or otherwise acquired. When the difference in shear wave velocity exceeds ±1%, it is recommended that the incidence angle be limited from 40°-60°. If the velocity of the test object and calibration block is measured and found to be within ±1% of each other, a 40°-70° incidence angle range may be used. Since most steels have a velocity of 0.127-0.128 in/μs, these steels would all be able to use the same calibration block assuming that attenuation is properly accounted for.

JIS Z 3060: 2015 [13] includes three different methods to directly or indirectly measure the shear wave velocity of the test object and calibration block:

1. Fabricate a block with a reference reflector from the test object material. Calculate the incidence angle of the test object and the calibration block by using measurements of the physical distance of the reflector from the index point and the depth of the reflector.
2. Perform pitch-catch measurement on the test object and calibration block in a single-V path and calculate the incidence angle by using measurements of the physical distance between the transducer index points and the thickness of the plate.
3. Directly measure the shear wave velocity of the plate by using a normal incidence shear wave probe to measure backwall signals. The shear wave velocity of the calibration block and test object can either be directly computed using a calibration feature with successive shear wave backwall skip signals (i.e., similar to velocity measurements using a normal

incidence longitudinal wave probe) or the velocity ratio between the calibration block and test object can be computed using the known thickness and measured shear wave backwall signals of each plate.

If the incidence angle is measured, the velocity ratio can be calculated using Snell's Law as follows:

$$\frac{\sin \theta_{test\ object}}{\sin \theta_{cal\ block}} = \frac{V_{test\ object}}{V_{cal\ block}}$$

Assuming that the calibration block incidence angles are truly 60° and 70° (i.e., velocity of calibration block matches the assumed velocity), the incidence angles measured in the test object are 62.6° and 74.4° for a 2.5% increase in velocity and 61° and 71.6° for a 1.0% increase in velocity.

All of these methods rely on the orientation of the probe used to measure the velocity or incidence angle matching the orientation of the probe that will be used during scanning. For instance, if the PAUT line scanning will be performed with the probe oriented along the rolled direction, then the measurement of the shear wave velocity or incidence angle shall be performed in the same direction. As an example, checking the depth and index distance from the corner trap signal which is produced from scanning the edge of the plate transverse to the rolled direction cannot be used to verify the velocity along the rolled direction. Fabrication of a calibration block is also sensitive to the orientation of the plate in relation to the orientation of the scanning direction.

In fact, the direction of sound propagation in regards to the through-thickness direction is also critical. For instance, typically calibration blocks are cut from material and flipped so that the through-thickness direction forms the width of the calibration block, as shown for the block on the left side of Figure 5.64. This is performed in order to provide for greater depths of the SDH reflectors and avoid the need for very thick plates. Due to the complex and layered grain structure found in TMCP steels, the velocity at the surface of the plate will differ from the velocity in the middle of the plate. Therefore, calibration blocks for TMCP steels must have the correct scanning surface and scanning direction (i.e., through-thickness and rolled direction) compared with the test object as shown on the right side of Figure 5.64.

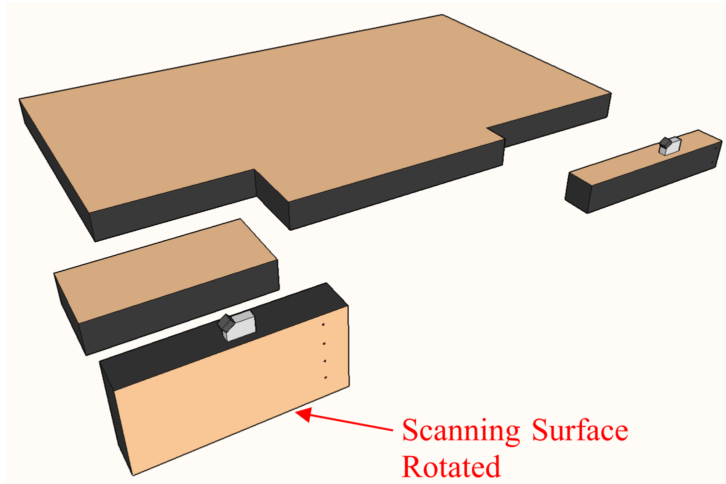

Figure 5.64 Calibration Block Rotation

5.7.2.2 Oblique to rolled direction

While normal incidence shear wave probes can be used to quickly ascertain whether a plate has acoustic anisotropic behavior (i.e., the velocity is different in the rolled and transverse to rolled directions) by rotating the probe from polarization in the rolled direction to the transverse to rolled direction, caution may be necessary to use it for measuring the velocity in the oblique orientation. For scanning along oblique orientations in acoustic anisotropic materials, JIS Z 3060 requires that the velocity be accounted for by measuring the incidence angle using an angle beam probe(s) rather than directly measuring the velocity with the normal incidence shear wave probe. While the technical reason for this requirement is not explained in JIS Z 3060, it is likely due to the fact that two different measurements are possible with the normal incidence shear wave probe which could result in miscalculations. Measurement of the incidence angle through either fabrication of a reference standard or using the pitch-catch method results in measurement of the true refraction angle at the maximum amplitude indication. There may still be two indications apparent on the screen, but the maximum amplitude indication would be used for measurement of the incidence angle. The JIS code does not require additional amplitude be added for scanning in the oblique orientation, but it does require that the calibration standard be acoustically equivalent to the test object with velocity within ±2% and sensitivity correction within ±2 dB compared to the test block along with additional limits on the incidence angle depending on the ratio of the velocity of the test object to the calibration block in the orientation of the scanning direction.

Based on the experimental results, additional requirements are recommended for acoustically anisotropic materials. It is recommended that all materials with a birefringence ratio (i.e., ratio of velocity in the rolled and transverse to rolled direction) of 1% or greater be defined as acoustically anisotropic in Annex K. Based on the experimental test results additional requirements on the incidence angle and addition of amplitude are recommended for scanning of acoustically anisotropic materials in the oblique orientation with respect to the rolled direction. It is recommended to limit the incidence angle to 40°-60° for scanning of acoustic anisotropic plates at an oblique orientation to the rolled direction. It is also recommended that 4 dB be added to the reference sensitivity to account for the sound loss due to the beam splitting.

These requirements do not require the velocity or beam incidence angle be measured in the oblique orientation. Therefore, while guidance is provided in the commentary that caution must be taken when measuring the velocity of the plate in the oblique orientation using a normal incidence shear wave probe, this measurement is not necessary. Rather, acoustic anisotropic materials are identified using the shear wave velocity measurements in the rolled and transverse to rolled directions and checking against the 1% limit on difference.

6. PAUT SCANNING PROCEDURES AND ACCEPTANCE CRITERIA

Simulations were performed using CIVA-UT [47] to aid in the development of the PAUT scanning procedures and acceptance criteria. The simulations incorporated weld flaws with a size similar to the critical flaw sizes developed during the FFS parametric studies. These flaws serve as a "lower bound" flaw set from which improved acceptance criteria were developed to consistently reject these flaws. As long as flaws of this size or larger are consistently rejectable, the procedure can be deemed effective at removing critical flaws from service. Therefore, the acceptance criteria are grounded in fracture mechanics but use amplitude rather than flaw size measurements for detection and rejection.

A parametric study using CIVA evaluated the effects of variations in the amplitude response of weld flaws deemed critical per the FFS studies. The CIVA parametric study provided a rational comparison of the amplitude from the target critical weld flaws to the acceptance criteria amplitude limits. These data were used to develop a rational fracture mechanics based PAUT inspection procedure and acceptance criteria which will detect and reject critical weld flaws. The parametric models varied the plate thickness along with the flaw type, size, position, tilt, and skew of target critical weld flaws in order to compare the maximum amplitude of the indication response with the reference amplitude and acceptance criteria amplitude limits.

6.1 Reference Standard Reflectors

6.1.1 Comparison of current PAUT amplitude-based acceptance criteria

The first step in developing the PAUT scanning procedures and acceptance criteria was to compare three PAUT amplitude-based acceptance criteria which are used to inspect bridge welds including: (1) AWS D1.5:2015 Annex K, (2) CSA W59:2018, and (3) ISO 19285:2017 Level 2. All three acceptance criteria utilize a maximum amplitude and length sizing approach to classify flaws as acceptable/rejectable so it is possible to directly compare them. To perform this comparison, the reference amplitude must be converted to be equivalent since AWS and CSA use 1.5 mm (0.06") diameter SDHs for reference amplitude (i.e., TCG) while ISO uses a 3 mm (0.12") diameter SDHs.

CIVA modeling was used to convert the reference amplitude for a 3 mm diameter SDH to the equivalent reference amplitude for a 1.5 mm diameter SDH. The 5 MHz PAUT, 2.25 MHz conventional UT, and 2.25 MHz PAUT CIVA models were used to compare the difference in amplitude between 3 mm diameter SDHs and 1.5 mm diameter SDHs at varying depths and beam angles. As shown in Table 6.1, the change in reference amplitude was approximately +4 dB for the 3 mm diameter SDH compared with a 1.5 mm diameter SDH. This correlated well with data from previous work [50] in which a similar study using CIVA was performed to compare the reference amplitude of SDHs ranging from 1 mm to 6 mm diameter in 1 mm increments for a 5 MHz conventional UT probe. For all of the following plots, +3.9 dB was used to convert the reference amplitude of the 3 mm diameter SDH to the 1.5 mm diameter SDH.

Table 6.1 Change in Reference Amplitude for 3 mm dia. SDH vs. 1.5 mm dia. SDH

Probe	**Δ(dB)**
5 MHz PAUT	3.7
2.25 MHz PAUT	4.2
2.25 MHz conventional UT	3.9
Average	**3.9**

AWS D1.5:2015 Annex K classifies the flaws into four categories (Class A, B, C, and D) and provides maximum flaw lengths for each classification. AWS D1.5:2015 Annex K does not modify the acceptance criteria depending on the plate thickness. In other words, the acceptance criteria are exactly the same for 0.5” thick welds as 4” thick welds. Because there is separate acceptance criteria for flaws located near the surface and middle of the weld, two lines are plotted for AWS Annex K when compared to the ISO and CSA acceptance criteria. Only the acceptance criteria for tension welds are plotted.

The CSA W59:2018 acceptance criteria was developed by converting the traditional conventional UT tables to a single table which can be applied at any beam angle [14]–[16]. It incorporates TCG and uses a 1.5 mm diameter SDH for reference. The intent was to create an acceptance criteria which would give an equivalent level of quality to the traditional conventional UT inspection but allow the use of different sized probes and/or PAUT. The acceptance criteria is similar to AWS Annex K in that the flaws are classified into four categories (Class A, B, C, and D) and provides maximum flaw lengths for each classification. In fact, the only differences in the flaw lengths is that the Class B flaws are allowed up to 0.75” in length for cyclic welds per CSA W59 rather than 0.5” for tension welds according to AWS Annex K. Different criteria are given for static and cyclic welds, but only the cyclic criteria are compared in the figures below. The CSA W59 acceptance criteria depend on the plate thickness as well as whether the flaw is located near the surface.

ISO 19285:2017 [17] Level 2 corresponds to what would be typically required for bridge welds. It can be evaluated using either flaw height and length sizing or maximum amplitude and flaw length. The amplitude-based acceptance criteria depend on the plate thickness and provides maximum amplitude for certain flaw lengths. Unlike the AWS and CSA acceptance criteria, the ISO acceptance criteria does not depend on whether the flaw is near the surface of the plate or whether the weld is in tension or compression. Because the ISO acceptance criteria depends on the plate thickness, the ISO acceptance level for the thinnest and thickest plate thickness in each range of plate thicknesses will be plotted to compare to the AWS and CSA acceptance criteria.

The following four plots (Figure 6.1 through Figure 6.4) display the comparison of the three different acceptance criteria for various plate thickness ranges. These plate thickness ranges were chosen based on the thickness classifications in the ISO and CSA acceptance criteria. Any flaw that is above the acceptance criteria lines would be rejectable while those that fall under the acceptance criteria lines would be acceptable. Therefore, the acceptance criteria that have lines further towards the bottom-left corner are more conservative since the area above the line is increased (i.e., more flaws will be rejectable).

As can be seen in these plots, AWS Annex K is the least conservative acceptance criteria for very thin plates (i.e., 5/16” to 9/16”) while the proposed CSA acceptance criteria is the most conservative. In fact, there is more than a 15 dB difference between the CSA and AWS Annex K acceptance criteria for short flaws. For standard bridge welds with plates between 9/16” to 2.5” thick, the AWS Annex K and ISO acceptance criteria yield very similar results. The CSA acceptance criteria is still very conservative compared to the other acceptance criteria. For very thick plates (i.e., 2.5” to 4”) the ISO acceptance criteria seems to be the least conservative with

AWS Annex K falling between ISO and CSA. For thick plates, the difference between the AWS Annex K and CSA acceptance criteria is much smaller, but the CSA proposed acceptance criteria is still the most conservative.

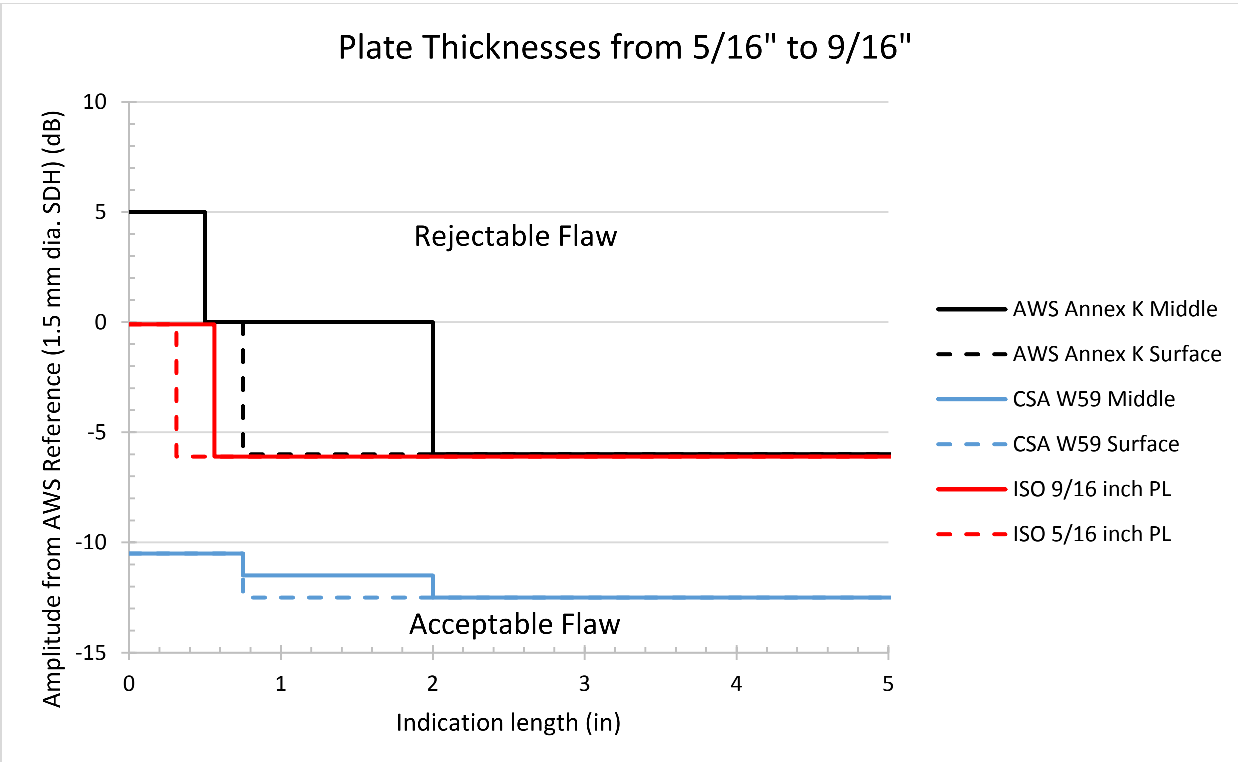

Figure 6.1 Comparison of Amplitude-based Acceptance Criteria for 5/16” to 9/16” Plates

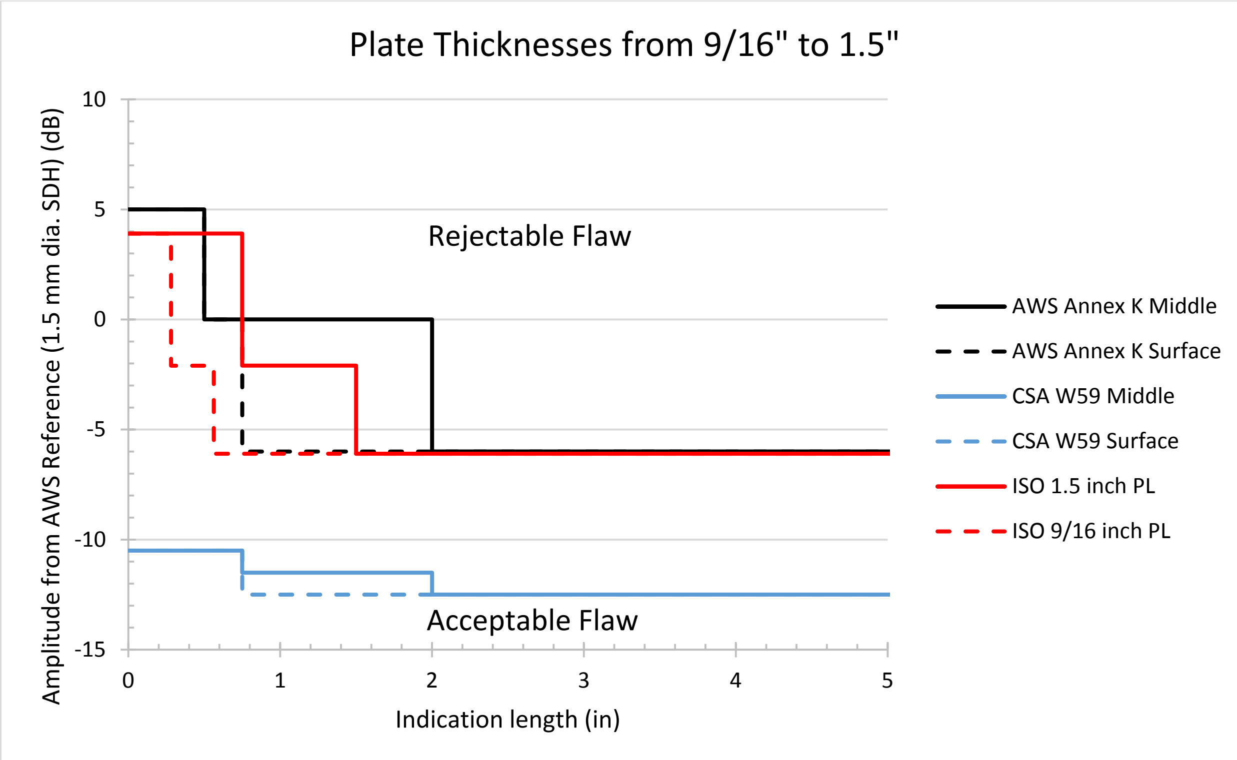

Figure 6.2 Comparison of Amplitude-based Acceptance Criteria for 9/16” to 1.5” Plates

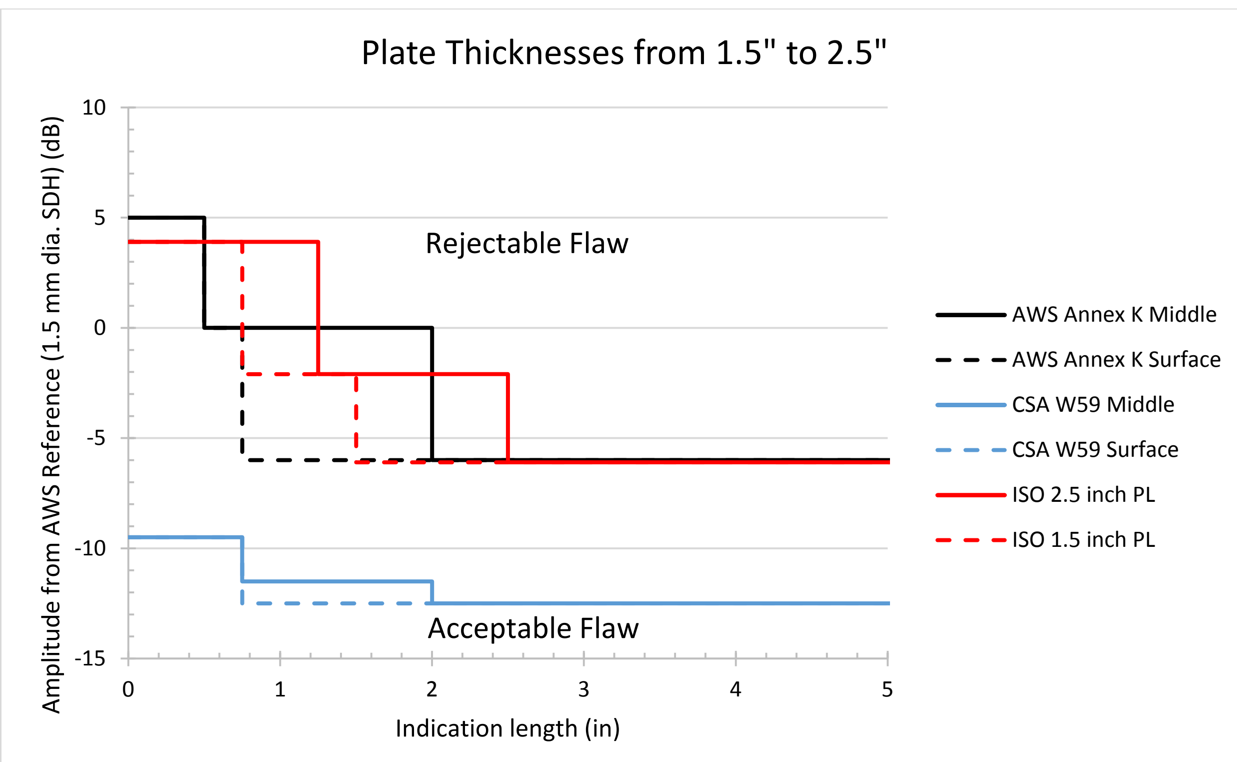

Figure 6.3 Comparison of Amplitude-based Acceptance Criteria for 1.5” to 2.5” Plates

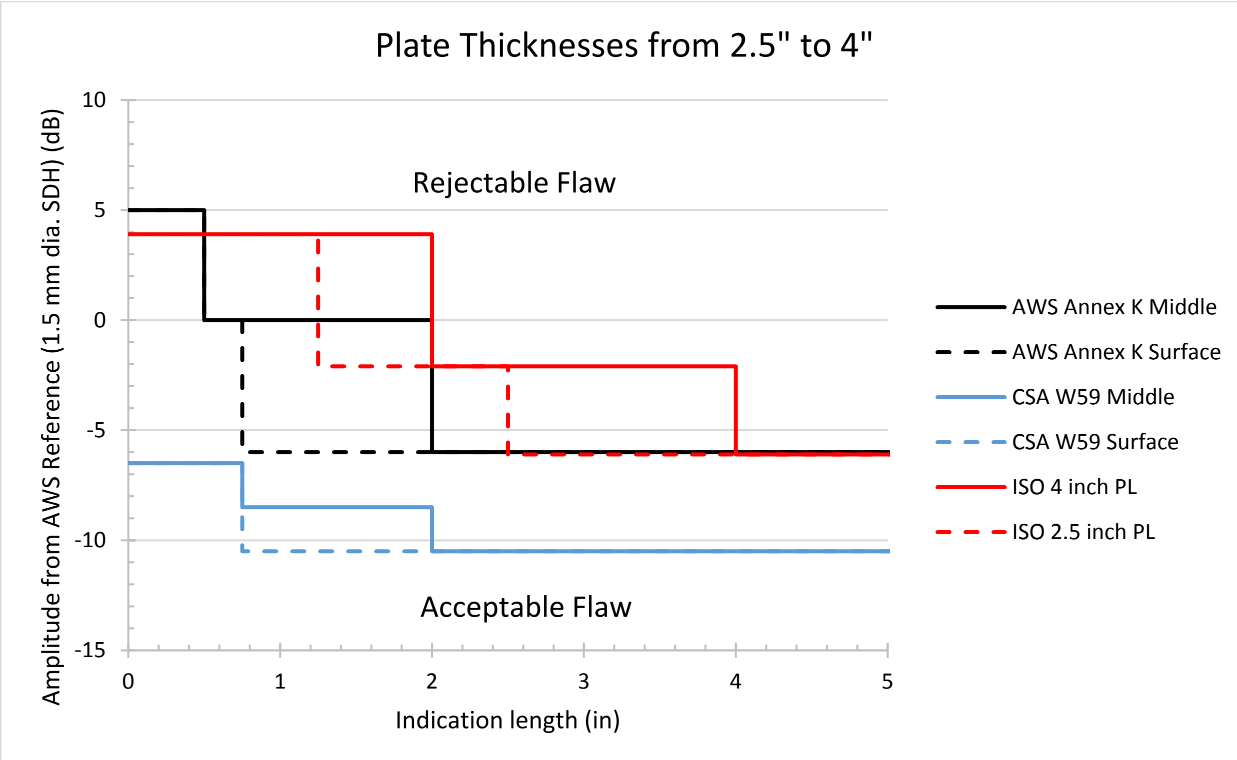

Figure 6.4 Comparison of Amplitude-based Acceptance Criteria for 2.5” to 4” Plates

Considering that there is no literature on the development and justification of AWS Annex K acceptance criteria, it is very helpful to quantitatively compare AWS Annex K to other acceptance criteria to determine whether it seems reasonable. It must be noted, though, that this data only serves as a comparison between different acceptance criteria and that there is no justification between one being right or wrong. No literature has been found which documents the development and basis of the ISO 19285 acceptance criteria. Members of the ISO PAUT committee were contacted and, while a response was received that the request was forwarded to the expert of the ISO working group, no additional information was ever received. While literature [14]–[16] has been documented outlining the steps that the CSA working group took to attempt to provide a consistent level of quality as the original conventional UT amplitude tables, in the end, that approach also involved averaging three very different amplitude tables into one “equivalent” table along with some minor manual manipulation.

6.1.2 Recommendation for AWS on reference standard reflectors

While correction for differences for attenuation and velocity between the calibration block and the test object may be provided through the use of certain probes and incidence angles or through the use of a transfer correction, it can also be provided by using a calibration block which is acoustically equivalent to the test object. Thus, fabrication of additional calibration blocks which are acoustically equivalent to the various steels commonly used in a shop may be prudent. As discussed previously, the orientation and scanning face of the calibration block is also critical for acoustic anisotropic material such as TMCP processed steel. Therefore, guidance is provided on recommendations for proper calibration block design. Due to the necessary sensitivity for flaw detection and rejection discussed in the following sections, it is recommended that the 1.5 mm (0.06") diameter SDH reference standard reflector be used for calibration and setting reference amplitude. This is the same reference standard reflector which is currently being used in AWS Annex K; therefore, no changes to the code in regards to the reference standard reflector are necessary.

Calibration blocks can be machined from a strip of steel removed from a plate with 0.06" (1.5 mm) diameter SDHs drilled through the width. In order to provide enough sound paths for TCG calibration, it is recommended that one SDH be placed near the surface of the plate and the other placed either in the center or third-point depending on the plate thickness. This provides for many possible TCG points as shown in Figure 6.5. It is recommended that the current limit of a minimum of 3-point TCG be carried forward in the new version of Annex K, but nine or more TCG points are possible from this block. The hole near the surface should be placed at least 0.2" away from the surface in order to distinguish the first leg indication from the second leg indication. The hole 0.2" away (minimum) from the surface should not be scanned with a skip off of the near surface since the small ligament between the edge of the hole and surface of the plate can result in increased amplitude. This is similar to a corner trap from a surface breaking flaw. CIVA analysis was performed to determine the minimum ligament for the SDH from the surface of the plate in order to use it for skipping off of the backwall. It was determined that a 0.5" minimum depth from the surface of the plate should be provided in order to skip from the near surface. It is recommended that this limit be included in the calibration block geometry requirements in Annex K.

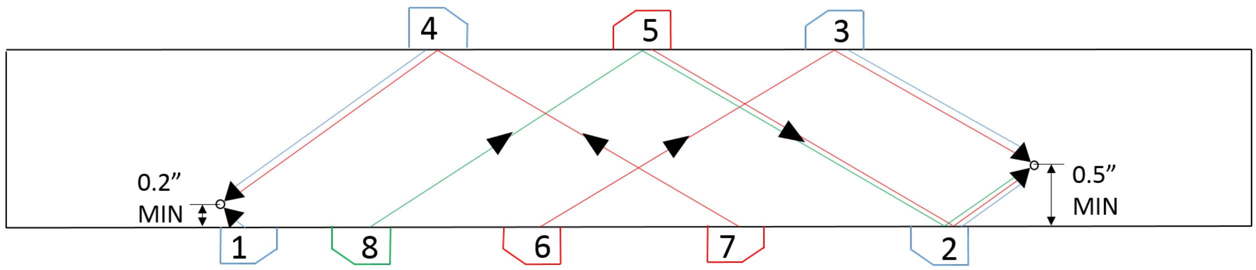

Figure 6.5 Possible TCG Scanning Positions

The width of the block should be large enough to accommodate for the beam spread without funneling the sound beam along the calibration block at long sound paths. The JIS Z 3060 code includes the following equation for estimating a suggested minimum width of the calibration block:

$$W > 2 \times \lambda \times S/D$$

Where:

W: width of the calibration block

λ: wavelength

S: maximum sound path to be used

D: width of the transducer

Using typical values in this equation such as a 11.7” sound path which would represent a 4” depth at 70° incidence angle, the minimum width of the block would be 2.1” for a 2.25 MHz probe with a 16 mm width and 1.7” for either a 2.25 MHz probe with a 20 mm width or a 5 MHz probe with a 10 mm width. Therefore, a 2” width will likely be adequate for most blocks although a narrower block may be appropriate if it is used over shorter sound paths. It is recommended that Annex K include requirement that the calibration block be of sufficient width to allow for adequate beam spread at the longest sound path used for calibration. It is recommended that the JIS code equation be provided in the commentary as a recommended minimum width of the calibration block.

Finally, the length of the block should be adequate to accommodate multiple skips for TCG calibration and pitch-catch comparison to the test object. Therefore, it is recommended that the spacing of the two holes be wide enough to provide for the double V-path in the pitch-catch setup for the 70° incidence angle. This will also provide adequate clearance for multiple skips for the TCG calibration.

The holes should also be spaced far enough from the end of the plate to limit the corner trap signal from affecting the TCG calibration. For instance, as a PAUT probe is swept over the SDH for TCG calibration, the high incidence angle can hit the corner trap before the low incidence angle have been calibrated. If the corner trap signal has greater amplitude than the SDH, the corner trap amplitude will incorrectly be used for the TCG calibration rather than the SDH amplitude. There are two ways to avoid this issue: (1) space the SDH far enough from the end of the plate so that the corner trap is not reached at the high incidence angles or (2) separate the incidence angle range into multiple groups and perform TCG calibration on each group separately. For instance, the 40°-70° incidence angle range could be split into a 40°-60° range and a 60°-70° range and each range swept over the SDH independently. The TCG for each angle range is then combined within the instrument software to provide for a single TCG covering the entire angle range. This is particularly an issue for long sound paths such as skipping in second or third leg on the calibration block since the coverage between the 40° beam and the 70° is quite large.

Based on preliminary CIVA analysis, it is recommended that the SDHs should be spaced at least 5” from the end of the plate for a 1” plate thickness but that the TCG may still require splitting into two groups for long sound paths. The recommended dimensions for a 1” thick calibration block are shown in Figure 6.6 but the SDH spacing and plate width may be modified based on the specific probe used in the inspection. The dimensions for the plate length, width, SDH depth, spacing, and placement may all be different for different plate thicknesses. For instance, the recommended dimensions for a 2” thick calibration block are shown in Figure 6.7. This plate would also require the TCG to be split into two groups for long sound paths such as the 3rd leg 4.5” depth TCG point. The 2.5” width was determined by using the 70° incidence angle for a 2.25 MHz 16 mm wide probe (equivalent to 5 MHz 8 mm wide probe) for the 3rd leg 4.5” depth TCG point since this point would cover 1st and 2nd leg scanning for 2” thick material. It should be noted that machining a 0.06” dia. SDH through 2.5” thick material may be difficult due to the short length of available drill bits.

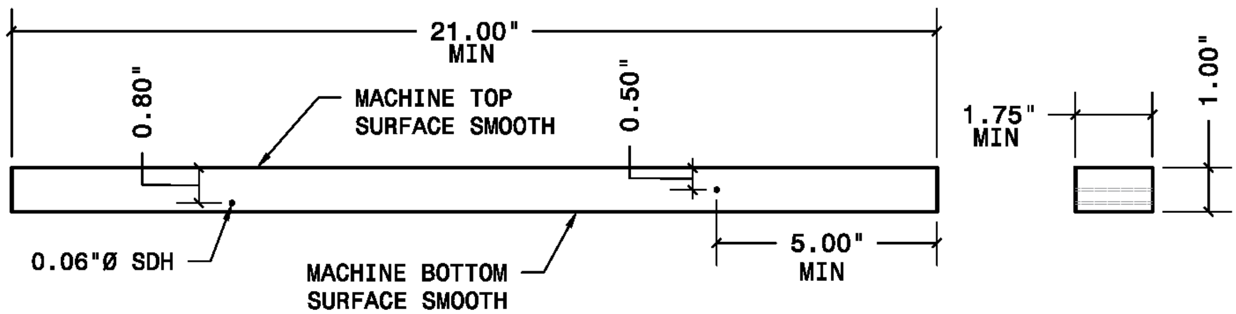

Figure 6.6 Recommended Calibration Block for 1” Thick Plate

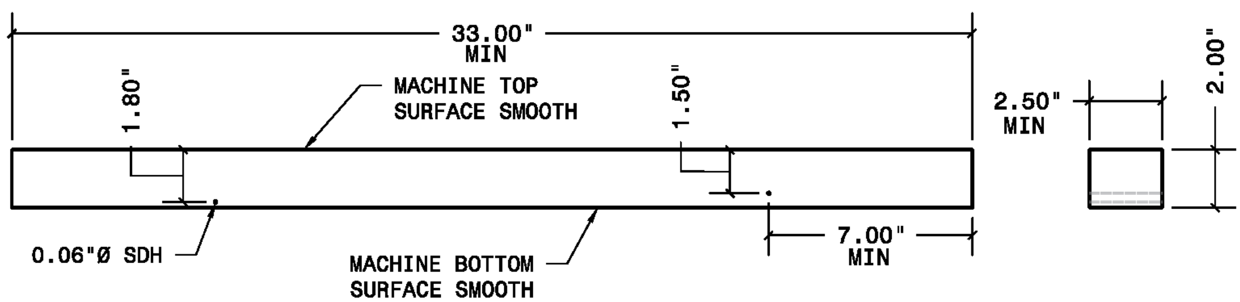

Figure 6.7 Recommended Calibration Block for 2” Thick Plate

Finally, it is recommended that Annex K require the calibration block to be similar in temperature to the test object when calibration is performed. During the attenuation experimental testing, differences in attenuation measurements were noted when measurements were taken at different temperatures. It is recommended that the temperature limits from the AWS D1.1 PAUT proposal of ±25 °F be included in AWS D1.5 Annex K.

6.2 CIVA Modeling of Target Critical Weld Flaws

The second parametric study using CIVA evaluated the effects of variations in the amplitude response of weld flaws deemed critical per the fitness-for-service calculations. This provides a rational comparison of the amplitude from the critical weld flaws to the acceptance criteria amplitude limits. The parametric models varied the plate thickness along with the flaw type, size, position, tilt, and skew of weld flaws in order to compare the maximum amplitude of the indication response with the reference amplitude.

6.2.1 Maximum amplitude

The study included comparing the maximum amplitude of the weld flaw to the amplitude of a SDH at similar depth and incidence angle. This would be equivalent to the maximum amplitude which would be reported during raster scanning if TCG was used with a 1.5 mm (0.06") diameter SDH. Note: conventional UT would report the inverse of this number as that approach involves changing the gain (up or down) to obtain the same amplitude in full-screen height as the SDH reference standard. It should be noted that the probe remained perpendicular to the weld axis for all simulations so the "Flaw Skew" case involved skewing the longitudinal axis of the weld flaw in relation to the weld axis. This results in angular skew between the probe and the flaw. CIVA modeling was performed with the 2.25 MHz 16x16 mm aperture PAUT probe with an angular range of 45°-70°, unless otherwise noted.

Specimen matrices for planar surface flaws and planar embedded flaws are given in Table 6.2 and Table 6.3. The ligament is defined as the distance from the bottom of the flaw to the backwall of the plate. Therefore, all surface flaws were near the backwall, rather than near the scanning surface. It is anticipated that similar results will be found for flaws near the scanning surface since TCG accounts for the sound loss due to attenuation. Also, since simulations were performed for 0.5", 2", and 4" plate thicknesses, the 4" surface flaw results would be equivalent to skipping off of the backwall for a flaw near the scanning surface in a 2" thick plate. All simulations were performed including one half skip (i.e., 1st and 2nd leg), as shown in Figure 6.8. Tilt was defined as positive (+) for tilt away from the probe which would maximize signals in 1st leg and negative (-) for tilt towards the probe which would maximize signals in 2nd leg as shown in Figure 6.9.

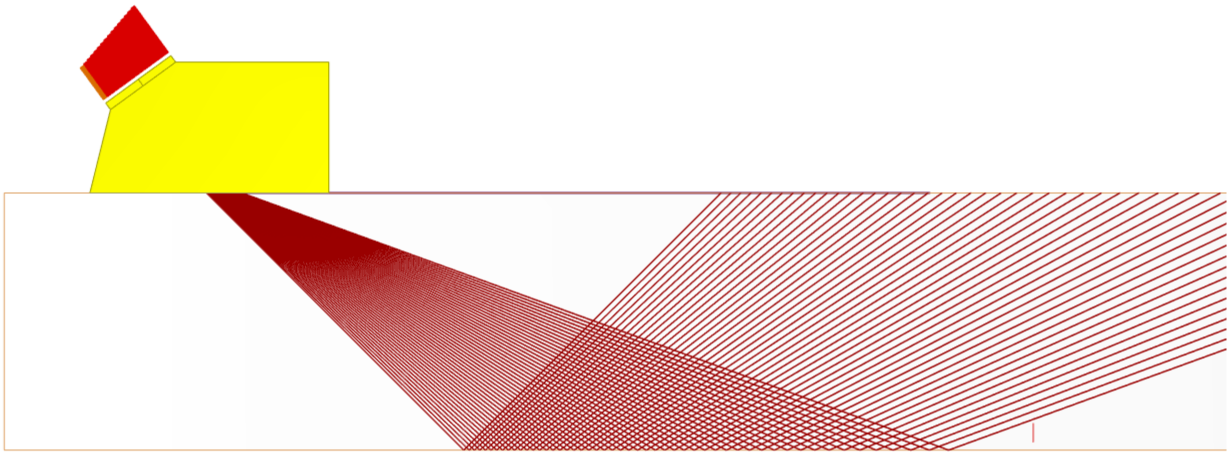

Figure 6.8 CIVA Flaw Model

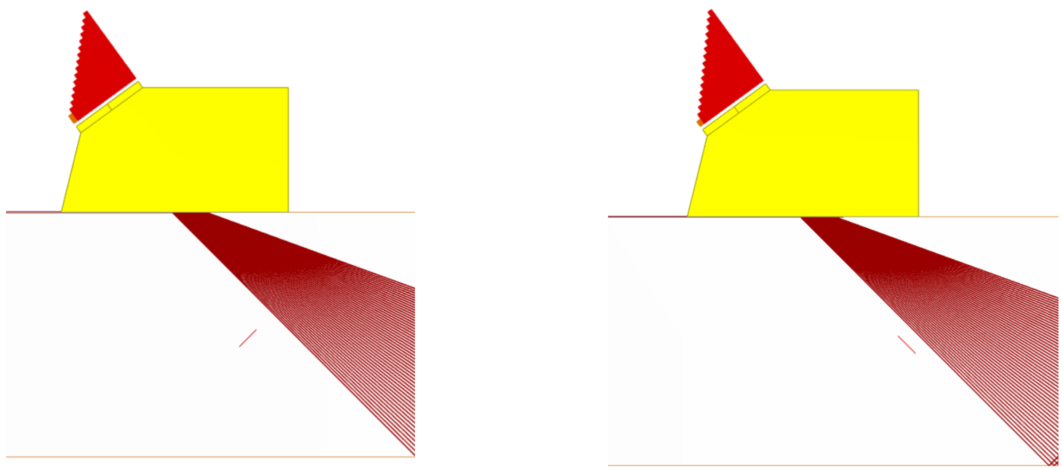

Figure 6.9 (left) Positive Tilt; (right) Negative Tilt

Table 6.2 Planar Surface Flaw Specimen Matrix for 2.25 MHz 16x16 mm

<table>
<tr><th>Flaw Height</th><th>Flaw Length</th><th>Ligament</th><th>Flaw Tilt</th><th>Flaw Skew</th><th>Plate Thickness</th></tr>
<tr><td>0.025”</td><td>0.025”, 0.05”, 0.10”, 0.15”</td><td>0”</td><td>0°</td><td rowspan="11">0°</td><td rowspan="5">0.5”, 2”</td></tr>
<tr><td rowspan="2">0.05”</td><td>0.05”, 0.10”</td><td rowspan="2">0.03”</td><td>0°, 5°, -5°, 30°, -30°, 45°, -45°</td></tr>
<tr><td>0.15”</td><td rowspan="7">0°</td></tr>
<tr><td>0.10”</td><td>0.10”, 0.15”, 0.20”</td><td>0.06”</td></tr>
<tr><td>0.15”</td><td>0.15”, 0.20”, 0.25”</td><td>0.06”</td></tr>
<tr><td>0.025”</td><td>0.025”</td><td>0”</td><td rowspan="4">4”</td></tr>
<tr><td>0.05”</td><td>0.05”</td><td>0.03”</td></tr>
<tr><td>0.10”</td><td>0.10”</td><td>0.06”</td></tr>
<tr><td>0.15”</td><td>0.15”</td><td>0.06”</td></tr>
<tr><td>0.05”</td><td>0.15”</td><td>0.06”</td><td>5°, 30°, -30°</td><td rowspan="2">0.5”</td></tr>
<tr><td>0.10”</td><td>0.15”</td><td>0.06”</td><td>5°, -5°, 30°, -30°, 45°, -45°</td></tr>
<tr><td>0.05”</td><td>0.05”, 0.10”, 0.15”</td><td>0.03”</td><td rowspan="2">0°</td><td rowspan="2">0°, 5°, 10°, 20°</td><td rowspan="2">0.5”</td></tr>
<tr><td>0.10”</td><td>0.10”, 0.15”</td><td>0.06”</td></tr>
<tr><td>0.10”</td><td>0.10”</td><td>0”, 0.06”, 0.125”, 0.25”, 0.375”, 0.5”, 0.625”</td><td>0°</td><td>0°</td><td>2”</td></tr>
</table>

Table 6.3 Planar Embedded Flaw Specimen Matrix for 2.25 MHz 16x16 mm

<table>
<tr><th>Flaw Height</th><th>Flaw Length</th><th>Ligament</th><th>Flaw Tilt</th><th>Flaw Skew</th><th>Plate Thickness</th></tr>
<tr><td>0.05”</td><td>0.05”</td><td rowspan="11">Mid-Thickness</td><td>0°</td><td rowspan="5">0°</td><td rowspan="4">0.5”, 2”</td></tr>
<tr><td>0.10”</td><td>0.10”</td><td>0°, 5°, -5°, 30°, -30°, 45°, -45°</td></tr>
<tr><td>0.15”</td><td>0.15”</td><td>0°</td></tr>
<tr><td>0.20”</td><td>0.20”</td><td>0°</td></tr>
<tr><td>0.15”</td><td>0.15”</td><td rowspan="2">5°, -5°, 30°, -30°, 45°, -45°</td><td rowspan="2">2”</td></tr>
<tr><td>0.20”</td><td>0.20”</td><td>0°, 5°, 10°</td></tr>
<tr><td rowspan="2">0.10”</td><td>0.10”</td><td rowspan="5">0°</td><td rowspan="5">0°, 5°, 10°, 20°</td><td rowspan="4">2”</td></tr>
<tr><td>0.30”</td></tr>
<tr><td>0.15″</td><td>0.15”</td></tr>
<tr><td>0.20”</td><td>0.20”</td></tr>
<tr><td>0.10”</td><td>0.10”</td><td>0.5”</td></tr>
</table>

CIVA includes two methods for modeling planar flaws. One uses an analytical model which combines the Kirchhoff and GTD models to capture both the specular reflection and tip diffraction, respectively. The other model uses an FEA solver by meshing the area around the flaw to compute the tip diffraction rather than using an analytical model. This model is referred to in CIVA as the “Transient FEM” model. The Transient FEM solver is more accurate for very small flaws where the flaw size is smaller than the wavelength, but it is much more computationally expensive with approximately 1,000 times longer computation time. For this reason, the combined

Kirchhoff/GTD model was used except for a brief comparison of the two models and to demonstrate whether the Kirchhoff/GTD model was valid.

In order to compare the Kirchhoff/GTD model to the Transient FEM model, the probe was first swept across the weld flaw using a scan increment of 0.5 mm (0.02”) to determine the Kirchhoff/GTD maximum amplitude, shown in Figure 6.10. The probe was then placed at the location where the maximum amplitude occurred for the Kirchhoff/GTD model, but the Transient FEM model was used to compute the maximum amplitude, shown in Figure 6.11. As expected, it was found that the Kirchhoff/GTD model would overestimate the amplitude for very small flaws (0.025”x0.025”) but gave reasonably similar results for 0.05”x0.05” and larger flaws. This correlates with the traditional methodology that UT can only detect flaws greater than one-half of the wavelength. For the 2.25 MHz probe, the wavelength is 0.056” so one-half of the wavelength is 0.028”.

The two models mostly gave similar results for the large flaws, but it should be noted that the Transient FEM model was only computed for one probe location in rather than incrementally sweeping across the flaw. To illustrate error from this assumption, the probe was swept over the flaw with a 0.5 mm increment using the Transient FEM model in two cases and found that the difference between the Kirchhoff/GTD and the Transient FEM models decreased considerably for the larger flaws, with updated differences of 2 dB or less. Therefore, it was determined that the Kirchhoff/GTD model could be used for all future CIVA modeling but that the amplitude of the 0.025” high flaws was not valid for the 2.25 MHz probe.

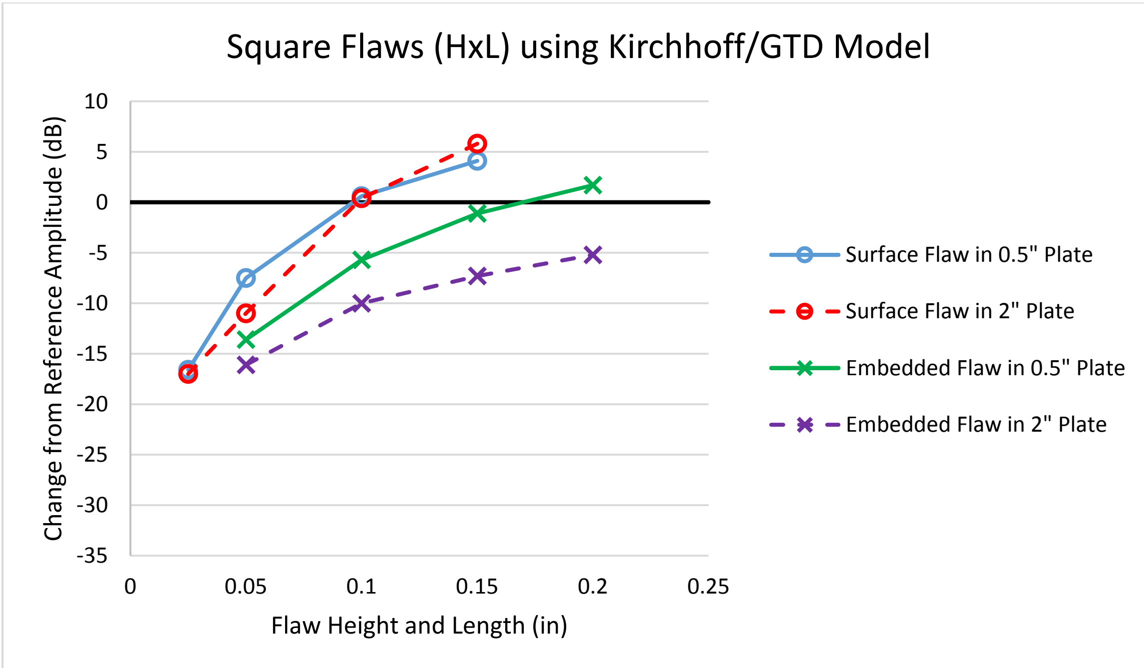

Figure 6.10 Square Flaws using Kirchhoff/GTD Model

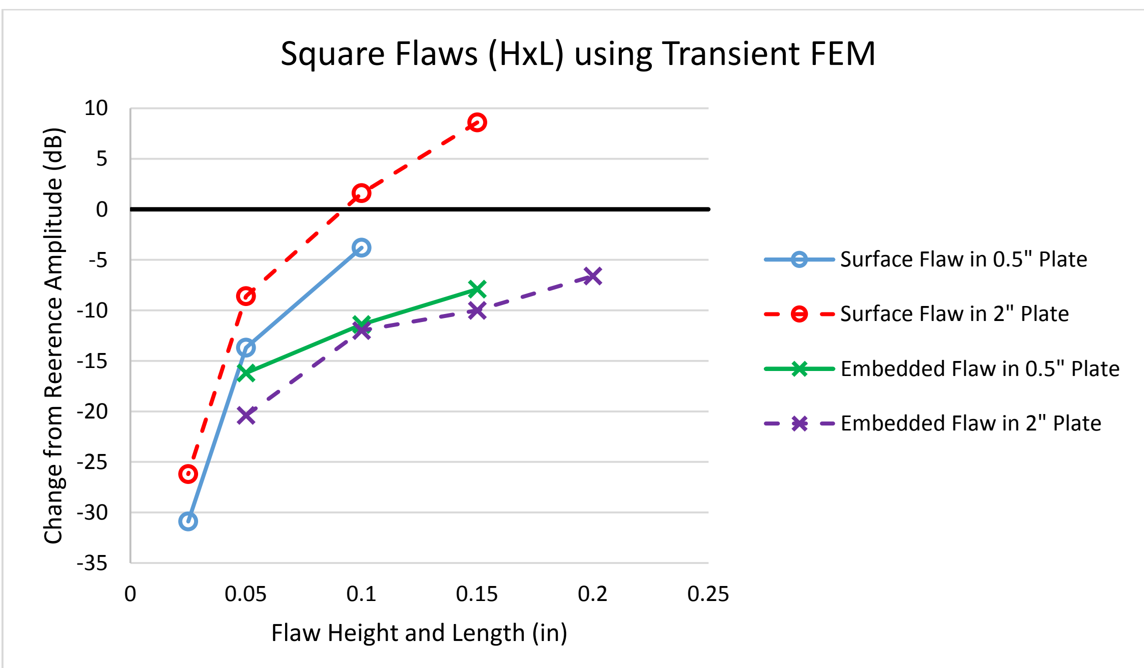

Figure 6.11 Square Flaws using Transient FEM Model

The results for planar surface/near surface flaws is shown in Figure 6.12. As expected, flaws with larger flaw height and length produced larger maximum amplitude. The maximum amplitude varied from -11 dB for a 0.05"x0.05" (H x L) flaw in a 2" plate to +10 dB for a 0.15"x0.25" (H x L) flaw in a 2" plate. For the 0.5" plate, the amplitude of the flaws was typically maximized at approximately 65° incidence angle while the incidence angle for peak amplitude for the 2" plates was approximately 56°. Referring back to the critical flaw sizes developed during the analytical FFS program, a 0.05"x0.05" surface flaw would have been acceptable in all cases except for thickness transitions under 8 ksi stress range. A 0.15"x0.25" surface flaw would have been rejectable for all cases.

Figure 6.10 displays the maximum amplitude for vertical embedded flaws located at the mid-thickness depth of 0.5" and 2" thick plates. The maximum amplitude varied from -16 dB for a 0.05"x0.05" flaw in a 2" plate up to +2 dB for a 0.20"x0.20" flaw in a 0.5" plate. Referring back to the critical flaw sizes calculated during the analytical FFS program, a 0.05"x0.05" embedded flaw would be acceptable under all conditions while a 0.20"x0.20" flaw would be rejectable for all cases. The 0.10"x0.10" embedded flaw would only be rejectable for embedded flaws in thickness transition welds with a stress range of 8 ksi, and the maximum amplitude was -10 dB for a vertical 0.10"x0.10" embedded flaws in a 2" plate.

Therefore, at first glance, it seems that the critical amplitude according to FFS would be somewhere between -16 dB and +2 dB when compared to a 1.5 mm (0.06") diameter SDH. One must remember that this is for vertical flaws where the amplitude was maximized with the probe perpendicular to the flaw. Therefore, flaws with tilt or skew will likely have much lower maximum amplitude.

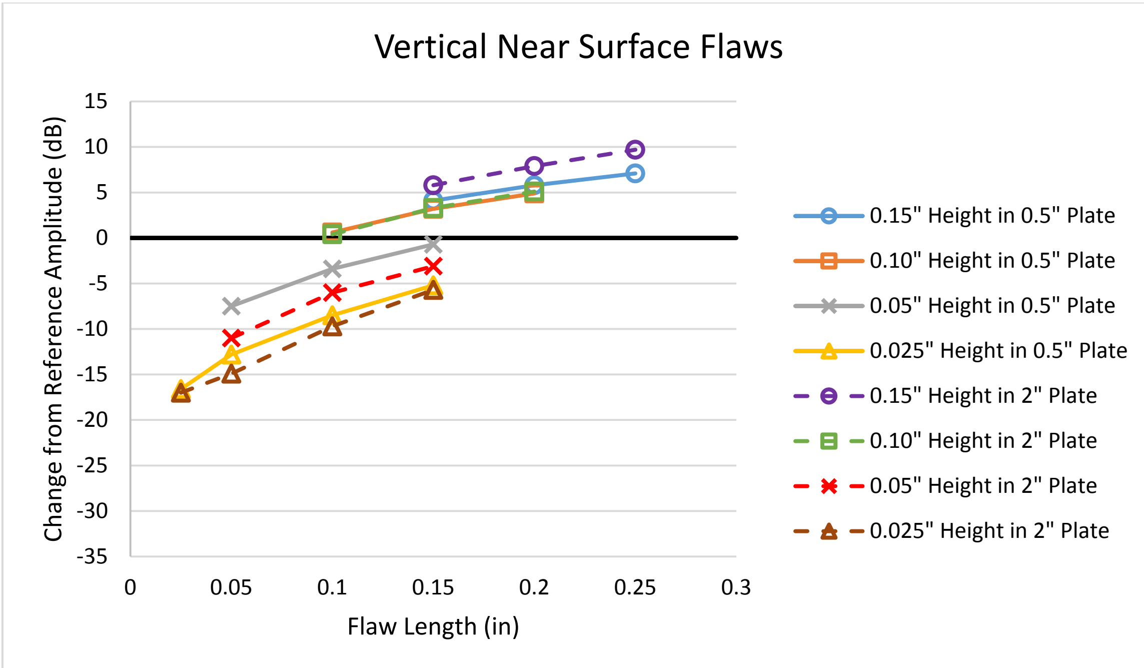

Figure 6.12 Maximum Amplitude of Near Surface Flaws

The effect of flaw tilt on near surface flaws is shown in Figure 6.13. It was found that the maximum amplitude tended to be more sensitive to flaw tilt in the 0.5" plate than the 2" plate. This is thought to be due to the increased sound path for greater thickness plates which results in more beam spread. In general, tilt of ±5° did not result in a large decrease of amplitude compared with vertical flaws. For tilt of ±30° or more, the drop of amplitude compared to vertical flaws was up to 8 dB. For instance, the maximum amplitude of the 0.05"x0.05" flaw in the 0.5" plate with -45° tilt was -15.2 dB while it was -7.5 dB when vertical (0° tilt).

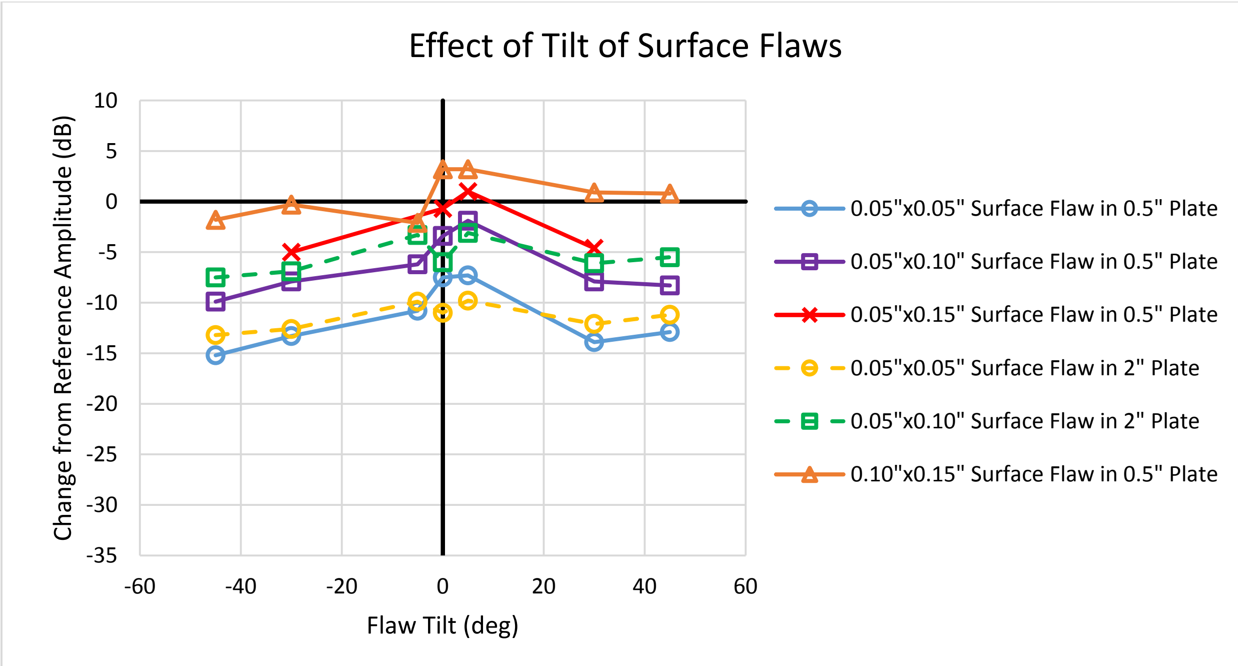

Figure 6.13 Effect of Tilt on Surface Flaws

The effect of flaw tilt on embedded flaws is shown in Figure 6.14. The maximum amplitude tended to be more sensitive to changes in flaw tilt for larger flaws. In general, tilt of ±5° did not result in a large change in amplitude. (Note: it is believed that some of the reason for the drop in amplitude from 0° tilt to ±5° for the 0.10”x0.10” flaw in a 0.5” plate is due to near field effects). For tilt of ±30° or more, the amplitude increased in all cases for embedded flaws. This is the opposite behavior compared with surface flaws where large amount of tilt decreased the amplitude. The change in amplitude for embedded flaws varied from nearly 0 dB for the 0.10”x0.10” flaw in a 0.5” plate to +15 dB for the 0.20”x0.20” flaw in the 2” plate. Therefore, an amplitude limit of -10 dB seems reasonable to reject all embedded flaws of 0.10”x0.10” and larger, regardless of the flaw tilt.

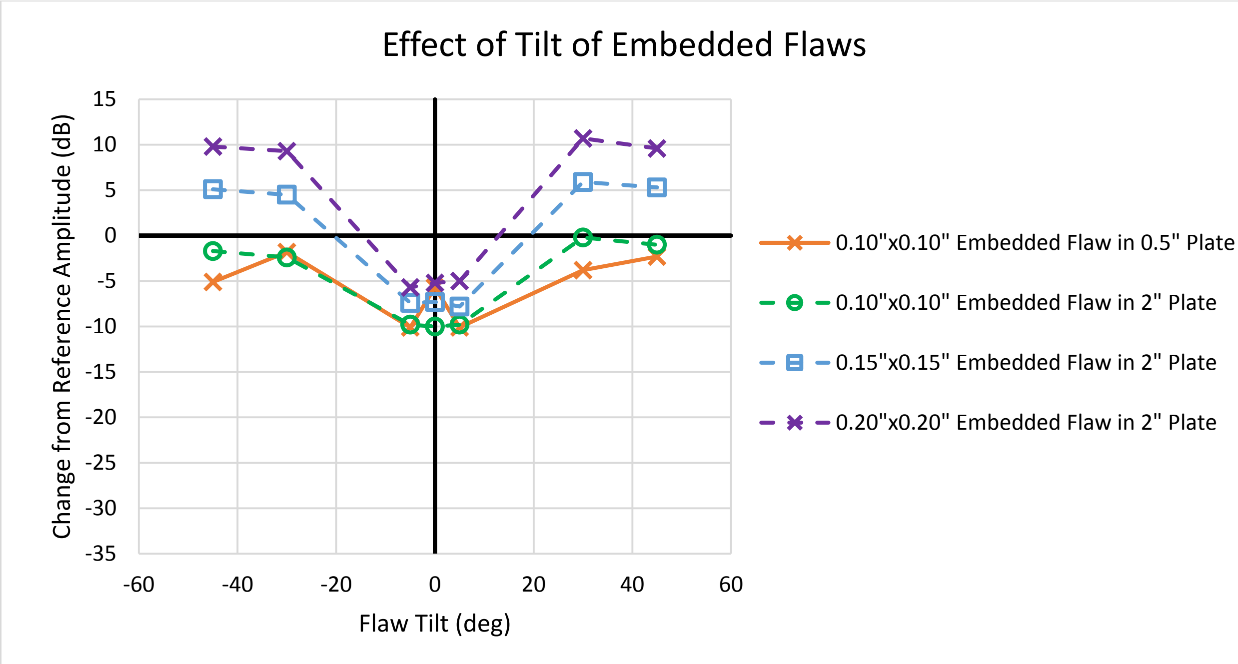

Figure 6.14 Effect of Tilt on Embedded Flaws

While the probe should be perpendicular to the longitudinal axis of the flaw if evaluated using raster scanning, the effect of flaw skew should be included in the determination of an amplitude limit for flaw detection using encoded line scanning. During encoded line scanning, the probe is kept perpendicular to the weld axis even though the flaw may be skewed compared with the weld axis. The effect of skew between the probe and the flaw is shown in Figure 6.15 for surface flaws and Figure 6.16 for embedded flaws. For these CIVA models, the flaw was skewed in relation to the weld axis and the probe remained perpendicular to the weld axis. After moving the probe perpendicular to the weld axis to maximize the amplitude, the probe was then translated parallel to the weld axis to further maximize the amplitude. This additional translation was performed since the maximum amplitude may not occur when the probe is centered on a skewed flaw due to the sound being reflected horizontally along the weld axis.

As expected, the amplitude decreased when the flaw was skewed compared to the probe axis. The drop in amplitude was greater for longer flaws and for longer sound paths. The increased drop in amplitude for longer flaws is believed to be due to the fact that the sound is reflecting off of the skewed flaw at different moments in time along the length of the flaw. For instance, the amplitude of a 0.05”x0.15” flaw was lower than a 0.05”x0.05” flaw when the flaw was skewed by 10° or greater. It is believed that the larger drop for longer sound paths is due to the sound traveling further away from the probe horizontally along the weld axis.

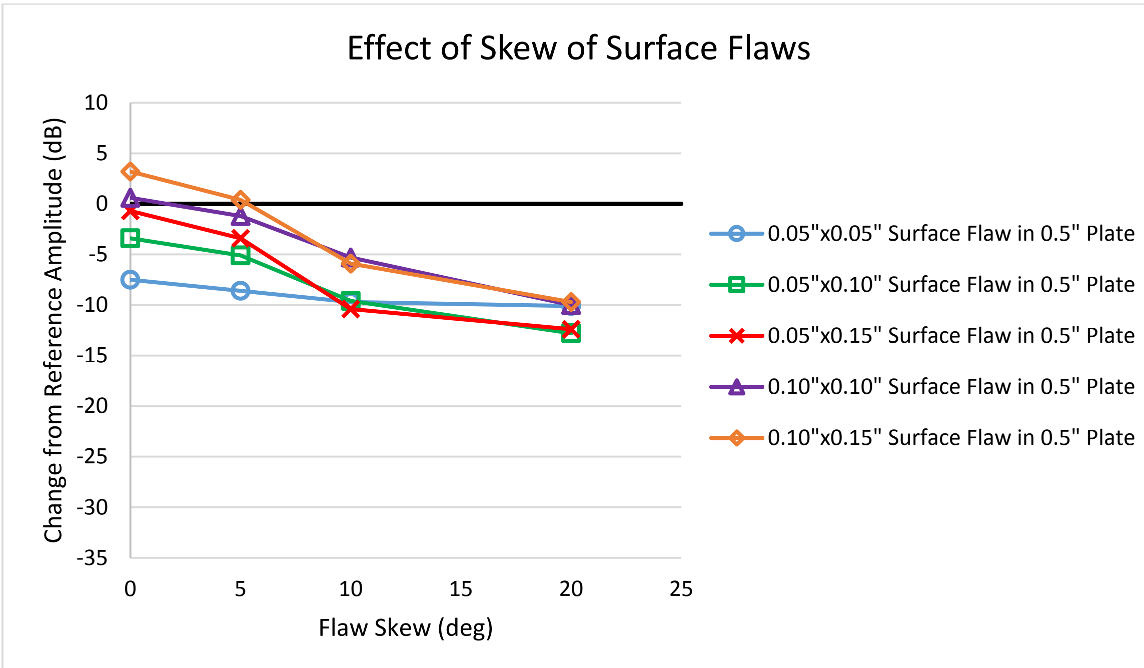

Figure 6.15 Effect of Skew on Surface Flaws

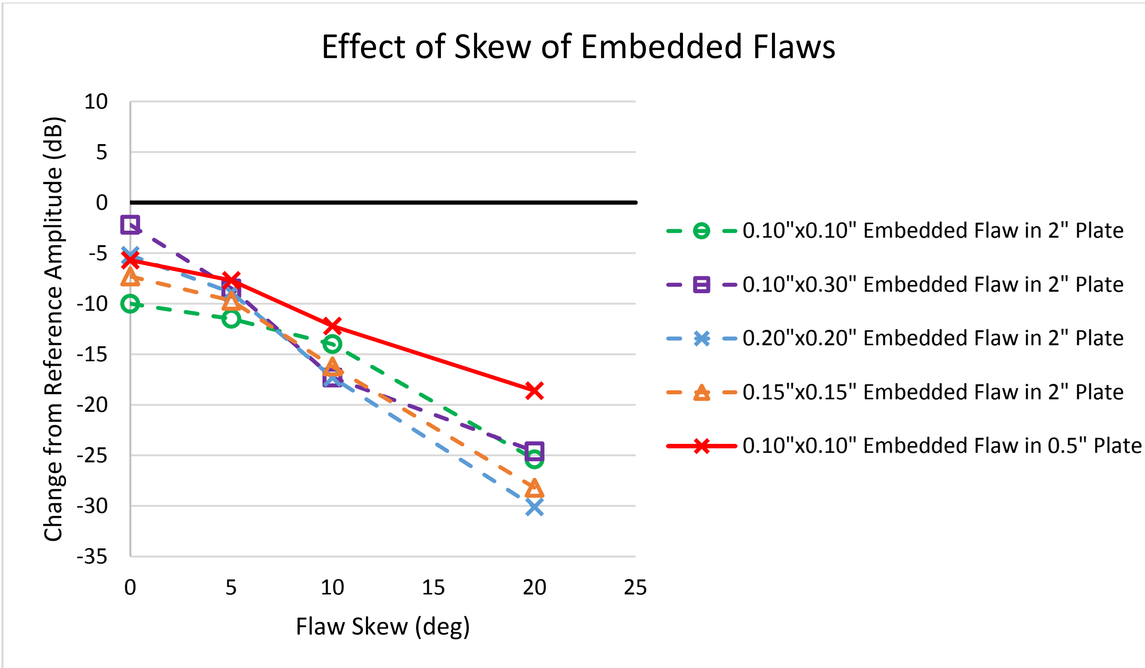

Figure 6.16 Effect of Skew on Embedded Flaws

Finally, the effect on the maximum amplitude due to changes in the ligament distance is shown in Figure 6.17. For these models, a vertical surface flaw had the ligament distance increased until the flaw reached the mid-thickness of the plate. Therefore, the ligament of 0.95" case is equal to the embedded flaw result shown previously. The amplitude remained nearly constant until the ligament distance reached 0.375". The amplitude then decreased for ligament distances greater than 0.375" until reaching 0.625". The amplitude was nearly constant for ligaments greater than 0.625". This is a similar result as the CIVA simulations that were performed to determine the distance that a SDH would need to be placed away from the surface of the plate in order to avoid obtaining increased amplitude when skipping off of the backwall. In the SDH model, it was found that a ligament of 0.5" was needed in order for the effect of the backwall to be negligible.

The ASME Code Case 2235 [30] fracture mechanics based acceptance criteria considers a near surface flaw to be considered as a surface flaw if the ligament distance is less than or equal to half of the flaw height. For the 0.10"x0.10" flaw, the maximum ligament distance to be considered a surface indication would be 0.05". In this case, the total flaw height would be considered as 0.15" since the ligament is included in the flaw height for near surface flaws. Based on the results in

Figure 6.17, it seems that the amplitude should remain relatively high over small ligament distances for near surface flaws. ASME Code Case 2235 acceptance criteria considers all flaws with a ligament greater than half the flaw height to be embedded. According to the CIVA results, embedded flaws with small ligaments would have greater amplitude than those with larger ligament. Therefore, placement of the embedded flaw at the mid-thickness depth for the CIVA models is slightly conservative considering that the critical flaw size was determined through FFS assuming embedded flaws were at the quarter thickness depth.

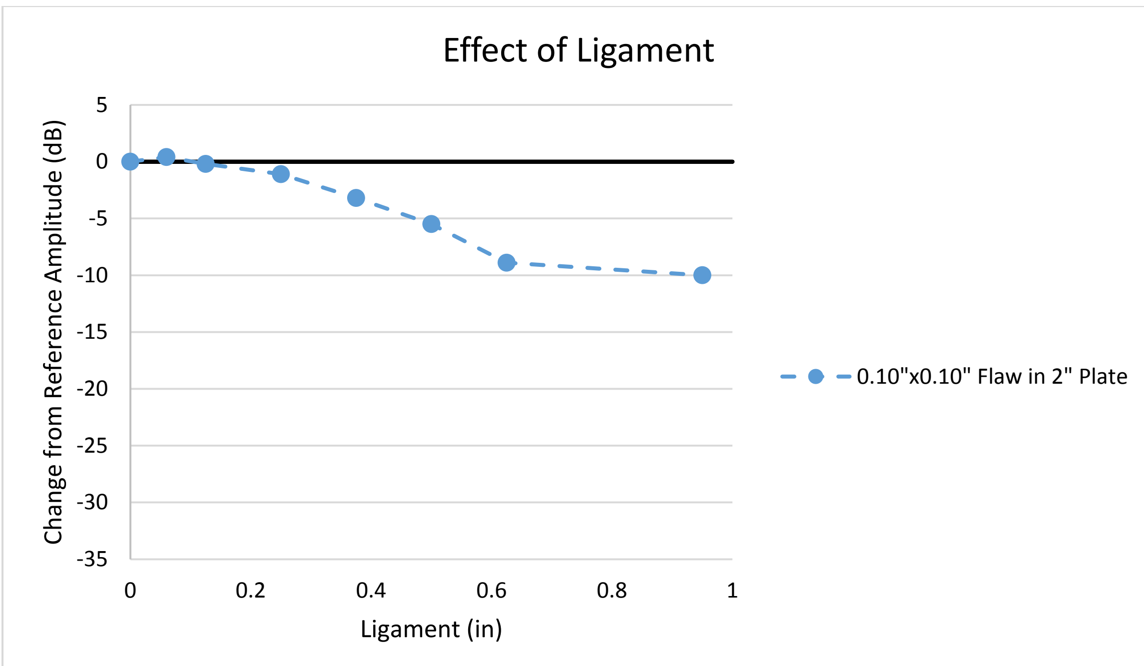

Figure 6.17 Effect of the Ligament Distance

The specimen matrix for volumetric flaws is given in Table 6.4. All flaws were assumed to be spherical and slag was modeled with a density and shear wave velocity equivalent to alumina (ρ=3.97 g/cm^3; v_s=5800 m/s) since this is very similar to typical slag density according to prior research [35], [36]. This was also recommended by CIVA training staff to be used for modeling of slag inclusions. The density and velocity is important since the product of these two properties forms the acoustic impedance. The amount of ultrasonic energy which is reflected off of or transmitted through an indication is related to the change in acoustic impedance from steel to the indication medium. Since the slag is assumed to be perfectly bonded to the steel, some sound can propagate through the slag inclusion. Porosity, on the other hand, is a result of an air pocket which has much different density and shear wave velocity (ρ=0.001 g/cm^3; v_s=0 m/s). Therefore, if the slag inclusion is not perfectly bonded to the steel, the amount of sound reflecting off of the surface will be greatly increased.

Comparing the results for slag in Figure 6.18 and porosity in Figure 6.19, the spherical slag inclusions had much lower amplitude than the spherical porosity of similar diameter. The largest amplitude for slag was -14 dB for a 0.25" diameter near surface inclusion. Porosity had much larger amplitude (-5 dB) for a 0.25" diameter near surface pore and -13 dB for a 0.08" diameter near surface pore. Due to the fact that so much sound was propagating through the slag inclusions rather than reflecting off of them, the results from the porosity models were used for the determination of volumetric flaw detection and rejection amplitude limits.

Table 6.4 Volumetric Flaw Specimen Matrix for 2.25 MHz 16x16 mm

<table>
<tr><th>Flaw Diameter</th><th>Flaw Type</th><th>Ligament</th><th>Plate Thickness</th></tr>
<tr><td>0.08"</td><td rowspan="3">Slag</td><td rowspan="6">0.06", Mid-Thickness</td><td>0.5"</td></tr>
<tr><td>0.12"</td><td>0.5", 2"</td></tr>
<tr><td>0.25"</td><td>2"</td></tr>
<tr><td>0.08"</td><td rowspan="5">Porosity</td><td>0.5", 2"</td></tr>
<tr><td>0.125"</td><td>0.5"</td></tr>
<tr><td>0.25"</td><td>0.5", 2"</td></tr>
<tr><td>0.03"</td><td>0.02"</td><td>0.5"</td></tr>
<tr><td>0.125"</td><td>Mid-Thickness</td><td>2"</td></tr>
</table>

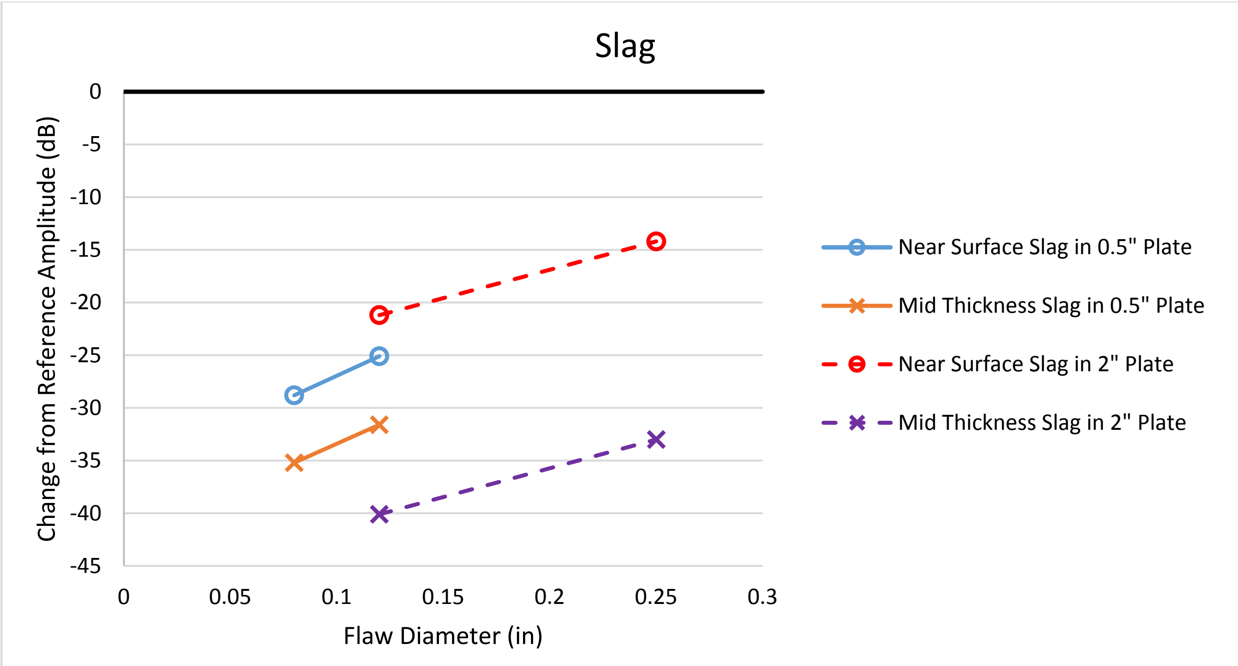

Figure 6.18 CIVA Slag Results

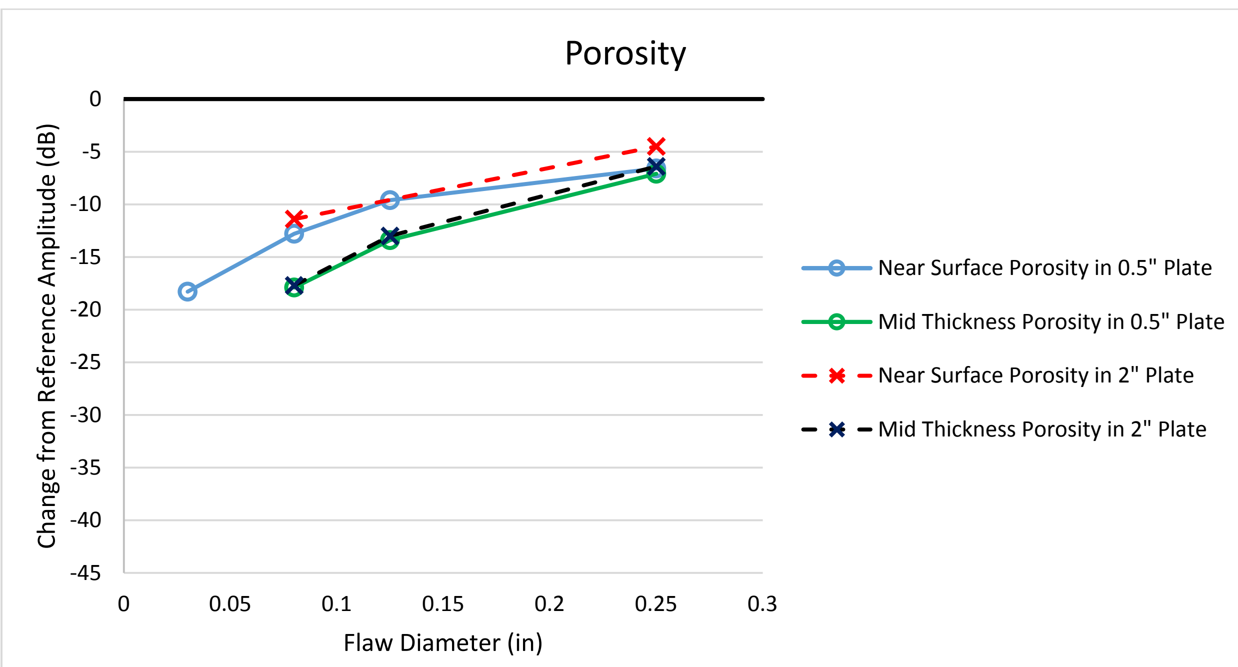

Figure 6.19 CIVA Porosity Results

All of the results reported above for planar and volumetric flaws were modeled using a 2.25 MHz 16x16 mm probe. Additional models were performed to compare the results if different frequency and apertures were used. The specimen matrix shown in Table 6.5 is for a 5 MHz 10x10 mm aperture and Table 6.6 is for 2.25 MHz 10x10 mm and 24x24 mm apertures.

Table 6.5 Planar Flaw Specimen Matrix for 5 MHz 10x10 mm

<table>
<tr><th>Flaw Height</th><th>Flaw Length</th><th>Ligament</th><th>Flaw Tilt</th><th>Flaw Skew</th><th>Plate Thickness</th></tr>
<tr><td>0.025”</td><td>0.025”</td><td>0”</td><td rowspan="11">0°</td><td rowspan="4">0°</td><td rowspan="4">0.5”, 2”</td></tr>
<tr><td>0.05”</td><td>0.05”</td><td>0.03”</td></tr>
<tr><td>0.10”</td><td>0.10”</td><td>0.06”</td></tr>
<tr><td>0.15”</td><td>0.15”</td><td>0.06”</td></tr>
<tr><td rowspan="2">0.05”</td><td>0.05”</td><td rowspan="2">0.03”</td><td rowspan="2">0°, 5°, 10°, 20°</td><td rowspan="2">0.5”</td></tr>
<tr><td>0.15”</td></tr>
<tr><td>0.10”</td><td>0.10”</td><td>0”, 0.06”, 0.125”, 0.25”, 0.5”</td><td rowspan="5">0°</td><td>2”</td></tr>
<tr><td>0.05”</td><td>0.05”</td><td rowspan="4">Mid-Thickness</td><td rowspan="4">0.5”</td></tr>
<tr><td>0.10”</td><td>0.10”</td></tr>
<tr><td>0.15”</td><td>0.15”</td></tr>
<tr><td>0.20”</td><td>0.20”</td></tr>
</table>

Table 6.6 Planar Flaw Specimen Matrix for 2.25 MHz 10x10 mm and 24x24 mm

<table>
<tr><th>Flaw Height</th><th>Flaw Length</th><th>Ligament</th><th>Flaw Tilt</th><th>Flaw Skew</th><th>Plate Thickness</th></tr>
<tr><td>0.025”</td><td>0.025”</td><td>0”</td><td rowspan="4">0°</td><td rowspan="4">0°</td><td rowspan="4">0.5”, 2”, 4”</td></tr>
<tr><td>0.05”</td><td>0.05”</td><td>0.03”</td></tr>
<tr><td>0.10”</td><td>0.10”</td><td>0.06”</td></tr>
<tr><td>0.15”</td><td>0.15”</td><td>0.06”</td></tr>
</table>

As expected, use of a high frequency probe resulted in higher amplitude for very small flaws. The wavelength for the 5 MHz probe is half the wavelength of the 2.25 MHz probe so the one-half wavelength flaw height would correspond to 0.013” rather than 0.025”. Therefore, the comparison of the 0.025”x0.025” flaw using Transient FEM found that Kirchhoff/GTD model only overestimated the amplitude by less than 4 dB for the 5 MHz probe rather than over 9 dB for the 2.25 MHz probe. Therefore, the Kirchhoff/GTD results of 0.025” high flaws and larger seem to be valid for the 5 MHz probe.

The 5 MHz 10x10 mm results for the vertical surface and embedded flaws are compared to 2.25 MHz 16x16 mm in Figure 6.20. For the near surface flaws, the amplitude using the 5 MHz probe was always equal to or greater than the amplitude from the 2.25 MHz probe. The largest increase of amplitude from the 5 MHz probe compared with the 2.25 MHz probe was +5 dB occurring for the 0.05”x0.05” surface flaw in the 2” plate. For the embedded flaw, the amplitude was slightly lower for the 5 MHz probe compared with the 2.25 MHz probe with the largest decrease being -3 dB.

The effect of skew was also compared for the 5 MHz and 2.25 MHz probes since the probes have different beam spread. It was found that the 5 MHz probe did not have significantly different results for skewed flaws compared with the 2.25 MHz probe with all results within 3 dB. Finally, the effect of ligament distance is compared to the 2.25 MHz probe in Figure 6.21. The amplitude consistently decreased as the ligament was increased for the 5 MHz probe. This differs from the 2.25 MHz results where the amplitude is mostly consistent for all ligaments 0.25” or less.

Overall, the difference in results between the 2.25 MHz and 5 MHz probe did not seem significant enough to warrant modification to the flaw detection and rejection amplitude limits described in Section 6.3 and 6.4 of this report. Therefore, it is proposed that the same acceptance criteria and scanning procedures be used for inspection with 2.25 MHz or 5 MHz probes. Any increase in amplitude for the 5 MHz probe compared with the 2.25 MHz probe such as near surface flaw results and ligament distance results will result in conservative assessment of the flaw for detection and rejection since the 2.25 MHz probe was used in the development of the amplitude limits. The slightly lower amplitude for embedded flaws and the slight differences due to flaw skew for the 5 MHz probe compared with the 2.25 MHz probe is not considered to be significant since all results were within 3 dB.

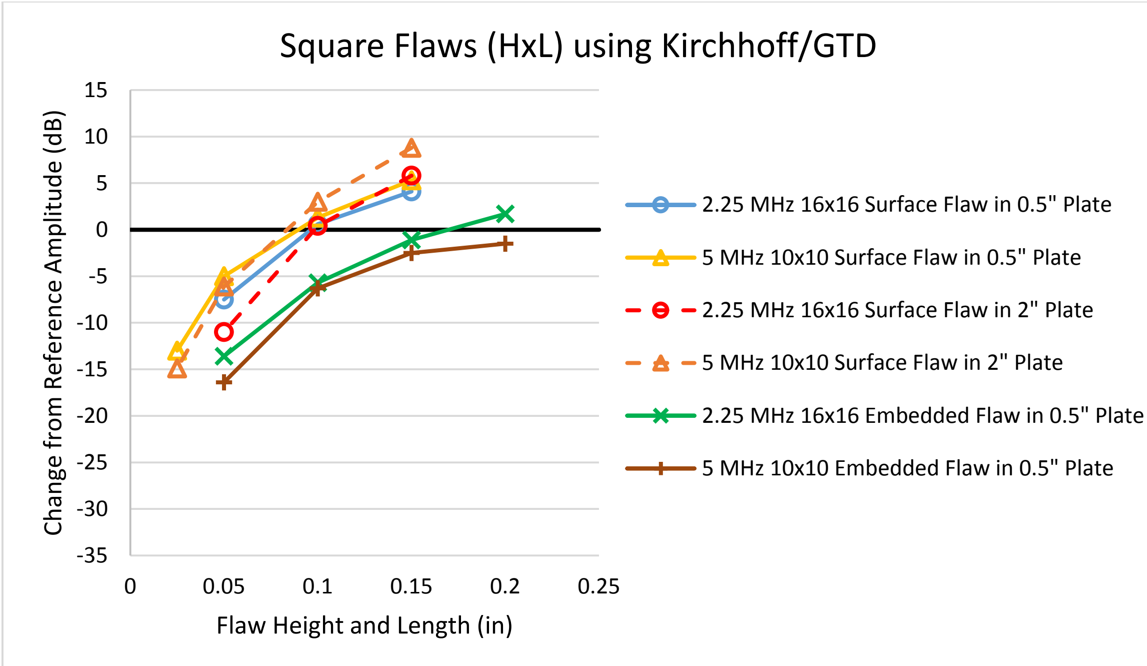

Figure 6.20 Amplitude of Vertical Flaws using 5 MHz 10x10 mm

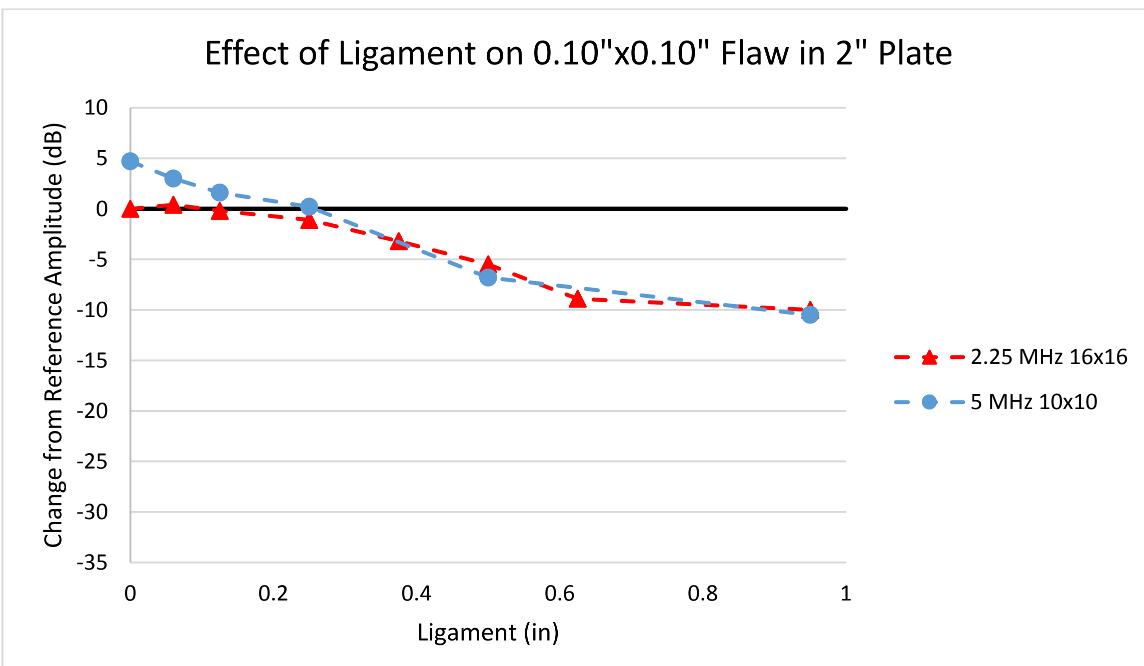

Figure 6.21 Effect of Ligament Distance for 5 MHz probe

The effect of using different apertures for 2.25 MHz probes is shown in Figure 6.22 - Figure 6.24 for surface flaws in 0.5”, 2”, and 4” plates. While the 10x10 mm aperture resulted in the highest amplitude responses for flaws in the 0.5” plate, it had equivalent amplitude as the 16x16 mm aperture for flaws in the 2” and 4” plates. Rather, the 24x24 mm probe had lower amplitudes for all of the plates.

As shown in the acoustic property CIVA parametric results shown in Chapter 5, the amplitude from the SDH decreases more quickly for the 10x10 mm aperture compared to the 16x16 mm aperture for depths greater than 1” due to increased beam spread. Therefore, based on the near surface flaw results along with the attenuation and beam spread results, it seems reasonable to use 5 MHz 10x10 mm and 2.25 MHz 10x10 mm aperture probes for testing of 0.5” plates and thinner. While the CIVA results show that these probes may be used for thicker plates as well, affects from attenuation will likely result in larger corrections during calibration for the 5 MHz probe, and the increased beam spread will result in large TCG gains at long sound paths. The 2.25 MHz 16x16 mm aperture would be preferable for thicker plates due to a more focused beam at longer sound paths.

It should be noted that the 2.25 MHz 16x16 mm aperture probe is not inadequate for thin plates since this probe was utilized in the determination of the flaw detection and rejection limits which considered 0.5” thick plates. Therefore, use of the smaller aperture probes rather than the 16x16 mm aperture probe would be slightly conservative based on the proposed amplitude limits. Finally, based on the CIVA results of the SDHs shown in Chapter 5 as well as the near surface flaw shown below, it is not recommended to use a 2.25 MHz aperture as large as 24x24 mm since this could result in poor resolution and decreased amplitude of flaws near the probe.

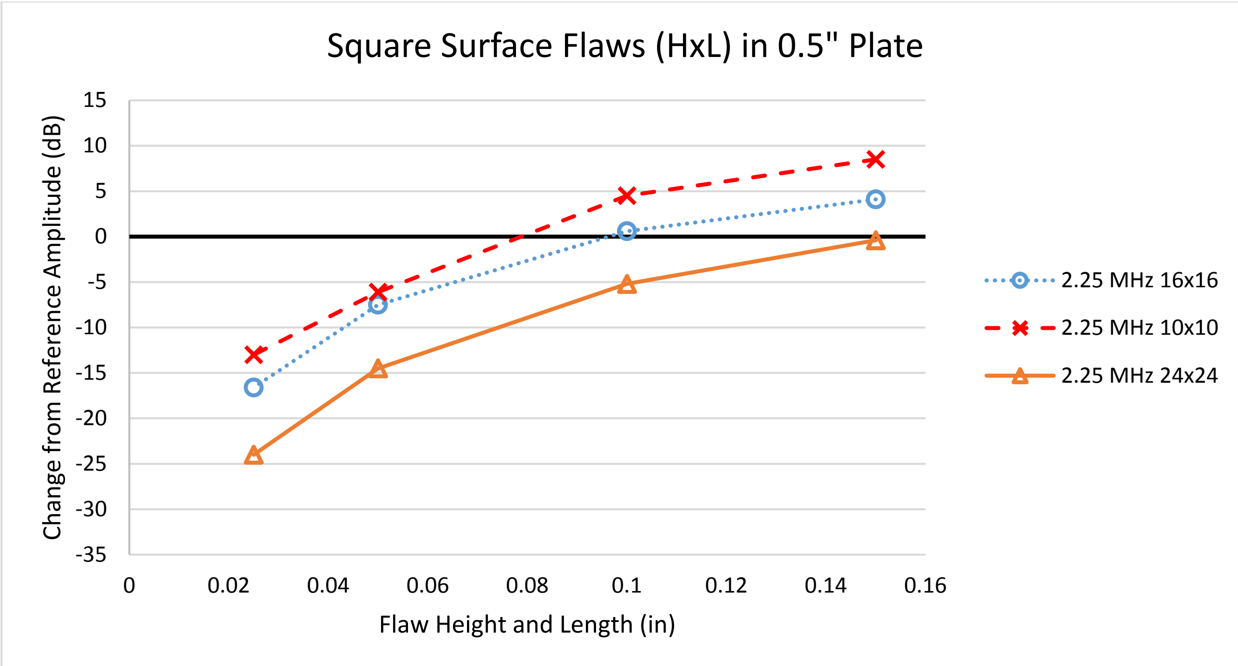

Figure 6.22 2.25 MHz Apertures for Surface Flaws in 0.5” Plate

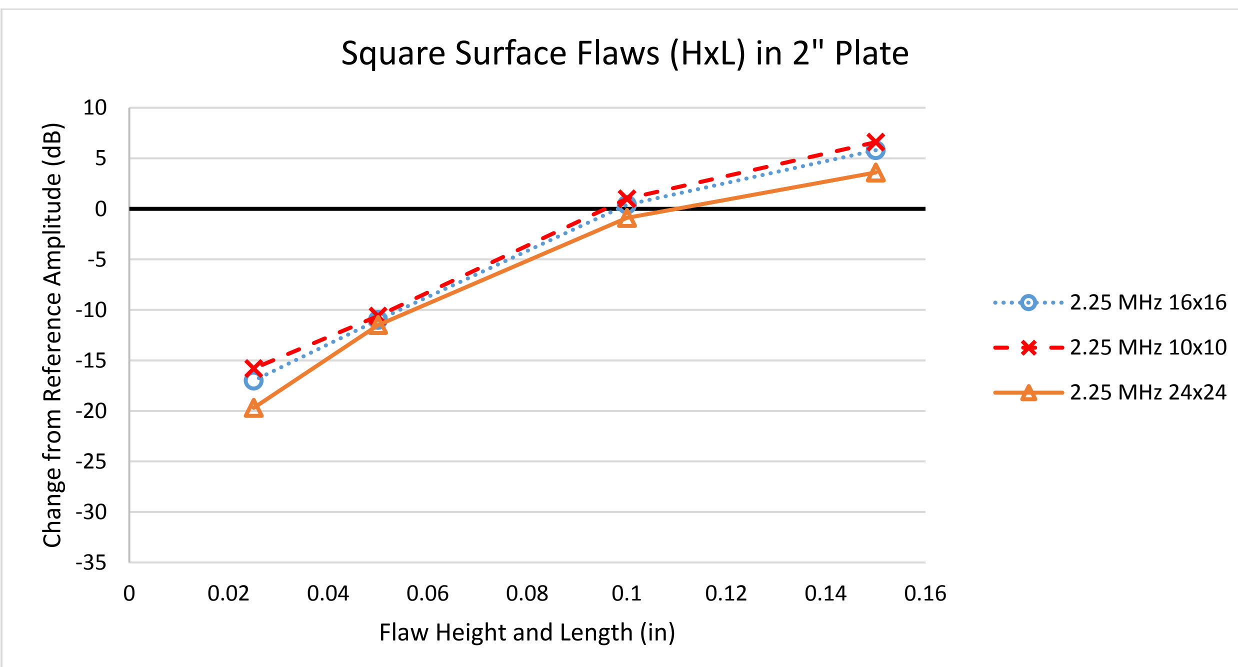

Figure 6.23 2.25 MHz Apertures for Surface Flaws in 2” Plate

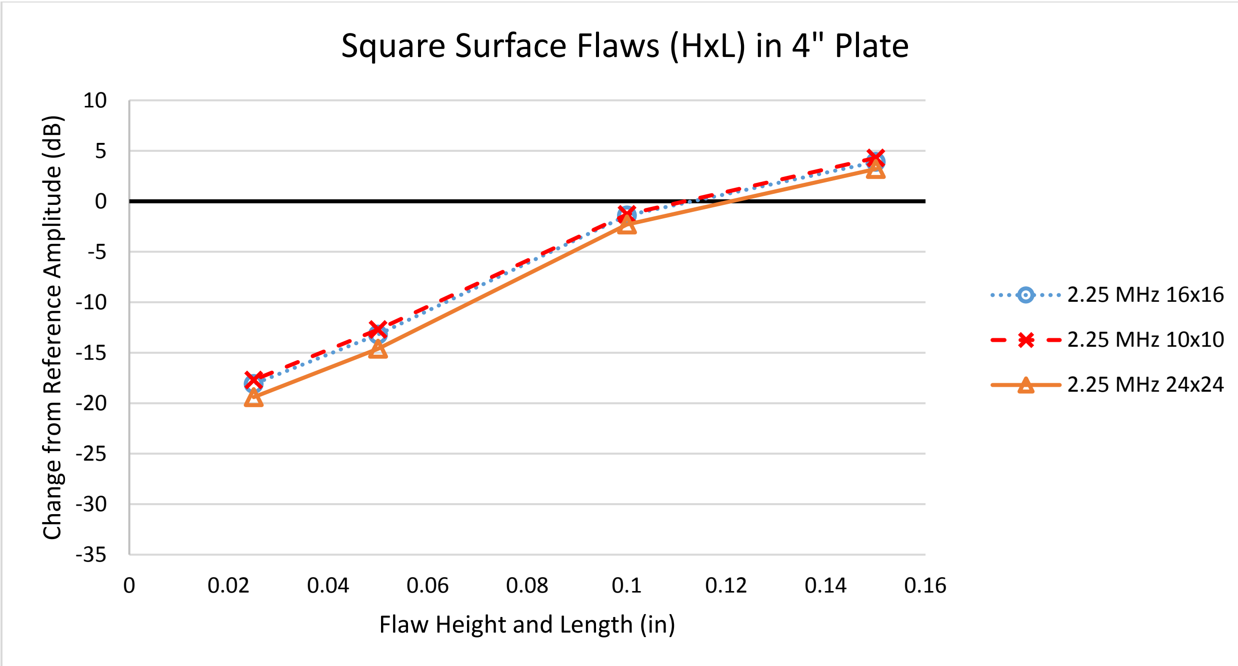

Figure 6.24 2.25 MHz Apertures for Surface Flaws in 4” Plate

6.2.2 Amplitude profile

All of the results reported above for CIVA models of flaws assume that the probe is moved perpendicular to the weld axis until the amplitude of the flaw is peaked. Only the peak amplitude was reported. The previously reported plots where the maximum amplitude was shown for various flaw parameters were used to determine the amplitude limits for an accept/reject criteria assuming that raster scanning will be performed as explained in detail in Section 6.3.

In order to develop recommendations for line scanning procedures, plots were made which show the amplitude of the flaw compared to the SDH along this entire scanning path as the beam is swept over the flaw perpendicular to the weld axis. Plots where the amplitude is reported at each index point as the probe is swept over the flaw were used in the development of the flaw detection amplitude limit, number of required line scans parallel to the weld axis, and limits on the location of these line scans for adequate weld coverage as explained in detail in Section 6.4. By capturing the amplitude profile as the probe is swept over the flaw perpendicular to the weld axis, the relationship of the change in amplitude based on movement of the probe away from the optimum index offset was determined.

There are two ways use this relationship to improve flaw detection as discussed in Section 6.4: (1) to determine limits on the number and location of line scans to keep the probe within the optimum index location and (2) determine a limit on the amplitude at the worst case index location which would still detect critical weld flaws. Obviously, the number of line scans must be reasonable from an economic standpoint and the procedure must be written in such a way that there is reasonable consistency with how it is applied. The flaw detection amplitude should also not be set so low that an unreasonable number of indications require raster scanning only to be found as acceptable. This is discussed in depth in Section 6.4. Table 6.7 displays the specimen matrix where the maximum amplitude was reported for each index offset as a 2.25 MHz 16x16 mm aperture with 45°-70° incidence angle range was swept over the flaw.

Table 6.7 Planar Flaw Amplitude Profile Specimen Matrix for 2.25 MHz 16x16 mm

<table>
<tr><th>Flaw Height</th><th>Flaw Length</th><th>Ligament</th><th>Flaw Tilt</th><th>Flaw Skew</th><th>Plate Thickness</th></tr>
<tr><td rowspan="3">0.05”</td><td>0.05”</td><td rowspan="3">0.03”</td><td rowspan="2">0°, 5°, -5°, 30°, -30°, 45°, -45°</td><td rowspan="8">0°</td><td rowspan="2">0.5”, 2”</td></tr>
<tr><td>0.10”</td></tr>
<tr><td>0.15”</td><td>0°</td><td>0.5”</td></tr>
<tr><td>0.10”</td><td>0.15”</td><td>0.06”</td><td>0°, 5°, -5°, 30°, -30°, 45°, -45°</td><td>0.5”</td></tr>
<tr><td>0.15”</td><td>0.15”</td><td>0.06”</td><td>0°</td><td>0.5”, 2”</td></tr>
<tr><td>0.05”</td><td>0.05”</td><td rowspan="4">Mid-Thickness</td><td>0°</td><td>2”</td></tr>
<tr><td>0.10”</td><td>0.10”</td><td rowspan="3">0°, 5°, -5°, 30°, -30°, 45°, -45°</td><td>0.5”, 2”</td></tr>
<tr><td>0.15”</td><td>0.15”</td><td>2”</td></tr>
<tr><td>0.20”</td><td>0.20”</td><td>0°, 5°, 10°</td><td>2”</td></tr>
</table>

Figure 6.25 displays the results for vertical surface flaws in a 0.5” plate with the index offset (i.e., distance from nose of wedge to flaw centerline) along the horizontal axis and the amplitude in relation to the reference standard along the vertical axis. The relative drop in amplitude from the peak amplitude is similar as the probe is swept over all of the flaws, regardless of their size. Movement of the probe of 0.5” from the location of the peak amplitude resulted in a drop of 6 dB for the flaws with 0.05” height. Movement of the probe of approximately 0.75” of the location of the peak amplitude resulted in a 6 dB drop for the flaws with 0.15” height.

The results for the 0.05”x0.05” flaw when tilted is shown in Figure 6.26. The flaw tilt affected the distance that the probe could be moved for a 6 dB drop from the maximum amplitude. For instance, since the peak amplitude occurs at 45° incidence angle for flaws with a 45° tilt, the amplitude profile plot is skewed rather than symmetric for changes in the index offset from the peak location. This is because the amplitude starts to level off once the 70° incidence angle hits the flaw and drops off quickly after peaking the 45° incidence angle since only the beam spread is hitting the flaw. It should be noted that, along with impacting the sensitivity to probe movement, changes in the flaw tilt will also affect the maximum amplitude.

Figure 6.27 displays the results of the amplitude profile due to probe index movement for vertical surface flaws in a 2" thick plate. The amplitude is much less sensitive to the index offset location for the 2" thick plate than the 0.5" thick plate since the incidence angle range covers much more area in the thicker plate. In general, the amplitude is within 6 dB of the peak as long as the flaw is being directly hit by sound over the incidence angle range. The sharp drop off on either side of the flat portion occurs when the sound does not directly hit the flaw when viewed on a ray tracing plot of the sound beam. Instead, the flaw is being hit by just the beam spread. Figure 6.28 shows the 0.05"x0.05" surface flaw in the 2" thick plate when tilted. Once again, the scanning index plot drops off very slowly where the flaw is hit directly by the sound over the incidence angle range from 45°-70°. Once the probe has passed completely over the flaw so that it does not directly hit the flaw with sound at 45°, the amplitude drops off very quickly.

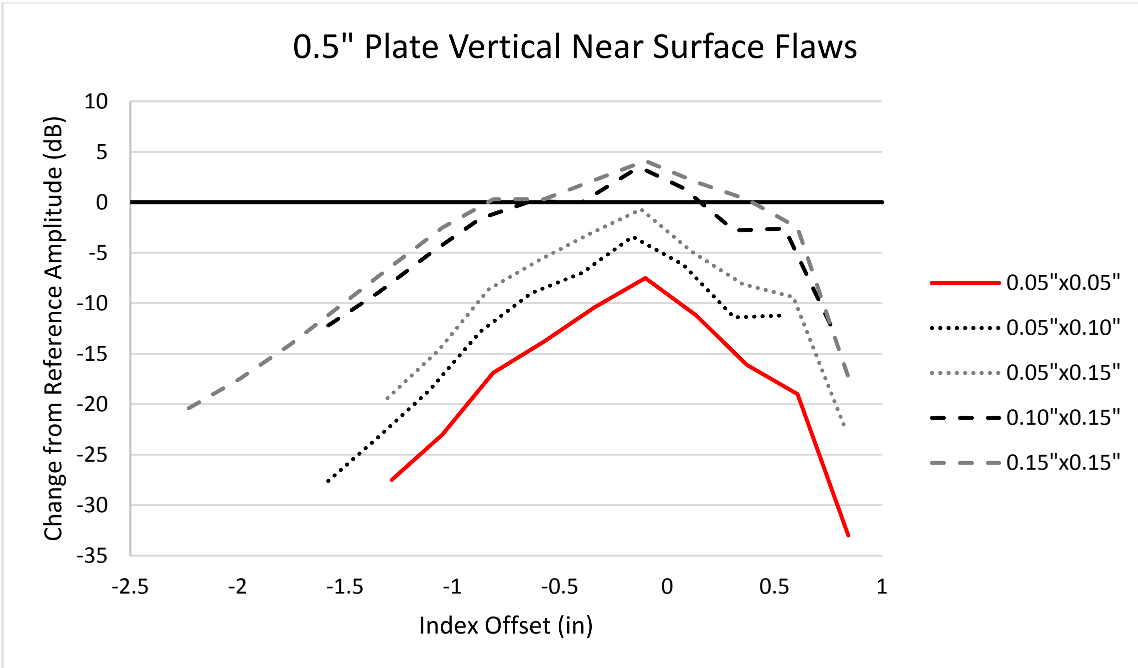

Figure 6.25 Amplitude Profile Results for Surface Flaws in 0.5” Plate

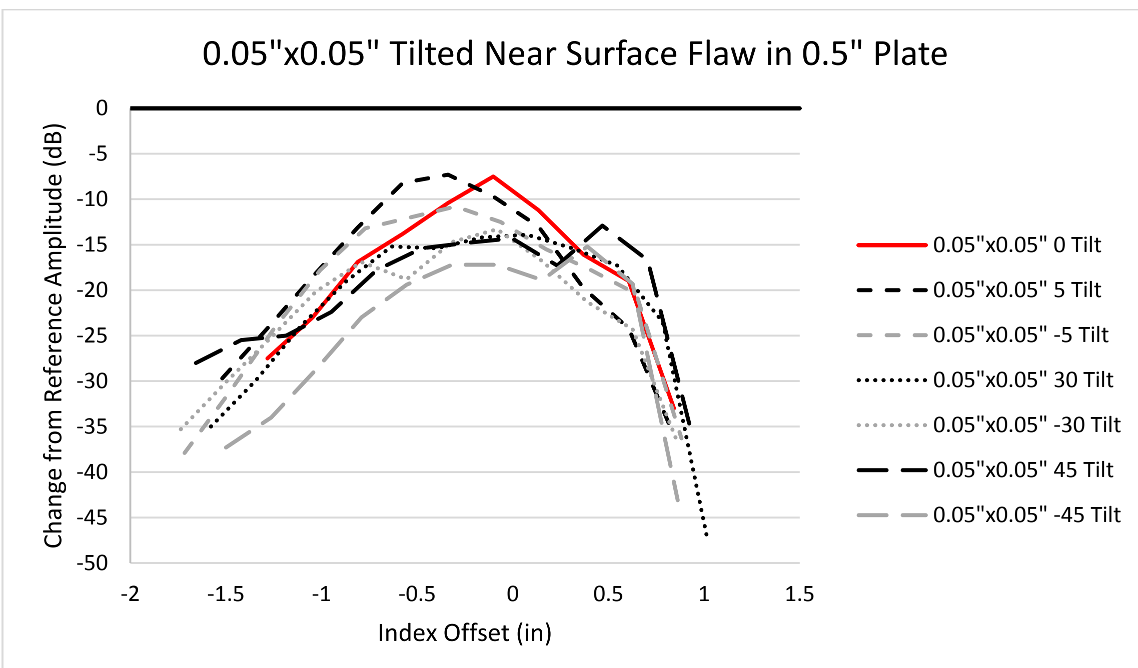

Figure 6.26 Amplitude Profile Result for Tilt of 0.05”x0.05” Surface Flaw in 0.5” Plate

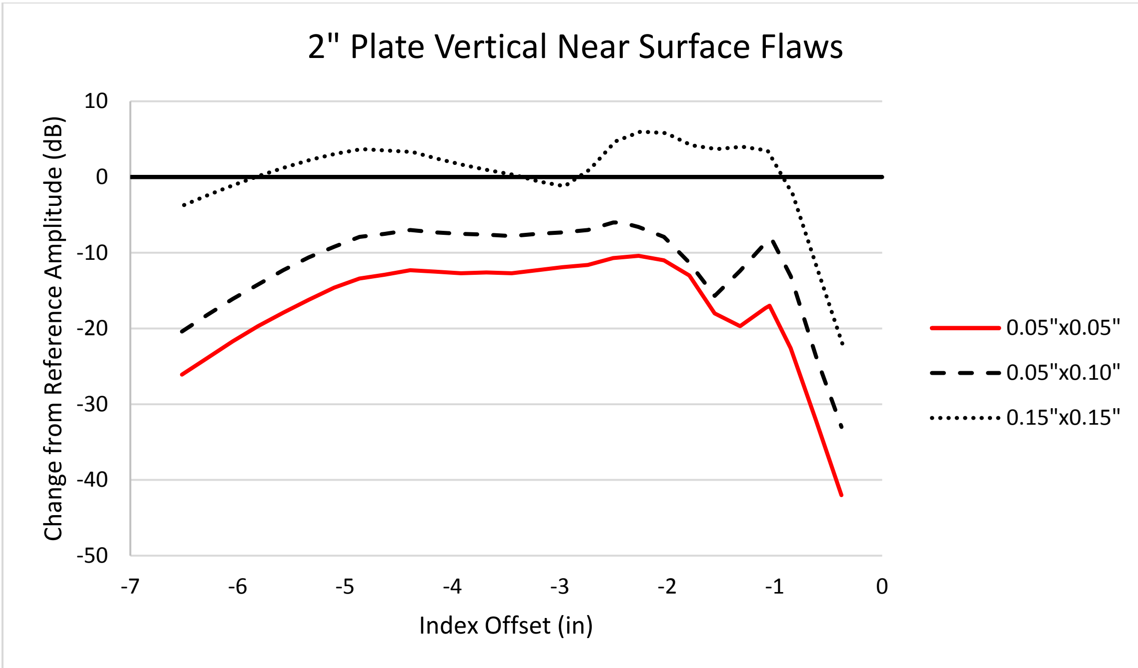

Figure 6.27 Amplitude Profile Result for Surface Flaws in 2” Plate

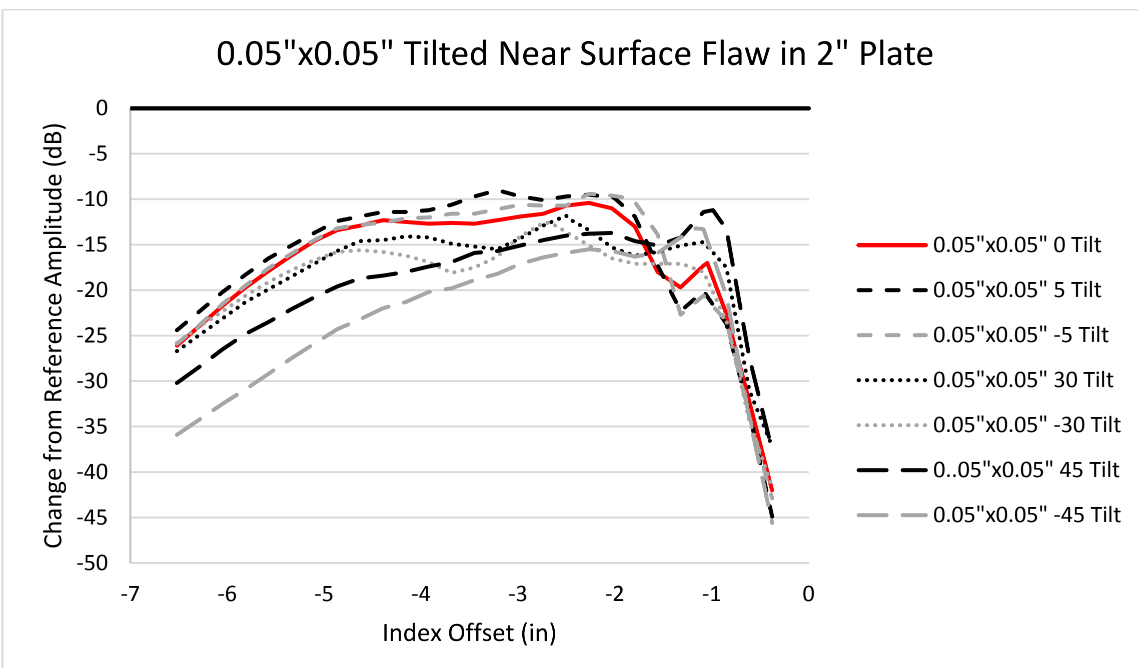

Figure 6.28 Amplitude Profile Result for Tilt of Surface Flaw in 2” Plate

Figure 6.29 displays the amplitude profile for vertical embedded flaws in a 2” plate. The embedded flaws had two locations where the amplitude increased with a sharp decrease between them. The two locations of increased amplitude correlate to peaking the amplitude in 1st and 2nd leg. As previously noted, the peak amplitude increases for embedded flaws when they are tilted 30° or more.

As shown in Figure 6.30, the amplitude is also very sensitive to changes in the index offset for embedded flaws tilted 30° or more. One thing to keep in mind is that scanning is required from both sides of the weld so positive tilt from one side would be similar to negative tilt from another side and vice versa. For instance, a +30° flaw from one side of the weld would be the same as a -30° flaw from the other side. For tilted flaws, keeping the angular range within ±4° of perpendicular to the flaw resulted in an amplitude drop of approximately 6 dB from the peak. Considering that the peak amplitude for these flaws was considerably higher than the peak amplitude for vertical or ±5° tilted flaws, the incidence angle range which is effective for flaw detection can be increased further since the vertical or ±5° tilted flaws will control. Thus, while the amplitude for embedded flaws tilted 30° or more is sensitive to small movements of the probe, the amplitude of these flaws is generally greater than the amplitude from vertical flaws as long as coverage is provided in two crossing directions.

Finally, the amplitude profile for a 0.10”x0.10” embedded flaw in a 0.5” thick plate is shown in Figure 6.31. As discussed previously, the peak amplitude was not as sensitive to the tilt in the 0.5” plate compared to the 2” thick plate due to the shorter sound path. Similar results are seen for this flaw as the embedded flaws in the 2” plate. The following plots demonstrate the sensitivity of the amplitude to probe location and flaw position, tilt, and skew according to analyses performed using CIVA. Therefore, even with the additional sound coverage provided by PAUT sector scans, raster scanning will be required for flaw detection in order to peak the indication amplitude.

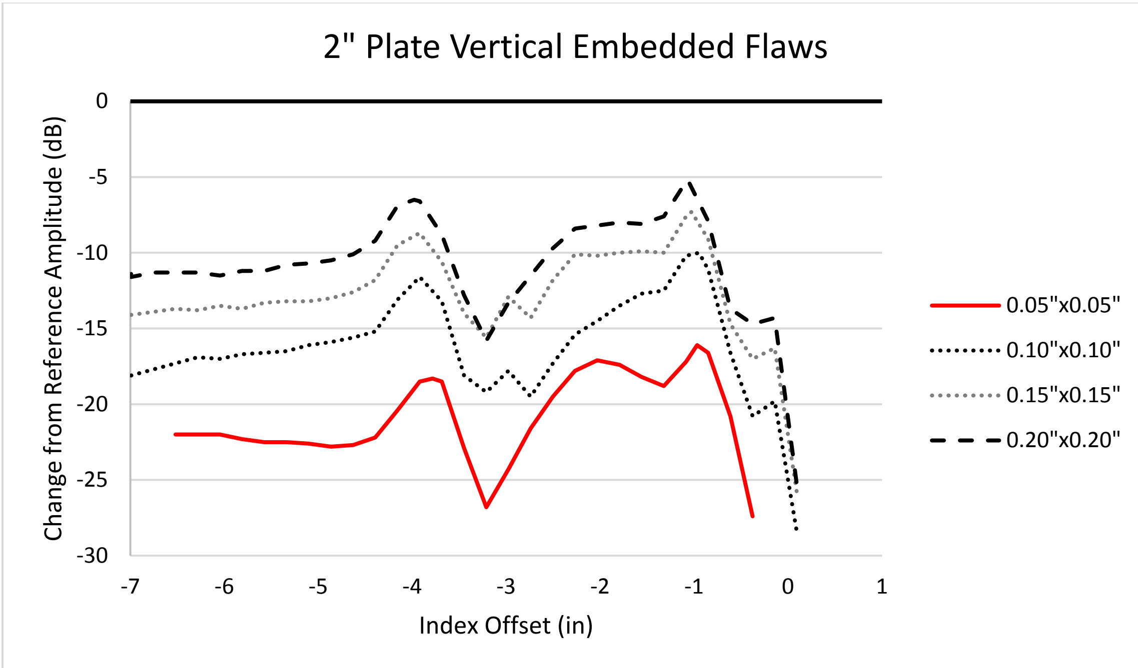

Figure 6.29 Amplitude Profile Result for Embedded Flaws in 2” Plate

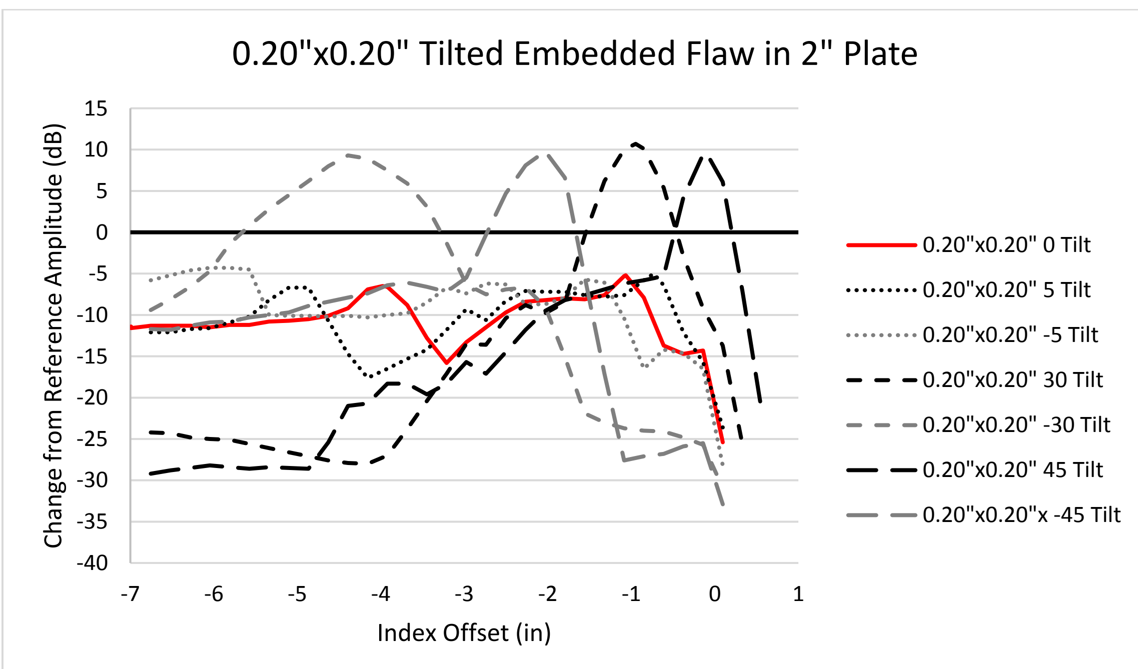

Figure 6.30 Amplitude Profile Result for Tilt of Embedded Flaw in 2” Plate

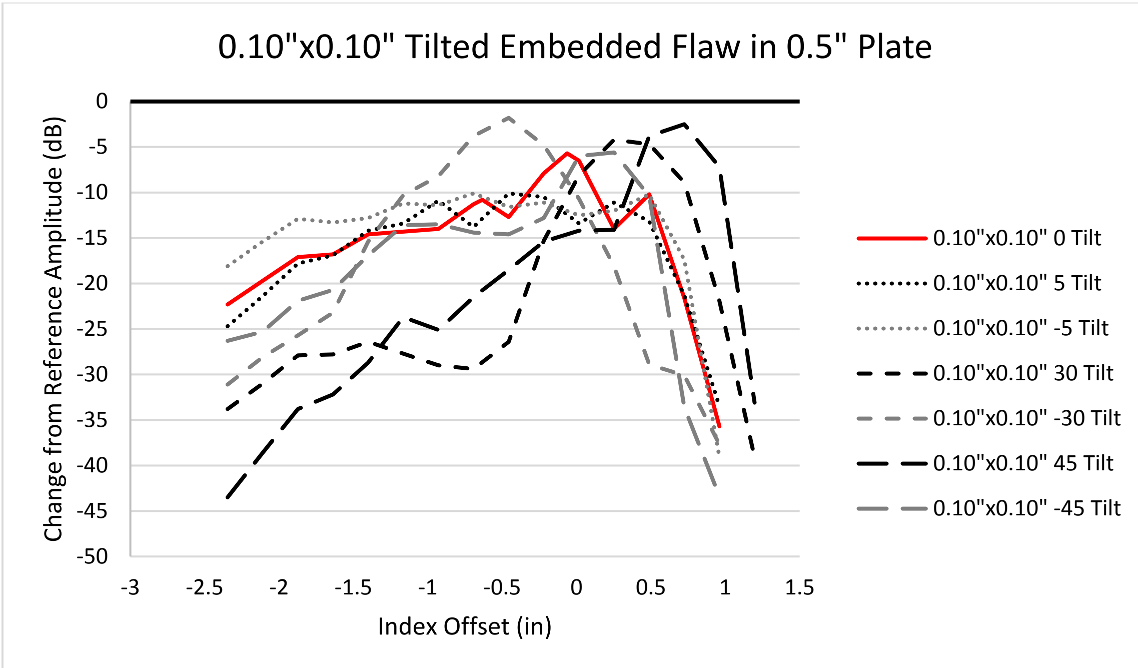

Figure 6.31 Amplitude Profile Result for Tilt of Embedded Flaw in 0.5” Plate

6.3 Amplitude Limit for Rejection of Flaws

6.3.1 CIVA modeling

Modifications to the AWS D1.5 Annex K acceptance criteria were developed in order to improve detection and rejection of critical weld flaws. The approach to the inspection procedure is to use line scanning for detection of weld flaws and follow-up raster scanning to evaluate rejection of weld flaws. The amplitude which will be compared to the acceptance criteria limits will be the maximum amplitude measured during raster scanning. Raster scanning will involve scanning the indication over the entire incidence angle range from both sides of the weld while also rotating the probe. Compared with line scanning, raster scanning will maximize the amplitude since it will involve movement of the probe to account for unknown parameters such as flaw tilt, flaw skew, and flaw location.

In order to develop the amplitude limit for flaw rejection, CIVA analysis was performed using a 2.25 MHz PAUT probe with an active aperture of 16 mm by 16 mm and an angular range of 45°-70°. Using CIVA, the maximum amplitude which would be found during typical raster scanning with TCG was determined. The CIVA analysis was performed on flaws similar in size to the critical planar and volumetric flaws. The amplitude from the indications was referenced to the amplitude of a 1.5 mm (0.06”) diameter SDH at a similar sound path, with positive amplitude having a higher response than the SDH and negative amplitude having a smaller response than the SDH. Therefore, positive results are more severe than negative results. Flaw tilt of planar flaws were evaluated at 0°, ±5°, ±30°, and ±45°. Obviously, the lowest maximum amplitude measured over all of these conditions controls in order to reject critical flaws regardless of their tilt. In other words, the smallest possible amplitude which would result from raster scanning, regardless of the actual flaw tilt, forms the basis of the rejection limit.

Since the critical flaw size depends on the stress range, stress concentration from thickness transitions, and the through-thickness location of the flaw, different critical flaw sizes are possible depending upon these inputs. Therefore, the critical flaw sizes for surface and embedded flaws in equal thickness and thickness transition welds were evaluated for 4 ksi and 8 ksi stress ranges. Plate thicknesses of 0.5” and 2” were used to account for variations due to the probe near field and natural beam shape. The results of the parametric CIVA modeling for the controlling maximum amplitude compared to the 1.5 mm (0.06”) diameter SDH are shown in Table 6.8 and Table 6.9 for critical planar and volumetric flaws, respectively.

Table 6.8 CIVA Results of Controlling Maximum Amplitude for Critical Planar Flaws

Stress Range	**Flaw Location**	**Weld Type**	**Critical Planar Flaw**		**Comparable CIVA Analysis**			
			Height (in)	**Length (in)**	**Height (in)**	**Length (in)**	**Plate Thickness (in)**	**Controlling Maximum Amplitude (dB)**
4 ksi	Embedded	Equal	0.20	0.20	0.20	0.20	0.5/2	-6
		Transition	0.17	0.17	0.15	0.15	0.5/2	-8
	Surface	Equal	0.10	0.13	0.10	0.15	0.5/2	-2
		Transition	0.06	0.08	0.05	0.10	0.5/2	-10
8 ksi	Embedded	Equal	0.14	0.14	0.15	0.15	0.5/2	-8
		Transition	0.08	0.08	0.10	0.10	0.5/2	-10
	Surface	Equal	0.06	0.08	0.05	0.10	0.5/2	-10
		Transition	0.02	0.03	0.025	0.025	0.5	-38

Table 6.9 CIVA Results of Controlling Maximum Amplitude for Critical Volumetric Flaws

Stress Range	Flaw Location	Weld Type	Critical Volumetric Flaw		Comparable CIVA Analysis		
			Height (in)	Length (in)	Diameter (in)	Plate Thickness (in)	Controlling Maximum Amplitude (dB)
4 ksi	Embedded	Equal	0.22	0.41	0.25	0.5/2	-7
		Transition	0.24	0.24	0.25	0.5/2	-7
	Surface	Equal	0.23	0.31	0.25	0.5/2	-7
		Transition	0.08	0.11	0.08	0.5/2	-13
8 ksi	Embedded	Equal	0.14	0.14	0.125	0.5/2	-13
		Transition	0.08	0.08	0.08	0.5/2	-18
	Surface	Equal	0.06	0.08	0.08	0.5/2	-13
		Transition	0.02	0.03	0.03	0.5	-18*

*Result may not be valid since standard analytical CIVA model is not valid due to small flaw size relative to the wavelength

The results of this analysis are further summarized in Table 6.10 by combining the results of embedded and surface flaws for the same stress range and weld type (i.e., equal thickness or thickness transition). This forms the basis of possible acceptance criteria amplitude limits to be applied to the raster scanning results. The acceptance criteria amplitude limit varies from -6 dB (i.e., indication amplitude 6 dB below reference amplitude) for critical planar flaws in equal thickness welds under 4 ksi stress range to -18 dB for critical embedded volumetric flaws in thickness transition welds under 8 ksi stress range. It should be noted that critical surface planar and volumetric flaws in thickness transition welds under 8 ksi stress range is not included in this table since the critical flaw size according to fracture mechanics was so small that the standard analytical CIVA models are not valid (i.e., approximately half the wavelength of the 2.25 MHz probe).

Table 6.10 Raster Scanning Acceptance Criteria Limits from CIVA

Stress Range	Weld Type	Planar Flaws	Volumetric Flaws
4 ksi	Equal Thickness	-6 dB	-7 dB
4 ksi	Thickness Transition	-10 dB	-13 dB
8 ksi	Equal Thickness	-10 dB	-13 dB
8 ksi	Thickness Transition (Embedded Flaws Only)	-10 dB	-18 dB

6.3.2 Comparison to current amplitude-based acceptance criteria

Figure 6.32 compares the acceptance criteria amplitude limits from the CIVA analysis in Table 6.10 to the current acceptance criteria in AWS D1.5 Annex K for flaws in the middle half of tension welds. In this figure, the maximum amplitude from the indication compared to the 1.5 mm (0.06") diameter SDH is on the vertical axis and the indication length is along the horizontal axis. Combinations of amplitude and length which fall below the line would be accepted while those above the line are rejected. For instance, AWS Annex K would accept an indication which was up to 5 dB above reference (i.e., 5 dB greater amplitude than the 1.5 mm (0.06") diameter SDH) as long as the indication length is 0.5" or less. Also, AWS Annex K would accept any indication which is more than 6 dB below reference (i.e., amplitude of -6 dB or less compared with the 1.5 mm (0.06") diameter SDH) regardless of the indication length.

It is apparent from Figure 6.32 that the CIVA amplitude limit results are more conservative than the AWS Annex K acceptance criteria limits since the AWS Annex K line is above the CIVA results. For instance, Annex K acceptance criteria has higher amplitude limits for Class A and B flaws than any of the CIVA results. Therefore, there is more area for indications to fall under the Annex K line in the acceptable zone rather than the CIVA results. Once again, since Annex K also allows for evaluation of amplitude based on the initial line scan, it is unlikely that the amplitude used to compare to the acceptance criteria will be the maximum flaw amplitude due to possible flaw tilt, skew, and location in relation to the probe. The lack of maximizing the flaw amplitude which is compared to the acceptance criteria for Annex K would compound the differences between an evaluation using Annex K and using raster scanning with the CIVA determined limits.

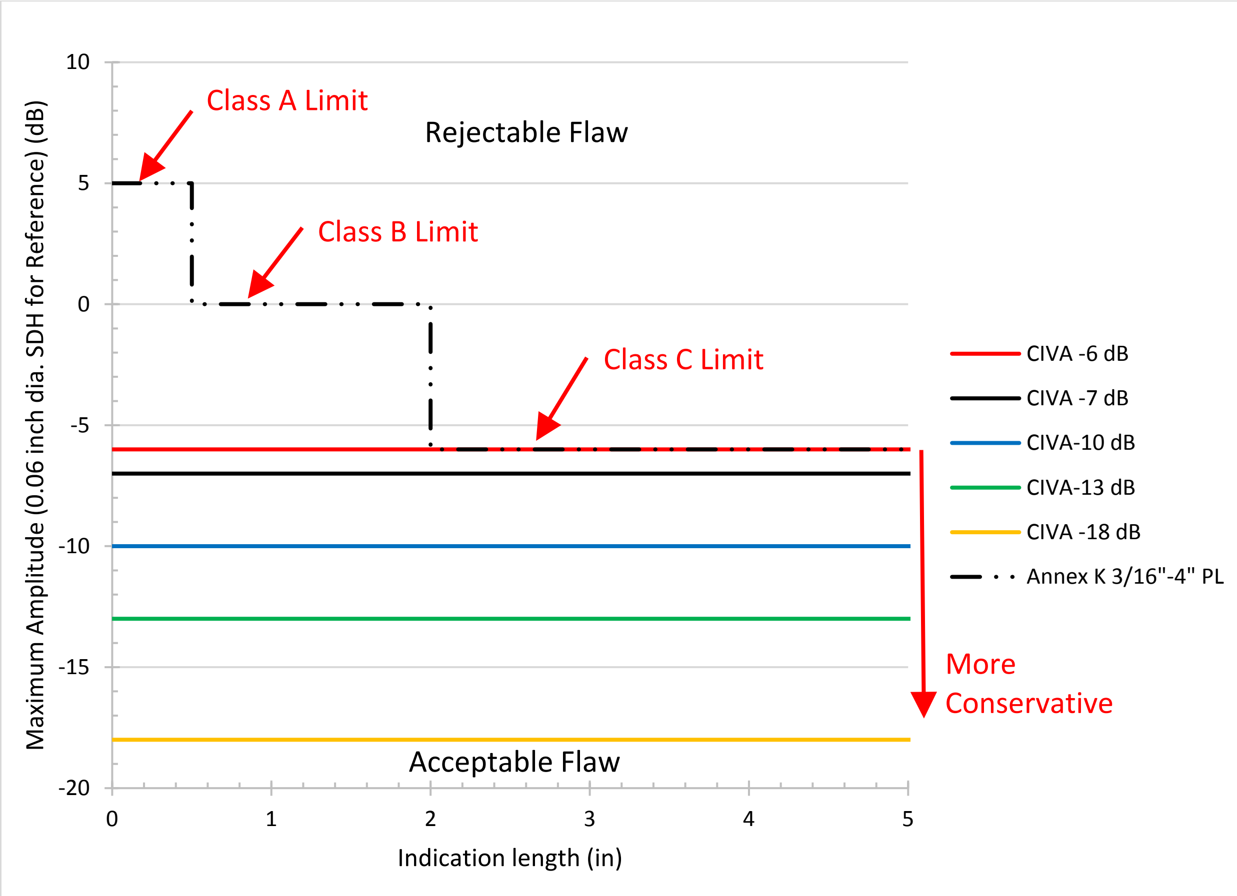

Figure 6.32 Comparison of CIVA Results to AWS D1.5 Annex K Acceptance Criteria

In order to compare the proposed amplitude limits from CIVA to the conventional UT amplitude limits, the conventional UT amplitude limits must be inverted from positive to negative integers. This is due to the fact that the conventional UT and PAUT have very different approaches to obtain the indication amplitude. Conventional UT according to AWS D1.5 requires modifying the instrument gain in order to force the indication amplitude to match the reference amplitude of the 1.5 mm (0.06") diameter SDH. Therefore, indications with high amplitude result in a low (or negative) Indication Rating since instrument gain is removed in order to bring the indication amplitude down to reference amplitude. For instance, in Figure 6.33 (left), the indication exceeds the reference amplitude at reference gain. Therefore, this indication has greater amplitude than the reference standard. In Figure 6.33 (right), 4 dB gain was removed from the instrument to bring the indication amplitude to the level of the reference amplitude. Assuming that the attenuation factor would be zero in this case, this indication would have an Indication Rating of -4 dB. This is opposite of PAUT testing where the indications with high amplitude result in a more positive reported amplitude compared to the reference amplitude. For instance, PAUT inspection of the indication in Figure 6.33 would have a reported amplitude of +4 dB compared to the reference amplitude.

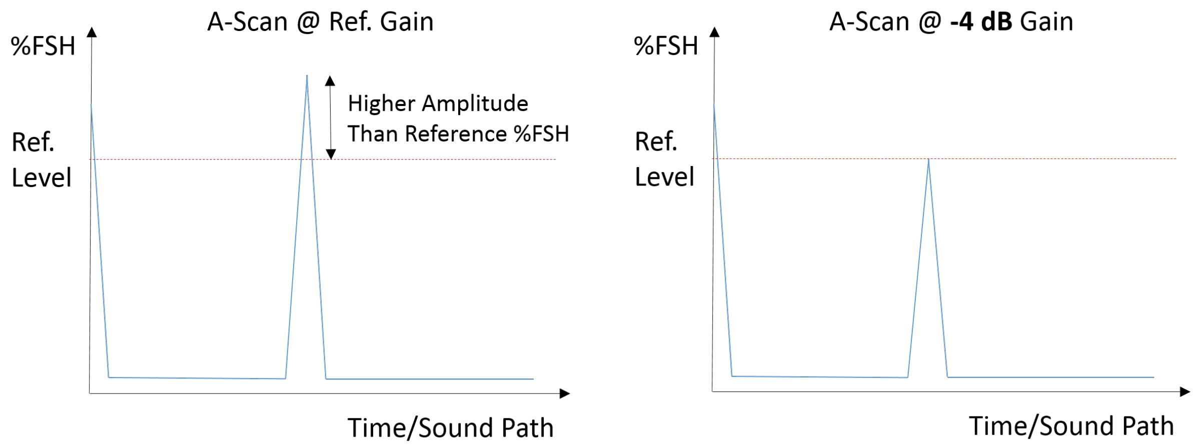

Figure 6.33 Conventional UT Amplitude Measurement

Figure 6.34 compares the acceptance criteria amplitude limits from the CIVA analysis in Table 6.10 to the current acceptance criteria in AWS D1.5 Clause 6 conventional UT for flaws in the middle half of the tension welds after inverting the positive to negative values for the conventional UT tables. Conventional UT in Clause 6 includes separate criteria depending on the plate thickness and incidence angle used in the inspection. Therefore, rather than having one line like Annex K, there are eight different lines for conventional UT acceptance limits. It is apparent that the conventional UT acceptance criteria are more conservative than AWS D1.5 Annex K since the CIVA results from -6 dB to -13 dB correlate quite well to the conventional UT limits while they were in the acceptable range for Annex K.

Therefore, although it may seem that the CIVA results are overly conservative when compared to Annex K, they correlate quite well to the conventional UT acceptance criteria which at least appears to have provided good historical performance when used for UT inspection. It is also very important to remember that the amplitude limits from CIVA were derived completely independent of the Clause 6 conventional UT acceptance criteria by modeling critical flaws derived from fracture mechanics. Therefore, while the similarities of the CIVA results to traditional acceptance criteria helps to bolster confidence in the newly derived amplitude limits, these limits are not based solely on the historical performance of workmanship-based acceptance criteria but rather FFS.

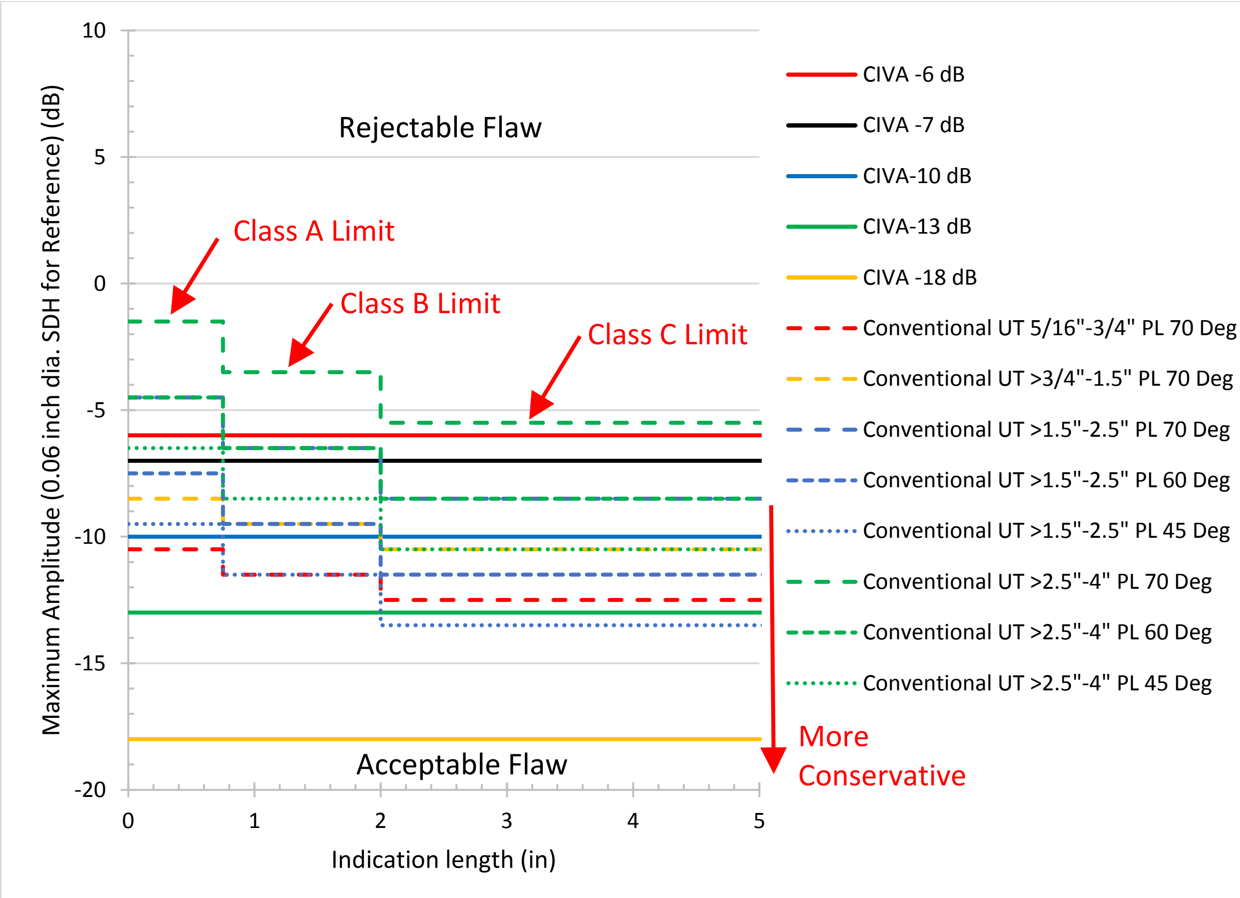

Figure 6.34 Comparison of CIVA Results to AWS D1.5 Clause 6 Conventional UT Acceptance Criteria

The 2018 edition of the CSA W59 code [10] includes an alternative acceptance criteria based on TCG rather the fixed attenuation approach. This acceptance criteria was based on the CSA fixed attenuation conventional UT tables which are similar to the AWS D1.5 Clause 6 conventional UT tables. The CSA W59 alternative TCG acceptance criteria may be applied to conventional UT or manual raster scanned PAUT. Encoded PAUT is specifically noted as an alternative ultrasonic system which is subject to a written agreement between the engineer and contractor along with development of an appropriate scanning procedure and acceptance criteria. The CSA TCG acceptance criteria were derived by combining the amplitude limits for the various incidence angles in the fixed attenuation tables along with correction for the difference in true attenuation compared to the fixed attenuation model [14]–[16]. By taking this approach, the CSA code attempts to recreate the same level of quality using the TCG acceptance criteria as the traditional fixed attenuation acceptance criteria.

Figure 6.35 compares the TCG acceptance criteria in CSA W59-18 to the CIVA results for flaws in the middle half of the tension welds. Since the CSA TCG acceptance criteria depends on the plate thickness, there are three different criteria plotted in this figure. It can be seen that the CIVA results of -7 dB and -10 dB cross the CSA acceptance criteria and, therefore, are quite similar. The CIVA result of -6 dB would have been rejectable regardless of the indication length according to the CSA TCG acceptance criteria for all of the plate thicknesses. Therefore, the -6 dB limit would be slightly less conservative to the CSA TCG limits. On the other hand, the CIVA results of -13 dB and -18 dB would be acceptable regardless of the indication length and therefore would be more conservative.

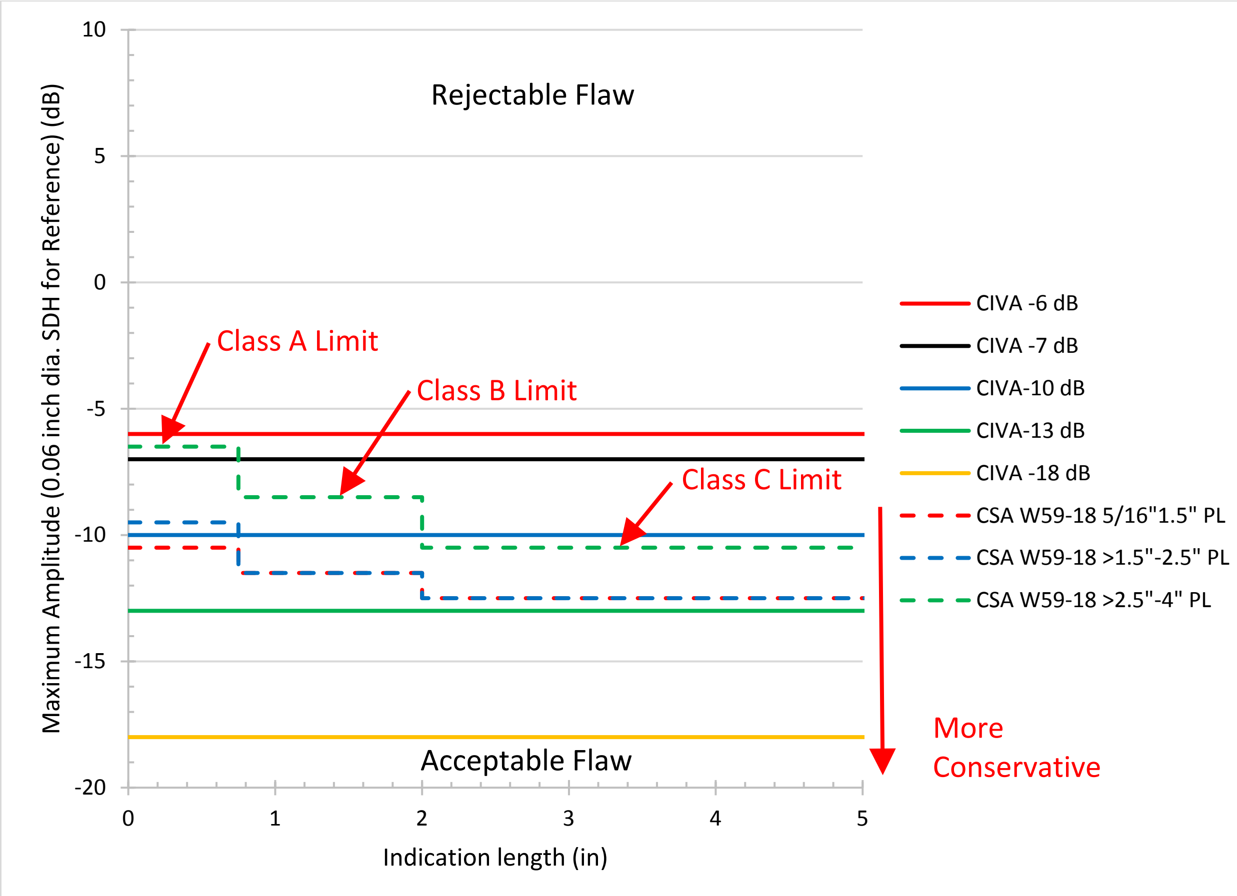

Figure 6.35 Comparison of CIVA Results to CSA W59 TCG Acceptance Criteria

6.3.3 Verification testing of weld flaw samples

Initial verification of the CIVA analysis was performed by rescanning the round robin specimens with two different PAUT probes and using a standard AISI 1018 steel calibration block with 1.5 mm (0.06") diameter SDHs for TCG. Testing was performed using a Zetec Topaz 16 with a Zetec AXL-2.25 MHz PAUT probe with 16 active elements (i.e., active aperture of 16 mm by 20 mm) and with a Zetec AM-5 MHz PAUT probe with 16 active elements (i.e., active aperture of 9.6 mm by 10 mm). In general, it was found that the amplitude from the flaws was greater using the 5 MHz probe compared with the 2.25 MHz probe. This is not surprising since the wavelength is smaller for the 5 MHz probe and it is more sensitive to small flaws.

This testing found that the lowest maximum amplitude from a planar flaw which would be rejectable according to fracture mechanics (excluding the extremely small critical size calculated for surface flaws in thickness transition welds under 8 ksi) was +3.6 dB for a vertical crack which had an intended size of 0.17" high by 0.40" long. Therefore, this flaw would have been rejectable according to the amplitude limits found during the CIVA analysis.

The round robin specimens also included some very small planar flaws which would only be rejectable according to fracture mechanics as a surface flaw in thickness transition weld under 8 ksi. The lowest maximum amplitude from these flaws was -5.3 dB for a surface breaking crack which had an intended size of 0.02" high by 0.04" long. Therefore, this flaw would also have been rejectable according to the amplitude limits found during the CIVA analysis.

The lowest maximum amplitude from a volumetric flaw was -13 dB for a near surface group of porosity which had an intended size of 0.09" high by 3.31" long with a maximum pore diameter measured with RT of 0.05". This pore diameter is similar to the critical volumetric flaw used in the CIVA analysis for the 4 ksi thickness transition and 8 ksi equal thickness cases. This flaw would have been rejectable according to the amplitude limits found during the CIVA analysis for these cases. It is noted that current RT acceptance criteria would have also rejected this flaw.

Final verification of the CIVA analysis was performed by an ASNT Level III UT/Level II PAUT technician. Round robin specimens with low amplitude indications were utilized for this testing along with additional flawed weld specimens which were acquired specifically for this testing. These specimens were acquired since they included known weld flaws which were small in size relative to many of the flaws included in the round robin specimens.

The final verification testing involved line scanning the samples for flaw detection followed by raster scanning for evaluation of acceptance. As the flaw detection amplitude limit which would require follow-up raster scanning was unknown at the time (explained further in the following section), all indications with an amplitude greater than -20 dB during the initial line scanning were further investigated with raster scanning to determine the maximum amplitude. Testing was performed with an Olympus Omniscan MX2 with a 2.25L16-AWS1 PAUT probe which is a 2.25 MHz probe with 16 active elements (active aperture of 16 mm by 16 mm).

Table 6.11 shows the results from this testing for all intended flaws located in the test plates. This table includes the flaw type, intended flaw height and length, the rejection rate from the round robin results for conventional UT, the maximum measured flaw length from the line scanning, and the maximum amplitude from the follow-up raster scanning. The flaw length was measured using the 6dB drop method, and the flaw length of scattered indications not separated by more than 2L was combined to determine the overall flaw length. Caution should be taken if comparing the results of this testing to the current Annex K acceptance criteria since the reported amplitude for each flaw was peaked during raster scanning. The maximum amplitude and measured length were used to evaluate each flaw using five different criteria based on the CIVA results:

1. rejection of flaws with maximum amplitude ≥ -13 dB
2. rejection of flaws with maximum amplitude ≥-13 dB and ≥1” long (i.e.., reject scattered low amplitude flaws such as porosity)
3. rejection of flaws with maximum amplitude ≥ -10 dB
4. rejection of flaws with maximum amplitude ≥ -8 dB
5. rejection of flaws with maximum amplitude ≥ -6 dB

All of the intended flaws had a maximum amplitude equal to or greater than -13 dB. Therefore, all of the intended flaws are rejectable under the first criteria (i.e., ≥ -13 dB).

The second criteria was meant to reject low amplitude flaws such as slag or porosity that were over 1” long and would likely be applied in conjunction with another criteria based solely on the amplitude. Six flaws are rejectable under this criteria including three lack of fusion flaws, two slag flaws, and one porosity grouping. All of the rejectable flaws under this criteria were also rejectable to all of the other amplitude-only criteria with the exception that the porosity would have been acceptable if the rejection limit was set to -6 dB. Therefore, it may not be necessary to apply the second criteria in conjunction with the other amplitude-only criteria.

The third criteria (i.e., ≥ -10 dB) rejected all intended flaws except for a 0.14” by 0.37” crack. This crack is vertical and embedded so the amplitude response relied on tip diffraction. This specimen included weld reinforcement on both faces of the weld so the entire incidence angle range could not be swept over the flaw before the front of the probe contacted the weld reinforcement. Therefore, the incidence angles were confined to high angles, and the maximum amplitude was measured at the 67° incidence angle. Rather, CIVA analysis for similar flaws had a maximum amplitude at ~60° incidence angle (since the reinforcement was not modeled in CIVA). According to the critical flaw size for embedded planar flaws, the critical flaw size for a similar aspect ratio for the 4 ksi stress range in an equal thickness weld was approximately 0.13” by 0.31”. Therefore, this crack would have been critical, but since this plate was not included in the round robin testing program the rejection rate according to conventional UT is unknown.

Three of the intended flaws are acceptable according to the fourth criteria (i.e., ≥ -8 dB). This includes the previously mentioned vertical, embedded crack along with a very small surface breaking crack (0.02”x0.04”) and a very small slag inclusion (0.06”x0.03”). The small surface breaking crack had a rejection rate of 40% according to the conventional UT round robin results while the small slag inclusion had a 0% rejection rate for conventional UT.

Five of the intended flaws are acceptable according to the fifth criteria (i.e., ≥ -6 dB). This includes the three flaws from the fourth criteria along with two groupings of porosity. Once again, it should be mentioned that this testing was performed on the round robin plates with the lowest amplitude indications. Therefore, it is likely that the indications in the other round robin plates would have been rejected to this criteria.

Finally, any amplitude-based acceptance criteria will have variability from differences in probe parameters, calibration procedures and standards, probe pressure, and final probe location at maximum amplitude. Therefore, while verification testing is important to provide physical test results to verify the CIVA modeling, specific maximum amplitude values measured by a technician could be expected to vary by ~±4 dB.

Table 6.11 Experimental Verification Testing of Flaw Rejection Amplitude Limit

Drawing Details			UT Rejection Rate	Line Scan Results	Raster Scan Results					
						Rejection Limit				
Flaw Type	Flaw Height	Flaw Length		Maximum Measured Length	Maximum Amplitude	-13 dB	-13 dB & 1" long	-10 dB	-8 dB	-6 dB
HAZ Crack	0.18	0.52	NA	0.99	8.0	Y	N	Y	Y	Y
Porosity	0.10	0.73	NA	0.79	-6.2	Y	N	Y	Y	N
LOF	0.11	0.63	NA	1.14	10.8	Y	Y	Y	Y	Y
HAZ Crack	0.14	0.57	NA	0.83	-0.6	Y	N	Y	Y	Y
Slag	0.10	0.74	NA	0.79	2.3	Y	N	Y	Y	Y
Crack	0.14	0.37	NA	0.51	-12.1	Y	N	N	N	N
LOF	0.18	0.50	NA	1.10	11.8	Y	Y	Y	Y	Y
LOF	0.12	0.64	NA	1.14	15.5	Y	Y	Y	Y	Y
Toe Crack	0.19	0.49	NA	0.55	2.9	Y	N	Y	Y	Y
Toe Crack	0.11	0.61	NA	0.87	-1.0	Y	N	Y	Y	Y
Slag	0.09	0.92	NA	0.63	-4.2	Y	N	Y	Y	Y
HAZ Crack	0.14	0.45	NA	0.87	3.7	Y	N	Y	Y	Y
IP	0.10	0.88	NA	0.83	5.5	Y	N	Y	Y	Y
Slag	0.32	0.37	100%	0.55	1.7	Y	N	Y	Y	Y
Slag	0.16	0.18	100%	0.47	2.9	Y	N	Y	Y	Y
Slag	0.10	0.90	100%	1.73	-1.8	Y	Y	Y	Y	Y
Porosity	0.09	3.31	80%	3.39	-8.0	Y	Y	Y	Y	N
Toe Crack	0.02	0.04	40%	0.28	-8.4	Y	N	Y	N	N
LOF	0.03	0.06	80%	0.36	-3.6	Y	N	Y	Y	Y
Slag	0.06	0.03	0%	0.39	-8.2	Y	N	Y	N	N
Slag	0.17	3.61	100%	3.47	0.9	Y	Y	Y	Y	Y

6.3.4 Recommendation for AWS

Based on the CIVA analysis of critical planar flaws and the experimental testing, it is recommended that the acceptance criteria amplitude limit for flaw rejection be set at 10 dB under the amplitude from the 1.5 mm (0.06”) diameter SDH (i.e., -10 dB). As shown in Table 6.11, this limit would result in rejection of all intended flaws from the verification testing except for the 0.14”x0.37” embedded crack. As stated previously, it is believed that the weld reinforcement which limited access and, hence, limited the use of the incidence angles which could be swept over this flaw resulted in the low amplitude response. Therefore, it is recommended to set the

Automatic Rejection Level (ARL) as 10 dB under Standard Sensitivity Level (SSL) for tension welds. These indications would be considered Class A defects and be automatically rejected regardless of length.

The CIVA analysis of critical volumetric flaws found that the amplitude associated with critical pores may be as low as -13 dB. Volumetric flaws such as slag and porosity are typically made up of scattered grouping of individual discontinuities. In order to reject large groups of volumetric discontinuities that include a critical sized pore, it is recommended that indications which have a maximum amplitude between -13 dB and -10 dB during the follow-up raster scanning be rejected if the length of the entire grouping of discontinuities exceeds 1”. It is recommended that a new amplitude limit referred to as the Evaluation Level (EVL) be set at 13 dB under SSL, and indications which exceed the EVL but are less than the ARL be defined as Class B indications.

Measurement of the flaw length will be needed for rejection evaluation of Class B indications or limits for repair of Class A defects. It is recommended that the length measurement for flaws use the 6 dB drop method during the manual raster scan. Some PAUT acceptance criteria use a standard amplitude limit for length measurement rather than the 6 dB drop. In these cases, the length is determined to encompass the full extent of the flaw which has amplitude greater than this limit. While use of this method has some merit, oversizing of indications with saturated signals may occur.

It is worth commenting that an amplitude limit of 18 dB below SSL was initially going to be recommended for the length measurement of indications which are above the EVL but less than the ARL (i.e., Class B). (*The -18 dB limit corresponds to the amplitude limit for detection of flaws during the encoded line scan as will be described in the following section.*) Therefore, length measurement of Class B flaws would have involved measuring the extents where the signal exceeds the flaw detection limit. In essence, this would have ensured that any indications which would be considered as detectable are included in the evaluation against the 1” length limit. Since 6 dB drop on flaws with maximum amplitude between -13 dB and -10 dB will essentially be equivalent to the -18 dB limit (i.e., -19 dB and -16 dB, respectively), it was finally decided to recommend the use of the familiar 6 dB drop method for all length measurements. This will provide consistency for Class A and Class B flaws, along with flaws in compression welds.

It should also be noted that the existing requirements on spacing between Class B flaws from each other and the edge of the plate have been retained. Finally, it is recommended that for all indications investigated in follow-up manual raster scanning a screenshot be required and data documented at the location of maximum indication amplitude.

6.4 Amplitude Limit for Detection of Flaws

6.4.1 CIVA modeling

As stated previously, the approach to the inspection procedure is to use line scanning for detection of weld flaws and raster scanning to evaluate rejection of weld flaws. Therefore, the amplitude limit for detection of weld flaws will need to be set such that it will detect critical weld flaws during the line scan regardless of the flaw tilt, skew, and position in relation to the probe. The detection amplitude limit by definition must be lower than the acceptance criteria rejection limit since the rejection limit is compared to the maximum possible amplitude following raster scanning.

In order to develop the amplitude limit for flaw detection, CIVA analysis was performed using the same probe as was used in the flaw rejection limit (i.e., 2.25 MHz PAUT probe with an active aperture of 16 mm by 16 mm and an angular range of 45°-70°). The CIVA analysis was performed on the same size flaws used in the flaw rejection which are similar in size to the critical planar and volumetric flaws. Since the amplitude was always referenced to the 1.5 mm (0.06”) diameter SDH at a similar sound path, the reported amplitude is similar to that which would be found during typical line scanning with TCG. Positive amplitude represents a higher amplitude response than the SDH and negative amplitude represents a smaller amplitude response than the SDH.

Encoded line scanning involves using the incidence angle range of PAUT focal laws to provide coverage of the entire weld volume and HAZ. As shown in Figure 6.36, the PAUT probe is moved in a direction parallel to the weld axis at a constant index offset and with the probe orientation remaining perpendicular to the weld axis.

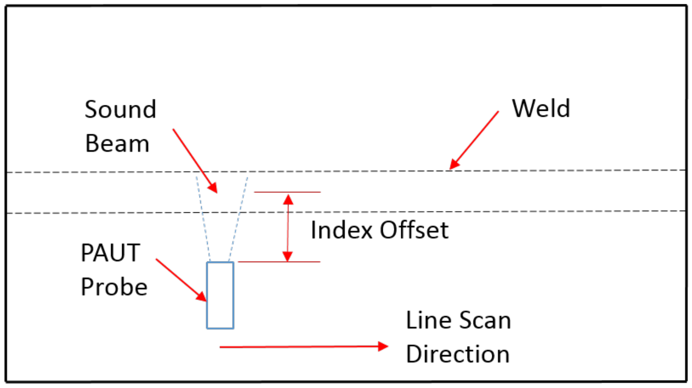

Figure 6.36 Encoded Line Scanning

Due to the amplitude being strongly affected by the interaction of the flaw tilt and sound beam incidence angle, full coverage of the weld volume and HAZ should be provided in two crossing directions (i.e., nearly perpendicular sound beam directions), as shown in Figure 6.37. This can be provided by either scanning from both sides of the weld or combining first and second leg index offset scans from the same side of the weld. Due to the effects of attenuation and beam spread on long sound paths, scanning from both sides of the weld is preferred rather than relying on second leg scans with long sound paths. This has already been incorporated in Annex K by requiring butt welds be tested from the same face but opposite sides of the weld axis where access is possible.

JIS Z 3060 [13] which uses a DAC curve approach requires that the plate be flipped and scanning performed in first leg from the other face of the weld when the sound path exceeds 250 mm (9.8"). For a 70° incidence angle, this would correspond to a depth of 3.4" which would be exceeded for second leg scanning of plates thicker than 1.7". Therefore, it may be reasonable to set limits on the maximum sound path which can be used for sound coverage in order to limit the effects of attenuation and beam spread. For instance, coverage could still be provided for shorter sound paths through the use of additional line scans at a different index offset or flipping the plate and scanning from both weld faces. A reasonable limit may be limiting the sound path used for full coverage to 12" since this would still allow for full coverage to be provided at the 70° incidence angles for second leg in 2" thick plates (i.e., 4" deep TCG point). The recommendations for changes to Annex K included a statement that the probe dimensions shall be chosen in order to optimize the beam formation within the area of coverage. No exact sound path limit was provided.

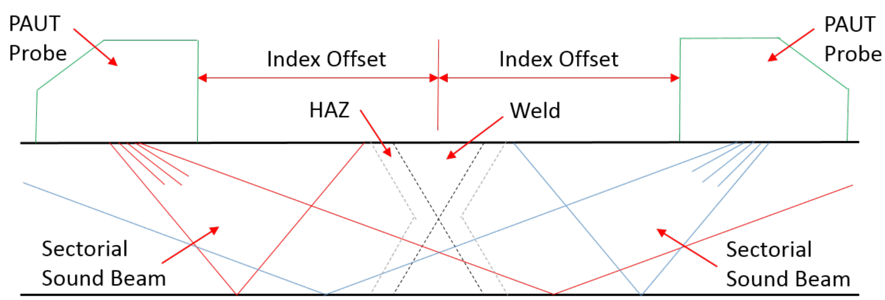

Figure 6.37 Line Scanning Sound Coverage

In order to develop the amplitude limit for detection of flaws, the probe was moved across the weld flaws perpendicular to the weld axis (i.e., the index offset was varied) in the CIVA simulations. The largest amplitude for all of the focal laws (i.e., incidence angles) was documented at 6 mm (0.24") increments of the index offset, as shown in Figure 6.38. The maximum amplitude across the incidence angle range for each index offset represents the largest amplitude which would occur if a line scan was performed using the same index offset. The indication amplitude was documented at a small increment of possible index offsets. The amplitude limit for flaw detection was subsequently determined in order to detect critical weld flaws for any possible index offset used in line scanning (i.e., combination of possible probe and flaw locations). The only stipulation is that the flaw must be within the coverage of the incidence angle range which is already provided through minimum scanning coverage requirements. In other words, as long as full coverage was provided of the weld and HAZ, the amplitude from the critical weld flaw would surpass this limit and therefore be detected during line scanning.

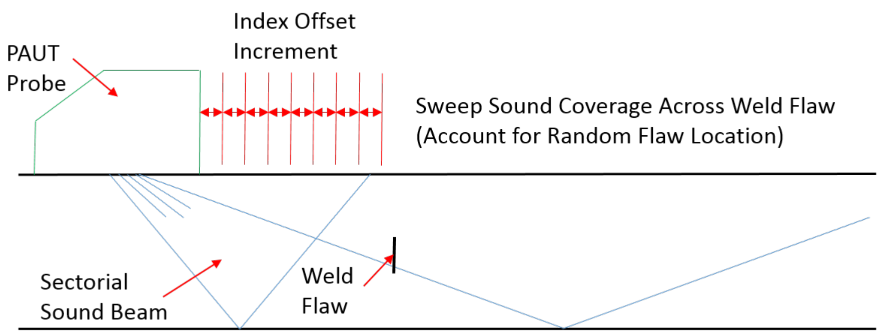

Figure 6.38 Index Offset Increment

Since the flaw tilt is also an unknown parameter, the tilt of planar flaws was evaluated at 0°, ±5°, ±30°, and ±45°. Flaw tilt away from the probe (i.e., maximum amplitude in 1st leg) was defined as positive tilt while tilt towards the probe (i.e., maximum amplitude in 2nd leg) was defined as negative tilt, as shown in Figure 6.39. Since the minimum scanning coverage requirements provide for full coverage in two crossing directions, flaws tilted away from the probe when scanned from one side of the weld would be tilted towards the probe when scanned from the other side of the weld. Therefore, all necessary analysis could be performed by sweeping the probe over the flaw in 1st and 2nd leg. The smaller of the amplitude from the 1st leg results for positive flaw tilt or 2nd leg results for negative flaw tilt was used as the controlling amplitude for flaw detection in order to ensure that the flaw would be detected by only requiring sound coverage in two crossing directions. Therefore, it did not matter whether the sound beam which would impact the flaw was provided in 1st or 2nd leg as long as the full weld volume and HAZ is covered by sound in two crossing directions.

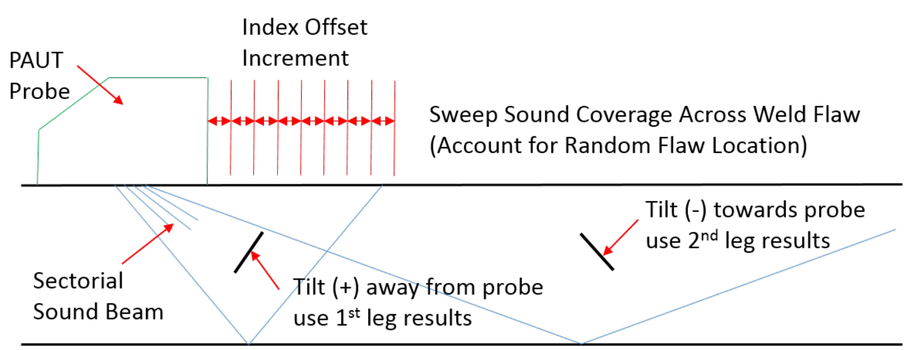

Figure 6.39 Flaw Tilt during Line Scanning

Figure 6.30 previously displayed the amplitude of a 0.2”x0.2” embedded planar flaw at mid-thickness depth in a 2” thick plate as the probe is swept over the flaw in 1st and 2nd leg. When there is no tilt, the amplitude varies from -5 dB to -15 dB compared to the 1.5 mm (0.06”) diameter SDH until the weld flaw is no longer within the sound beam coverage at which point the amplitude drops quickly (i.e., 0” Index Offset). When the flaw is tilted from vertical by 30° or 45°, the maximum amplitude increases to +10 dB when the sound beam is nearly perpendicular to the weld flaw. For the negative tilt cases, this occurs at Index Offsets of -4” to -2” where the flaw is impacted by sound in 2nd leg. For positive tilt cases, it occurs at Index Offsets of -1” to 0” where the flaw is impacted by sound in the 1st leg. When the sound beam is nearly parallel to the tilted flaws (i.e., 1st leg of negative tilted flaws and 2nd leg of positive tilted flaws), the amplitude drops off considerably with amplitudes of ~-25 dB. Therefore, sound coverage in two crossing directions is required in order to provide for detection of tilted flaws.

The critical flaws from Table 6.8 and Table 6.9 for the CIVA analysis used to develop the acceptance criteria rejection limits were also used in the study for the amplitude limits for flaw detection. The controlling amplitude over all possible index offset positions were tabulated for various flaw tilt and possible incidence angle ranges. The controlling amplitude was used to determine the overall minimum amplitude possible during line scanning for critical weld flaws. This amplitude could then be used to form the basis of the amplitude detection limit for encoded, line scanning which would require follow-up raster scanning for evaluation of acceptance.

Table 6.12 includes the results from the CIVA flaw detection analysis for planar flaws without any skew (i.e., the flaw length is parallel to the weld axis). This table presents the minimum possible peak amplitude during a line scan as long as the flaw was within sound coverage provided in two crossing directions. It presents parametric results for various sized planar flaws, various flaw tilt, and various incidence angle ranges. The controlling line scan amplitudes (i.e., minimum peak amplitude depending on the chosen index offset) are highlighted in yellow for each flaw and incidence angle range. The maximum amplitude (i.e., from raster scanning) is also provided in the table.

Table 6.12 CIVA Flaw Detection Results for Planar Flaws

Flaw Parameters					Maximum Amplitude (dB)	Minimum Peak Line Scan Amplitude for Incidence Angle Range (dB)				
Location	**Height (in)**	**Length (in)**	**Plate Thickness (in)**	**Tilt (deg)**		**45° - 70°**	**50° - 70°**	**55° - 65°**	**45° - 55°**	**45° - 50°**
Embedded	0.20	0.20	2	0	-5	-16	-16	-14	-15	-15
				+/- 5	-6	-16	-12	-12	-16	-16
				+/- 30	9	-10	-10	-9	-9	-9
				+/- 45	9	-12	-12	-10	-6	4
	0.15	0.15	2	0	-7	-17	-15	-15	-17	-17
				+/- 5	-8	-17	-13	-13	-17	-17
				+/- 30	5	-11	-10	-1	-11	-11
				+/- 45	5	-15	-15	-12	-8	0
	0.10	0.10	0.5	0	-6	-14	-14	-14	-10	-10
				+/- 5	-10	-13	-13	-12	-13	-13
				+/- 30	-4	-11	-11	-8	-11	NA
				+/- 45	-6	-15	-15	-15	-13	-6
	0.10	0.10	2	0	-10	-21	-20	-17	-21	-21
				+/- 5	-10	-20	-18	-17	-20	-20
				+/- 30	-2	-14	-10	-7	-14	-14
				+/- 45	-2	-17	-17	-17	-8	-5
Surface	0.10	0.15	0.5	0	3	-3	-3	1	-3	-3
				+/- 5	-2	-8	-8	-8	-5	-4
				+/- 30	0	-13	-13	-7	-10	-10
				+/- 45	-2	-17	-17	-15	-6	-6
	0.05	0.10	0.5	0	-3	-11	-9	-6	-11	-11
				+/- 5	-6	-12	-12	-12	-11	-11
				+/- 30	-8	-15	-15	-11	-15	-9
				+/- 45	-10	-15	-15	-15	-11	-11

For some of the flaws, especially those with large tilt, the amplitude is very sensitive to the probe location. For instance, the 0.20"x0.20" embedded flaw with 45° tilt has a maximum amplitude of +9 dB from raster scanning, but a minimum peak amplitude during possible line scan locations of -12 dB even with full coverage from two crossing directions. Therefore, the amplitude of this flaw could be 21 dB below the maximum during the line scanning, even with providing full coverage in two crossing directions. This highlights the need for follow-up raster scanning rather than evaluating flaw rejection on the line scan results.

The incidence angle ranges shown in Table 6.12 were chosen in order to investigate whether limits should be placed on the incidence angle used in the scan plan. Limiting the incidence angle range, while providing less sound coverage, may result in larger amplitudes for flaw detection. This would be similar to the requirement in Annex K where the incidence angle used in the line scan must be within ±10° of the weld fusion face. Rather than perform five different analyses for each flaw (one for each incidence angle range investigated), the individual incidence angle which had the largest amplitude across the 45°-70° angular range was documented for each index offset evaluated (0.24" increment). The minimum amplitude for each incidence angle range could then be determined from this data since, as the probe is swept over the flaw, the maximum amplitude at each index point will occur at a slightly different incidence angle.

For example, referring back to the 0.20"x0.20" flaw with 45° tilt, the maximum amplitude is +9 dB but the minimum amplitude during line scanning using the 45°-70° incidence angle range was -12 dB. It is anticipated that the maximum amplitude would occur at an incidence angle of 45° since this would be perpendicular to the flaw. Therefore, limiting the incidence angle range closer during the line scan to 45° should result in a larger amplitude. This was confirmed in the CIVA analysis since the minimum amplitude over the 45°-55° incidence angular range was -6 dB and over the 45°-50° incidence angular range was +4 dB. Obviously, the amplitude of this flaw is very sensitive to the incidence angle as is typical for tilted lack of fusion flaws.

Along with limiting the sound coverage, limiting the incidence angle range assumes that the flaw tilt is known. Lack of fusion flaws are typically assumed to have the same tilt as the fusion face. However, one must also consider if the flaw is a vertical crack or tilted at ±5°. Returning once again to the example of the 0.20"x0.20" flaw, if the weld had a 45° bevel face and the incidence angular range was limited to either 45°-55° or 45°-50° but the weld flaw was tilted at ±5°, the minimum peak line scan amplitude would be -16 dB for all possible index offsets. Therefore, using a flaw detection limit of -6 dB or +4 dB would be very unconservative and the critical weld flaw would not be detected. While limiting the incidence angle range may be helpful for flaws with known tilt in order to better maximize the amplitude, it does not help when the flaw tilt is vertical or otherwise unknown.

Table 6.13 includes the results from the CIVA flaw detection analysis for volumetric flaws. Since these flaws were modeled as spherical porosity, there is no flaw tilt or skew. As expected, spherical flaws are not as sensitive to probe location (i.e., index offset). For instance, the minimum amplitude during line scanning is relatively unaffected by the different combinations of incidence angle ranges evaluated. Still, a loss of amplitude of 7 dB was typical for the line scan amplitude compared to the maximum possible during raster scanning.

Table 6.13 CIVA Flaw Detection Results for Volumetric Flaws

Flaw Parameters				Controlling Maximum Amplitude (dB)	Minimum Line Scan Amplitude for Incidence Angle Range (dB)				
Location	**Height (in)**	**Length (in)**	**Plate Thickness (in)**		**45° - 70°**	**50° - 70°**	**55° - 65°**	**45° - 55°**	**45° - 50°**
Embedded	0.25	0.25	0.5	-7	-13	-13	-10	-13	-13
	0.25	0.25	2	-6	-13	-13	-12	-10	-10
	0.125	0.125	0.5	-13	-16	-16	-16	-15	-15
	0.125	0.125	2	-13	-20	-20	-18	-17	-17
	0.08	0.08	0.5	-18	-21	-21	-21	-21	-21
	0.08	0.08	2	-18	-25	-25	-23	-22	-21
Surface	0.25	0.25	0.5	-7	-12	-9	-9	-12	-12
	0.25	0.25	2	-5	-12	-12	-8	-8	-6
	0.08	0.08	0.5	-13	-18	-18	-17	-15	-15
	0.08	0.08	2	-11	-22	-22	-18	-15	-13
	0.03	0.03	0.5	-18	-28	-28	-22	-18	-18

Similar to the raster scanning amplitude limits, the CIVA results could be further summarized by combining the results for flaw sizes comparable to the critical flaw sizes. The flaw detection limits for the 4 ksi and 8 ksi stress ranges for equal thickness and thickness transition welds is shown in Table 6.14. For planar flaws, limiting the incidence angle range to 55°-65° resulted in the largest line scan amplitudes, but only by a few dB compared to using 45°-70°. Using an incidence angle range of 55°-65° would result in much less coverage than using 45°-70°. Therefore, based on these results, it seems that using an incidence angle range from 45°-70° is justified without the need for additional scan plan requirements beyond providing full coverage of the entire weld volume and HAZ in two crossing directions.

Table 6.14 Summary of CIVA Flaw Detection Amplitude Results w/o Flaw Skew

	Planar Flaw Amplitude (dB)					Volumetric Flaw Amplitude (dB)				
	45° - 70°	50° - 70°	55° - 65°	45° - 55°	45° - 50°	45° - 70°	50° - 70°	55° - 65°	45° - 55°	45° - 50°
4 ksi (Equal)	-17	-17	-14	-16	-16	-13	-13	-12	-13	-13
4 ksi (Transition)	-17	-16	-15	-17	-17	-22	-22	-18	-15	-15
8 ksi (Equal)	-17	-16	-15	-17	-17	-22	-22	-18	-17	-17
8 ksi (Transition - Embedded)	-21	-20	-17	-21	-21	-25	-25	-23	-22	-21

As explained previously and shown in Figure 6.36, encoded line scanning is performed by keeping the probe perpendicular to the weld axis while probe movement is parallel to the weld axis. All of the previous CIVA analysis assumed that the flaw was aligned parallel to the weld axis and, therefore, the probe is perfectly perpendicular to the weld flaw. While this is a valid assumption for raster scanning where the probe will be rotated as well as translated, it may be unconservative for line scanning.

In order to account for this effect, the change in amplitude due to flaw skew was evaluated. CIVA analysis of embedded and surface vertical weld flaws in 0.5” and 2” plates with 5°, 10°, and 20° skew was performed and compared to the results with no skew. Since the sound is reflected to the side of skewed planar flaws as shown in Figure 6.40, lateral movement of the probe along the weld axis was performed as well as sweeping the probe over the flaw perpendicular to the weld axis (Note: this figure represents the centerline of the sound beam, but the beam actually has beam spread and width).

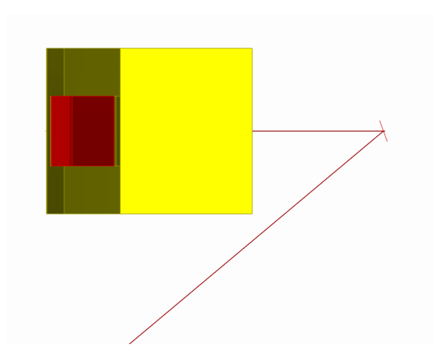

Figure 6.40 Flaw Skew

The maximum amplitude for flaws with skew was shown previously in Figure 6.15 for surface flaws and Figure 6.16 for embedded flaws. As the flaw skew is increased, the drop in amplitude increases, especially for larger flaws. This is due to the fact that the beam is hitting different parts of the flaw at different time which causes the amplitude to drop more severely. Flaws with long sound paths also had larger drop in amplitude since the beam reflected off of the skewed flaw travel a further distance transverse to the probe. For instance, the embedded flaws in the 2” thick plate had greater drop in amplitude at than the embedded or surface flaws in the 0.5” thick plate. The flaw and plate combinations chosen for this analysis correspond to those included in Table 6.12.

In order to account for the effect of flaw skew on flaw detection, the drop in amplitude from the analysis of the vertical flaw with skew was added to the results of the tilted flaws without skew for each individual flaw. This assumes that the drop in amplitude from flaw skew will be similar for tilted and vertical flaws.

This assumption was checked for the 0.20”x0.20” embedded flaw in a 2” thick plate by modeling flaws with both skew and tilt and comparing the results to the estimated values. It was determined that this assumption was reasonable. For instance, in the case of 5° skew, the drop in amplitude due to skew on the vertical flaws was -4 dB. The drop in amplitude due to skew on the tilted flaws varied from -2 dB to -5 dB depending on the flaw tilt. In the case of 10° skew where the drop in amplitude due to skew on the vertical flaws was -12 dB, the drop in amplitude for the tilted flaws varied from -7 dB to -15 dB.

The flaw detection limits including the effect of skew on the planar flaws are given in Table 6.15 for 5° skew and Table 6.16 for 10° skew. In general, including the 5° skew resulted in a -2 dB to -3 dB decrease in the flaw detection amplitude while the decrease was -9 dB to -12 dB for 10° skew. Since the drop in amplitude due to skew is greater for larger flaws, the 4 ksi equal thickness weld had lower flaw detection amplitude than the 4 ksi transition or 8 ksi equal thickness welds. Since the volumetric flaws were assumed to be spherical, the volumetric flaws were not affected by flaw tilt or skew; therefore, the volumetric flaw results are the same as those in Table 6.14.

Table 6.15 Summary of CIVA Flaw Detection Amplitude Results w/ 5° Flaw Skew

	Planar Flaw Amplitude (dB)					Volumetric Flaw Amplitude (dB)				
	45° - 70°	50° - 70°	55° - 65°	45° - 55°	45° - 50°	45° - 70°	50° - 70°	55° - 65°	45° - 55°	45° - 50°
4 ksi (Equal)	-20	-20	-18	-20	-20	-13	-13	-12	-13	-13
4 ksi (Transition)	-19	-17	-17	-19	-19	-22	-22	-18	-15	-15
8 ksi (Equal)	-19	-17	-17	-19	-19	-22	-22	-18	-17	-17
8 ksi (Transition - Embedded)	-23	-22	-19	-23	-23	-25	-25	-23	-22	-21

Table 6.16 Summary of CIVA Flaw Detection Amplitude Results w/ 10° Flaw Skew

	Planar Flaw Amplitude (dB)					Volumetric Flaw Amplitude (dB)				
	45° - 70°	50° - 70°	55° - 65°	45° - 55°	45° - 50°	45° - 70°	50° - 70°	55° - 65°	45° - 55°	45° - 50°
4 ksi (Equal)	-28	-28	-26	-28	-28	-13	-13	-12	-13	-13
4 ksi (Transition)	-26	-24	-24	-26	-26	-22	-22	-18	-15	-15
8 ksi (Equal)	-26	-24	-24	-26	-26	-22	-22	-18	-17	-17
8 ksi (Transition - Embedded)	-25	-24	-22	-25	-25	-25	-25	-23	-22	-21

The proposed PAUT annex for AWS D1.1 was reviewed after performing the CIVA analysis. The proposed PAUT annex for D1.1 will utilize an incidence angle range from 40°-70° rather than the 45°-70° incidence angle range in D1.5 Annex K. One of the authors of the proposed D1.1 PAUT annex was contacted in order to obtain an explanation for the increase in the incidence angle range from 45° to 40°. It was noted that the incidence angle range was increased to enlarge the sound coverage area and to aid in verification of corner trap signals. The AWS D1.1 proposed PAUT annex also includes a requirement that the HAZ be covered with incidence angle range from 40°-60° in order to increase the detectability of corner trap signals from surface breaking HAZ cracks. The author of the proposed D1.1 PAUT annex stated that incidence angle was limited at 40° since standing wave signals were produced sometimes at 35° and this seemed risky since it was close to the first critical angle.

Subsequently, additional CIVA analysis was performed on a subset of flaws with an extended incidence angle range of 40°-70°. This was used to verify that the previously determined flaw detection amplitude limits using the 45°-70° incidence angle range would be appropriate for use with a 40°-70° incidence angle range. All of these results with the 40°-70° range were within ±1 dB of the results given in Table 6.14 for flaws without skew. Therefore, it was determined that the incidence angle range could be extended from 45°-70° to 40°-70° without significantly altering the necessary flaw detection limits.

6.4.2 Verification testing of weld flaw samples

In order to verify the CIVA results, physical testing was performed on weld samples with known weld flaws. These specimens included the round robin test plates as well as additional test plates with small weld flaws. None of the plates were fabricated with acoustically anisotropic material. This testing was performed in conjunction with final verification testing of the flaw rejection limits by an ASNT Level III UT/Level II PAUT technician. The weld samples were scanned with an Olympus Omniscan MX2 with a 2.25L16-AWS1 PAUT probe which is a 2.25 MHz probe with 16 active elements (active aperture of 16 mm by 16 mm). Some supplemental line scanning was performed with a 5L64-A12 PAUT probe which is a 5 MHz probe with 32 active elements (active aperture of 19.2 mm by 10 mm) in order to evaluate the differences between the 2.25 MHz and 5 MHz probes.

The weld samples were scanned after performing TCG calibration on an AISI 1018 calibration block with 1.5 mm (0.06") diameter SDHs. The reference amplitude was set to 80% FSH and +12 dB scanning gain was added. Line scanning was performed using an incidence angle range of 40°-70° with full coverage of the weld volume and HAZ in two crossing directions. No additional requirements were imposed on the scan plan. All indications with an amplitude greater than -20 dB were further investigated through raster scanning for flaw rejection verification testing, as previously explained.

Since some of the plates had reinforcement on both faces of the plate, these plates were line scanned in 1st leg from each side of the weld and each face of the plate (i.e., four line scans). This was also performed for the plates which were thicker than 0.75" since the TCG did not extend beyond 2" depth. Subsequently, the 2nd leg portion of the scan would have extended beyond the last TCG point. Scanning of the 0.75" thick plates was performed with two line scans; one from each side of the weld using 1st and 2nd leg to cover the entire weld and HAZ in two crossing directions. Some of these plates had additional scans performed from the other face of the plate to verify whether all of the intended weld flaws would still have been detected if full coverage was provided from that face.

The results of the verification testing is shown in Table 6.17 for the intended weld flaws. This table includes the maximum amplitude for each flaw after evaluating each of the line scans necessary for full coverage in two crossing directions. It also includes the maximum amplitude from the follow-up raster scanning which was previously reported. All of the results provided in the table are from testing with the 2.25 MHz probe, but the amplitude with the supplemental line scans with the 5 MHz probe was found to be similar. Since +12 dB scanning gain was added to the line scans and the Olympus Omniscan MX2 instrument truncates the A-scan at 250% FSH, the maximum amplitude during the line scan was truncated at -2.1 dB.

As expected, the maximum amplitude from the line scan can be significantly lower than the maximum amplitude from the raster scanning. The largest difference between the line scan and the raster scan (excluding truncated line scan results) was for the slag which was 0.16”x0.18”. This flaw had a maximum amplitude during the line scans from Face A of the plate of -9.9 dB while the follow-up raster scan was +2.9 dB. This is a difference of 12.8 dB which is approximately a factor of four times as much amplitude.

The intended flaw with the smallest maximum amplitude after evaluating each line scan necessary for full coverage was -13.9 dB for the embedded vertical crack which was 0.14”x0.37”. <u>Therefore, all of the intended flaws would be detected for any flaw detection limit of -14 dB or less.</u> All of the flaw detection limits for planar flaws determined through the CIVA analysis and presented in Table 6.14 are below -14 dB so use of the CIVA results would have resulted in all of the intended flaws to be detected. None of the weld flaws in the weld flaw samples had any skew relative to the weld axis. For this reason, the maximum line scan amplitude should be compared to the limits in Table 6.14 rather than those in Table 6.15 or Table 6.16.

Table 6.17 Verification Testing of Flaw Detection Results

Drawing Details			Line Scan Results	Raster Scan Results
Flaw Type	**Flaw Height (in)**	**Flaw Length (in)**	**Maximum Amplitude (dB)**	**Maximum Amplitude (dB)**
HAZ Crack	0.18	0.52	-2.1*	8.0
Porosity	0.10	0.73	-10.5	-6.2
LOF	0.11	0.63	-2.1*	10.8
HAZ Crack	0.14	0.57	-2.1*	-0.6
Slag	0.10	0.74	-6.4	2.3
Crack	0.14	0.37	-13.9	-12.1
LOF	0.18	0.50	-2.1*	11.8
LOF	0.12	0.64	-2.1*	15.5
Toe Crack	0.19	0.49	-2.1*	2.9
Toe Crack	0.11	0.61	-2.1*	-1.0
Slag	0.09	0.92	-3.0	-4.2
HAZ Crack	0.14	0.45	-2.1*	3.7
IP	0.10	0.88	-2.1*	5.5
Slag	0.32	0.37	-2.1* (Face A) -2.1* (Face B)	1.7
Slag	0.16	0.18	-9.9 (Face A) -2.1* (Face B)	2.9
Slag	0.10	0.90	-3.4 (Face A) -2.1* (Face B)	-1.8
Porosity	0.09	3.31	-8.7 (Face A) -12.5 (Face B)	-8.0
Toe Crack	0.02	0.04	-8.3	-8.4
LOF	0.03	0.06	-2.8	-3.6
Slag	0.06	0.03	-12.1	-8.2
Slag	0.17	3.61	-2.1*	0.9

*A-scan was truncated at 250% FSH with +12 dB scanning gain which correlates to -2.1 dB

During the verification testing, there were many unintended indications which crossed the initial detection limit threshold of -20 dB, excluding geometric indications from weld reinforcement and surface roughness. While some of these unintended flaw detections seem to correlate to actual unintended flaws, most of these indications seemed to be spurious repeating signals on the high incidence angle (70°), as shown in Figure 6.41 (left). Sometimes these repeating signals also appeared at the low incidence angle (40°), as shown in Figure 6.41 (right). These spurious indications also appeared during scanning of clean production welds which had been inspected with digital RT and had no noted indications. The spurious indications were only noticed in the scanning with the 2.25L16-AWS1 probe and not with the 5L64-A12 probe. After further investigation, it was determined that these indications are likely due to grating lobes due to the large pitch of the 2.25 MHz probe (1 mm) compared with the wavelength (1.45 mm). From the literature [51], grating lobes typically appear when the pitch is greater than the wavelength although they may appear for a slightly smaller pitch as well. The spurious indications seemed sensitive to changes to the surface roughness of the plates, even though the surface roughness was typical of production welds. Grating lobes may reflect off of the surface roughness which may explain why they appeared on locations with more roughness. Follow-up raster scanning on the detected locations of the spurious indications found no relevant indications greater than -20 dB, which confirms that they are noise. Due to the prevalence of these grating lobe signals throughout the line scans, it was determined to exclude indications which were characterized as grating lobe indications from follow-up raster scanning.

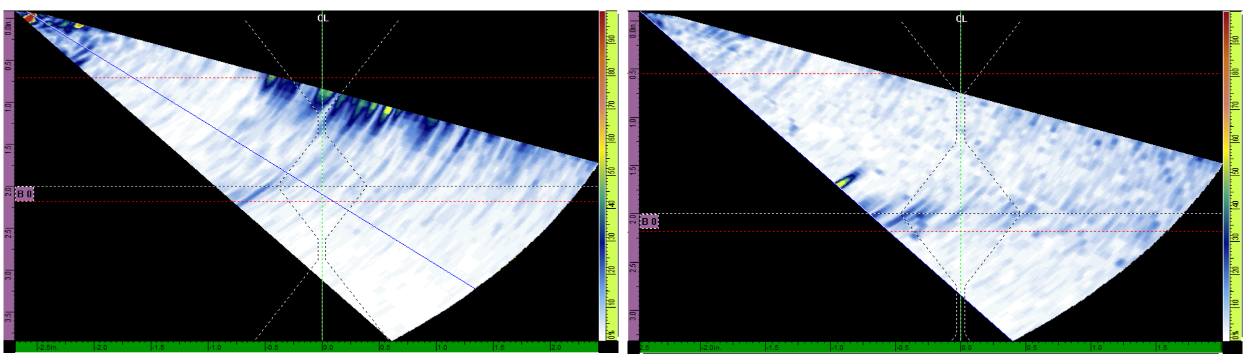

Figure 6.41 Spurious Signals on High Incidence (left) and Low Incidence (right) Angles

Table 6.18 summarizes the detection and rejection results of unintended indications during the verification testing. When the flaw detection limit was set at -20 dB, 36 unintended indications (excluding geometric indications) were detected that required follow-up raster scanning. Of those 36 indications, 33 indications had a maximum amplitude during raster scanning which was less than -13 dB; therefore, these indications would be accepted under all of the flaw rejection limits previously discussed. Three unintended indications were detected above -20 dB which would be rejected if the flaw rejection limit were set at -13 dB, while only one of these indications would be rejected if the flaw rejection limit were set at -10 dB or higher.

As the flaw detection limit is shifted up (more positive), the number of unintended indications drops dramatically, but indications may be missed which would have been rejected during follow-up raster scanning. For instance, if the flaw detection limit were set at -18 dB, the number of acceptable unintended indications which are detected and require follow-up raster scanning decreases from 33 to 18. Increasing the flaw detection limit to -16 dB, decreases the number of acceptable unintended indications to only 8, but one of the unintended indications which would have been rejectable if the rejection limit were set to -13 dB would not have been detected. Thus, that indication would now be accepted since it was effectively missed.

Due to the high rate of unintended indications found during the testing of the weld flaw specimens, a clean production weld 32 inches long by 2 inches thick was obtained and scanned. This specimen was specifically obtained to get a feel for what level of "noise" might be expected in clean shop production welds. Other than grating lobe signals, only two indications (excluding geometric indications) were noted greater than -20 dB during four line scans with the 2.25 MHz probe and no indications (excluding geometric indications) appeared above this threshold with the 5 MHz probe. Neither of the two indications detected with the 2.25 MHz probe exceeded the -18 dB detection limit. Therefore, excluding the grating lobe indications, it is anticipated that very few unintended indications would be identified above a flaw detection threshold of -18 dB in clean welds.

Table 6.18 Number of Unintended Indications Detected during Verification Testing

	Line Scan Amplitude Thresholds			
Raster Scanning Amplitude Threshold	**Detected at -20 dB**	**Detected at -18 dB**	**Detected at -16 dB**	**Detected at -14 dB**
Accepted (<-13 dB)	33	18	8	2
Rejected > -13 dB	3	3	2	1
Rejected > -13 dB & 1" long	0	0	0	0
Rejected > -10 dB	1	1	1	1
Rejected > -8 dB	1	1	1	1
Rejected > -6 dB	1	1	1	1

6.4.3 Recommendation for AWS

Based on the CIVA results for planar flaws along with the verification testing, it was determined to set the amplitude limit for flaw detection at 18 dB under the SSL (i.e., -18 dB). In Annex K, this is referred to as the disregard level (DRL) since indications with amplitude lower than this limit during the line scans will not require additional raster scanning. As stated, this limit provided adequate sensitivity for all intended flaws in the verification testing, along with detecting all unintended indications that were -13 dB or greater when performing follow-up raster scanning. Therefore, this limit seems to set a good compromise between adequate detection of critical flaws and adequate sensitivity so that the number of harmless indications which require follow-up raster scanning is minimal.

According to the CIVA analysis, the -18 dB limit would overestimate the lowest possible amplitude from a critical flaw with skew. This may possibly result in missing a critical flaw, but based on the verification testing, it seems that the CIVA results for flaw detection were slightly conservative. For instance, the CIVA results for a flaw without skew showed that an amplitude limit of -17 dB would result in detection of all critical flaws, but the minimum amplitude measured during verification testing for a comparable flaw was actually -14 dB. Assuming the amplitude of flaws with 5° skew are comparably overestimated, a flaw detection limit of -18 dB should detect critical flaws with 5° skew as the CIVA analysis for these flaws gave an amplitude limit of -20 dB. In other words, no further reduction below SSL seems to be required.

Flaws with 10° skew or greater may have much lower amplitude than the flaw detection limit proposed. For instance, the CIVA results for 10° skew was -28 dB and would be much lower for 20° skew. Setting an amplitude limit this low would result in a large amount of indications which would be acceptable and would likely result in manual raster scanning of most if not all of the weld. This would eliminate the economic advantage of encoded line scanning. The likelihood of planar flaws with skew is expected to be low since the LOF and incomplete penetration flaws will likely be aligned along a fusion face. Also, the current requirements for follow-up scanning for transverse flaws using scanning Pattern D or E will be retained. These requirements will allow for detection of flaws transverse to the weld axis and may aid in detecting highly skewed flaws.

It is recommended that 12 dB over SSL be added to the scanning gain during encoded line scanning of tension welds in order to provide adequate screen height of indications greater than the flaw detection limit. After applying 12 dB of scanning gain, an indication which is greater than 40% FSH will require follow-up raster scanning assuming that reference amplitude is set at 80% FSH.

6.5 Compression Weld Acceptance Criteria

The flaw detection and rejection limits discussed previously were derived using the critical flaw sizes. These sizes were computed assuming that the weld is in a tension member for the FFS analysis. AWS traditionally has separate acceptance criteria for tension and compression welds for both conventional UT and Annex K. For conventional UT in accordance with Clause 6, the rejection limits for compression welds are ~6 dB lower (less conservative) than for tension welds. There is also a slight modification to the Class C length limits as the maximum length for compression welds is 2" regardless of the through-thickness location while there are tighter limits for tension welds in the top or bottom quarter of the weld thickness. For Annex K, the amplitude limits are exactly the same for compression and tension welds, but the maximum length are slightly different for compression and tension welds. The Class C length limits are carried over from Clause 6 with the smaller length for near surface flaws in tension welds. The Class B length limits are also slightly different with compression welds having a maximum length of 0.75" and tension welds having a maximum length of 0.5".

Rather than include separate acceptance criteria for tension and compression welds, the CSA W59:2018 code only includes separate acceptance criteria for statically-loaded and cyclically-loaded structures. Therefore, while bridges would fall under cyclically-loaded, tension and compression welds would be evaluated using the same acceptance criteria.

Since the critical flaw size of compression welds was not specifically determined (and could not be using FFS), the acceptance criteria for compression welds would either be based on workmanship criteria or on the results for tension welds. It is recommended that the flaw detection and rejection limits determined for tension welds be used to form the *basis* of compression weld rejection criteria. It is believed to be prudent to use the same scanning procedure requirements in order to ensure that any critical flaws be detected. The proposed acceptance criteria for tension welds does not rely on length measurement for indications greater than -10 dB. Therefore, purely modifying the maximum length of flaws similar to what is currently in Annex K does not seem reasonable since this would be a very low amplitude for automatic rejection of flaws in compression welds. Rather, any modification to the acceptance criteria rejection limits for compression welds should involve shifting the amplitude limit. One option would be to shift the amplitude limit +6 dB based on the shift that is in the existing Clause 6 amplitude tables. However, this would be contrary to Annex K and CSA W59:2018 which use the same amplitude limits for both compression and tension welds in cyclically loaded structures.

Table 6.19 displays the raster scanned results from the raster scanned verification testing as shown in Table 6.11 but with flaw rejection amplitude limits of -4 dB, -2 dB, and 0 dB. The conventional UT rejection rate from the round robin testing is also shown using the AWS D1.5 Clause 6 compression and tension criteria. Based on this data, setting the rejection limit to -4 dB would result in rejection of all flaws which were rejectable by at least one technician per the round robin testing using the conventional UT compression tables. Setting the rejection limit to -2 dB would result in acceptance of a LOF flaw which was 0.03”x0.06” and was rejectable by 60% of the technicians per the round robin testing using the conventional UT compression tables. Setting the rejection limit to 0 dB would result in acceptance of an HAZ crack, toe crack, and slag inclusion which was rejectable by all of the technicians per the round robin testing using the conventional UT compression tables. This is in addition to the acceptable flaws from the -2 dB rejection limit.

The amplitude limits from the existing Clause 6 conventional UT acceptance criteria for compression welds varies depending on the incidence angle and plate thickness. Based on these amplitudes along with the results from the round robin, it seems reasonable to set the ARL for compression welds to 0 dB (i.e., equal to the SSL). While this would result in a shift of 10 dB from the tension criteria, it seems reasonable from a workmanship standpoint. It is also recommended that compression welds be evaluated based on the results from the encoded line scan rather than requiring follow-up manual raster scan of each indication. The criticality of flaws in compression welds is much lower than in tension welds and does not warrant the additional effort to maximize the signal. With these recommendations, compression welds will be essentially tested similar to how they are in the 2015 edition of Annex K since evaluation would be performed on encoded line scans only. With this modification to the ARL for compression welds, the new version of Annex K would still be 5 dB more conservative than the old criteria which sets the ARL at +5 dB.

Based on conventional UT tables, it seems reasonable for the EVL to be set ~-4 dB. This is very close to the old Class C limit of -6 dB for flaws which are acceptable when 2” or less. Therefore, it is recommended that the EVL be set at -6 dB with a length limit of 2”. This essentially duplicates the Class C criteria of Annex K, but are now labeled as Class B in the proposed version. Since follow-up raster scanning is not required for compression welds, the detection limit (i.e., disregard level (DRL)) would be set to the same amplitude as the EVL of -6 dB. Finally, the length measurements for compression welds can be determined using the 6 dB drop method on the encoded line scan results similar to the current Annex K requirements.

Table 6.19 Verification Testing of Flaw Rejection Amplitude Limit (Compression Welds)

Drawing Details			Conventional UT Rejection Rate		Raster Scan Results						
					Max Amp (dB)	Rejection Limit					
Flaw Type	Flaw Height (in)	Flaw Length (in)	Tension	Compression		-10 dB	-8 dB	-6 dB	-4 dB	-2 dB	0 dB
HAZ Crack	0.18	0.52	NA	NA	8.0	Y	Y	Y	Y	Y	Y
Porosity	0.10	0.73	NA	NA	-6.2	Y	Y	N	N	N	N
LOF	0.11	0.63	NA	NA	10.8	Y	Y	Y	Y	Y	Y
HAZ Crack	0.14	0.57	NA	NA	-0.6	Y	Y	Y	Y	Y	N
Slag	0.10	0.74	NA	NA	2.3	Y	Y	Y	Y	Y	Y
Crack	0.14	0.37	NA	NA	-12.1	N	N	N	N	N	N
LOF	0.18	0.50	NA	NA	11.8	Y	Y	Y	Y	Y	Y
LOF	0.12	0.64	NA	NA	15.5	Y	Y	Y	Y	Y	Y
Toe Crack	0.19	0.49	NA	NA	2.9	Y	Y	Y	Y	Y	Y
Toe Crack	0.11	0.61	NA	NA	-1.0	Y	Y	Y	Y	Y	N
Slag	0.09	0.92	NA	NA	-4.2	Y	Y	Y	N	N	N
HAZ Crack	0.14	0.45	NA	NA	3.7	Y	Y	Y	Y	Y	Y
IP	0.10	0.88	NA	NA	5.5	Y	Y	Y	Y	Y	Y
Slag	0.32	0.37	100%	60%	1.7	Y	Y	Y	Y	Y	Y
Slag	0.16	0.18	100%	100%	2.9	Y	Y	Y	Y	Y	Y
Slag	0.10	0.90	100%	100%	-1.8	Y	Y	Y	Y	Y	N
Porosity	0.09	3.31	80%	0%	-8.0	Y	Y	N	N	N	N
Toe Crack	0.02	0.04	40%	0%	-8.4	Y	N	N	N	N	N
LOF	0.03	0.06	80%	60%	-3.6	Y	Y	Y	Y	N	N
Slag	0.06	0.03	0%	0%	-8.2	Y	N	N	N	N	N
Slag	0.17	3.61	100%	100%	0.9	Y	Y	Y	Y	Y	Y

6.6 Comparison to Radiographic Testing

Currently, most tension bridge welds are only inspected with RT, except for fracture critical welds which are inspected with RT and UT. Compression welds may be tested with either RT or UT. There are select states that have replaced RT with UT for tension welds, but this is very unique. Bridge owners have traditionally preferred RT to UT due to the simple interpretation of an RT image which can be saved and easily retrieved for permanent record. Conventional UT reports, on the other hand, are tabulated results of the indications which were detected by the UT technician.

RT is known to be more sensitive to volumetric flaws such as slag inclusions and porosity while UT is more sensitive to planar flaws such as lack of fusion and cracks. This was very apparent during this research project as most of the lack of fusion flaws in the round robin plates were not discernable with RT while they were rejectable according to most conventional UT and PAUT inspections.

Slag and porosity while easily detectable with RT had low rejection rates with PAUT according to Annex K. Since the rejection rates for these flaws was much greater for conventional UT, it is likely that the poor rejection rate for PAUT was due to differences between the acceptance criteria of PAUT and conventional UT as well as the lack of raster scanning with PAUT in order to maximize the amplitude. Therefore, while slag and porosity often have low amplitude with UT (conventional UT or PAUT) compared with planar flaws, it is not to say that volumetric flaws cannot be detected with UT. This is apparent in the previously reported verification testing results for flaw detection and rejection shown in Table 6.17 and Table 6.11 where setting reasonable amplitude limits resulted in detection and rejection of the volumetric flaws.

Digital RT images of the round robin test plates are included in the Appendix. In addition to the intended flaws in the weld specimens, RT images are available for two of the three unintended flaws which were detected and rejected if the amplitude limit was set at -13 dB. One of these indications (maximum amplitude of -10.8 dB during raster scanning) was apparent on the RT image, shown in Figure 6.42. It had a maximum length of 0.03" which would be acceptable for all thicknesses according to the RT acceptance criteria in AWS D1.5 Clause 6. The other unintended flaw (maximum amplitude of -11.2 dB during raster scanning) was not apparent on the RT image since it was on the edge of the plate.

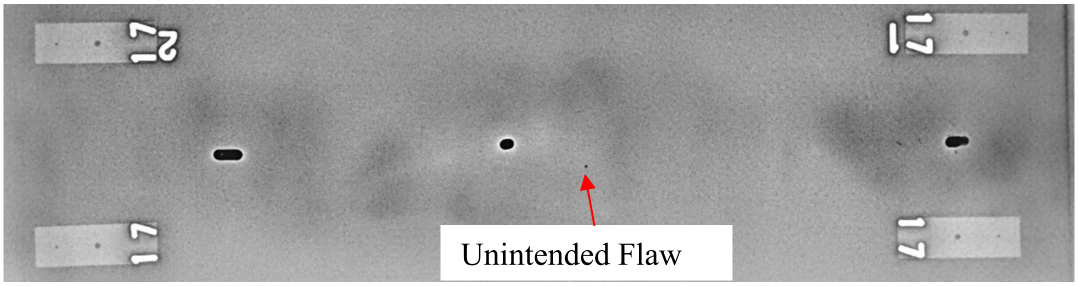

Figure 6.42 RT Image of Unintended Weld Flaw

If confronted with choosing either RT or UT, it seems that UT would be the preferred inspection method based on the increased sensitivity of planar flaws, which are more critical according to FFS, along with the ability to detect and reject volumetric flaws. It is recommended that future research include a round robin testing program where the rejection rate using PAUT with the proposed revisions to AWS Annex K would be compared to the rejection rate for RT. Performance qualification of PAUT technicians requiring the detection and rejection of critical planar and volumetric weld flaws during an independently-administered practical examination would provide additional verification that PAUT is providing adequate sensitivity to critical flaws of all types.

6.7 Technician Performance Qualification

6.7.1 Current AWS requirements

The round robin testing showed that there was a large amount of variability in inspection results using the PAUT Annex K and conventional UT codes. While some of this variability may be due to differences in inspection equipment, equipment settings, and scanning procedures, a large portion of this variability is due to human factors and inconsistencies. For instance, it is likely that the large amount of variability in the reported location of the same flaw was primarily caused by poor calibration of encoders. It was noted that technicians would often consistently report multiple flaws either to the left or right of their actual location. This offset in flaw location was sometimes quite large resulting in a large number of detected flaws which did not meet the API RP 2X requirements for reported flaw location.

The inspection variability due to human factors would likely be improved if PAUT technicians were required to pass practical examinations which were administered by independent entities.

These proposed examinations would include inspection of flawed weld specimens using AWS D1.5 Annex K. The test plates should include known flaws which are comparable to the critical flaw size used to determine the acceptance criteria.

Since AWS D1.5 and ASNT SNT-TC-1A do not currently have any guidance on critical weld flaw size, it is unknown what size flaws are included in the practical examinations performed in accordance with ASNT SNT-TC-1A [52]. In addition, ASNT SNT-TC-1A only requires that a minimum of one flawed specimen be used for the practical examination without any guidance on the number of flaws, type of flaw, orientation of flaw, or requirement for blank specimens. It states that the flawed specimen should be representative of the component that would be tested, but that interpretation is left to the ANST Level III. Finally, no minimum requirements for passing the practical examination is provided. It states that at least ten different checkpoints requiring an understanding of NDT variables and the employer's procedural requirements should be included in the practical exam. It also states that the candidate should detect all discontinuities and conditions specified by the NDT Level III. Finally, it notes that while it is normal to score the practical on a percentile basis, practical examinations should contain checkpoints or gateway tasks that failure to successfully complete will result in failure of the examination.

The 2016 edition of SNT-TC-1A included a sample checklist for guidance on the development of practical examinations. This checklist is not specific to any method or level and may be modified as needed in accordance with the Level III. The sample checklist includes a possible breakdown of a scoring rubric and sample limits on flaw detection, false calls, and flaw evaluation. The ten categories listed in this sample checklist include:

1. Knowledge of NDT Procedure
2. Equipment and Material
3. Test Specimen Care and Custody
4. Operations
5. Detection of Indications
6. Interpretation of Indications
7. Evaluation of Indications
8. Documentation and Records

9. General Health and Safety
10. General Observable Conduct

Since there is no guidance on the flaw size in the practical exam specimen, the weld flaws included in the specimen could be extremely large such that anyone who understands the very basics of PAUT inspection would be able to detect them and would pass the practical exam. In this case, the examination is not performing the intended function of testing the competency of the individual. This would be like giving a structural engineer a single question exam on steel design where they only had to compute the tension stress by dividing the given force by the given area and deeming that they are now qualified to design a bridge.

ASNT SNT-TC-1A states that the technician should demonstrate familiarity with and ability to operate the NDT equipment, record, and analyze the resultant information to the degree required. The "degree required" statement is very non-specific and leaves the decision on whether the technician has adequate performance completely to the ASNT Level III administering the exam. It also states that the Level II PAUT technician should detect all discontinuities and conditions specified by the NDT Level III. There are no requirements on the accuracy of flaw location measurements or limitations on the number of false calls.

Discussion is merited on the self-policing of the NDT industry according to ASNT SNT-TC-1A. There are no specific requirements on the difficulty of the practical test or on the method for grading the practical test. It is the NDT firm's advantage to have as many technicians pass the exam and be available for inspection duties. It is also difficult for NDT firms to have a large number of samples available or to have specimens which have not been used for previous tests. The test specimens may be reused from technician to technician within an NDT inspection firm or even reused for reexamination of candidates who previously failed (or passed) the exam.

It is interesting that ASNT SNT-TC-1A includes no discussion on characterization of flaw type yet AWS D1.5 Annex K requires that flaws characterized as cracks be rejected. In other words, the current training and certification program for PAUT technicians does not include any requirements on the ability to characterize flaws, but it is expected that these technicians will be able to accurately characterize the flaw type when they perform weld inspections per AWS D1.5 Annex K. (*As noted, the round robin phase of the research showed the current workforce has limited reliability in this skill.*)

The AWS D1.1 proposal for PAUT inspection has modifications to the personnel qualification requirements including doubling the minimum number of hours of work time experience in PAUT from 160 hours to 320 hours and requiring that the practical exam consist of at least two flawed specimens representing joint types to be examined with each specimen containing a minimum of two flaws. It is believed that doubling the minimum number of hours of work time experience is unlikely to result in a large improvement in PAUT inspection quality. In fact, it may actually have the opposite effect as a technician who is not properly performing any given task will become more entrenched in the wrong practice and become more confident that he or she is actually doing it correctly. In short, requiring a PAUT technician (or any individual performing any task) to perform additional work time experience does not necessarily mean that the technician will perform "better" as it unclear whether the technician is performing the inspection correctly in the first place. For example, a technician who has not properly demonstrated that they can detect and reject critical weld flaws but has 320 hours of work experience incorrectly performing PAUT inspections is unlikely to be any better than he was after he completed the first 160 hours of incorrect PAUT inspections. Rather than doubling the required work time experience, improving the meaningfulness of the practical examination and setting more defined requirements for passing the practical examination would likely result in greater improvement in technician performance.

While there is merit to increasing the number of flawed specimens and the number of flaws tested during the practical examination, it does not seem reasonable to require a minimum number of flaws per flawed specimen as this only provides the candidate with a minimum number of hits per plate that they need to find. It would be much better to have a random set of specimens with various number of weld flaws mixed with blank specimens which do not have any flaws. This way the candidate does not know how many flaws there are per plate and does not expect that there should be a flaw in each plate. This results in a much a more realistic practical exam since the number of flaws in a weld is always unknown in an inspection. Other guidance on the development of a performance test to evaluate reliability of a nondestructive testing system is given in MIL-HNBK-1823A [53].

Some states have started to recognize the need for improved practical examination of UT technicians. For example, NYSDOT has an Ultrasonic Testing Technician Program included in their Steel Construction Manual [54]. This program requires prospective UT technicians who wish to be certified by NYSDOT to pass examinations provided by NYSDOT. These examinations include an open and closed book exam worth 25% each as well as a practical exam worth 50%. NYSDOT also keeps a list of Certified UT Technicians available on their web page. One of the administrators of this UT certification program stated that a large percentage of prospective UT technicians have failed their state's exam. In fact, they are lessening the required time between initial test and the retest in order to make it easier for retesting. This case study highlights the need for independent examination of UT technicians.

TxDOT [55] also includes a hand-on examination administered in-house in addition to the requirements of the AWS code and employer's Written Practice. A TxDOT official who administers this exam was contacted to confirm the type and size of flaws used in this exam. TxDOT has a specific plate for each geometry including T and corner joints and a thickness transition butt weld. Each plate has multiple flaws which are of various types including both planar and volumetric flaws. These flaws are typically Class A rejectable defects in accordance with Clause 6 tension weld conventional UT tables.

While the NYSDOT and TxDOT programs are for additional practical examination of conventional UT technicians, Florida DOT is currently implementing a program to test PAUT technicians. This program involves practical examination of each PAUT technician using an in-house test block and QA inspector trained in PAUT. The flaws chosen for this block are specific to the response of FDOT's internal research. An FDOT official stated that this qualification was deemed necessary based on the level of training that technicians were receiving in typical PAUT training courses. Since FDOT is interested in replacing RT with PAUT, the selection of flaws for the practical examination were determined to be critical and was one of the reasons that this qualification is performed in-house.

6.7.2 Recommendations for AWS

As PAUT use becomes more prevalent, it will be important for the PAUT technician qualification requirements to be standardized across individual agencies. In speaking with these states, it became clear that having an independent central organization which would administer a reasonable practical examination using Annex K would be beneficial. By standardizing the practical examination, PAUT technicians would not need to take a separate exam to satisfy the individual requirements of each agency. Rather than having many separate examinations with one flawed plate, a standardized examination could be much more thorough and still take less time overall.

A good example of a thorough, standardized qualification requirement this is the Certified Welding Inspector (CWI) examination. Instead of having separate exams for each agency, prospective CWIs only need to qualify through AWS. The AWS CWI examination process includes a three-part examination which extends over a full day. Two parts of the exam cover welding background (i.e., closed book) and code requirements (i.e., open book) while the third part is a practical examination using weld specimens. The CWI examination is set by AWS and proctored at defined locations throughout the year. Therefore, the CWI examination has a controlled level of difficulty and clearly defined expectations which covers visual examination of welds for all agencies. It is recognized that requiring independent practical examination of PAUT technicians will result in additional cost but this may be necessary to implement the removal of RT requirements in lieu of in-depth PAUT inspection. It is believed that a meaningful practical examination could be performed in a single day.

Additional research should be performed to develop a PAUT technician qualification program which utilizes independent and consistent evaluation of technicians. This study could compare practical examination results to shop performance in order to develop a quantitative practical examination which will adequately evaluate candidates for bridge weld inspections. Based on the research and what was discussed above, the performance qualification requirements in the following sections are proposed.

6.7.2.1 Practical examination parameters

The practical examination should involve meaningful performance testing that is conducted by an independent party. Optimally, the test would be administered by a third-party that has developed a realistic test procedure which is acceptable to all agencies.

The practical examination should evaluate detection, location, and rejection of realistic weld specimens with critical flaws. In addition, the practical examination should include evaluation of following parameters:

- Familiarity and application of Annex K requirements
- Development of an appropriate scan plan and documentation of essential variables
- Use of proper equipment
- Proper calibration for reference sensitivity and acoustic properties
- Proper application of the two-part inspection procedure (i.e., line scan and follow-up raster scanning)
- Proper documentation and reporting

6.7.2.2 Specimen details

The specimens used in the practical examination should be fabricated from steel that have acoustic properties which are representative of the typical steels encountered in bridge weld inspection but also include some specimens in which calibration adjustments are required to account for variation in acoustic properties. The specimens should also be representative of the configuration of the welds which will be inspected by the technicians during future applications of Annex K. This includes thickness transitions and weld reinforcement if both will be encountered.

The number of flaw specimens shall be large enough such that the number of flaws per plate will be varied, and blank specimens should be included in the lineup of plates to be tested. The technicians should be instructed to detect and report all relevant indications and should be informed that a plate may not necessary contain any flaws. Based on the previous research, including the round robin, it is believed that at least four weld specimens should be used with a weld length of approximately 18 inches. Weld specimens which are too short may not adequately capture errors from encoded line scanning. More weld specimens may be necessary in order to adequately include possible weld configurations and acoustic properties (i.e., proper calibration practices) that technicians may encounter during weld inspection.

The number of flaws included in the weld specimens should be adequate to verify satisfactory performance. Both volumetric and planar discontinuities should be included in the set of weld flaw specimens. It is recommended that at least one slag inclusion, porosity grouping, lack of fusion flaw, and vertical planar flaw (i.e., crack or incomplete penetration) should be included. Variations in the flaw size and through-thickness location will also be necessary in order to verify that the scanning procedures for flaw detection and rejection are properly being followed. Therefore the absolute minimum number of flaws included in the practical exam is recommended to be five. Use of more flaws and weld specimens would allow for variation in flaw size and location (through-thickness depth, tilt, and location along weld axis) which would provide additional information on the scatter of results from human factors.

6.7.2.3 Pass/fail criteria

It is believed that the formulas and minimum performance levels included in API RP 2X are appropriate for the bridge industry for evaluating flaw detection, sizing, and location during the practical examination. API RP 2X includes minimum recommended performance levels for UT technicians using the following two formulas:

$$P = \frac{L_c}{L_a} \times 100 \qquad \text{Formula 1}$$

$$R = \left(\frac{L_c}{L_1}\right)\left(1 - \frac{L_f}{L_1}\right) \times 100 \qquad \text{Formula 2}$$

Where:

P = percentage of actual reflectors correctly detected and sized, 0 to 100

R = overall rating including penalty for false calls, 0 to 100

L_a = length of actual reflector contained in the test plate

L_c = credited length for indications that have been correctly sized and located. (Credit is given for the lesser of the reported length or actual length of the flaw.)

L_1 = accumulative length of all indications by the technician, right or wrong

L_f = accumulative length of indications above the stated disregard level where no reflector exists

To be correctly sized, this document recommends that the reported dimensions be within a factor of two of true dimensions (i.e., one-half to twice the actual dimension). To be correctly located, this document recommends that the centerline of the reported indication be within the boundary of the actual indication or within ½ inch of the actual centerline of the indication (whichever is greater). API RP 2X suggests that a score of 70 or above for Formula 1 and a score of 50 or above for Formula 2 be used as minimum performance for ultrasonic technicians.

When the round robin test results were used to calculate the performance of each conventional UT and PAUT technician, two of the five conventional UT technicians and zero of the four PAUT technicians met these levels. The primary reason for the PAUT technicians not meeting the minimum performance was due to errors in flaw location. As stated, this is thought to be due to issues with the use of encoders. Since the flaw has to be detected in order to count towards the performance requirements, the lower sensitivity with Annex K prior to the proposed modifications (i.e., no separate flaw detection limit for the line scans) will have also contributed to some of the low scores. The primary reason for the conventional UT technicians not meeting the minimum performance was due to poor accuracy for the flaw length measurement and some misses of long scattered porosity. The issues with flaw length measurement is likely due to the manual method for length measurement with conventional UT which lends itself to overestimating the actual length.

While the minimum scores provided by API RP 2X could be used to evaluate flaw detection and flaw location, the pass/fail criteria of the practical examination should also evaluate the following items in determining an overall practical examination score:

- Familiarity and application of Annex K requirements
- Development of an appropriate scan plan and documentation of essential variables
- Use of proper equipment
- Proper calibration for reference sensitivity and acoustic properties
- Proper application of the two-part inspection procedure (i.e., line scan and follow-up raster scanning)
- Evaluation of indications using the proper acceptance criteria
- Proper documentation and reporting

Using a checklist similar to that provided in the 2016 edition of ASNT SNT-TC-1A, a rubric should be developed which incorporates each of these items. By assigning points to each item, along with flaw detection and location criteria, technicians passing the practical examination will demonstrate adequate comprehension and application of the Annex K inspection procedure.

6.8 Flaw Sizing Acceptance Criteria for Alternative UT Methods

An acceptance criteria based on flaw height and length sizing is provided as an alternative method, given that the PAUT technician develops a written procedure according to specified requirements and that performance testing be performed on samples of similar material and with flaws similar to the rejectable size. This allows for other advanced ultrasonic methods such as FMC/TFM PAUT or TOFD to be used to inspect bridge welds provided that they can detect and reject critical weld flaws.

It is envisioned that the requirements for alternative ultrasonic systems and the accompanying acceptance criteria based on flaw sizing would be included in the main body of AWS D1.5, rather than included in Annex K. Annex K includes all necessary requirements and acceptance criteria for application of encoded line scanned PAUT. Annex K does not rely on accurate flaw height sizing and, therefore, does not require development and qualification of an individual flaw sizing procedure for the specific equipment and application method.

CSA W59-18 [10] includes minimum requirements for alternative ultrasonic systems in the main body of the code. Alternative ultrasonic systems include encoded PAUT and TOFD in W59, as only manual raster scanned PAUT are allowed to replace conventional UT without additional performance testing. Since AWS D1.5 Annex K covers encoded PAUT using amplitude and length acceptance criteria, it is recommended that the additional requirements for alternative UT methods in AWS D1.5 apply to any methods which do not fit within the requirements of conventional UT Clause 6 or Annex K.

6.8.1 Minimum requirements

The following requirements from CSA W59 are recommended for incorporation into AWS D1.5:

- Written agreement by the Engineer and Contractor prior to the examination allowing the use of the alternative inspection method.
- Certification of Level II or III in accordance with ASNT SNT-TC-1A for the specific method, if applicable. For instance, ASNT SNT-TC-1A includes qualification requirements for TOFD, but does not include additional qualification requirements for FMC/TFM PAUT.
- Documentation of inspection procedures in writing in accordance with recognized standards and accepted in writing by the Engineer.
- Written procedures that contains at a minimum the following information:
    - Specific technician training requirements
    - Types of weld joint configurations to be examined
    - Acceptance criteria
    - Type of UT equipment (manufacturer and model number)
    - Type of transducer, including frequency, size, shape, angle, and type of wedge
    - Scanning surface preparation and couplant requirements
    - Type of calibration test block(s) with appropriate reference reflectors
    - Method of calibration and calibration interval
    - Method of examination for laminations prior to weld evaluation
    - Scanning pattern and sensitivity requirements
    - Methods for determining discontinuity location, height, length, and amplitude level
    - Transfer correction methods for surface roughness, surface coatings, and part curvature, if applicable
    - Method of verifying the accuracy of the completed examination. This verification may be by reexamination using UT by others, other NDE methods, macroetch specimen, gouging, or other visual techniques accepted by the engineer
    - Documentation requirements for examinations, including any verification performed

    - Documentation retention requirements
- Demonstration of the system in order to achieve Engineer's approval
    - System demonstration on one or more demonstration blocks simulating the weld
    - Demonstration should provide adequate and repeatable detection of typical weld flaws and be used to set threshold parameters
- Acceptable performance of system demonstration should include:
    - Detection of all of the flaws in the demonstration block(s)
    - Recorded flaw sizes for critical weld flaws with reported flaw size that exceeds the acceptance criteria limits
    - Recorded flaw sizes for subcritical weld flaws with reported flaw size which is reasonably accurate

6.8.2 Acceptance criteria

The acceptance criteria used for the alternative UT methods which uses measurements of flaw height and length should be comparable to the acceptance criteria used in the recommendations for Annex K acceptance criteria for planar and volumetric flaws. As described in Section 6.3, the acceptance criteria for Annex K was developed using the critical flaw sizes computed using fracture mechanics.

As shown in Table 6.8, the -10 dB amplitude limit for flaw rejection was based on CIVA analysis of a 0.05"x0.10" planar surface flaw. This flaw was comparable to the 0.06"x0.08" critical planar surface flaw for a 4 ksi stress range thickness transition weld and an 8 ksi stress range equal thickness weld. The controlling planar embedded flaw had an amplitude of -8 dB according to CIVA using a 0.15"x0.15" planar embedded flaw. This flaw was comparable to the 0.17"x0.17" critical planar embedded flaw for a 4 ksi stress range thickness transition weld and the 0.14"x0.14" critical planar embedded flaw for an 8 ksi stress range equal thickness weld.

For the acceptance criteria used for the alternative UT methods, it is recommended that the flaw height and length limits be provided for various a/c ratios. Therefore, the results for the critical planar flaws noted above were summarized into the following tables. Table 6.20 includes a recommended acceptance criteria for planar embedded flaws measured using alternative UT methods. Table 6.21 includes a recommended acceptance criteria for planar surface flaws.

Table 6.20 Alternative UT Methods Acceptance Criteria for Planar Embedded Flaws

Flaw Height (in)	Flaw Length (in)	Interpolated Length (in) for Intermediate Height (in)
0.06	1.00	-
0.07	0.28	For 0.07<H<0.10, L=0.56-4.0*H
0.10	0.16	For 0.10<H<0.14, L=0.21-0.5*H
0.14	0.14	

Table 6.21 Alternative UT Methods Acceptance Criteria for Planar Surface Flaws

Flaw Height (in)	Flaw Length (in)	Interpolated Length (in) for Intermediate Height (in)
0.02	1.00	-
0.03	0.20	For 0.03<H<0.06, L=0.31-3.67*H
0.06	0.09	

As shown in Table 6.9, the -13 dB amplitude limit for flaw rejection of flaws 1" long or greater was based on CIVA analysis of a 0.125" diameter embedded volumetric flaw and a 0.08" diameter surface volumetric flaw. The embedded flaw was comparable to the 0.14" diameter critical volumetric embedded flaw for an 8 ksi stress range equal thickness weld. The surface volumetric flaw was comparable to the 0.08"x0.11" critical volumetric surface flaw for a 4 ksi stress range in a thickness transition weld and a 0.06"x0.08" critical volumetric surface flaw for an 8 ksi stress range in an equal thickness weld.

Since these flaws are the same sizes as the critical planar flaws, it is recommended that the limits provided in Table 6.20 and Table 6.21 be also be used for the maximum size of an individual volumetric flaw (i.e., maximum slag inclusion or pore). In addition, a maximum length of 1" is recommended for scattered indications such as a group of porosity. This is similar to the length requirement recommended for Annex K for flaws greater than -13 dB but less than -10 dB.

Since the inputs to the FFS study were for tension welds. The limits given in Table 6.20 and Table 6.21 will be overly conservative for compression welds. The recommendation for the Annex K amplitude limits for the compression acceptance criteria uses a 0 dB amplitude. This amplitude approximately correlated with the maximum amplitude of vertical 0.10”x0.10” planar surface flaw and a vertical 0.20”x0.20” planar embedded flaw from CIVA analysis. Note that this amplitude was based on traditional conventional UT amplitude limits rather than fracture mechanics. For compression welds, a 50% increase in critical flaw height and length given in Table 6.20 and Table 6.21 seems reasonable to compare with the Annex K acceptance criteria. Another strategy would be to set this limit based on a strength requirement and an acceptable amount of unfused material.

7. SUMMARY AND CONCLUSIONS

This research had the objectives of developing guidelines to evaluate CJP welds in steel bridges based on updated acceptance criteria and to develop proposed modifications to AWS D1.5. While AWS D1.5 currently includes PAUT inspection procedures in Annex K, these acceptance criteria were workmanship-based and were carried over from previous D1.1 conventional UT methods. AWS D1.5 did not provide means for alternative methods such as FMC/TFM PAUT or TOFD which are suited for evaluation of flaw criticality based on measurements of flaw size rather than amplitude responses.

The research has shown that (1) the critical flaw size of bridge welds could be developed using FFS, (2) a large amount of variability was possible when weld inspections were performed using current AWS D1.5 conventional UT and PAUT scanning procedures and the current workforce, (3) computer modeling could be used to evaluate ultrasonic responses of weld flaws and reference reflectors, (4) acoustic properties of bridge steels may vary widely and may not be isotropic, (5) revised acceptance criteria for Annex K could be developed to detect and reject critical weld flaws utilizing amplitude based criteria, and (6) additional technician performance requirements including independent practical examination were necessary.

Major findings of this research were that the current scanning procedures and acceptance criteria in Annex K did not correlate to traditional limits used in conventional UT per Clause 6 and were not adequate for rejection of critical weld flaws according to FFS. This research also found that differences in acoustic properties between the calibration block and test object could result in significant error in reference sensitivity for frequencies which were allowed in Annex K. The current version of Annex K does not include any requirements on calibration block acoustic properties. Variations in shear wave velocity were also found to be significant for common grades of bridge steels. These variations resulted in significant error in beam refraction angle which could result in inaccurate flaw location and significant loss of amplitude. These variations affect both conventional UT and PAUT. Proposed revisions to Annex K were provided in Section 5.7 of this report which would account for these differences, but similar revisions should be included in Clause 6 for conventional UT.

The final product of this research was proposed revisions to AWS D1.5 Annex K for improved flaw detection and rejection. These revisions include minimum requirements for technician qualification, requirements on the acoustic properties of calibration blocks in order to represent the conditions found in the test object, requirements on the scanning procedure and sound coverage, and requirements on acceptance criteria to detect and reject critical weld flaws.

Recommendations were also provided which would allow alternate UT methods such as full matrix capture (FMC) - total focusing method (TFM) PAUT or time-of-flight diffraction (TOFD) to be used in lieu of PAUT or conventional UT. Use of these methods rely upon written agreement by the Engineer and Contractor along with procedure development and demonstration on weld flaw specimens. Limits on acceptable flaw sizes which could be incorporated into an acceptance criteria based on flaw size measurements was also provided.

7.1 Summary of Principal Findings

The following summary provides the principal findings of this research.

7.1.1 Summary of critical flaw size

1. Stress concentrations at thickness transition butt welds result in significant reductions in the critical flaw size compared with equal thickness butt welds. Stress concentration factors from linear elastic finite element modeling were 1.8 at the surface of flange thickness transition welds and 1.4 at the surface of web thickness transition welds. A stress concentration factor of 1.6 is appropriate at the surface of flange thickness transitions when primary stresses are 75% of the nominal yield strength due to redistribution of stresses.
2. Based on review of prior research, Delta-K threshold (ΔK_{th}) values of 2.5 ksi$\sqrt{in}$ are appropriate for planar and volumetric flaws in CJP welds.
3. Based on CVN requirements for weld and base metal, minimum fracture toughness (K_{Ic}) values for fracture critical welds are likely to be 50 ksi$\sqrt{in}$ for Grade 36 through HPS 50W, 60 ksi$\sqrt{in}$ for Grade HPS 70W, and 75 ksi$\sqrt{in}$ for Grade HPS 100W.

4. The critical flaw size for CJP bridge welds are controlled by the fracture limit state when the effective cyclic stress range is 4 ksi or lower and the fatigue crack growth limit state when the effective cyclic stress range is 8 ksi or above.
5. The critical flaw size for embedded flaws ranged from 0.20”x0.20” for equal thickness welds with 4 ksi effective stress range to 0.08”x0.08” for thickness transition welds with 8 ksi effective stress range. The critical flaw size for surface flaws ranged from 0.10”x0.13” for equal thickness welds with 4 ksi effective stress range to 0.02”x0.03” for thickness transition welds with 8 ksi effective stress range.

7.1.2 Summary of round robin experimental testing

1. Issues with proper calibration of PAUT encoders resulted in error in reported flaw location for PAUT technicians. An offset along the weld axis in the reported flaw location compared to the actual flaw location was documented by many PAUT technicians.
2. The average flaw detection rate for PAUT and conventional UT were similar when a lenient detection criteria was utilized (“1 Inch Gap” detection criteria), but the average flaw detection rate for PAUT was lower than conventional UT when a more stringent detection criteria was utilized (API RP 2X detection criteria).
3. The average rejection rate was lower for PAUT in accordance with the 2015 edition of AWS D1.5 Annex K compared to conventional UT in accordance with the 2015 edition of AWS D1.5 Clause 6.
4. Reported measurements of the height and length of the same weld flaw varied considerably for individual PAUT, conventional UT, and TOFD technicians. The reported flaw height was typically larger than the actual flaw height for PAUT and TOFD technicians. Errors in flaw length measurement included both overestimating and underestimating the actual flaw length.
5. Average range between maximum and minimum Indication Rating for all flaws scanned with conventional UT was 10 dB.

7.1.3 Summary of acoustic property calibration requirements

1. Material models for bridge base metals were developed and benchmarked using experimental test results from previous research. The CIVA material attenuation parameter at 5 MHz was found to vary from 1.85 dB/in for Grade 36 to 0.33 dB/in for Grade HPS 100W for 3D CIVA models. The CIVA material attenuation parameter at 2.25 MHz was found to vary from 0.49 dB/in for Grade 36 to 0.13 dB/in for Grade HPS 100W for 3D CIVA models.
2. Variations in the grain structure of base metals may result in differences in the attenuation characteristics between the calibration block and test object. This may result in significant differences in the reported amplitude of weld defects unless properly accounted for during calibration. While limiting the transducer frequency to 2.25 MHz results in much less variation in amplitude compared with 5 MHz transducers, significant (>2 dB) amplitude differences are possible with 2.25 MHz transducers for bridge base metals with high attenuation. Therefore, it is recommended that the material attenuation of the calibration block and test object be measured through pitch-catch testing and corrective action be taken when there is more than a 2 dB difference at the longest sound path. Corrective action includes application of a transfer correction or use of a different calibration block.
3. Variations in shear wave velocity can result in significant (>2 dB) amplitude loss if not properly accounted for during calibration. It is recommended that the incidence angle range be limited to a maximum of 60° if the difference in velocity between the calibration block and the test object is greater than 1%. It is recommended that the maximum difference in velocity between the calibration block and the test object be limited to 2.5%.
4. The ultrasonic beam may split into two sound waves traveling at two different velocities when acoustic anisotropic materials are tested at oblique orientations to the rolled direction. It is recommended that materials be defined as acoustic anisotropic when the birefringence exceeds 1%. It is recommended that scanning of acoustic anisotropic materials at an oblique orientation to the rolled direction include 4 dB of additional sensitivity and that the incidence angle be limited to a maximum of 60°.

5. Experimental tests were performed on submerged arc welds to measure the changes in attenuation for sound passing through the HAZ or weld metal. The test results showed that the attenuation of sound passing through the HAZ or weld metal was typically lower than for sound passing only through base metal. Some locations did have higher attenuation for sound passing through the weld metal but the total loss of amplitude was only 2 dB.
6. The variation of shear wave velocity at different points across a plate was evaluated for three heats of steel. The experimental results showed that the variation was minimal with a maximum standard deviation of 0.0002 in/µs in either the rolled or transverse to rolled direction and a maximum standard deviation of 0.25% for the birefringence.

7.1.4 Summary of PAUT scanning procedures and acceptance criteria

1. The amplitude limits for the acceptance criteria in AWS D1.5 Annex K PAUT are significantly different than the amplitude limits in the Clause 6 conventional UT acceptance criteria. AWS D1.5 Annex K limits are less conservative than what is in Clause 6 with up to a 15 dB difference for the Class A limit.
2. It is recommended that the scanning procedure in Annex K be modified to use line scanning for flaw detection and follow-up raster scanning for determination whether a flaw is rejectable. Line scanning is preferred for flaw detection since it provides a permanent record through the encoded scan for documentation while raster scanning is preferred for flaw rejection since it maximizes the amplitude.
3. It is recommended that the disregard limit (DRL) of AWS D1.5 Annex K be set to -18 dB compared to the 0.06” diameter SDH reference reflector for flaw detection during the line scan. Flaws with amplitude greater than the DRL during the line scan would require follow-up raster scanning.
4. It is recommended that the automatic rejection limit (ARL) for follow-up raster scanning be set to -10 dB compared to the 0.06” diameter SDH reference reflector. All flaws with amplitude which exceeds this limit would be rejectable regardless of length.
5. It is recommended that the Class B amplitude limit for follow-up raster scanning be set to -13 dB compared to the 0.06” diameter SDH reference reflector. Flaws with amplitude which exceed this limit and have a measured length 1” or greater would be rejectable.

7.2 Recommendations for Future Research

While this research has resulted in important findings and recommendations for modifications for AWS D1.5 regarding application of PAUT for the inspection of bridge welds, additional research is suggested which could aid in application of these recommendations. Four topics of suggested research are proposed: (1) performing a round robin testing program to compare inspection results using RT to inspection results using PAUT in accordance with the revised version of Annex K including the proposed modifications, (2) developing a performance based qualification program for PAUT technicians and verifying improvement in inspection results, (3) developing specific scan plan recommendations for probe selection and line scan index offset for typical weld geometries, and (4) collecting additional data on variability of acoustic properties for other steel bridge base metals and SAW welds of other thicknesses.

The first research topic will compare round robin inspection results of RT and PAUT using the revised version of Annex K. While this research project used computer modeling and experimental test results to develop and verify the revisions to Annex K, the round robin results would be able to collect information on human factors and scatter in results. This study would aid in adoption of the revised Annex K inspection procedure to be used in lieu of RT by providing a direct comparison of inspection results using both methods.

The second research topic will involve development of PAUT technician qualification requirements which will adequately demonstrate use of the revised Annex K procedure. This research would involve the establishment of the number, size, and type of flaws needed for a meaningful practical examination. This research will also provide verification whether the PAUT inspection quality will meet or exceed RT after requiring proper training and performance testing of PAUT technicians along with the revisions to Annex K.

The third research topic will develop specific scan plan recommendations for typical weld geometries. Currently, there is no ANST Level III for PAUT; therefore, the ASNT Level II PAUT technicians are responsible for developing the scan plan. This includes probe selection, index offset location for line scans, and focal law configurations. As shown in this research, the probe frequency and aperture should be properly selected in order to result in optimal inspection results.

For instance, inspections of thick plates with long sound paths may require use of lower frequency and larger apertures in order to account for loss of amplitude due to attenuation and beam spread. This research has also shown that the amplitude response of flaws will be greatly influenced by probe location. Since typical bridge welds utilize very similar geometries based on the plate thickness, recommendations to probe parameters and index positions could be tabulated for typical welds. This would cut down on the effort for scan plan development and would result in more consistent inspections from technician to technician within the QA/QC process.

The fourth research topic will collect additional data on the variability of acoustic properties for steel bridge base metals and SAW welds. This research topic would involve collecting data on the variability of acoustic properties of applicable steel bridge grades along with the variability of acoustic properties at different locations within the same heat of steel. This research topic will aid in determining the overall scatter of typical steels and in developing refined calibration standards. This project should include combinations of possible heat treatment within each grade, including A709-50CR (i.e., A1010) since the acoustic properties of this mild stainless steel were not investigated during this research. The experimental tests on the attenuation characteristics of SAW welds was limited to two inch thick specimens during this research project. Therefore, it is recommended that this research topic include SAW welds of other thicknesses or welding parameters which are typically used in bridge fabrication.

APPENDIX

A.1 Flaw Height Measurement Scatter

Along with collecting data on the detection and rejection of known weld flaws using the current acceptance criteria, one of the primary objectives of the round robin testing program was to evaluate the ability of PAUT and TOFD technicians to accurately measure the overall dimensions of internal flaws (i.e., flaw height and flaw length) and to determine best practices for flaw sizing.

The flaw height reported by each PAUT, TOFD, and FMC/TFM technician is shown in the following plots. The originally intended flaw sizes are noted in the legend as the “Drawing”. As can be seen in the following figures, the reported flaw height for FMC/TFM is very consistent with the intended flaw height and, where available, was the size used for the actual flaw height shown in the round robin flaw details. Note that PAUT3 technician only reported flaw height for two of the eight flaws that were detected. Also, TOFD1 technician only reported flaw height for twelve of the eighteen flaws that were detected since it was reported that the extents of the flaw could not be discerned. TOFD2 technician did not report a location for Flaw 12. Table A.7.1 shows the standard deviation of the reported flaw height for each UT method compared to the intended flaw height (i.e. “Drawing”). FMC/TFM had the lowest standard deviation for reported flaw height and PAUT had the greatest standard deviation.

Table A.1 Standard Deviation of Reported Flaw Height

UT Method	Standard Deviation
PAUT	0.27”
TOFD	0.16”
FMC/TFM	0.05”

Figure A.7.1 displays all of the reported flaw height data for LOF flaws. The flaw height was oversized by PAUT and TOFD for all of the flaws, except for the results from TOFD2. A large amount of scatter was seen for the reported height of the same flaw. Some interesting results are Flaw 10 and Flaw 8. Flaw 10 had one reported result very similar to the FMC/TFM result and two reported results that were oversized by 2-3 times. Flaw 8 had almost no scatter between the three PAUT hits, but they were consistently oversized by 1.5 times the height reported by FMC/TFM.

Figure A.7.2 displays the reported flaw height scatter data for all of the cracks. Compared with the LOF flaws the scatter of the height sizing of the cracks was typically much smaller. Once again, the cracks were typically oversized. Figure A.7.3 displays the reported flaw height data for all of the porosity flaws. The porosity flaws were also oversized, with Flaw 12 up to almost 2 times the FMC/TFM height and Flaw 16 approximately 3 times the FMC/TFM height. Figure A.7.4 displays the reported flaw height data for all of the slag flaws. Once again, these flaws were typically oversized by up to 2 to 3 times the height reported by FMC/TFM.

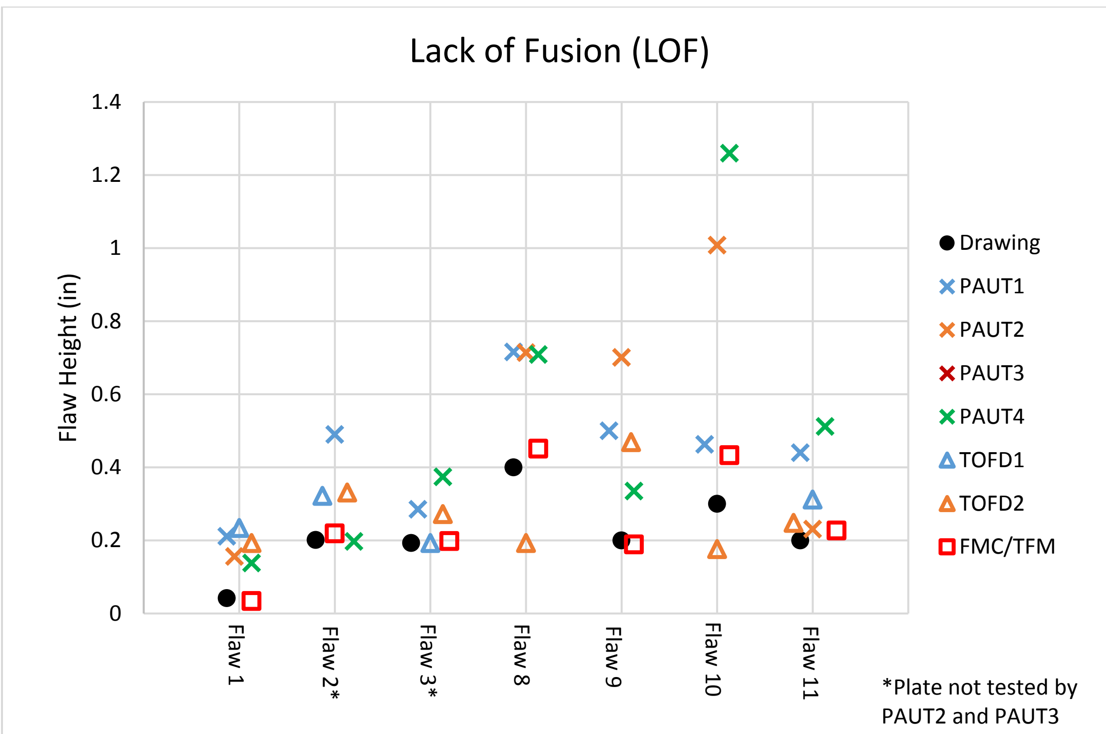

Figure A.1 Flaw Height Scatter for LOF Flaws

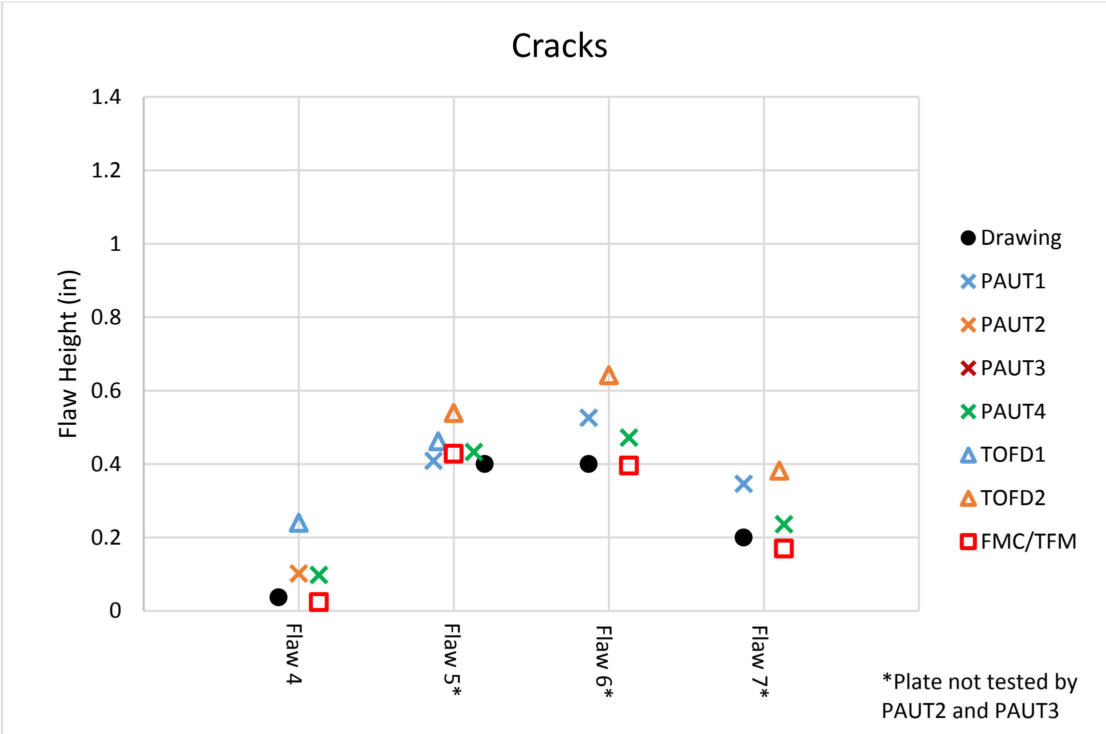

Figure A.2 Flaw Height Scatter for Cracks

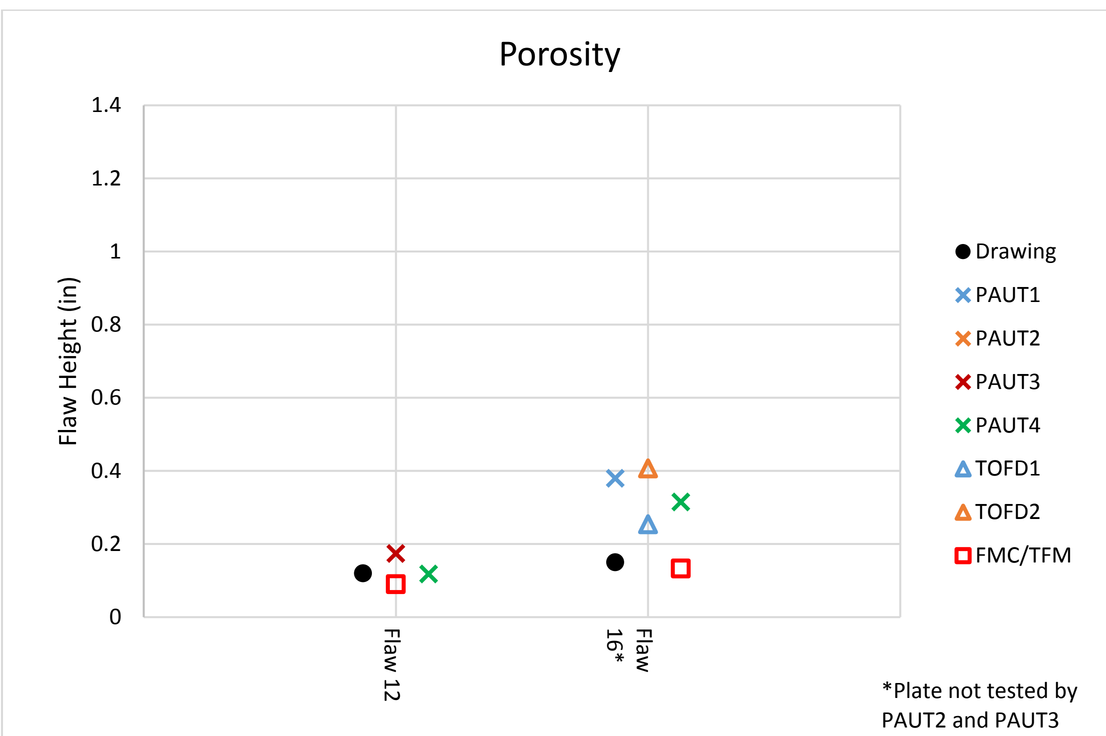

Figure A.3 Flaw Height Scatter for Porosity

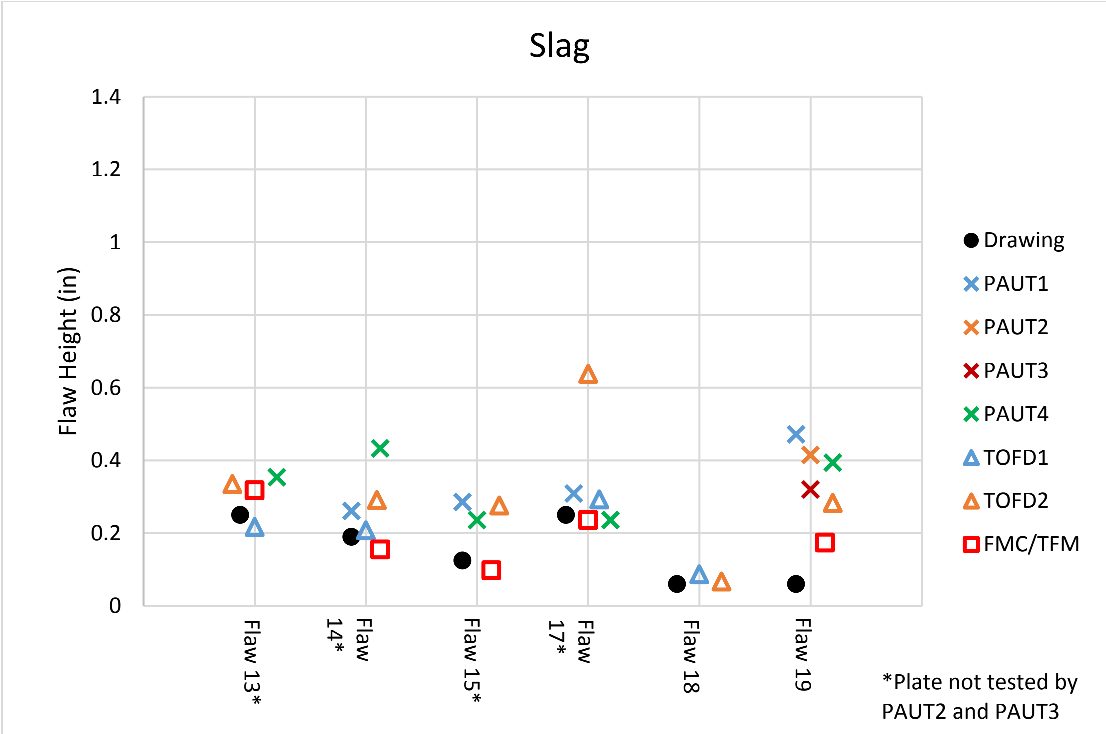

Figure A.4 Flaw Height Scatter for Slag

A.2 Flaw Length Measurement Scatter

Flaw length was reported for all inspection methods including: PAUT, conventional UT, TOFD, FMC/TFM, and digital RT. Table A.7.2 shows the standard deviation of the reported flaw length for each UT method compared to the intended flaw length (i.e. "Drawing"). FMC/TFM had the lowest standard deviation for reported flaw length and conventional UT had the greatest standard deviation.

Table A.2 Standard Deviation of Reported Flaw Length

UT Method	Standard Deviation
PAUT	0.48"
TOFD	1.03"
FMC/TFM	0.36"
Conventional UT	1.11"

Figure A.7.5 displays the reported flaw length data of LOF flaws. Flaw 1 is the only flaw which was apparent on the digital RT inspection. For all of the other flaws, the best estimate of the flaw length is the intended flaw length from the FlawTech drawings. It is apparent that the reported flaw length was typically oversized for PAUT, conventional UT, and FMC/TFM. The PAUT results for LOF flaws were typically oversized by up to 0.5”. The conventional UT results for LOF flaws were typically oversized by up to 1”, except for Flaw 11 which was undersized by conventional UT by 0.6”.

Figure A.7.6 displays the flaw length scatter data for cracks. It should be noted that the vertical scale is much larger for this plot since Flaw 4 had a tremendous amount of scatter. After reviewing the digital RT data, it was apparent that the plate with this flaw had scattered porosity throughout its length. While this would account for the reason for some of the large reported length measurements, it still does not account for the large scatter in results since all technicians scanned the same plate. Therefore, it would be expected that the technicians would still have had similar reported lengths encompassing all of the unintended flaws.

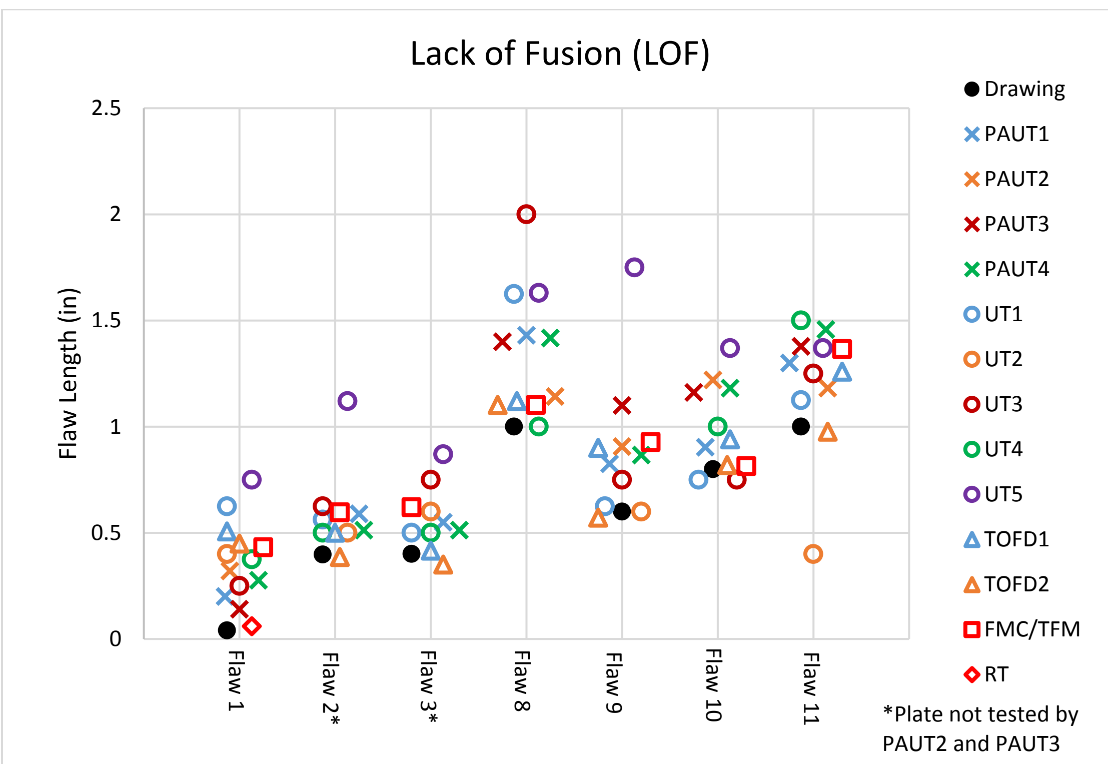

Figure A.5 Flaw Length Scatter for LOF Flaws

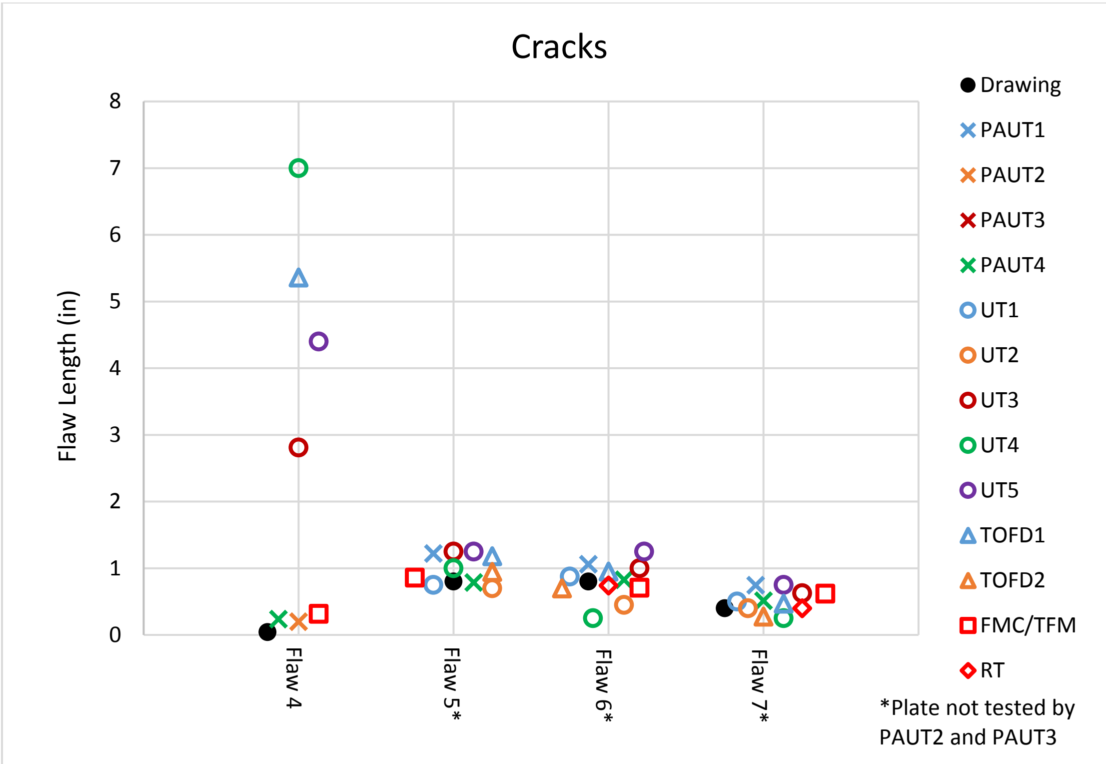

Figure A.6 Flaw Length Scatter for Cracks

Figure A.7.7 displays the reported flaw length data for the porosity flaws. Two lengths are reported for the digital RT inspection since, as reported previously, some of the weld flaws had unintended peripheral flaws outside the main grouping of porosity. It can be seen that porosity had a large scatter in reported results with some technicians overestimating the length and some underestimating the length. It seems that PAUT was slightly more consistent at measuring the flaw length than conventional UT. TOFD and FMC/TFM reported greatly undersized length for the porosity flaws in some cases.

Figure A.7.8 displays the reported flaw length data for slag flaws. Flaw 13-17 were typically oversized by PAUT and conventional UT with the oversizing up to 1” for conventional UT while the PAUT results were within 0.5”. Flaw 18 was the small slag inclusion which was not detected by any of the conventional UT or PAUT technicians. It was measured to be only 0.03” long in the digital RT results. Flaw 19 had a main grouping of slag and peripheral flaws. As can be seen in the reported results, some technicians reported the total flaw length while others reported a flaw length corresponding to the length of the main grouping of slag. Therefore, there were large variation of reported results for the same plate being tested by different technicians according to the same code.

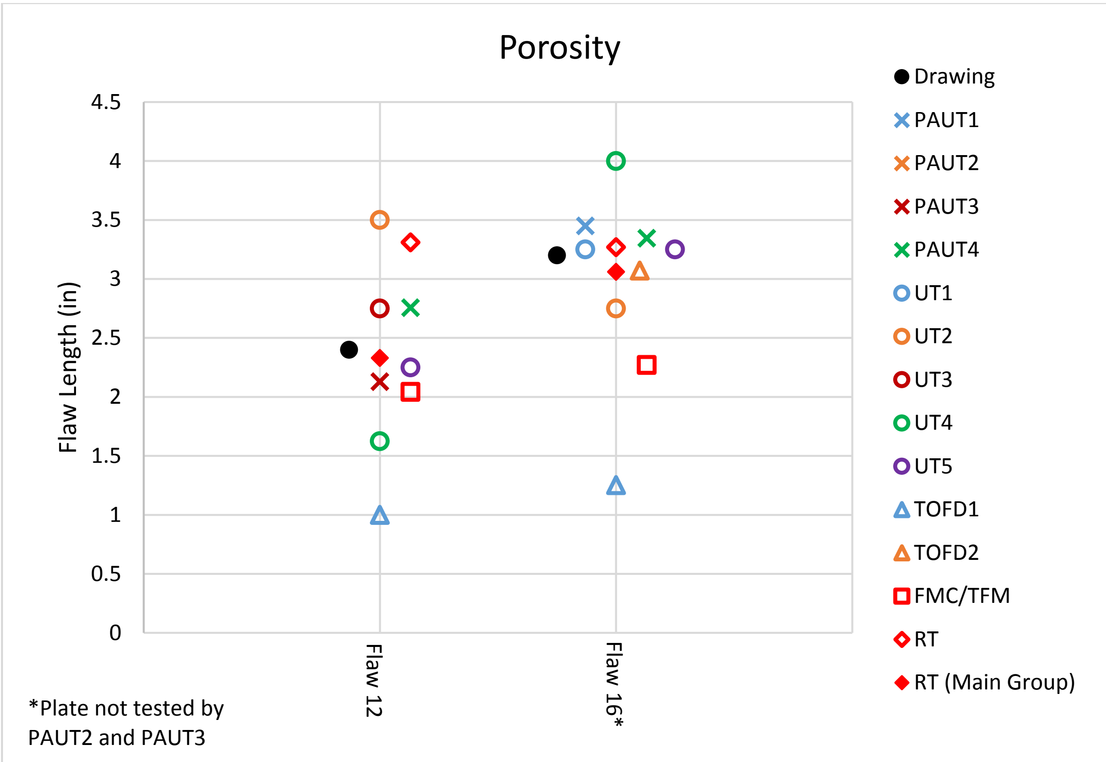

Figure A.7 Flaw Length Scatter for Porosity

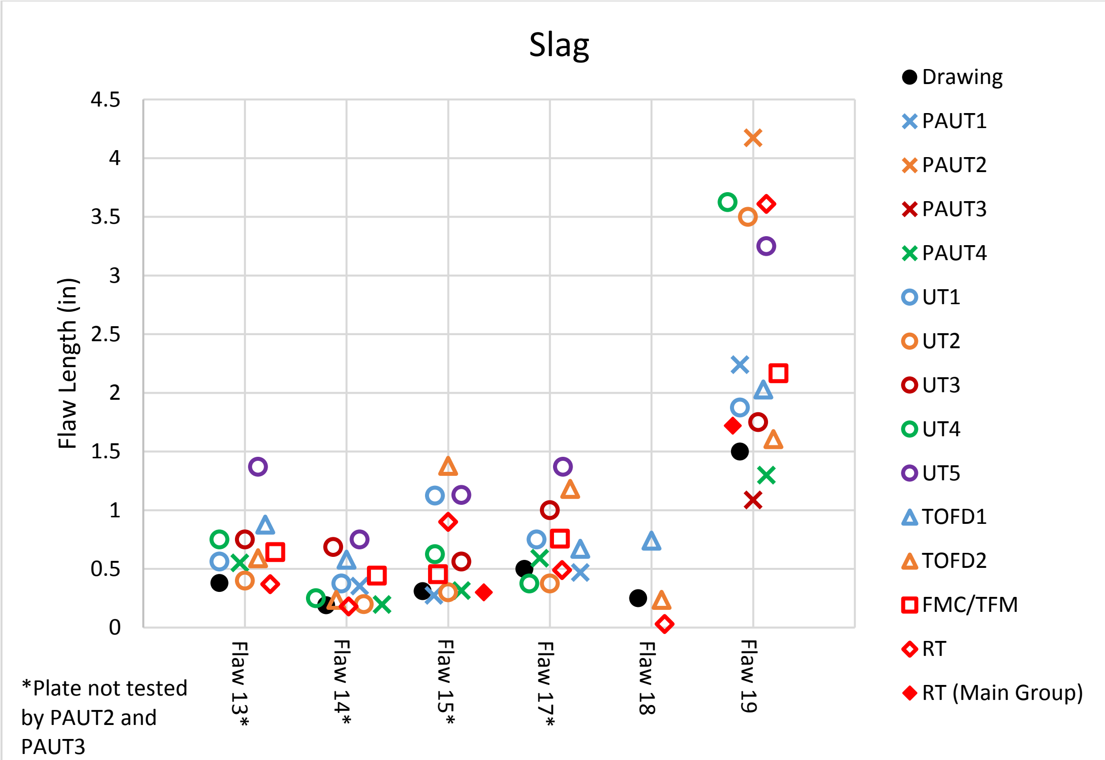

Figure A.8 Flaw Length Scatter for Slag

A.3 Round Robin Reported Amplitude

Previous studies [3], [26], [56], [57] have found that there is large scatter in reported amplitude between different technicians scanning the same flaw for conventional UT. As expected, the round robin data from this study showed the same trend. The average range between the maximum and minimum Indication Rating for all flaws scanned with conventional UT was 10 decibels (dB). This variability is much larger than the 3 dB difference used in the AWS D1.5 tension criteria for classification as either a Class A (Rejectable) or Class D (Acceptable) indication for welds up to 1.5" thick or the 5 dB difference for welds greater than 1.5" thick. If more technicians participated in the round robin study, the extremes in the difference in reported indication ratings would have only increased. Therefore, it should be expected that a flaw with amplitude close to the rejection limit would be found to be acceptable to some conventional UT technicians and rejectable to others.

It was found that lack of fusion indications have the greatest range (i.e., difference in maximum and minimum) in Indication Ratings, while porosity had the smallest range. This is likely due to the mirror-like quality of lack of fusion flaws where only a small movement of the probe results in a large change in amplitude while porosity is much less affected by adjustments in the probe location. Table A.7.3 summarizes the average range in reported indication rating by different flaw types.

Figure A.7.9 through Figure A.7.12 display the scatter in reported Indication Rating (amplitude) for each flaw. The figures are sorted by flaw type, similar to the height and length scatter plots. While there was a very large amount of scatter for each flaw, the Indication Rating was typically well into the Class A category for LOF and cracks. Flaw 1 in Figure A.7.9 and Flaw 4 in Figure A.7.10 had flaw classifications ranging from Class A to Class D which demonstrates how the scatter in reported amplitude can result in scatter in flaw rejection rate.

Table A.3 Average Range in Reported Conventional UT Indication Rating

Flaw Type	**Avg. Range**
LOF	12 dB
Crack	11 dB
Porosity	3 dB
Slag	9 dB

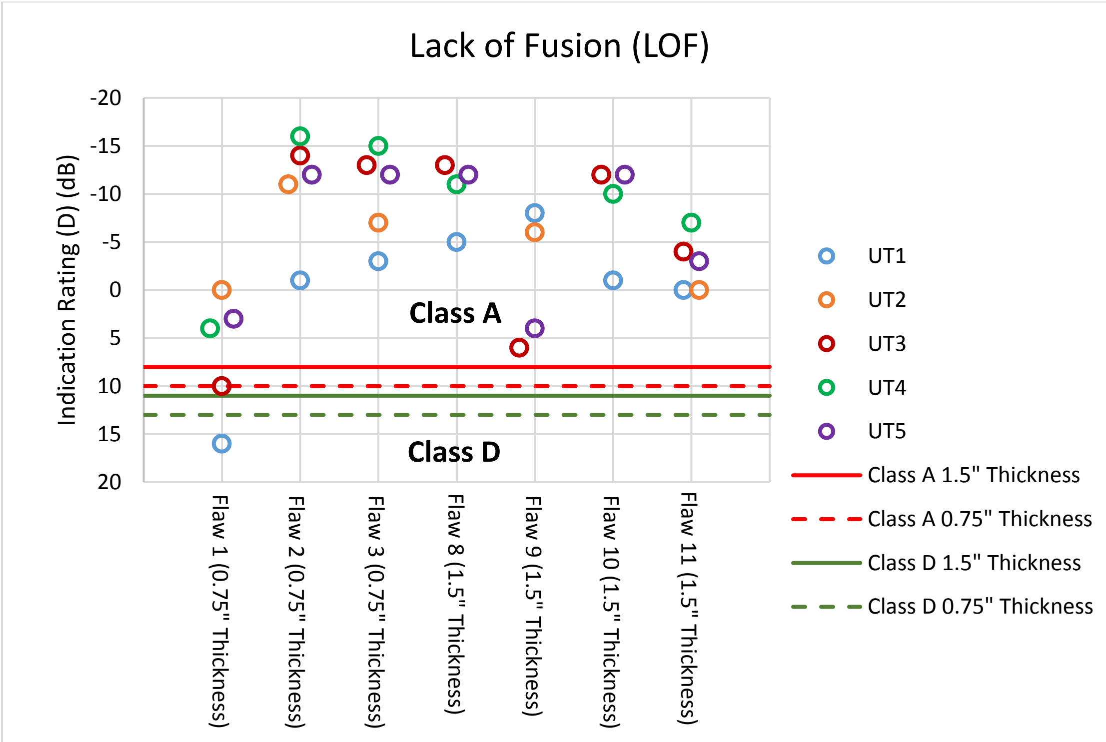

Figure A.9 Conventional UT Amplitude Scatter for LOF Flaws

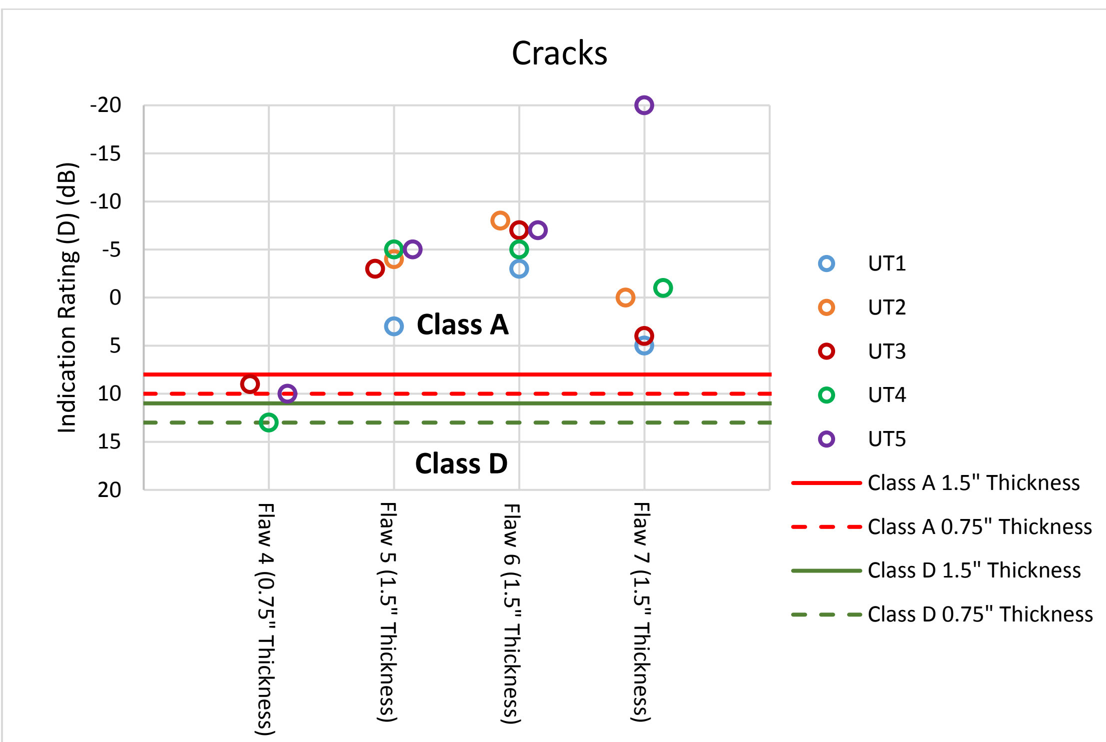

Figure A.10 Conventional UT Amplitude Scatter for Cracks

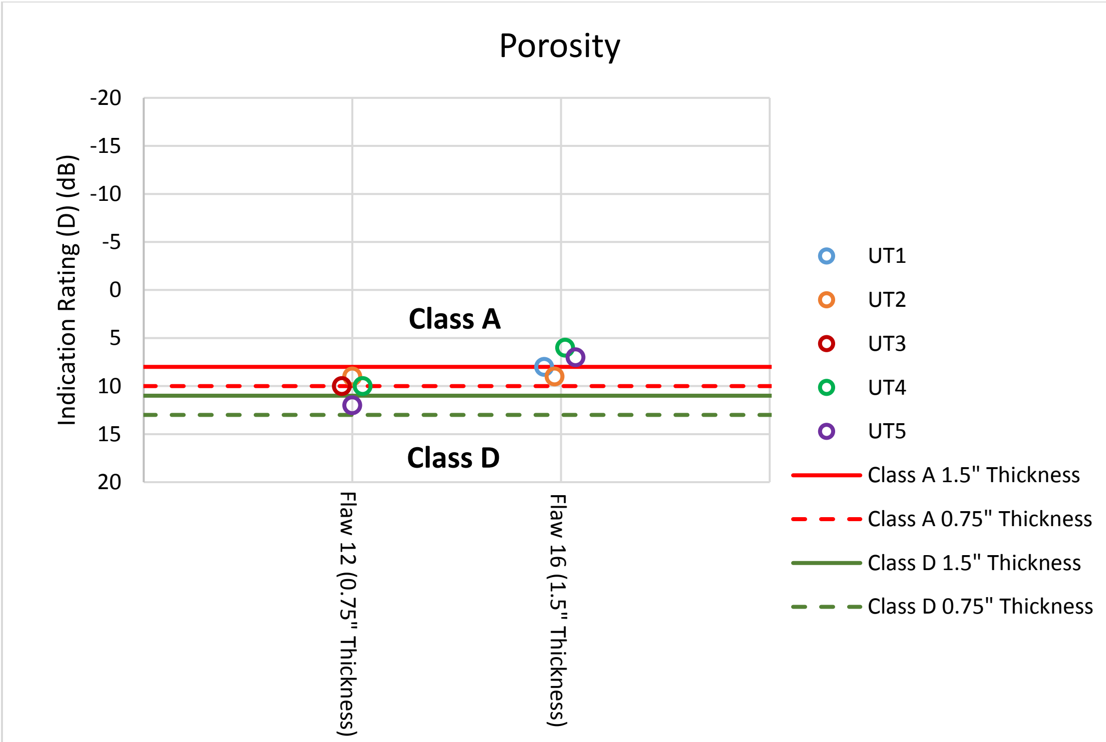

Figure A.11 Conventional UT Amplitude Scatter for Porosity

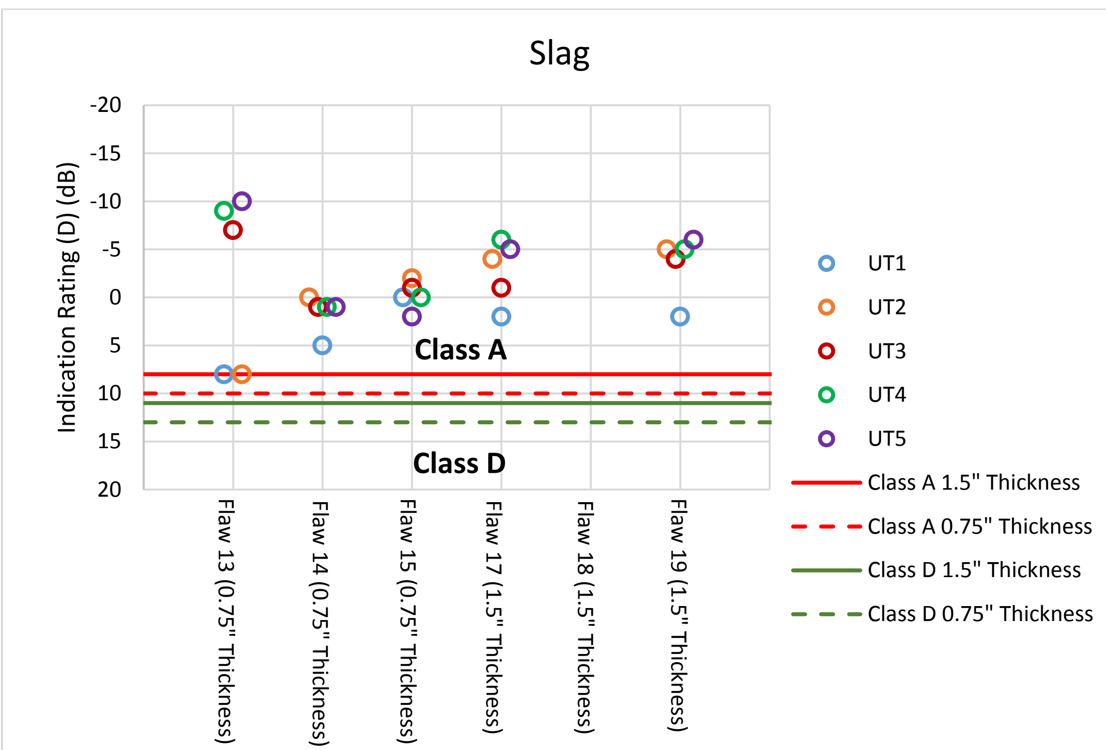

Figure A.12 Conventional UT Amplitude Scatter for Slag

A similar comparison was made for PAUT Annex K to investigate the range in reported amplitude, but one issue is that some PAUT technicians truncated the amplitude at 100% full screen height (FSH) while others reported amplitude readings up to 200% FSH. Therefore, comparing the maximum and minimum reported amplitude for each flaw is not as straightforward with PAUT since the truncated amplitude readings can give the appearance of a high range in amplitude due to the same flaw being reported as 100% and 200% FSH by different technicians or low range if all of the readings are at 100% FSH.

It was noted that the flaws that had a high amplitude with conventional UT also typically had a high amplitude with PAUT, but PAUT tended to have more outliers below the ARL (Class A) than conventional UT. This is thought to be caused by the lack of raster scanning to determine the maximum reported amplitude, but it also could be due to the differences in the acceptance criteria amplitude limits. Due to the truncation of the PAUT data, it was difficult to compare the difference in the magnitude of scatter between PAUT and conventional UT scans.

The amplitude was plotted against the flaw size (i.e., flaw height, flaw length, and flaw cross-sectional area) for both PAUT and conventional UT. As expected, the amplitude increases as the size of planar flaws increase (height, length, or cross-sectional area) for both PAUT and conventional UT. This shows that amplitude is appropriate for use in an ultrasonic acceptance criteria since an amplitude cut-off can be set such that large planar flaws are rejectable, if detected.

All planar flaws greater than 0.20" high x 0.40" length (cross-sectional area 0.08 in^2) had PAUT amplitude greater than 50% FSH (Class B). Recall that 50% FSH is equal to the reference amplitude for the 2015 version of Annex K. Conventional UT indication ratings for these planar flaws were greater than or equal to +6 dB (Class A up to 1.5" thickness and Class B for 1.5" to 2.5" thickness). Recall that this is equivalent to an amplitude of 6 dB below reference for PAUT. The maximum reported amplitude for PAUT would likely have been higher if the peak amplitude was determined by additional raster scanning rather than just reporting the maximum measured along the line scans.

Volumetric flaws did not have a correlation between size (height, length, or cross-sectional area) and amplitude for PAUT or conventional UT using the size of the overall grouping of flaws. It should be noted that the flaw size for porosity was taken to be the overall group of pores rather than the individual pore dimensions. It is likely that the individual pore dimensions also affect the ultrasonic response. The amplitude from volumetric flaws is likely more influenced by the flaw type (slag vs. porosity) and local differences in shape than the overall size of the grouped flaw.

A.4 Digital RT Images of Round Robin Specimens

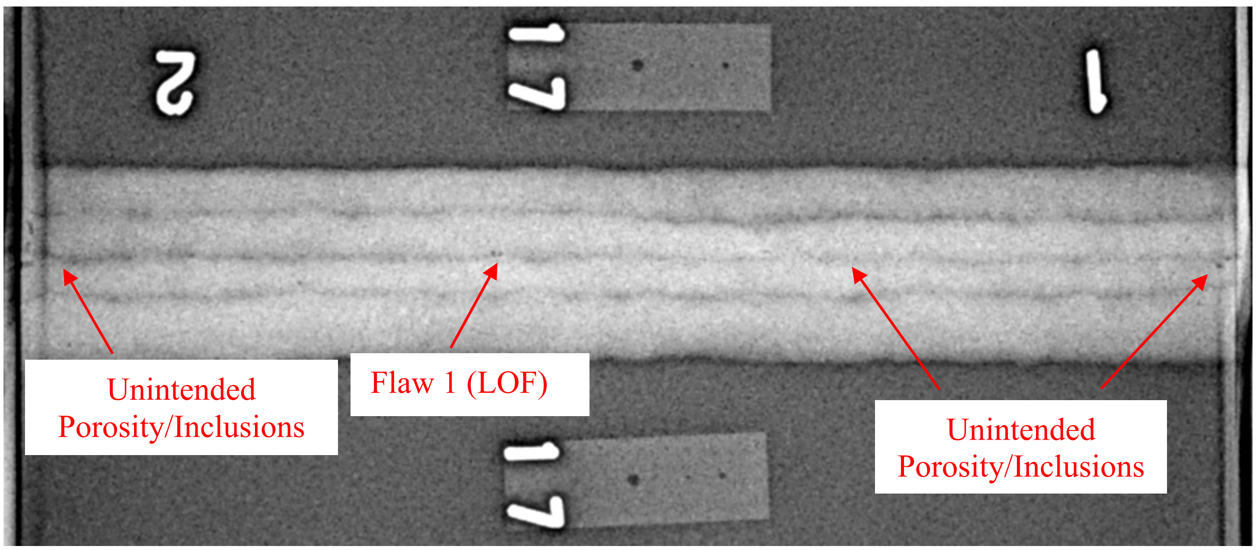

Figure A.13 Flaw 1 Digital RT Image

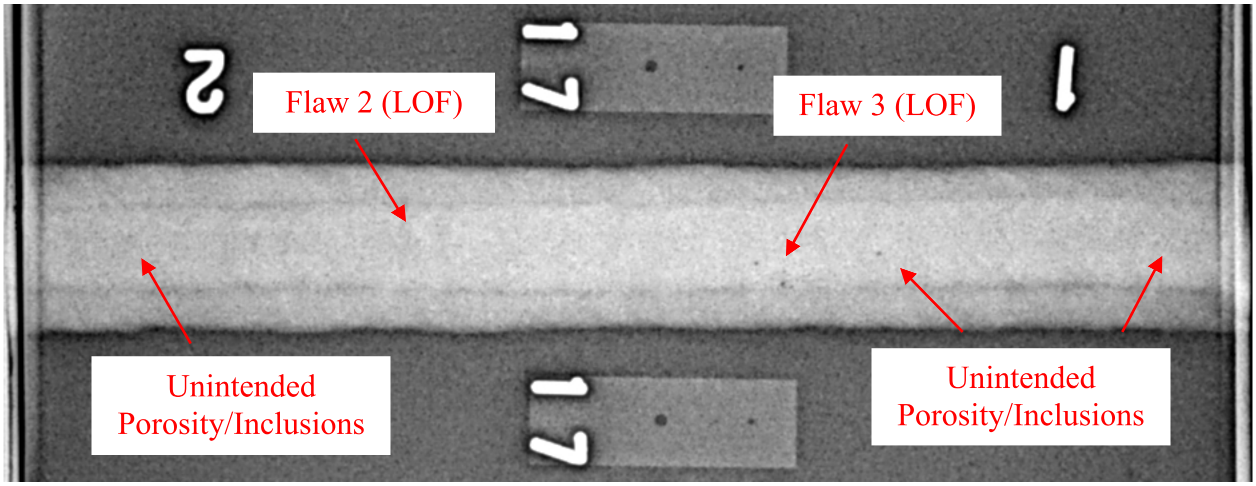

Figure A.14 Flaw 2 and 3 Digital RT Image

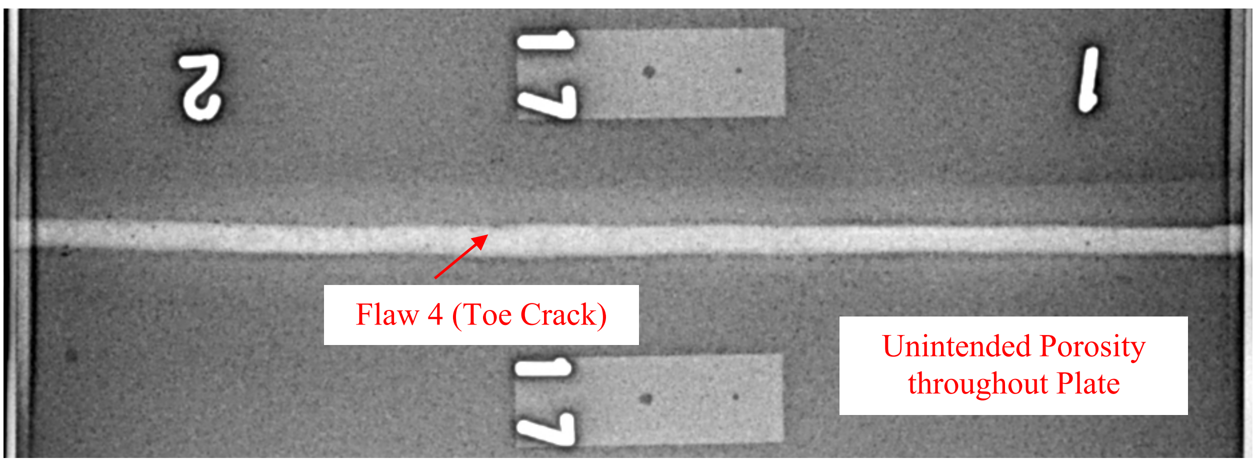

Figure A.15 Flaw 4 Digital RT Image

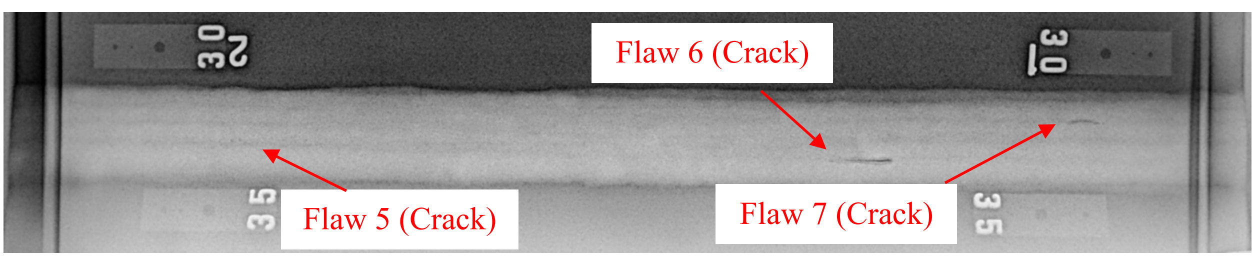

Figure A.16 Flaw 5-7 Digital RT Image

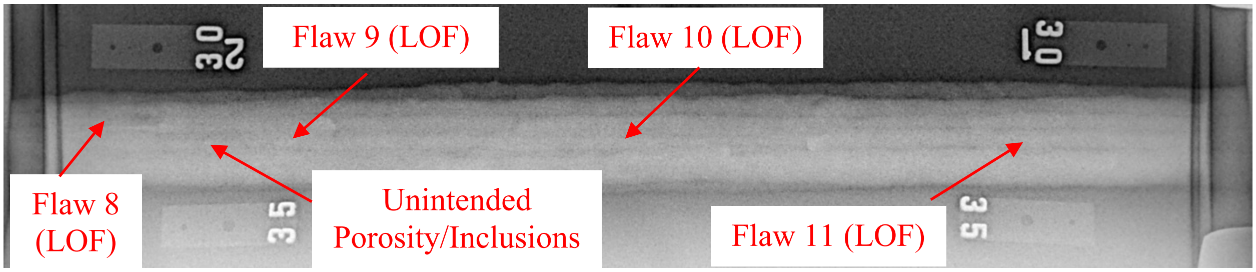

Figure A.17 Flaw 8-11 Digital RT Image

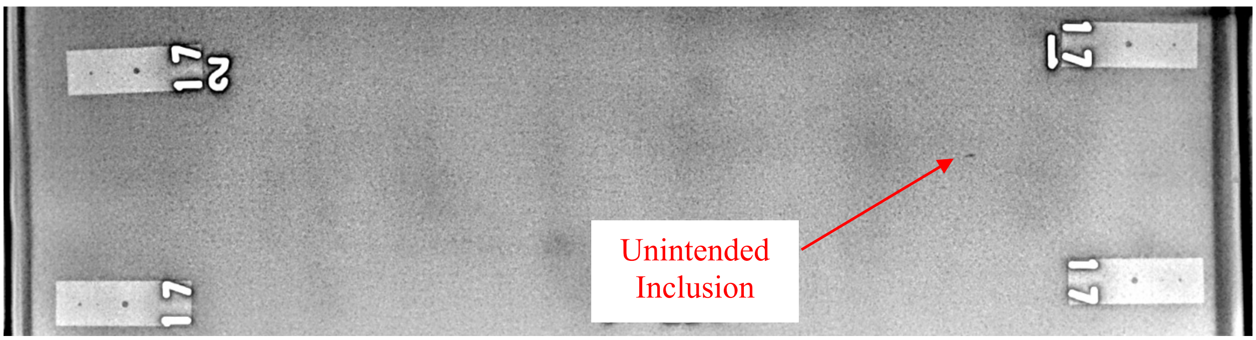

Figure A.18 Blank Plate Digital RT Image

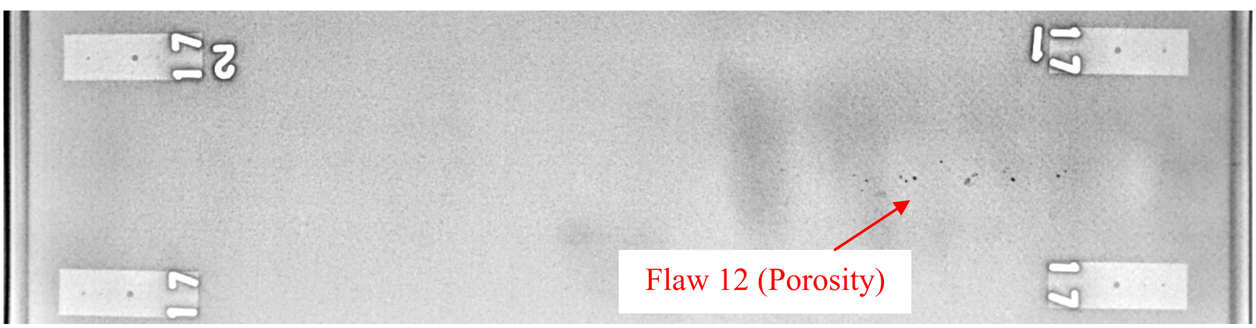

Figure A.19 Flaw 12 Digital RT Image

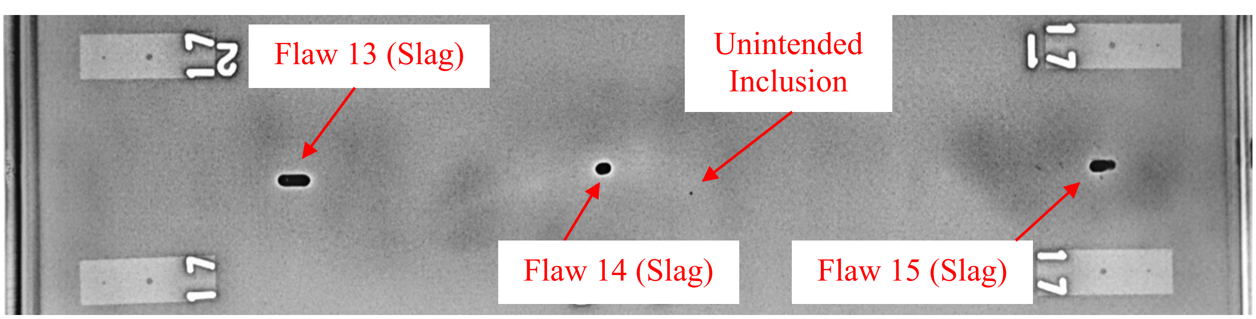

Figure A.20 Flaw 13-15 Digital RT Image

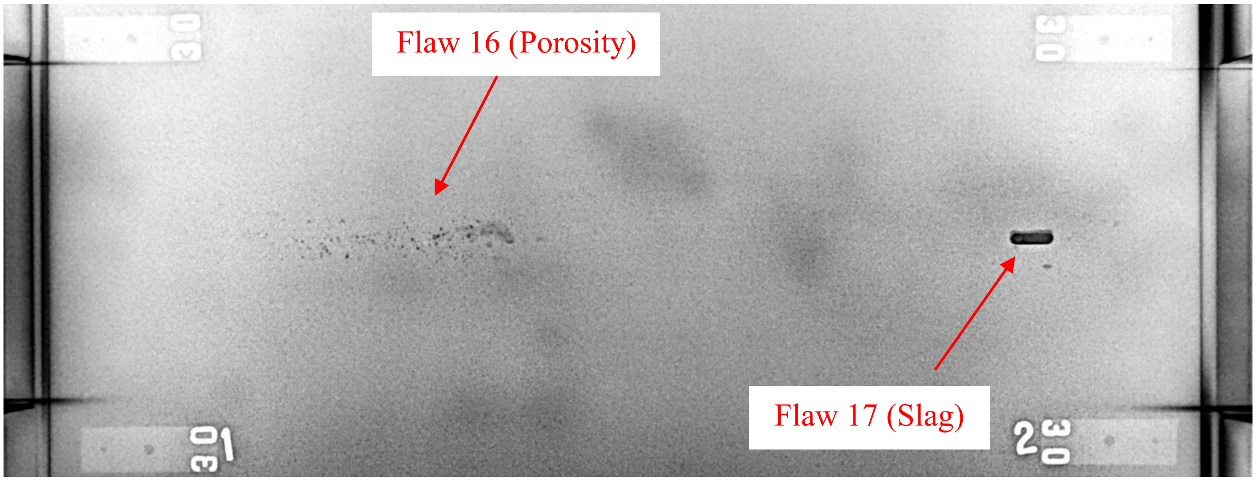

Figure A.21 Flaw 16 and 17 Digital RT Image

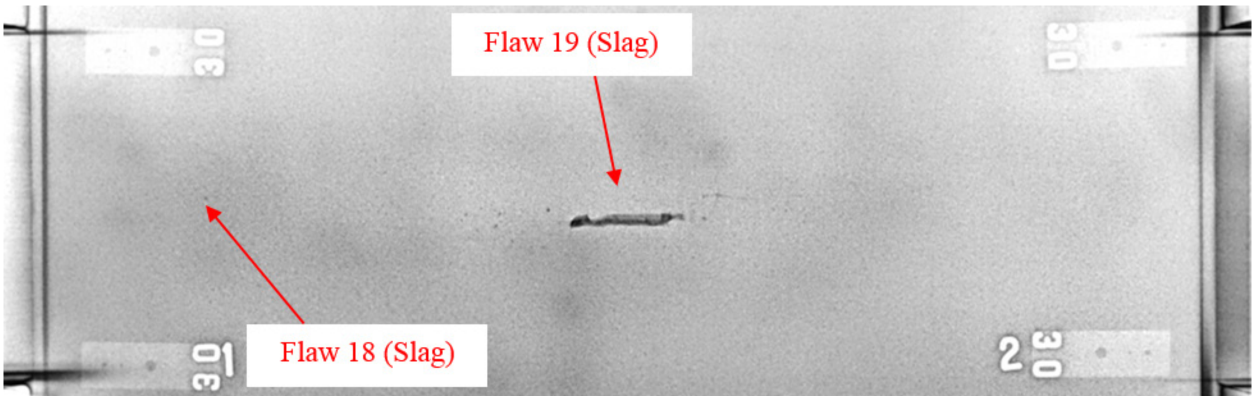

Figure A.22 Flaw 18 and 19 Digital RT Image

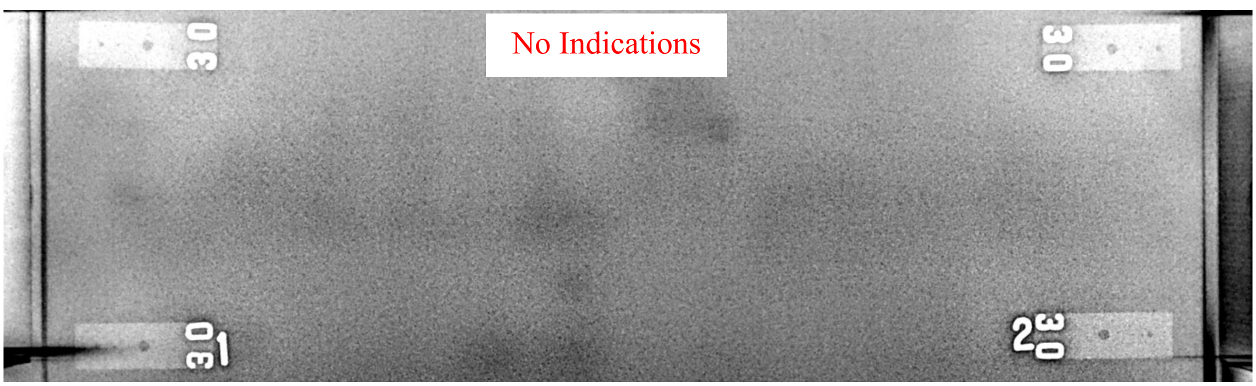

Figure A.23 Second Blank Plate Digital RT Image

REFERENCES

[1] O. Forli and K. O. Ronold, “NT Tech Report 427: Guidelines for Development of NDE Acceptance Criteria,” Oslo, Norway, 1999.

[2] P. B. Crosley and E. J. Ripling, *NCHRP Report 335: Acceptance Criteria for Steel Bridge Welds*. Washington, DC, 1990.

[3] T. J. Jessop, P. J. Mudge, and J. D. Harrison, *NCHRP Report 242: UT Measurement of Weld Flaw Size*. Washington, DC: National Research Council, 1981.

[4] AWS, *D1.1/D1.1M:2015 Structural Welding Code - Steel*, 23rd ed. Miami, FL: American Welding Society, 2015.

[5] AASHTO/AWS, *D1.5M/D1.5:2015 Bridge Welding Code*, 7th ed. Miami, FL: American Welding Society, 2015.

[6] M. Moles, “Defect Sizing in Pipeline Welds – What Can We Really Achieve?,” *Proc. ASME PVP Conf.*, vol. 484, pp. PVP2004-2811, 2004.

[7] B. Crowley, “Ultrasonic Attenuation of Bridge Steels and Narrow-gap Improved Electroslag Welds,” Purdue University, 2018.

[8] R. J. Connor, C. J. Schroeder, G. A. Washer, B. M. Crowley, and P. E. Fish, “NCHRP Project 14-35: Acceptance Criteria of Complete Joint Penetration Steel Bridge Welds Evaluated using Enhanced Ultrasonic Methods,” 2018.

[9] G. A. Shenefelt, “Ultrasonic Testing Requirements of the AWS 1969 Building Code and Bridge Specfications,” *Weld. J.*, vol. May, pp. 342–349, 1971.

[10] CSA, “W59-18: Welded Steel Construction.” CSA Group, Toronto, Canada, p. 550, 2018.

[11] ASME, *ASME BPVC Section V: Nondestructive Examination*, 2017th ed. New York, NY: The American Society of Mechanical Engineers, 2017.

[12] ASME, *ASME Code Case 2235-13: Use of Ultrasonic Examination in Lieu of Radiography*. 2013.

[13] Japanese Standards Association, *JIS Z 3060:2015 Method for Ultrasonic Testing for Welds of Ferritic Steel*, 2015th ed. Tokyo, Japan: Japanese Standards Association, 2015.

[14] P. Holloway, A. Crawford, S. Keay, and V. Vaidya, “Adapting CSA W59 ultrasonic inspections for use with distance-amplitude techniques,” in *NDT in Canada 2017 Conference*, 2017, p. 19.

[15] P. Holloway, "Structural UT : Variables Affecting Attenuation and Review of the 2 dB per Inch Model," *CINDE*, vol. 38, no. 3, pp. 6–11, 2017.

[16] P. Holloway, A. Crawford, S. Keay, and V. Vaidya, "Distance-Amplitude Techniques and their Adaptation to Structural Steel Weld Inspection," *Weld. J.*, vol. March, pp. 38–47, 2018.

[17] ISO, *Non-destructive testing of welds - Phased array ultrasonic testing (PAUT) - Acceptance Levels (ISO 19285:2017)*. Brussels: CEN, 2017.

[18] ISO, *Non-destructive testing of welds - Ultrasonic testing - Techniques, testing levels, and assessment (ISO 17640:2017)*. Brussels: CEN, 2017.

[19] P. T. Marks, *UT Classroom Training Book*, 2nd ed. Columbus, OH: The American Society for Nondestructive Testing, 2015.

[20] T. Armitt and M. Moles, "'Oscillating the Probe': Code Requirements and TOFD," *Mater. Eval.*, vol. 65, no. 11, 2007.

[21] K. IBA, "Method of Ultrasonic Angle Beam Examination for Welds of Ferritic Steels with Acoustic Anisotropy," *Trans. Iron Steel Inst. Japan*, vol. 27, no. 11, pp. 898–909, 1987.

[22] N. Rattanasuwannachart, C. Miki, S. Hirose, and H. Shirahata, "Acoustical Anisotropy and Non-Homogeneity of Rolled Steel Plates," *J. Struct. Eng. Eng. Appl. Mech.*, vol. 21, no. 1, p. 1s–9s, 2004.

[23] FHWA, "FHWA-HRT-14-074: Development of Phased-Array Ultrasonic Testing Acceptability Criteria (Phase I)," *TechBrief*, no. Phase I, pp. 1–15, 2014.

[24] FHWA, "FHWA-HRT-14-075: Development of Phased-Array Ultrasonic Testing Acceptability Criteria (Phase II)," *TechBrief*, no. Phase II, pp. 1–12, 2014.

[25] S. Wilkinson and S. M. Duke, "Comparative Testing of Radiographic Testing, Ultrasonic Testing and Phased Array Advanced Ultrasonic Testing Non Destructive Testing Techniques in Accordance with the AWS D1.5 Bridge Welding Code," 2014.

[26] G. Washer, R. Connor, and D. Looten, "Performance Testing of Inspectors to Improve the Quality of Nondestructive Testing," *Transp. Res. Rec. J. Transp. Res. Board*, vol. 2408, pp. 107–116, Dec. 2014.

[27] Q.Pro Technical Services, "Phased Array Ultrasonic Inspection for Glenn Washer." Houston, TX, p. 20, 2011.

[28] C. J. Schroeder, W. Hardy, P. Fish, and P. W. Sauser, “Comparison of Phased Array Ultrasound to Conventional Ultrasound and Radiographic Testing for Bridge Welds,” *Mater. Eval.*, vol. 75, no. 1, pp. 94–100, 2017.

[29] British Standards, *BS 7910:2005 Guide to methods for assessing the acceptability of flaws in metallic structures*. London: BSI, 2005.

[30] ASME, *ASME Code Case 2235-13: Use of Ultrasonic Examination in Lieu of Radiography*. New York, NY: The American Society of Mechanical Engineers, 2013.

[31] British Standards, “BS 7910:2013 - Guide to methods for assessing the acceptability of flaws in metallic structures,” London: BSI, 2014, p. 492.

[32] J. D. Harrison, “Basis for a Proposed Acceptance-standard for Weld Defects. Part 1: Porosity,” *Met. Constr. Br. Weld. J.*, vol. 4, no. 3, pp. 99–107, 1972.

[33] J. D. Harrison, “Basis for a Proposed Acceptance-standard for Weld Defects. Part 2: Slag inclusions,” *Met. Constr. Br. Weld. J.*, vol. 4, no. 7, pp. 262–268, 1972.

[34] J. D. Harrison and J. Doherty, “A Re-Analysis of Fatigue Data for Butt Welded Specimens Containing Slag Inclusions,” *Weld. Res. Int.*, vol. 8, no. 2, pp. 81–101, 1978.

[35] K. C. Mills and B. J. Keene, “Physical properties of BOS slags,” *Int. Mater. Rev.*, vol. 32, no. 1, pp. 1–120, Jan. 1987.

[36] K. C. Mills, “The Estimation Of Slag Properties,” 2011.

[37] J. W. Fisher, D. R. Mertz, and A. Zhong, *NCHRP Report 267: Steel Bridge Members Under Variable Amplitude Long Life Fatigue Loading*. Washington, DC: National Research Council, 1983.

[38] J. M. Barsom and S. R. Novak, *NCHRP Report 181: Subcritical Crack Growth and Fracture of Bridge Steel*. Washington, DC: National Research Council, 1977.

[39] Quest Integrity USA, “Signal Fitness-For-Service.” Quest Integrity USA, LLC, Seattle, WA, 2016.

[40] ASTM International, *A709-16: Standard Specification for Structural Steel for Bridges*, 2016th ed. West Conshohocken, PA: ASTM International, 2016.

[41] R. D. Medlock, “Qualification of Welding Procedures for Bridges: An Evaluation of the Heat Input Method,” University of Texas at Austin, 1998.

[42] AASHTO, *The Manual For Bridge Evaluation*, 2nd ed. Washington, DC: American Association of State Highway and Transportation Officials, 2011.

[43] American Petroleum Institute and ASME, *API 579-1/ASME FFS-1 Fitness-For-Service*, 2016th ed. Washington, DC: American Petroleum Institute, 2016.

[44] T. L. Anderson, *Fracture Mechanics: Fundamentals and Applications*, Third Edit. Boca Raton, FL: Taylor & Francis Group, 2005.

[45] M. D. Rana, O. Hedden, D. Cowfer, and R. Boyce, "Technical Basis for ASME Section VIII Code Case 2235 on Ultrasonic Examination of Welds in Lieu of Radiography," *J. Press. Vessel Technol.*, vol. 123, no. 3, p. 338, 2001.

[46] API, *API RP 2X: Recommended Practice for Ultrasonic and Magnetic Examination of Offshore Structural Fabrication and Guidelines for Qualification of Technicians*. Washington, DC: API Publishing Services, 2015.

[47] EXTENDE, "CIVA-UT." EXTENDE, Massy, France, 2017.

[48] ISO, *ISO 16811:2012 Non-destructive testing - Ultrasonic testing - Sensitivity and range setting*. Brussels: CEN, 2012.

[49] E. Ginzel and B. Pedersen, "Civa Modelling of Distance Amplitude Correction Curves on Flat Calibration Blocks," *NDT.net*, vol. 20, no. 5, pp. 1–8, 2015.

[50] E. Ginzel, "Fun With Civa," *NDT.net*, p. 12, 2011.

[51] Olympus NDT, *Phased Array Testing: Basic Theory for Industrial Applications*. Waltham, MA: Olympus NDT, 2010.

[52] ASNT, *Recommended Practice No. SNT-TC-1A (2016) Personnel Qualification and Certification in Nondestructive Testing*. Columbus, OH: The American Society for Nondestructive Testing, 2016.

[53] Department of Defense, "MIL-HDBK-1823A: Nondestructive Evaluation System Reliability Assessment," 2009.

[54] NYSDOT, *New York State Steel Construction Manual*, 4th ed. NYSDOT, 2018.

[55] TxDOT, *Standard Specifications for Construction and Maintenance of Highways, Streets, and Bridges*. Texas Department of Transporation, 2014.

[56] E. A. Ginzel, R. Thomson, and R. K. Ginzel, "A Qualification Process for Phased-Array UT using DNV RP-F118 Guidelines," *NDT.net*, pp. 1–12, 2011.

[57] R. E. Shaw Jr., "Ultrasonic Testing Procedures, Technician Skills, and Qualifications," *J. Mater. Civ. Eng.*, vol. 14, no. 1, pp. 62–67, 2002.